PART-II

Chapter- 4 Analysis

4.1 Channel geometry, hydraulics and load

Introduction

The movement and clearance of water and sediment from upslope largely depends on form and pattern of the river. Channel form in turn is influenced by the magnitude of discharge and flow regime character (Harvey 1969; Stevens et al., 1975). Later half of the 20^{th} century was an era of major advancement in understanding channel morphology and pattern through various channel parameters or variables. Fluvial scientists measured individual channel parameters both on field and in laboratories (flume tests) and attempted their relationships with many different parameters. Leopold and Maddock,1953 made relationships between parameters like discharge (Q), width (W), depth (D) and velocity (V) and their rate of variation to describe the morphology of river channels. Schumm (1974) examined the relationship between channel patterns, sediment load and gradient in a flume. Bagnold (1966) made a relation between stream power and sediment transport capacity, thereby suggested that stream power provided an integrative parameter for relating sediment transport to channel hydraulics. Bagnold's equation (1980) alongwith Parker's (1978) model suggested that for a given discharge and slope, a larger sediment load requires a wide channel. Leopold and Maddock (1953) explained the concavity of the longitudinal profile in terms of the downstream decrease of sediment load in relation to discharge. Keller (1972) proposed a five stages model of the development of pools and riffles in an alluvial river. Langbein and Leopold (1966) hypothesized that the meandering channel pattern represents a least work tendency, and equilibrium of power expenditure. Lewin (1977) classified meanders' pattern change as autogenic and allogenic. Autogenic changes in channels' meandering pattern refers to those changes which are inherent in rivers' regime, like changes due to channel migration,crevassing, neck cutoffs etc. whereas allogenic changes take place in response to external influences such as climatic fluctuation and human activities etc. Daniel (1971)

identified channel migration processes in terms of rotation, expansion and translation of look axes.

Water discharge increase downstream as the drainage area and the runoff from it increases. Water discharge in a channel cross section is the product of the mean velocity of the water with the cross-sectional area of the flow, or the width-depth product. One or more of these variables or parameters of the channel changes to accommodate the increased discharge, either downstream at a given moment, or a site through time. The relationships that reveal how the width, depth and velocity of the flow increase with discharge are called the hydraulic geometry of the river (Leopold and Maddock,1953).

The knowledge and understanding of point hydraulic variables (eg. Velocity, water depth, flow pattern, nature of flow etc.) is significant for various subjects ranging from hydraulic engineering, fluvial geomorphology to stream ecology (Chiu and Tung,2002; Rosenfeld et al., 2001 and Mérigoux et al., 2009). Leopold and Maddock (1953) introduced the hydraulic geometry approach whereby channel properties are treated as continuous functions of increasing discharge downstream. Water flow in open channels is determined by two opposing forces; ie., the gravitational force that pulls water downslope and frictional force that generates between the water molecules and that between water and channel boundary together resisting the flow (Chorley and Kennedy,1971). Further the increase in the rates of width and velocity is greater compared to the depth (Leopold et al.,1964; Wolman and Gerson,1978; Knighton,1998).

For understanding of channel hydraulics, sediment transport rate, sediment budget and habitat description, an analysis of river bed sediment analysis is an important prerequisite. Identification of changes in channel bed composition as a consequence of varied flow conditions and environmental factors can be achieved through accurate sampling of sediments.

4.1.1 Study Reach

The study reach for the present study extends from near the confluence point of Manzing and Sukha Khola with Chel River near Putharjhora Tea Garden, near the

mountain front below Gorubathan to confluence point of Chel River with Neora River (Fig. 4.1.1) in the downstream. The straight valley length of the reach is 20.93 km.

4.1.2 Materials and methods

A total of eighteen (18) cross profiles were taken at an equal interval of 2kms during February, 2017 all along the study reach of the Chel River to assess the nature of channel forms and patterns. The cross profiles with red colored labels were measured three times during 2014,2015 and 2017 to understand the channel configuration and bed elevation variation (Fig.4.1.1). Channel cross profiling was achieved by using dumpy level and measuring staffs considering several change points. The bench mark of 157 m of CWC Chel office located along NH-31C Road Bridge on Chel River at Odlabari has been used for calculation of reduced levels at all the stations. Channel depth was measured with the help of measuring staff. All the cross-profile readings were taken with Dumpy Level starting from right bank towards the left in the downstream direction of flow of river (Plate 4.1.2)**.** The drawn cross-profiles display a wide variation in terms of shape, configuration and degree of asymmetry.

Slope of the river bed is calculated employing the equation-

$$\theta = \tan^{-1}\frac{r}{h} \quad (1)$$

Where, 'θ' is the river bed slope, 'r' is difference of reduced level at the first and last points and 'h' is the horizontal distance between same two points.

Channel pattern is understood through the sinuosity index based on Friend and Sinha's method (1993) P,

$$P = Lcmax/LR, \quad (2)$$

Where LR is the overall length of the channel-belt reach measured along a straight line, and Lcmax is the mid-channel length of the same reach, or the mid-channel length of the widest channel, where there is more than one channel. Sinousity Index in fact is a measure of bending of a river. Lower value of it implies the channel is near to straight course and higher values shows more sinuous course.

Surface water velocity has been measured by dye tracing method and Current meter (Plate 4.1.1). Average discharge has been calculated for pre-monsoon and post- monsoon period.

The pattern of flow is understood by Reynolds Number

$$\mathbf{Re} = \rho \frac{\mathbf{VR}}{\boldsymbol{\mu}} \quad (3)$$

Where, Re= Reynolds' number

V= Mean velocity of flow,

R= Hydraulic Radius,

ρ = Density of water,

μ = Dynamic viscosity

Re<500 implies laminar flow, Re= 500-2000 implies transistional flow and Re> 2000 indicates turbulent flow.

The nature of flow is understood by Froude Number which is defined as

Fr = (Inertia force/ Gravity force) $^{1/2}$.

$$Fr = V/\sqrt{Dg} \quad (4)$$

Where, Fr = Froude number,

V = Mean flow velocity,

D= mean water depth,

g = acceleration due to gravity.

Fr<1 indicates sub-critical flow, Fr=1 indicates critical flow and Fr>1 indicates super critical nature of flow.

Discharge is calculated employing Leopold and Maddock (1953) as,

$$Q=WDV \quad (5)$$

Where, Q= discharge, W= width, D= depth and V= mean velocity.

An investigation on seasonal bed load sediment size variation along the study reach was achieved through pebble count method and by using Slide calipers (Plate 4.1.4).

Plate 4.1.1 Velocity measurement; Plate 4.1.2 - Cross profiling; Plate 4.1.3- depth measurement; Plate 4.1.4-Coarse sediment size measurement.

4.1.3 Cross Profiles

Cross-sectional form of natural channels is characteristically irregular in outline, locally variable and is roughly parabolic in shape. The shape of cross-section of a river channel is a function of the flow, the quantity and character of the sediment and the composition of the materials making up the bed and banks of the channel (Knighton, 1981).

The shape of the cross-section is described through the ratio of channel width to depth. The depth of flow in a channel is directly proportional to the force which the water exerts on the bed and to its ability to transport sediment (Leopold and Wolman, 1957).

Width, mean depth, cross-sectional area, wetted perimeter, hydraulic radius, maximum depth, bed width, width-depth ratio etc. are the important parameters commonly used to describe channel form (Fahnestock, 1963 and Knighton, 1981). Width and mean depth represent the gross dimension of a channel but do not uniquely define cross-sectional shape (Hey, 1978).

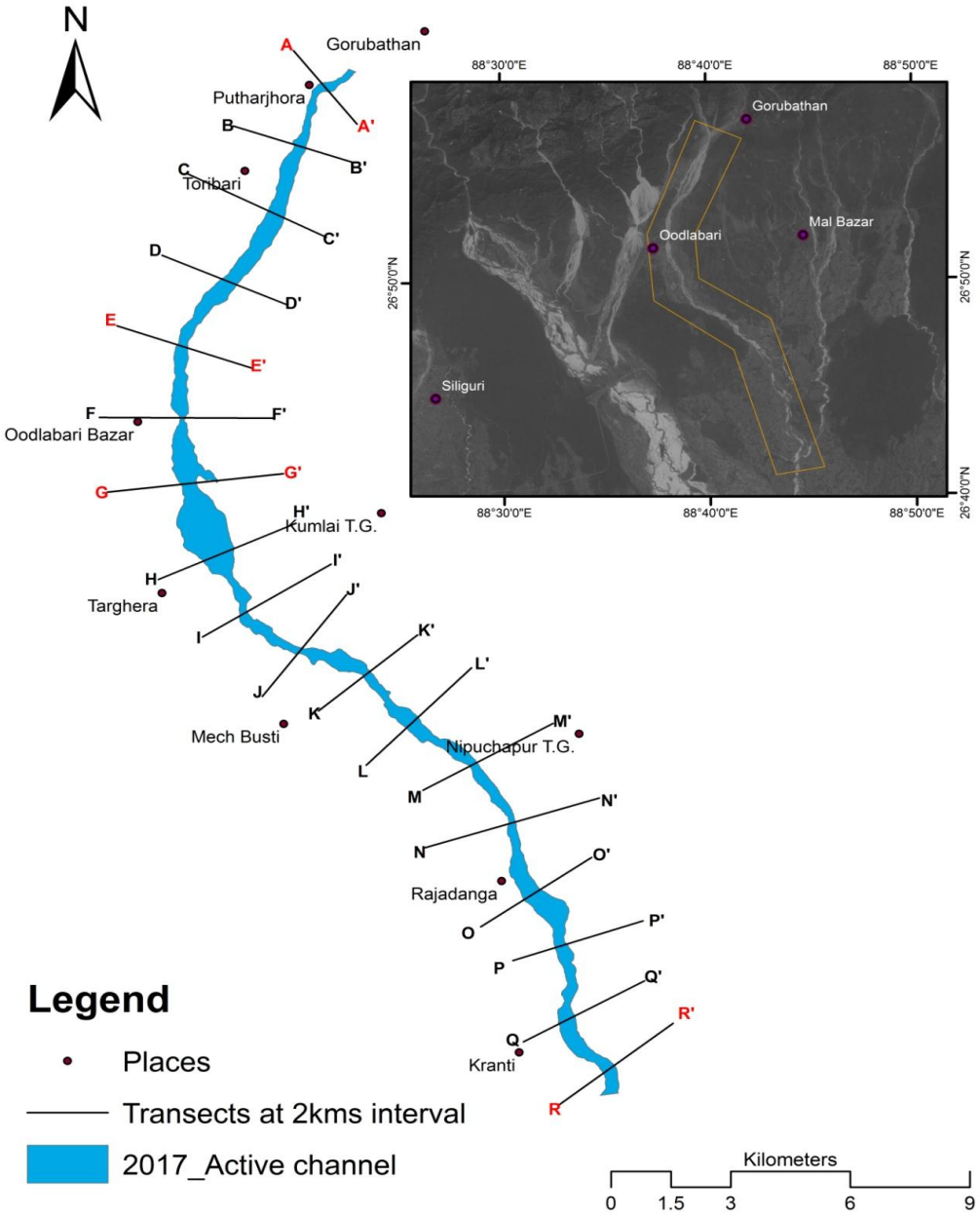

Figure 4.1.1 Positions of cross profiles drawn along the study reach. Red labeled cross profiles were measured during 2014, 2015 and 2017. Inset image showing regional setting of study reach.

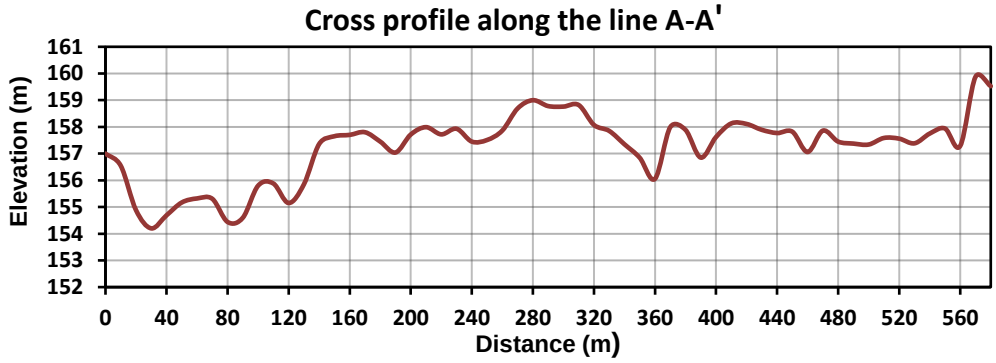
Cross profile along the line A-A'
Elevation (m)
161
160
159
158
157
156
155
154
153
152
0
40
80
120
160
200
240
280
320
360
400
440
480
520
560
Distance (m)

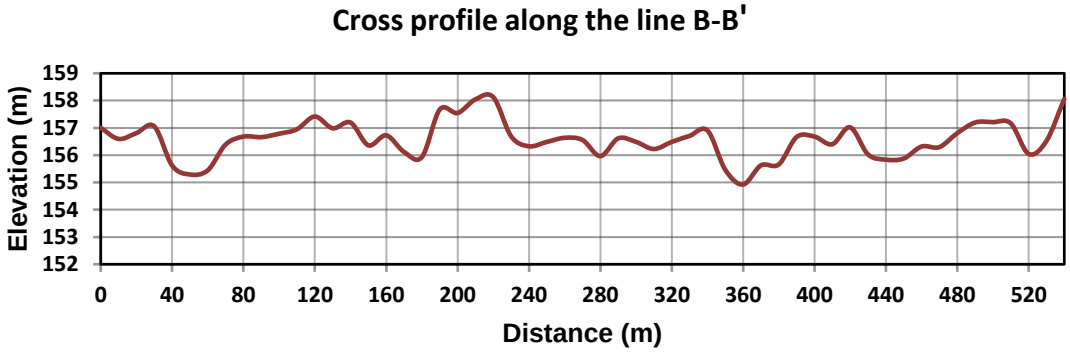
Cross profile along the line B-B'
Elevation (m)
159
158
157
156
155
154
153
152
0
40
80
120
160
200
240
280
320
360
400
440
480
520
Distance (m)

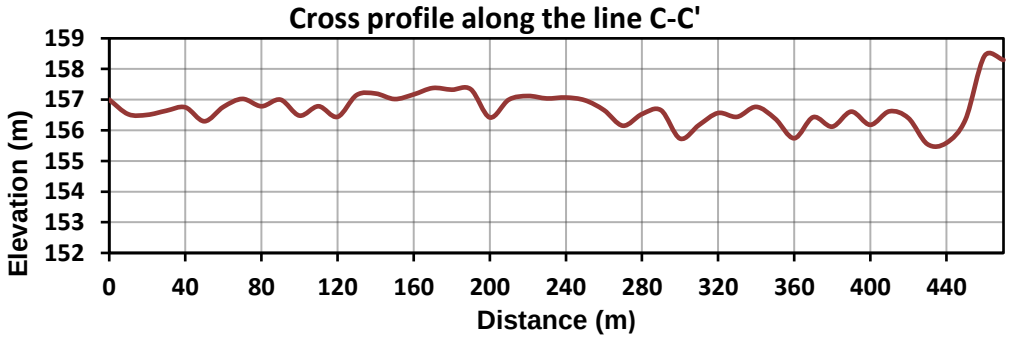
Cross profile along the line C-C'
Elevation (m)
159
158
157
156
155
154
153
152
0
40
80
120
160
200
240
280
320
360
400
440
Distance (m)

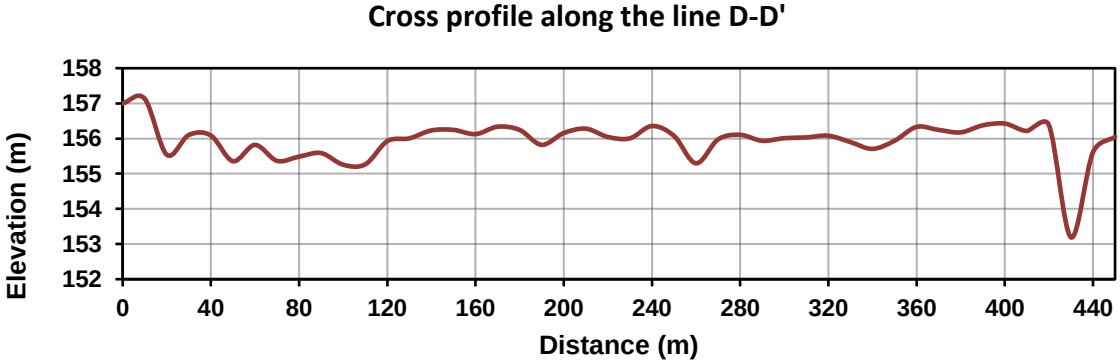
Cross profile along the line D-D'
Elevation (m)
158
157
156
155
154
153
152
0
40
80
120
160
200
240
280
320
360
400
440
Distance (m)

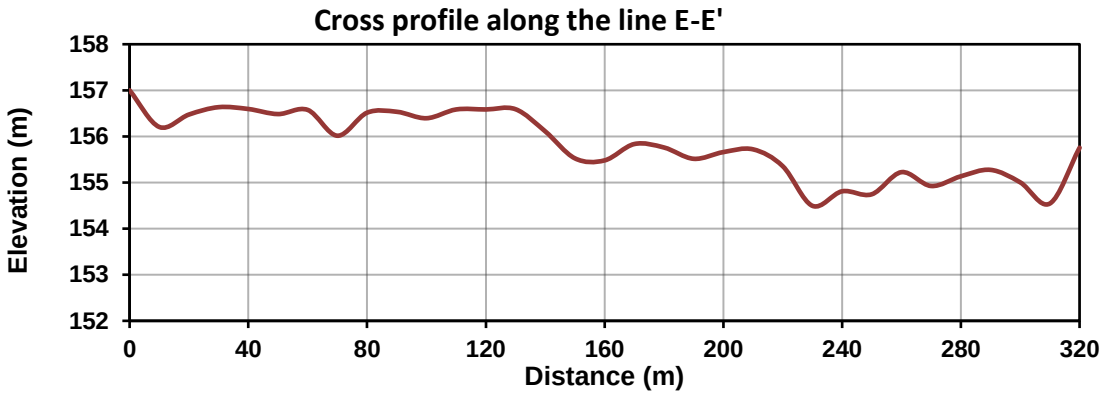
Cross profile along the line E-E'
Elevation (m)
158
157
156
155
154
153
152
0
40
80
120
160
200
240
280
320
Distance (m)

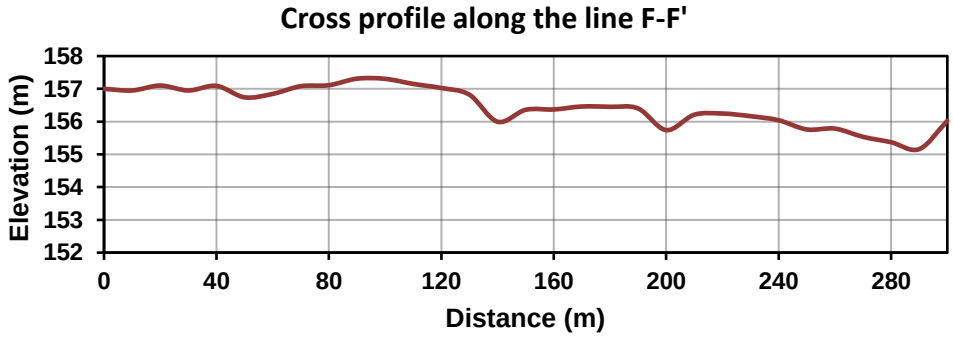
Cross profile along the line F-F'
Elevation (m)
158
157
156
155
154
153
152
0
40
80
120
160
200
240
280
Distance (m)

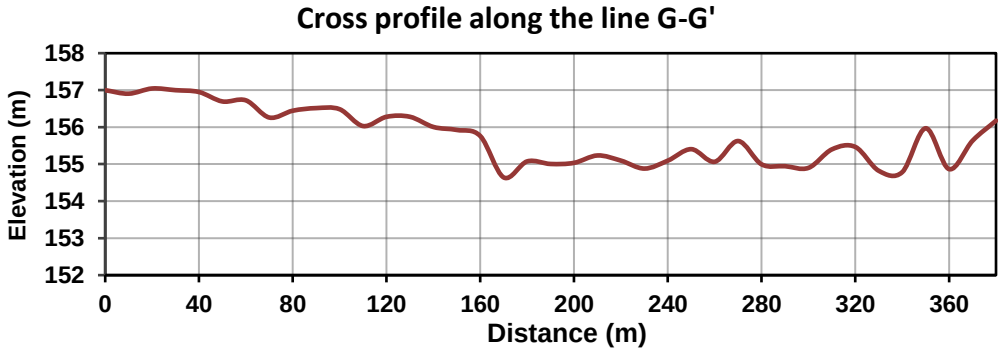
Cross profile along the line G-G'
Elevation (m)
158
157
156
155
154
153
152
0
40
80
120
160
200
240
280
320
360
Distance (m)

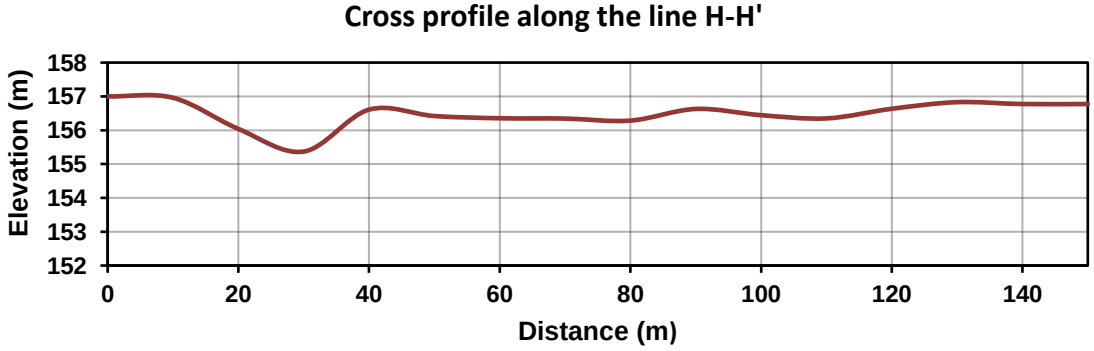
Cross profile along the line H-H'
Elevation (m)
158
157
156
155
154
153
152
0
20
40
60
80
100
120
140
Distance (m)

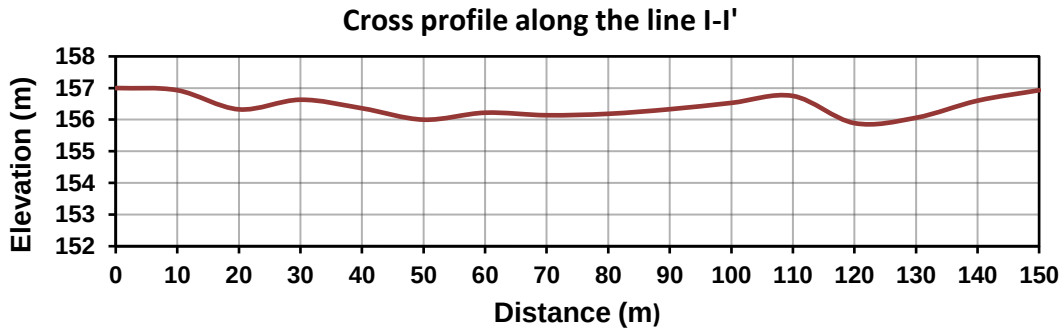
Cross profile along the line I-I'
Elevation (m)
158
157
156
155
154
153
152
0
10
20
30
40
50
60
70
80
90
100
110
120
130
140
150
Distance (m)

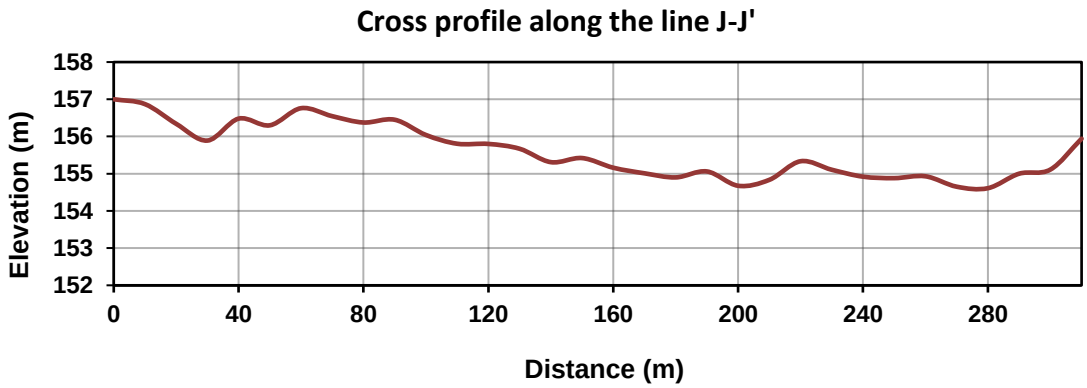
Cross profile along the line J-J'
Elevation (m)
158
157
156
155
154
153
152
0
40
80
120
160
200
240
280
Distance (m)

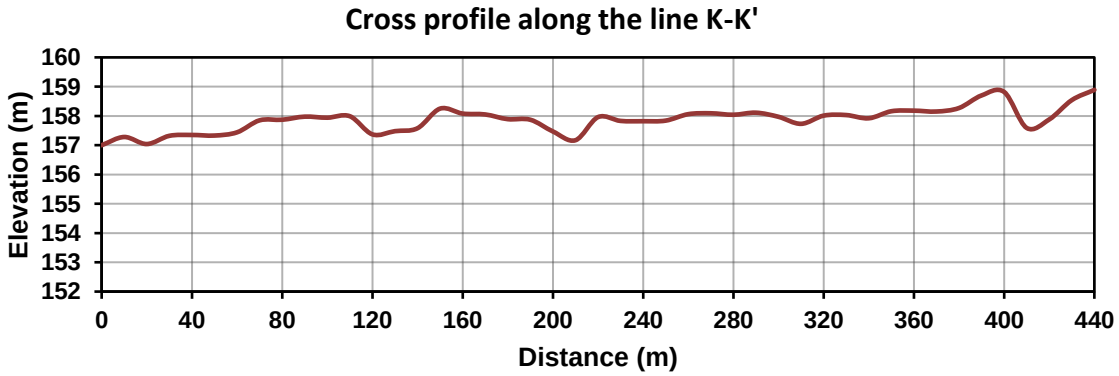
Cross profile along the line K-K'
Elevation (m)
160
159
158
157
156
155
154
153
152
0
40
80
120
160
200
240
280
320
360
400
440
Distance (m)

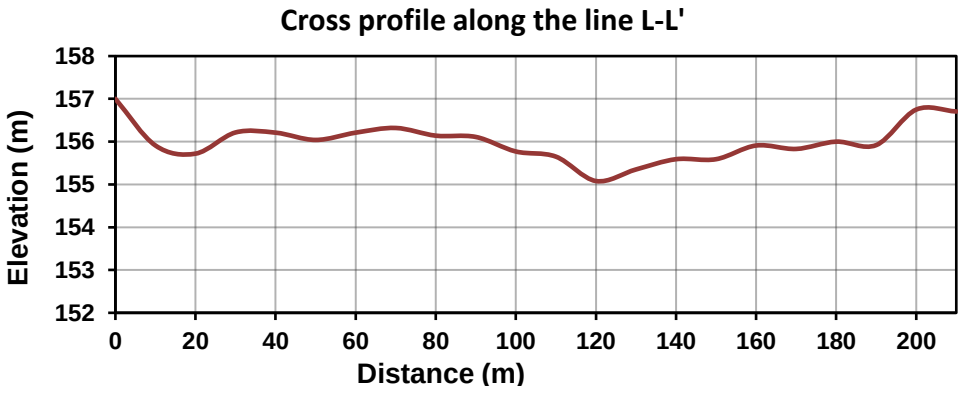
Cross profile along the line L-L'
Elevation (m)
158
157
156
155
154
153
152
0 20 40 60 80 100 120 140 160 180 200
Distance (m)

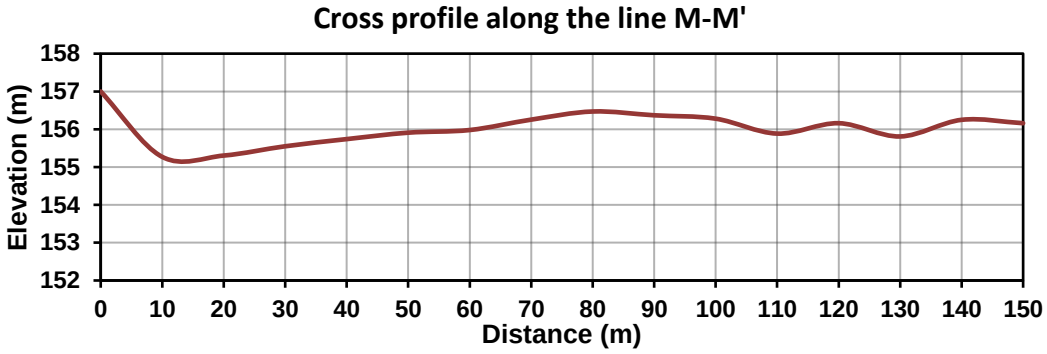
Cross profile along the line M-M'
Elevation (m)
158
157
156
155
154
153
152
0 10 20 30 40 50 60 70 80 90 100 110 120 130 140 150
Distance (m)

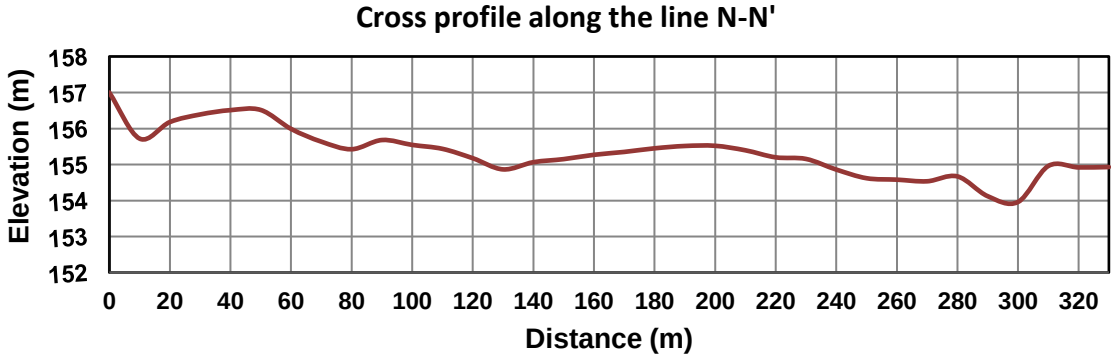
Cross profile along the line N-N'
Elevation (m)
158
157
156
155
154
153
152
0 20 40 60 80 100 120 140 160 180 200 220 240 260 280 300 320
Distance (m)

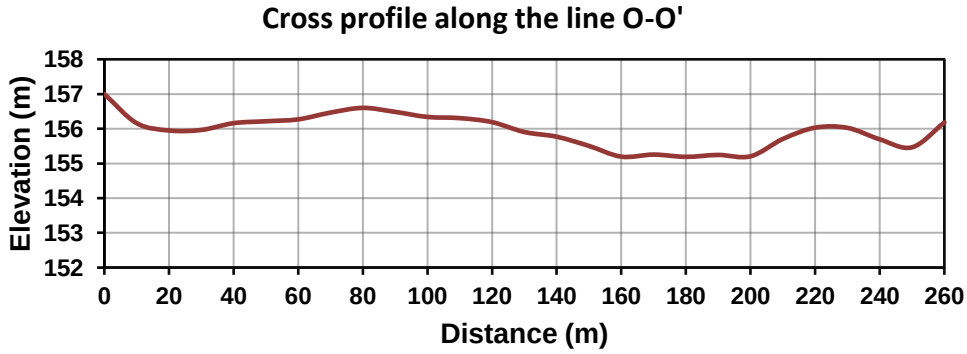
Cross profile along the line O-O'
Elevation (m)
158
157
156
155
154
153
152
0 20 40 60 80 100 120 140 160 180 200 220 240 260
Distance (m)

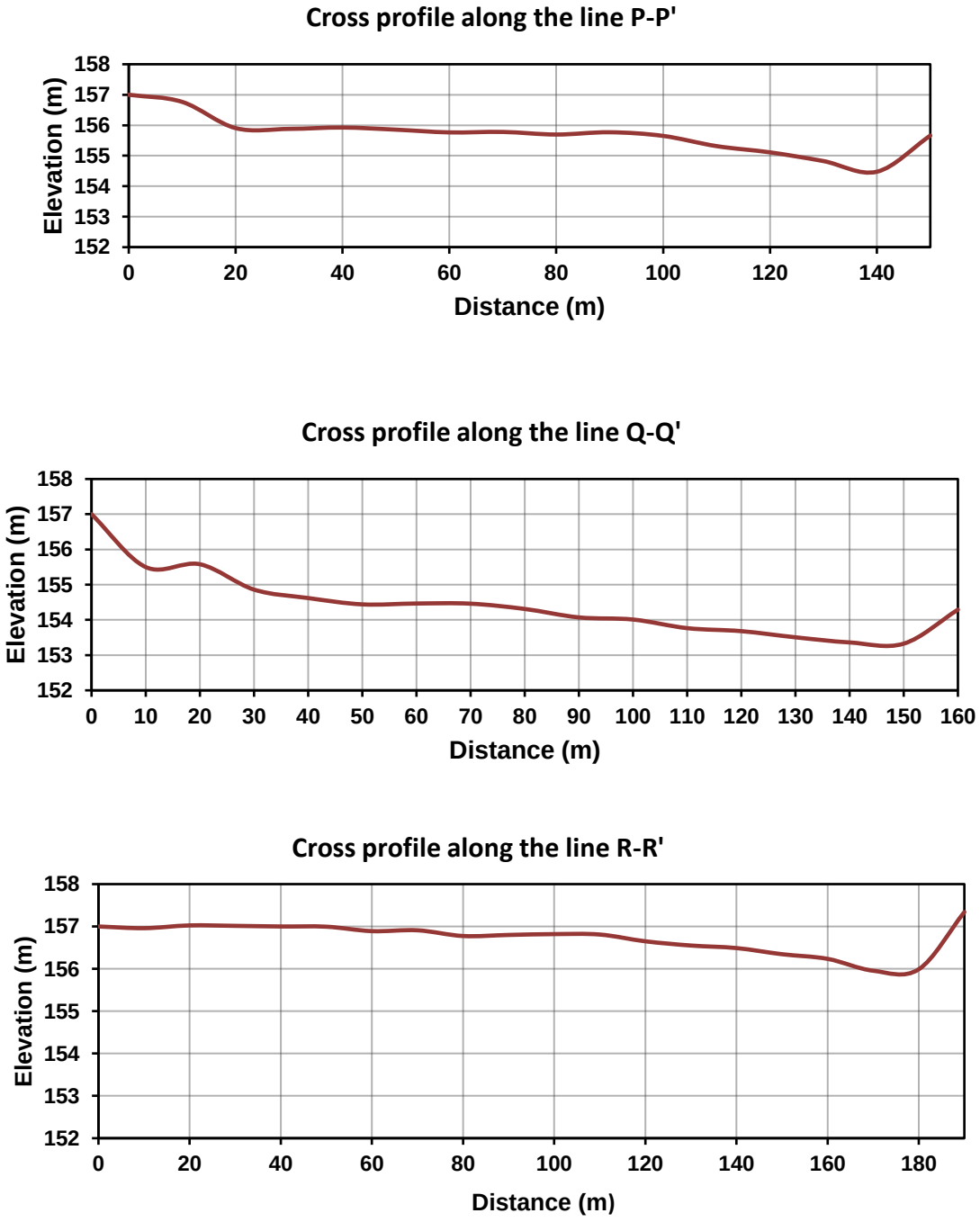

Figure 4.1.2 Cross sections at 2km interval along the study reach showing bed configuration during 2017.

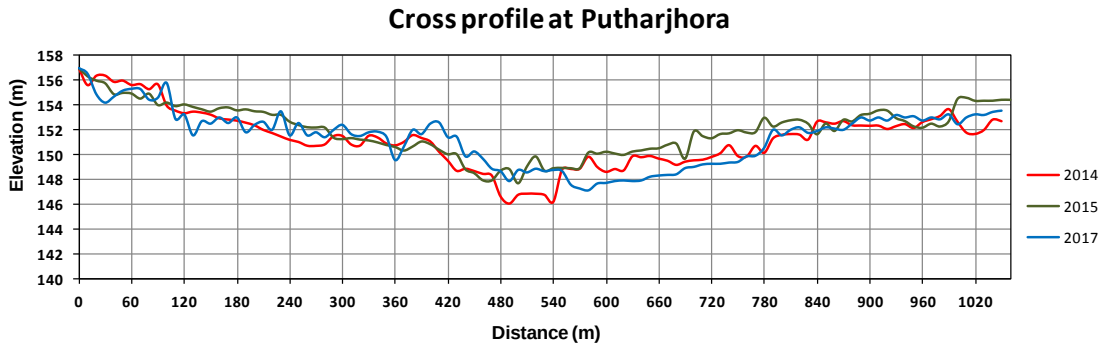
Cross profile at Putharjhora
Elevation (m)
158
156
154
152
150
148
146
144
142
140
0 60 120 180 240 300 360 420 480 540 600 660 720 780 840 900 960 1020
Distance (m)
2014
2015
2017

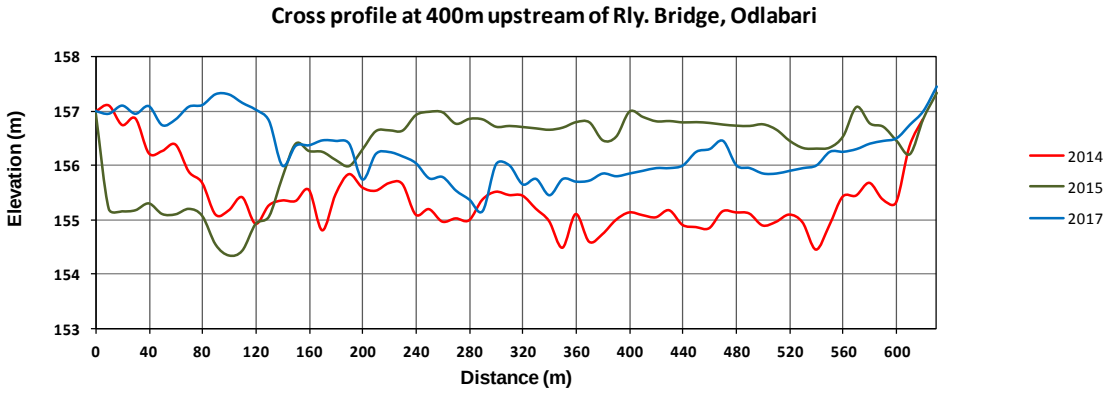
Cross profile at 400m upstream of Rly. Bridge, Odlabari
Elevation (m)
158
157
156
155
154
153
0 40 80 120 160 200 240 280 320 360 400 440 480 520 560 600
Distance (m)
2014
2015
2017

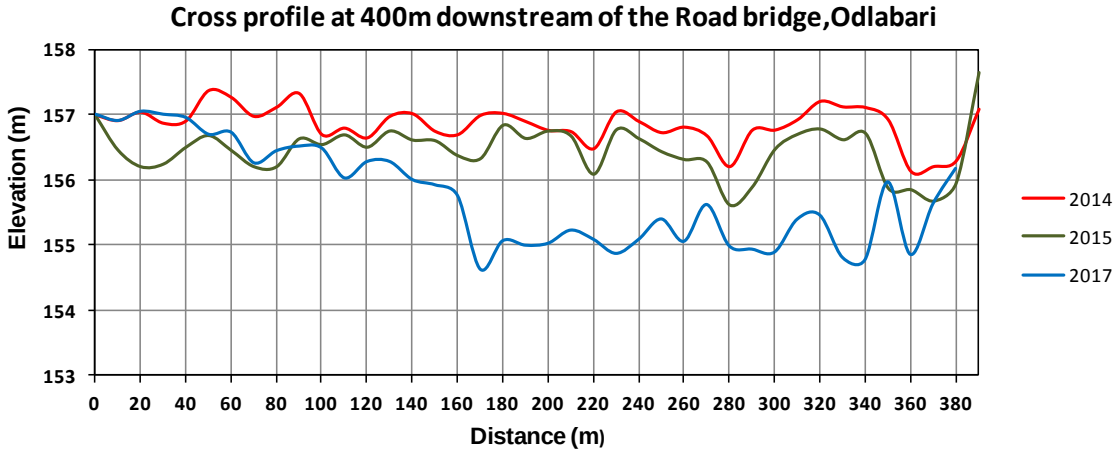
Cross profile at 400m downstream of the Road bridge,Odlabari
Elevation (m)
158
157
156
155
154
153
0 20 40 60 80 100 120 140 160 180 200 220 240 260 280 300 320 340 360 380
Distance (m)
2014
2015
2017

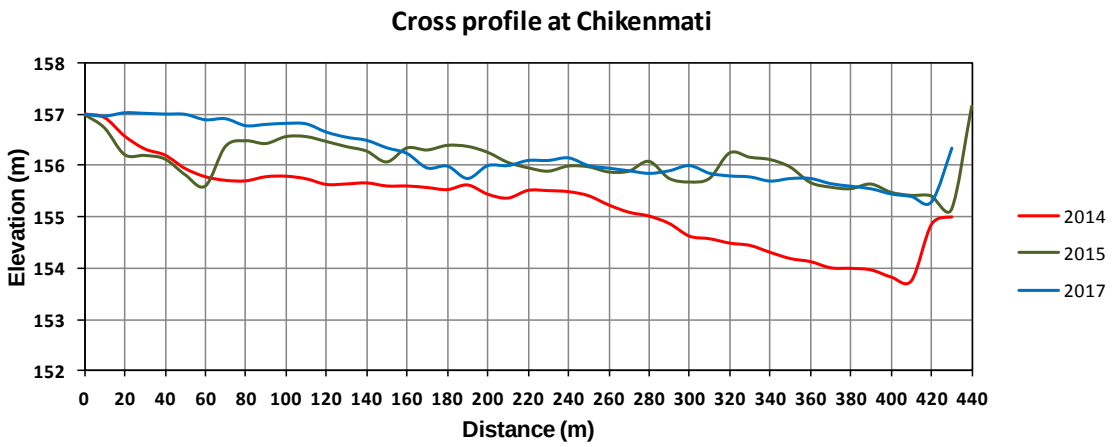

Figure 4.1.3 Superimposition of cross profile measured across three positions representative of three segments of the study reach showing variability in channel configuration.

4.1.3.1 Symmetrical and asymmetrical cross profiles

Symmetrical cross profiles are characterized by having the thalweg point at the middle of the cross section with same distance from both the banks (Morisawa, 1963). In fact, the slope, length and configuration of channel bed on both sides of the cross-sections are also same from the thalweg position. Contrary to this, in an asymmetric cross section thalweg point lies near to any of the either bank. Thus slope, length and configuration of channel bed on either side of the thalweg point will be different.

The entire cross profiles in the study area are asymmetrical in nature (Fig.4.1.2). They display typical braided pattern in the upper and middle segments of the study reach. The profiles are much changeable with several peaks and lows suggesting a number of channels filled with water and are separated by sand bars of different heights and sometimes with vegetative islands. The profiles P-P', Q-Q' and S-S' from the lower segment display somewhat single channel flow pattern as suggested by smoother and much less changeable curves. High rate of aggradations, distribution and redistribution of sediments by multiple channels, shifting of thalweg positions etc can be attributed for the asymmetrical cross profiles throughout the study reach.

4.1.3.2 Relationship between cross profiles (channel shape), velocity and turbulence.

Leighley (1934) related channel shape with regions of turbulence and realms of velocity across a river cross section. He divided the transverse section of a river into three regions – 1-an inner axial region of high velocity and moderate turbulence, 2-an outer realm of low velocity and low turbulence and 3- an area between the other two regions where turbulence is maximum and velocity is moderate (Fig.4.1.4).

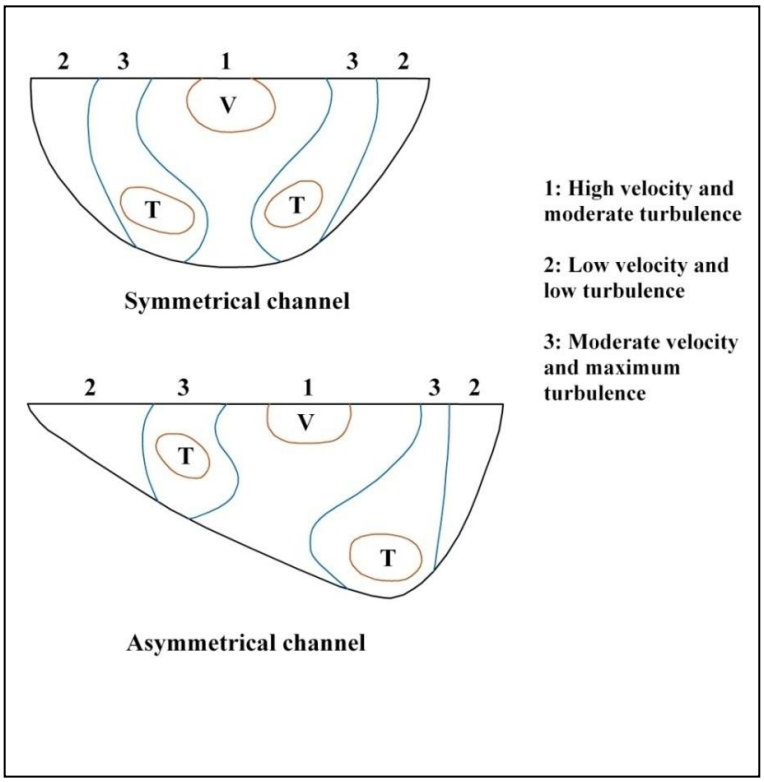

Figure 4.1.4 Relation between channel shape, velocity and turbulence (Leighley, 1934)

According to Morisawa, 1963, shape of the channel also determines the velocity distribution. Concepts of channel slope in relation to velocity and turbulence are important in understanding erosion of the channel and sediment transport through the reach (Hubbell and Matejka, 1959). A symmetric channel is characterized by high velocity present in the middle of the channel just below the surface (Knighton, 1988). Whereas in an asymmetric channel, velocity distribution is skewed and, indeed, may be

divided into two or more cells. As the study area is characterized by asymmetric cross sections throughout, velocity reduction due to flow separation towards the shallower

Sections are very common. This leads to large scale sedimentation whereas deeper and near bank portions witness scouring and erosion.

4.1.4 Depth

Distribution of depth across and along the channel largely governs the shape of the channel. Depth distribution across the channel depends largely on channel width, which again is dependent on discharge.

The field survey conducted during 2017 revealed a great spatial variation of depth at the different cross profiles in the study area (Plate 4.1.3 & Fig. 4.1.2). The maximum channel depth of 5m was recorded near Putharjhora at cross profile A-A' whereas the least channel depth of 1m was recorded at Cross profiles I-I' (near Odlabari) and R-R' at the middle and lower reaches respectively (Table 4.1.1). Huge amount of aggradation and multi-thread channel system hinders bed scouring and thus reduces channel depth in the study reach.

4.1.4.1 Seasonal variation of water depth

Huge amount of sediment aggradations, multiple channel and large channel width makes Chel River a relatively shallow river. The measured channel depth values along the study reach of River Chel during pre and post monsoon are all less than a meter. Seasonal variation of depth is much evident due to variation in discharge. The maximum depth near Putharjhora (A-A') cross profile is 0.27m and 0.55m during pre and post monsoon season. Whereas the last cross profile (R-R') near Kranti recorded maximum depths of 0.23m and 0.95m during pre and post monsoon seasons respectively. During pre-monsoon the highest maximum depth value (0.44 m) and lowest maximum depth value (0.16) were recorded in cross profiles M-M' and O-O' respectively. Whereas during the post monsoon highest maximum depth value (0.95m) and lowest maximum depth value of (0.45 m) were recorded at cross profiles F-F', M-M' and O-O' respectively (Table. 4.1.2 and 4.1.3). Higher discharge during monsoon months causes some amount

of bed scouring which results in recording of higher depth values during post monsoon season.

4.1.4.2 Width-Depth ratio

Width-depth ratio is one of the important parameters to understand the channel form. Relatively narrow and deep river with lower width-depth ratio is capable of moving more suspended sediment by turbulence and velocity of flowing water, but shallow wider channel, having large width-depth ratio, is more efficient to transport bed load by shear on the bottom of the stream (Coleman, 1969).

In the study area the highest width-depth ratio is measured near Mech-Busti at cross profile K-K' and the lowest corresponds to the last cross profile Q-Q' near Kranti (Table.4.1.1). The width-depth ratio changes continuously to adjust with the discharge, load type and slope of the bed. River discharge, rock type, slope, type of load being transported, type of sediment at the channel's perimeter, and rock uplift rate have all been shown to control river width (Schumm, 1960). Channel width appears to increase as a small power function of discharge, following the equation $w = aQ^b$ (Where, 'Q' is water discharge, 'w' is water surface width, 'a' and 'b' are constants) (Schumm, 1960). Several laboratory experiments and field studies yielded 'b' values between 0.3 and 0.5 (Carlston, 1968). Subsequent investigations suggest that channel perimeters with a high quantity of coarse-grained materials tend to be wide and shallow (Schumm, 1960).

Table 4.1.1 Width-depth ratio at different cross profiles.

Cross profiles	Width (m)	Maximum Depth (m)	Width-Depth ratio
A-A'	580	5	116.00
B-B'	540	3	180.00
C-C'	470	3	156.67
D-D'	450	4	112.50
E-E'	320	2.5	128.00
F-F'	300	2.3	130.43
G-G'	380	2.5	152.00
H-H'	150	1.5	100.00
I-I'	150	1	150.00
J-J'	310	2.5	124.00
K-K'	440	2	220.00
L-L'	210	2	105.00
M-M'	150	2	75.00
N-N'	330	3.2	103.13
O-O'	260	1.8	144.44
P-P'	150	2.5	60.00
Q-Q'	160	3.8	42.11
R-R'	190	1	190.00

Source: Field survey, 2017.

Table 4.1.2 Channel hydraulic variables measured during Pre-monsoon, 2017

						PRE MONSOON-2017								
Profile	**Slope**	**Surface water velocity (m/sec.)**	**Max. water depth (m)**	**Min. water depth (m)**	**Mean water depth (m)**	**Width (m)**	**Wetted Perimeter (m)**	**Cross Sec. Area (m^2)**	**Hydraullic Radius(m)**	**Width-Depth**	**Re**	**Fr**	**Available Shear Stress**	**Discharge (m3/sec.)**
A-A'	1.8996136	1.068	0.27	0.05	0.143	3.7	4.1	0.529	0.129	13.704	154390.16	0.902	2404.03	0.5651
B-B'	1.8666087	1.111	0.285	0.045	0.157	12	13.85	1.884	0.136	42.105	169293.25	0.895	2490.03	2.0931
C-C'	1.4177811	0.95	0.255	0.025	0.142	10.52	11.75	1.494	0.127	41.255	105388.3	0.627	1767.65	1.4191
D-D'	1.1028075	0.903	0.23	0.03	0.14	9.5	10.3	1.330	0.129	41.304	130616.08	0.771	1396.48	1.2010
E-E'	0.8756534	0.861	0.21	0.02	0.11	16.7	17.1	1.837	0.107	79.524	7954428.25	0.636	375.5	1.5817
F-F'	0.9166542	0.675	0.2	0.02	0.126	11.1	11.3	1.399	0.124	55.500	5129928.02	0.333	1112.61	0.9441
G-G'	0.5633903	0.717	0.3	0.15	0.225	5	5.15	1.125	0.218	16.667	175452.24	0.481	1206.91	0.8066
H-H'	0.5118286	0.665	0.25	0.11	0.164	9.2	9.5	1.509	0.159	36.800	1707944.56	0.076	797.17	1.0034
I-I'	0.5261514	0.514	0.71	0.04	0.278	12.9	13.5	3.586	0.266	18.169	152953.11	0.311	1370.67	1.8433
J-J'	0.4113766	0.68	0.295	0.01	0.142	24.7	25.35	3.507	0.138	83.729	105392.74	0.576	558.17	2.3850
K-K'	0.3724173	0.54	0.285	0.01	0.118	36.6	37.25	4.319	0.116	128.421	5714575.29	0.409	423.44	2.3322
L-L'	0.2960255	0.564	0.3	0.04	0.122	24.1	24.95	2.940	0.118	80.333	3458613.87	0.240	342.1	1.6583
M-M'	0.2139032	0.645	0.435	0.02	0.142	13.7	13.8	1.945	0.141	31.494	7816808.78	0.420	295.71	1.2548
N-N'	0.1718868	0.94	0.19	0.01	0.104	14.4	15.2	1.498	0.099	75.789	103746.76	0.931	166.08	1.4077
O-O'	0.7166542	0.564	0.16	0.02	0.079	23.2	24	1.833	0.076	145.000	3935103.26	0.523	686.48	1.0337
P-P'	0.181436	0.607	0.25	0.045	0.115	12.5	14.38	1.438	0.100	50.000	6797232.44	0.572	177.87	0.8726
Q-Q'	0.1336899	0.56	0.23	0.02	0.114	50	51.8	5.700	0.110	217.391	6902836.52	0.530	144.27	3.1920
R-R'	0.0381971	0.456	0.23	0.01	0.0854	47.1	48.5	4.022	0.083	204.783	35303283.4	0.042	31.07	1.8342

Table 4.1.3 Channel hydraulic variables measured during post-monsoon, 2017

						POST MONSOON-2017								
Profile	**Slope**	**Surface water velocity (m/sec.)**	**Max. depth (m)**	**Min. depth (m)**	**Mean depth (m)**	**Width (m)**	**Wetted perimeter (m)**	**Cross sec. area (m^2)**	**Hydraullic radius (m)**	**Width-depth ratio**	**Re**	**Fr**	**Available Shear stress**	**Discharge (m3/sec)**
A-A'	1.734228	1.985	0.545	0.11	0.266	7.2	9.3	1.915	0.206	13.211	457916.36	1.23	3502.34	3.801672
B-B'	1.845678	1.452	0.655	0.115	0.311	14.25	16.1	4.432	0.275	21.756	447724.09	0.8314	4982.26	6.434901
C-C'	1.674256	2.156	0.745	0.215	0.345	8.98	10.23	3.098	0.303	12.054	731413.58	1.1721	4972.36	6.6795036
D-D'	1.254376	1.236	0.66	0.15	0.278	14.31	15.74	3.978	0.253	21.682	349939.23	0.7486	3109.05	4.91703048
E-E'	0.753427	0.978	0.695	0.23	0.298	18.45	20.1	5.498	0.274	26.547	299674.57	0.5721	2021.06	5.3771418
F-F'	1.142786	0.456	0.45	0.155	0.211	10.45	11.78	2.205	0.187	23.222	9561207.92	0.317	2464.8	1.0054572
G-G'	0.543768	0.576	0.65	0.15	0.225	8.35	10.12	1.879	0.186	12.846	119785.83	0.3878	989.97	1.08216
H-H'	0.674298	0.678	0.655	0.175	0.316	16.56	18	5.233	0.291	25.282	220800	0.3851	1922.42	3.54794688
I-I'	0.742678	0.475	0.855	0.245	0.397	14.35	15.2	5.697	0.375	16.784	199428.35	0.2407	2729.73	2.70605125
J-J'	0.487429	0.968	0.75	0.21	0.24	22.85	25.34	5.484	0.216	30.467	234671.67	0.631	1034.5	5.308512
K-K'	0.586423	0.687	0.54	0.165	0.278	42.67	45.55	11.862	0.260	79.019	200415.02	0.4161	1497.7	8.14937262
L-L'	0.378644	0.658	0.455	0.155	0.196	37.56	39.87	7.362	0.185	82.549	136099.26	0.4746	685.63	4.84403808
M-M'	0.328976	0.405	0.45	0.215	0.315	25.65	27.89	8.080	0.290	57.000	131431.33	0.2304	934.62	3.27229875
N-N'	0.1986423	1.895	0.55	0.165	0.287	16.36	17.45	4.695	0.269	29.745	571190.14	1.1296	524.16	8.8976314
O-O'	0.1277564	0.895	0.45	0.135	0.198	27.45	28.56	5.435	0.190	61.000	190794.93	0.6423	238.43	4.8644145
P-P'	0.287257	1.975	0.755	0.3	0.287	17.34	19.22	4.977	0.259	22.967	572847.7	1.1773	729.41	9.8287455
Q-Q'	0.1267542	0.945	0.875	0.255	0.387	72.56	74.66	28.081	0.376	82.926	398149.82	0.4851	467.523	26.5362804
R-R'	0.1267865	0.585	0.95	0.165	0.578	86.97	89.25	50.269	0.563	91.547	369096.07	0.2457	700.3	29.4071661

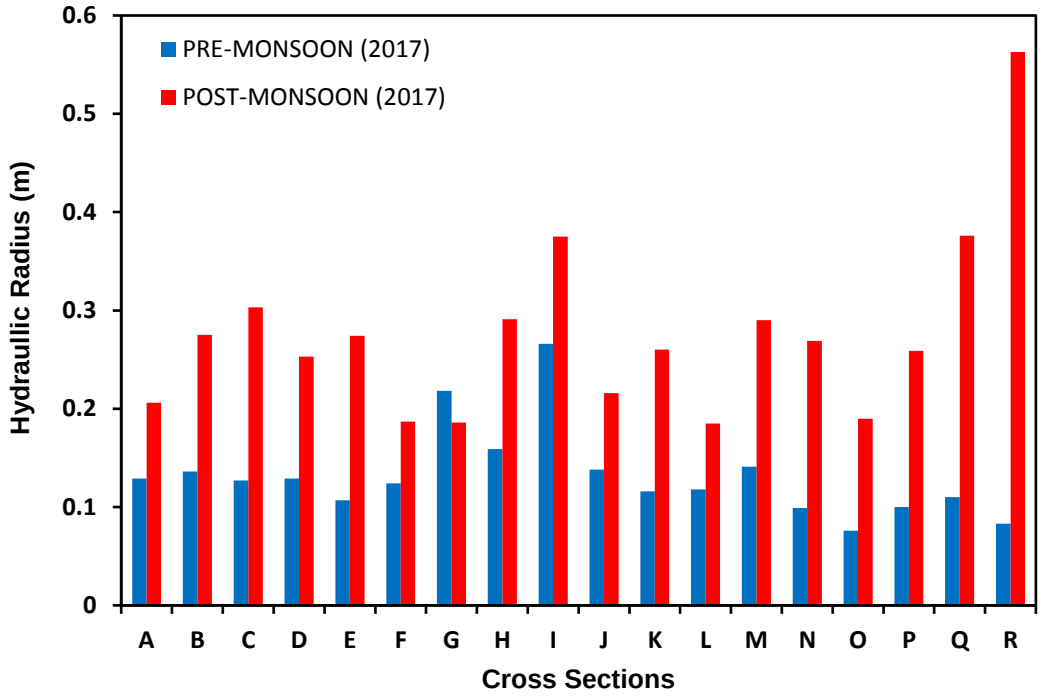

Figure 4.1.5 Hydraulic radius (m) variability at at surveyed cross-sections during pre-monsoon and post-monsoon, 2017.

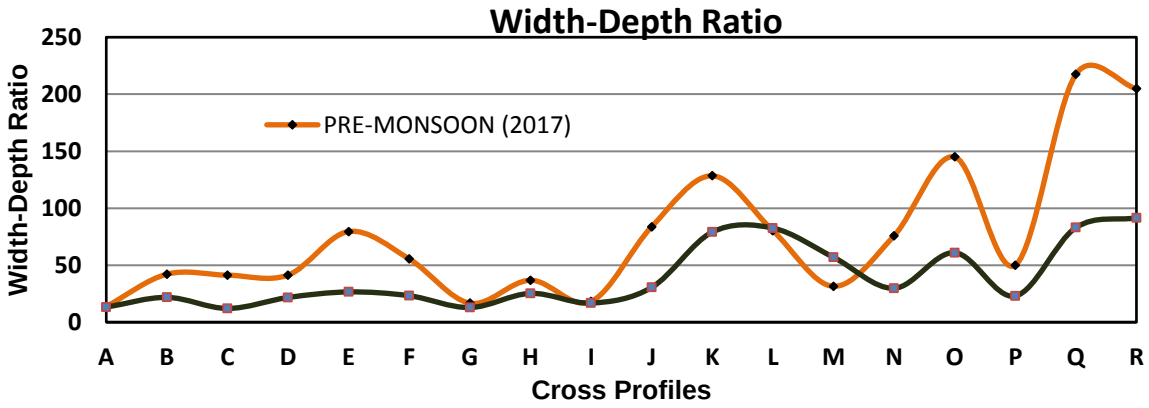

Figure 4.1.6 Width-Depth variability at at surveyed cross-sections during pre-monsoon and post-monsoon, 2017

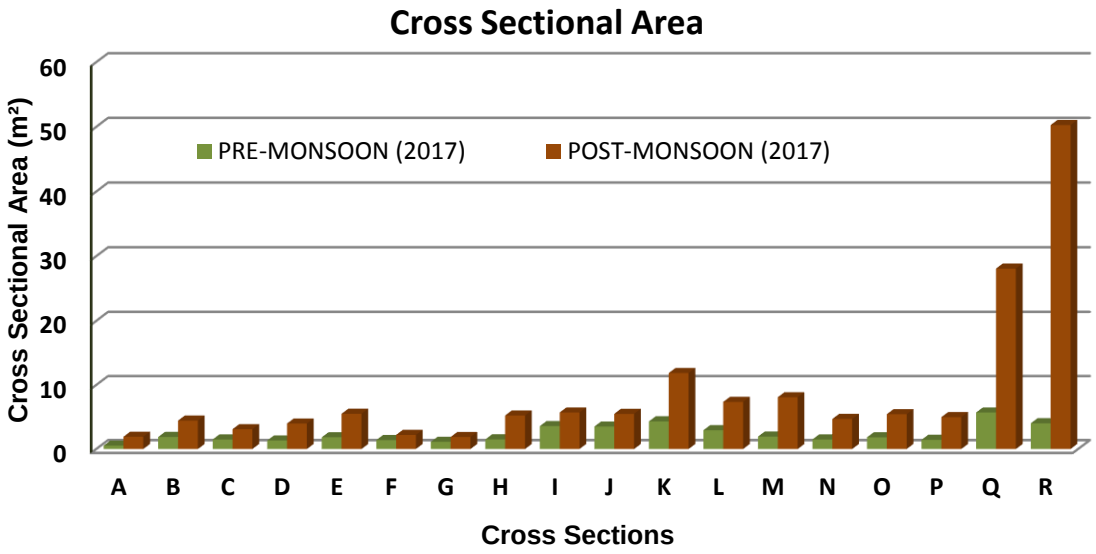

Figure 4.1.7 Cross Sectional Area (m^2) variability at at surveyed cross-sections during pre-monsoon and post-monsoon, 2017.

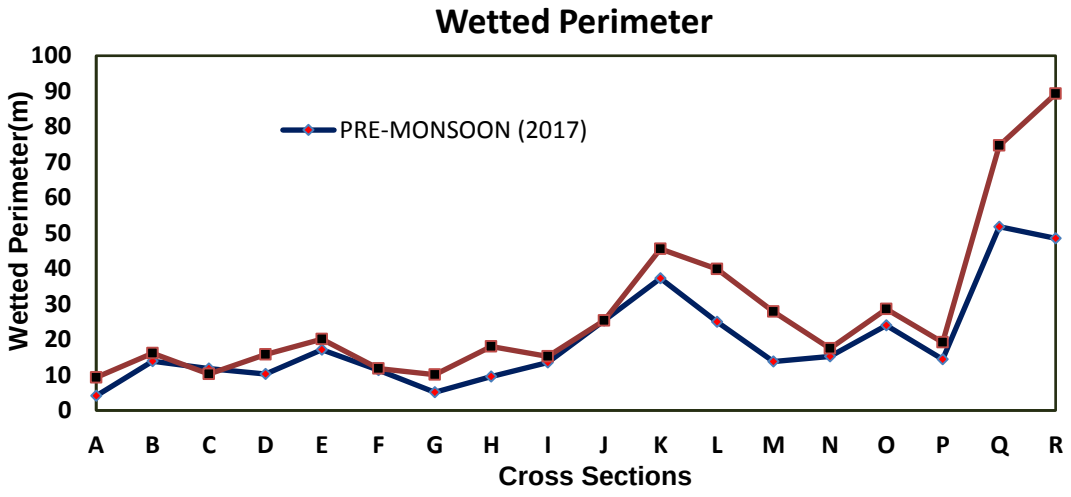

Figure 4.1.8 Wetted Perimeter (m) variability at at surveyed cross-sections during pre-monsoon and post-monsoon,2017.

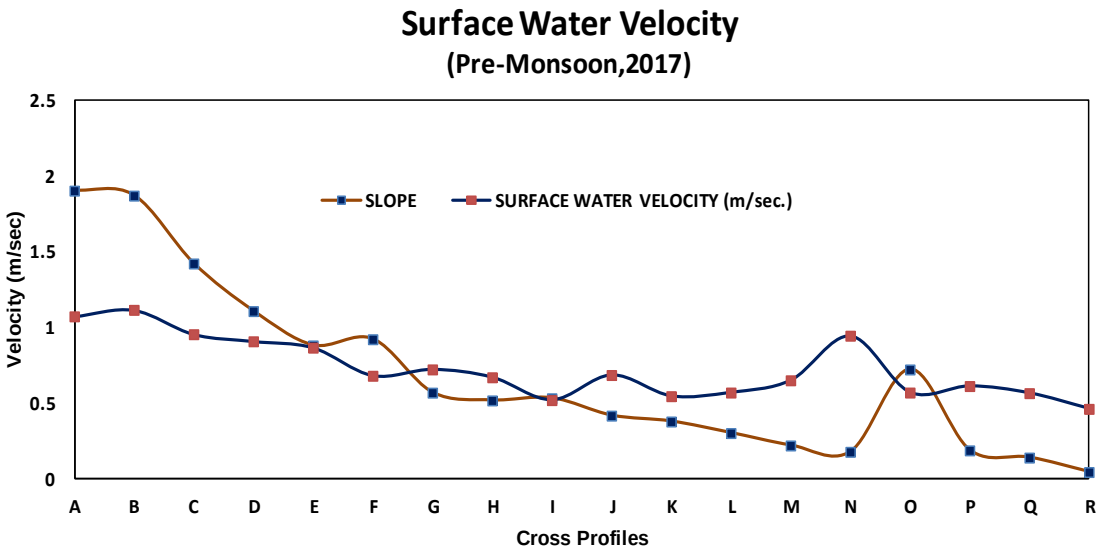

Figure 4.1.9 Surface water velocity (m/sec) variability in relation to slope at surveyed cross-sections during pre-monsoon, 2017.

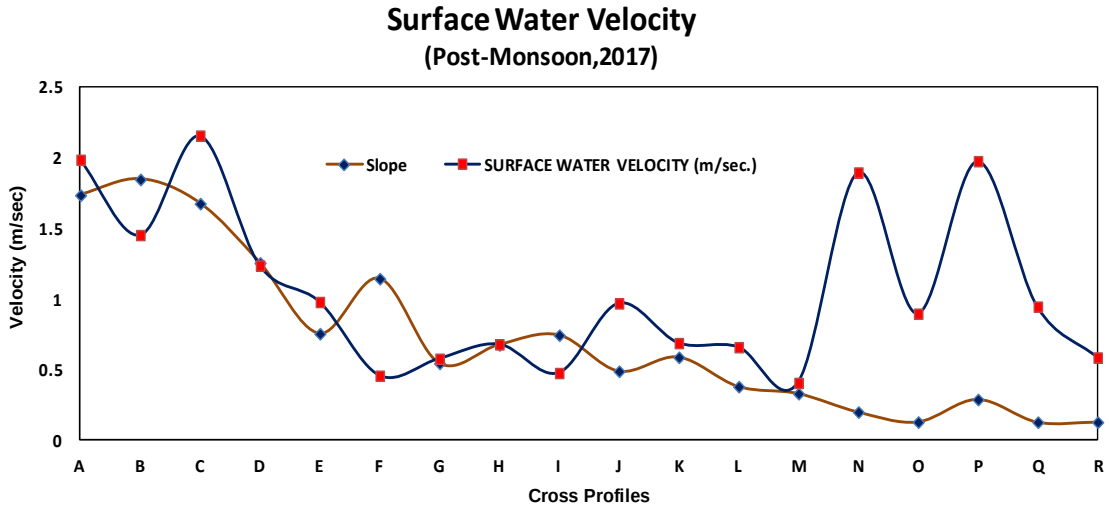

Figure 4.1.10 Surface water velocity (m/sec) variability in relation to slope at surveyed cross-sections during post-monsoon,2017.

Plate-4.1.5-4.1.8 Channel Bed material. (4.1.5) Colluvium bedded channel near headwaters, downstream of Chitong Bridge, Upper Ambiok TG (13.01.2016); (4.1.6) Boulder-bed hilly channel with step-pool morphology, upstream of Mukti bridge,Gorubathan,Darjeeling (08.08.2012);(4.1.7) Gravel stream-bed, 600m upstream of Railway bridge, Odlabari, Jalpaiguri (09.10.2012); (4.1.8) Sand and silt bed channel at Chikenmati near Kranti, Jalpaiguri (15.01.2016).

Plate 4.1.9-4.1.12-(4.1.9) Braided reach of river Chel in the upstream of railway bridge, odlabari; (4.1.10) Near bankfull flow submerging almost all mid channel bars of River Chel during monsoon month, 30.07.2017; (4.1.11) Very turbid water during monsoon flowing near under the railway bridge, odlabari, 10.09.2012. (4.1.12) Winter minimum flow, 01.02.2016.

4.1.5 Steady and Unsteady or Uniform and non-uniform flow of water

In steady flow the depth and velocity do not change in magnitude or direction with time. Unsteady flow occurs when depth and velocity fluctuate in magnitude or direction with time. When the stream depth and velocity is constant with distance along a channel, the flow is uniform (the gravitational and frictional components are in balance). If depth and velocity change with distance along a channel, flow is non-uniform or varied (Morisawa, 1985). The study area is characterized by great temporal and spatial variation of depth and velocity, which indicates the unsteady and non-uniform flow of water (Table-4.1.2 and 4.1.3). Near Putharjhora (cross-section-1) the maximum depths are 0.27

m and 0.55 m during pre-monsoon and post-monsoon respectively, while it is 0.21 m and 0.86 m respectively near Chickenmati (cross-section-19). The maximum and minimum Pre- monsoon depths of 0.9m and 0.16 m are recorded at cross sections 9 and 15 respectively. Whereas cross sections 18 and 6, 13 and 15 have recoded the minimum depth of 0.95 m and 0.45 m respectively (Table-4.1.2). In Post monsoon season all the cross sections exhibit greater depth than pre-monsoon season except cross section 9. The surface velocity of water also shows variability both spatially and seasonally. Maximum surface water velocity in pre-monsoon (1.11m/sec) was recorded at cross section 2 whereas maximum post-monsoon surface water velocity (2.16/sec) was recorded at cross section 3 (Table-4.1.3). Sudden increase of velocity at cross profile 14 and downstream can be attributed to the joining of tributary Kumlai Nadi. Minimum velocity (0.04 m/sec and 0.405m/sec) are measured at cross-section 18 and 13 for pre-monsoon and post-monsoon seasons respectively (Fig-4.1.9 and 4.1.10). Usually, natural stream flow varies to compensate and adjust at bends, contractions and expansions, obstructions etc. Stream flow can change quickly with time or space, such as in a hydraulic jump or hydraulic drop (Morisawa, 1985).

Table 4.1.4-Seasonal variation in maximum water depth and surface water velocity along the study reach.

Cross section	Maximum depth (m)		Maximum surface velocity (m/sec)	
	Pre-Monsoon	Post- Monsoon	Pre- Monsoon	Post- Monsoon
A-A'	0.27	0.545	1.068	1.985
B-B'	0.285	0.655	1.111	1.452
C-C'	0.255	0.745	0.74	2.156
D-D'	0.23	0.66	0.903	1.236
E-E'	0.21	0.695	0.661	0.978
F-F'	0.2	0.45	0.37	0.456
G-G'	0.3	0.65	0.717	0.576
H-H'	0.25	0.655	0.096	0.678
I-I'	0.9	0.855	0.514	0.475
J-J'	0.295	0.75	0.68	0.968
K-K'	0.285	0.54	0.44	0.687
L-L'	0.3	0.455	0.262	0.658
M-M'	0.435	0.45	0.495	0.405
N-N'	0.19	0.55	0.94	1.895
O-O'	0.16	0.45	0.46	0.895
P-P'	0.25	0.755	0.607	1.975
Q-Q'	0.23	0.875	0.56	0.945
R-R'	0.23	0.95	0.038	0.585

Source: Field survey, 2017

4.1.6 Pattern of flow:

An understanding about flow pattern in the piedmont reach of river Chel has been attempted with the help of Reynolds' number. It is a dimensionless number which includes the effects of the flow characteristics, velocity, and depth, and the fluid properties density and viscosity.

$$Re = \rho \frac{VR}{\mu} \quad (6)$$

Where, Re= Reynolds' number

V= Mean velocity of flow,

R= Hydraulic Radius,

ρ = Density of water,

μ = Dynamic viscosity

The ratio μ/ρ is Kinematic viscosity, commonly designated as ν (nu). Using this property,

Re= VR/ν

Reynolds' number has been calculated at all the cross-sections along the piedmont of the Chel River (Table-4.1.5) to identify the pattern of flow. The values of Reynolds Number at all the cross sections during both pre-monsoon and post-monsoon are more than 10000, indicating the turbulent flow pattern in the study area. In turbulent condition the flow is chaotic, being characterized by mixing of water masses with exchange of turbulent energy from one water mass to another. Eddies and other secondary flow patterns are superimposed on the primary downstream flow (Morisawa, 1985). During pre-monsoon season in cross-sections 5, 6, 11, 13, 16, 17 and 18, the flow is more turbulent (values of Reynolds Number are 7954428.25, 5129928.02, 5714575.29, 7816808.78, 6797232.44, 6902836.52, 35303283.41and 6385123.78 respectively), compared to other cross-sections, where the values are > 500000. Whereas during post-monsoon larger Reynolds

number are recorded in cross sections 3, 6, 14 and 16 (with values 731413.58, 9561207.92, 571190.14 and 572847.7 respectively. All other cross sections exhibit lower Reynolds number with values < 500000. The variation of sedimentation rate at different cross-sections is due to the variation of degree of turbulence, because the turbulence helps the river to lift heavier objects off the river bed and transport them downstream (Knighton, 1998). In very few channels water flow smoothly, generally obstacles on the river bed cause swirling vortices to form. In a dominant downstream flow, chaotic swirls develop. Turbulent flow occurs in complex winding channels and in rivers with riffle and pool sequences (Knighton, 1998).

4.1.7 Nature of flow:

The influence of gravity on water flow can be identified by the value of Froude Number. It is another dimensionless parameter frequently used to describe flow conditions. It is an index to the influence of gravity in flow situations where there is a liquid-gas interforce- such as an open channel. The Froude number is usually defined as

Fr = (Inertia force/ Gravity force) $^{1/2}$.

$$Fr = V/\sqrt{Dg} \qquad (7)$$

Where, Fr = Froude number,
V = Mean flow velocity,
D= mean water depth,
g = acceleration due to gravity.

The nature of flow at piedmont of the Chel River is identified by calculating the value of Froude Number at all the cross-sections (Table-4.1.5). During pre-monsoon season all the cross sections experienced Froude Number < 1, which indicates the sub-critical flow of water (Morisawa, 1985). Highest and lowest value is estimated at the cross-section 14 (0.931) and 18 (0.0415) respectively (Table-4.1.5). Whereas during post monsoon season four cross sections (1, 3. 14 and 16) experienced Super critical nature of flow with Froude number 1.23, 1.1721, 1.1296 and 1.1773 respectively. Rest of the cross sections

exhibits Froude number <1, suggesting sub critical nature of flow. Supercritical flows are characterized by the fact that surface waves cannot move upstream and standing waves are generated. Whereas subcritical flows are affected by the downstream disturbances wherein surface waves propagate upstream and no standing waves appears on the water surface. So, flow tends to be critical at cross section 14 and more sub-critical at cross section 18. Larger value of Froude Number (more critical flow) at 14 leads to scouring of river bed compared to shoaling. Higher value of Froude number at 14 is due to increased surface water velocity. Knighton (1998) mentioned that in most of the cases the flow in natural stream is generally sub-critical in nature. Altogether the piedmont reach of the Chel River, the region under study is characterized by subcritical and turbulent pattern of flow (Plate 4.1.13 and 4.1.14).

Table 4.1.5- Seasonal variation of Froude number and Reynolds number along the study reach.

Cross sections	$Re = \rho \frac{VR}{\mu}$		$Fr = \frac{v}{\sqrt{gD}}$	
	Pre-Monsoon	Post- Monsoon	Pre-Monsoon	Post- Monsoon
A-A'	154390.16	457916.36	0.902	1.23
B-B'	169293.25	447724.09	0.8952	0.8314
C-C'	105388.3	731413.58	0.6271	1.1721
D-D'	130616.08	349939.23	0.7705	0.7486
E-E'	7954428.25	299674.57	0.6362	0.5721
F-F'	5129928.02	9561207.92	0.333	0.317
G-G'	175452.24	119785.83	0.4812	0.3878
H-H'	1707944.56	220800	0.0757	0.3851
I-I'	152953.11	199428.35	0.3113	0.2407
J-J'	105392.74	234671.67	0.5763	0.631
K-K'	5714575.29	200415.02	0.409	0.4161
L-L'	3458613.87	136099.26	0.2395	0.4746
M-M'	7816808.78	131431.33	0.4195	0.2304
N-N'	103746.76	571190.14	0.931	1.1296
O-O'	3935103.26	190794.93	0.5227	0.6423
P-P'	6797232.44	572847.7	0.5716	1.1773
Q-Q'	6902836.52	398149.82	0.5297	0.4851
R-R'	35303283.41	369096.07	0.0415	0.2457

Source- Field survey,2017

Plate 4.1.13-4.1.14 Nature of flow. (4.1.13) Super critical flow near to mountain front, wherein there are some standing waves; (4.1.14) Subcritical flow far downstream wherein waves generated by field assistants are moving upstream on the water surface.

4.1.8 Water Discharge

Water discharge controls the width, depth and shape of the channel and velocity of water (Leopold and Maddock, 1953). Adjustment of a channel both at-a-station and downstream is mainly governed by the seasonal fluctuation of the water discharge (Richards, 1973). The measured discharges along the study reach of Chel River display widespread seasonal variability and are seemed to be largely governed by the fluctuation in the amount of rainfall in the whole basin especially in the upper catchments. The field measurements of discharge along the 36 kms long stretch at 18 cross profiles during the pre-monsoon and post-monsoon season reveal great seasonal variability (Table 4.1.2 and 4.1.3). During pre-monsoon the entire study reach exhibits very little amount of discharge availability with all the values recorded below $4m^3$/sec. The lowest (0.57 m^3/sec) and highest discharge (3.19 m^3/sec) corresponds to the first (A-A') and second last (Q-Q') cross profiles respectively (Table 4.1.2). There is significant increase in the recorded discharge values in all the cross profiles during the post-monsoon season. The lowest ($1m^3$/sec) and highest (29.4 m^3/sec) discharge correspond to F-F' and R-R' cross profiles respectively. In general, water discharge is increasing downstream with little fluctuations but its noteworthy that 6^{th} and 7^{th} cross profiles (F-F' and G-G') near Odlabari recorded lowest discharge during both pre and post monsoon season. This result can be attributed to the Bhabar nature of the sub-surface wherein much of the flow disappears under the

thick unsorted Himalayan sediment deposits in the form of base flow and again reappears on the surface much downstream increasing the total discharge in lower reaches. This high fluctuating discharge can be well related with the removal of vegetation in- stream and along stream banks which leads to non-cohesive channel bars and boundaries. These non-cohesive or less cohesive sediments both in-stream and on channel boundaries are continuously worked and reworked by the flowing water leading to multi-thread, shallow, ever-changing braiding pattern of flow.

4.1.9 Channel pattern

Channel pattern is understood through Friend and Sinha's method (1993) wherein the sinuosity index is the ratio between mid-channel length of the reach and channel-belt length of the same reach. Any local disturbance of flow lines between the straight banks will cause distortion of velocity and shear that result in secondary circulation. As the asymmetry increases, flow impinges on the banks and erodes them to form sinuous pattern (Schumm, 1963). The sinuosity index values calculated from Landsat 8, 2017 for the three segments of the study reaches are 1.1, 0.94 and 1.48 between Putharjhora-Odlabari, Odlabari-Nipuchapur T.G. and Nipuchapur T.G to Kranti respectively (Table 4.2.10). The sinuosity index value for the entire reach is 1.17 which implies the channel pattern is slightly braided in nature. Braided pattern is characterized by multiple-channels, flow separation, velocity and energy reduction and thus favors aggradation and consequent channel migration. The river bed gradient is 0.76 and much of the length of river bed and banks are composed of gravels and coarse-grained soil. Only the lower half of the lower reach (reach-c) is composed of fine-grained soils. Generally speaking, as gradient and particle size decreases, there is a corresponding increase in sinuosity (Williams, 1986).

4.1.10 Study on seasonal variation of coarse sediments (>2 mm) size along the study reach.

Since most of the study reach is composed of boulders, gravels and pebbles, only coarse sediments (intermediate axis > 2mm) have been sampled and taken as the

representative of the entire bed sediments. Thus, an investigation on seasonal bedload sediment size variation along the study reach was carried on by using Slide calipers.

Along each cross profile coarse sediments were randomly picked without looking downward whichever touched the toe of the surveyor. This method of sample collection is called step-toe procedure. Then with the help of slide caliper, the intermediate axis of each sediment was measured and recorded (Fig.4.1.11). The entire process was repeated until a desired number of 100 sediment samples per cross profile were achieved. The measured sediment sizes were arranged in a frequency distribution table with a Wentworth scale showing only class limits. The mean sediment size along each cross profile during pre-monsoon and post-monsoon are used further to represent the variation of annual mean coarse sediment size variation along the long profile of the study reach.

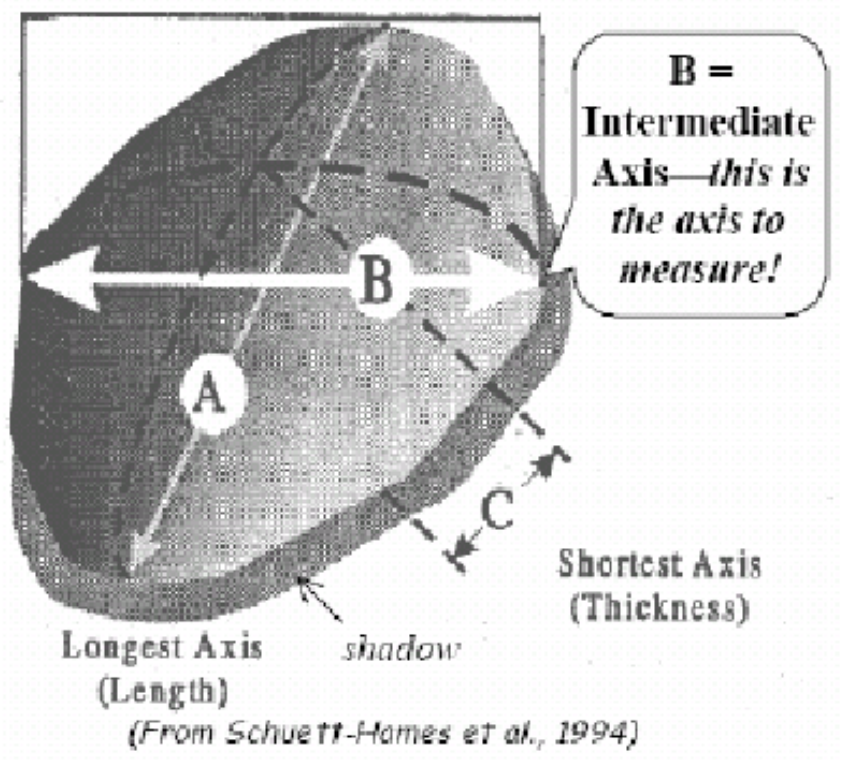

Figure 4.1.11 Different axis of a pebble for determining its size.

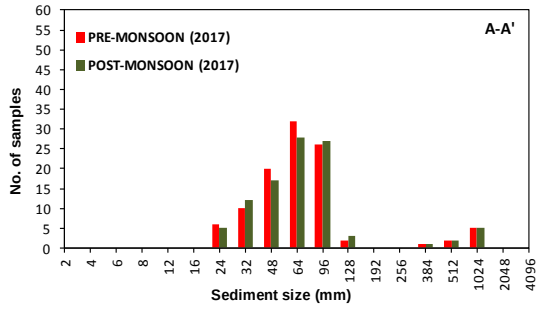
A-A'
PRE-MONSOON (2017)
POST-MONSOON (2017)
No. of samples
Sediment size (mm)

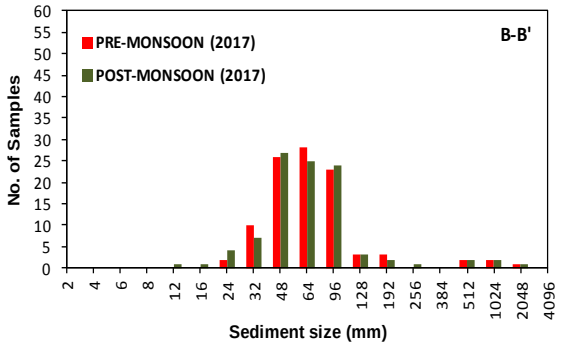
B-B'
PRE-MONSOON (2017)
POST-MONSOON (2017)
No. of Samples
Sediment size (mm)

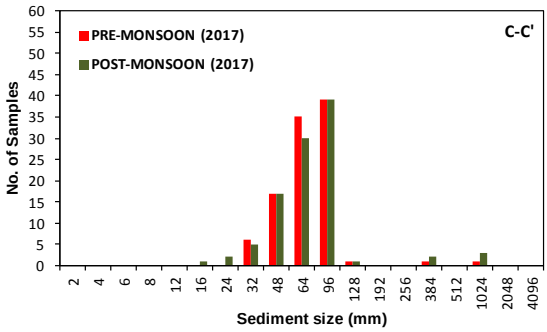
C-C'
PRE-MONSOON (2017)
POST-MONSOON (2017)
No. of Samples
Sediment size (mm)

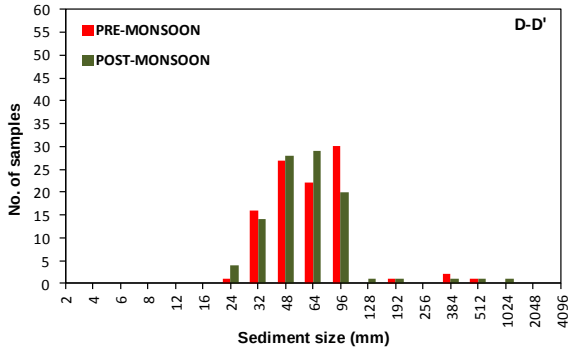
D-D'
PRE-MONSOON
POST-MONSOON
No. of samples
Sediment size (mm)

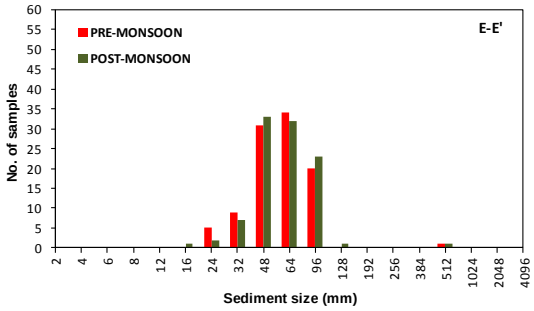
E-E'
PRE-MONSOON
POST-MONSOON
No. of samples
Sediment size (mm)

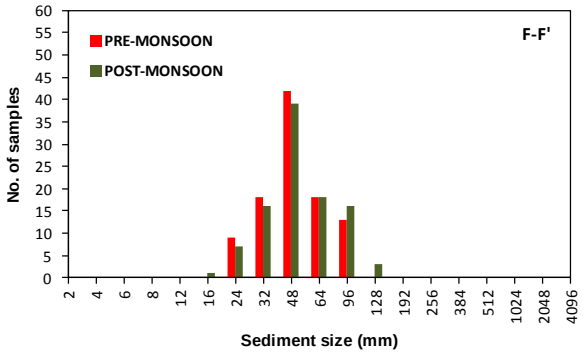
F-F'
PRE-MONSOON
POST-MONSOON
No. of samples
Sediment size (mm)

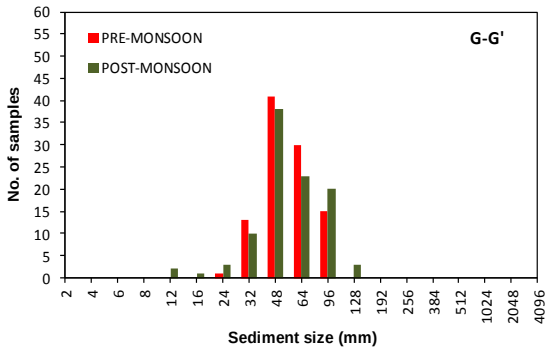
G-G'
PRE-MONSOON
POST-MONSOON
No. of samples
Sediment size (mm)

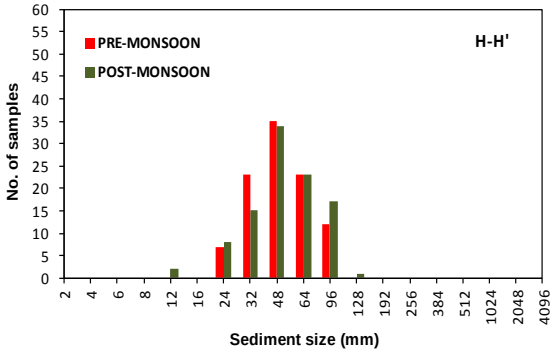
H-H'
PRE-MONSOON
POST-MONSOON
No. of samples
Sediment size (mm)

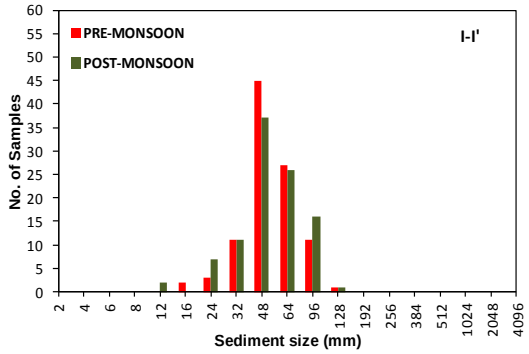
PRE-MONSOON
POST-MONSOON
I-I'
No. of Samples
Sediment size (mm)

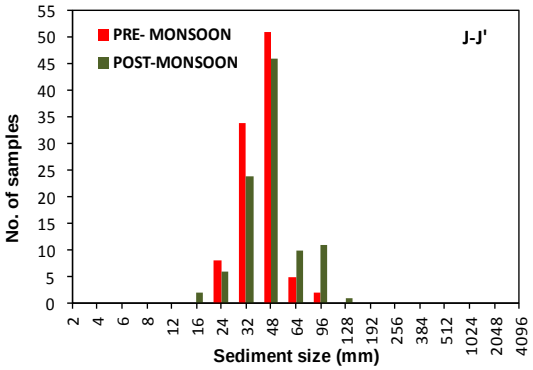
PRE- MONSOON
POST-MONSOON
J-J'
No. of samples
Sediment size (mm)

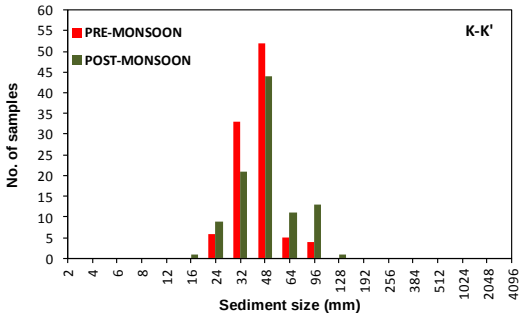
PRE-MONSOON
POST-MONSOON
K-K'
No. of samples
Sediment size (mm)

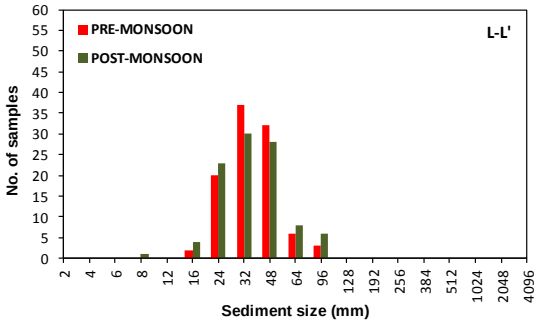
PRE-MONSOON
POST-MONSOON
L-L'
No. of samples
Sediment size (mm)

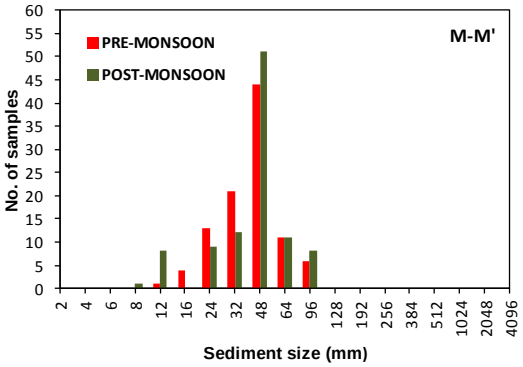
PRE-MONSOON
POST-MONSOON
M-M'
No. of samples
Sediment size (mm)

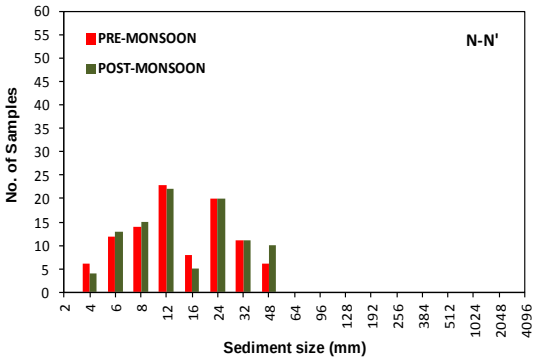
PRE-MONSOON
POST-MONSOON
N-N'
No. of Samples
Sediment size (mm)

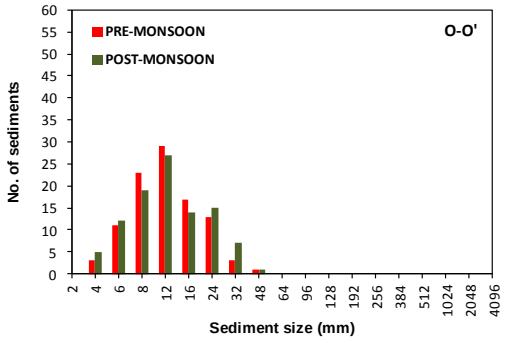
PRE-MONSOON
POST-MONSOON
O-O'
No. of sediments
Sediment size (mm)

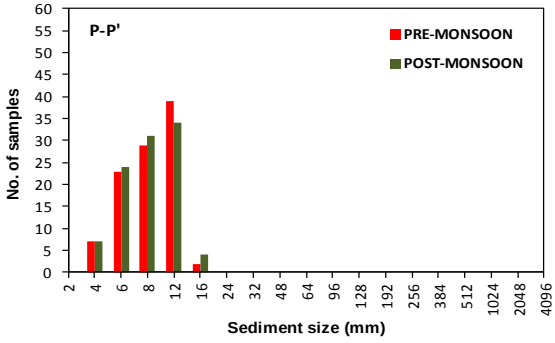
P-P'
PRE-MONSOON
POST-MONSOON
No. of samples
Sediment size (mm)

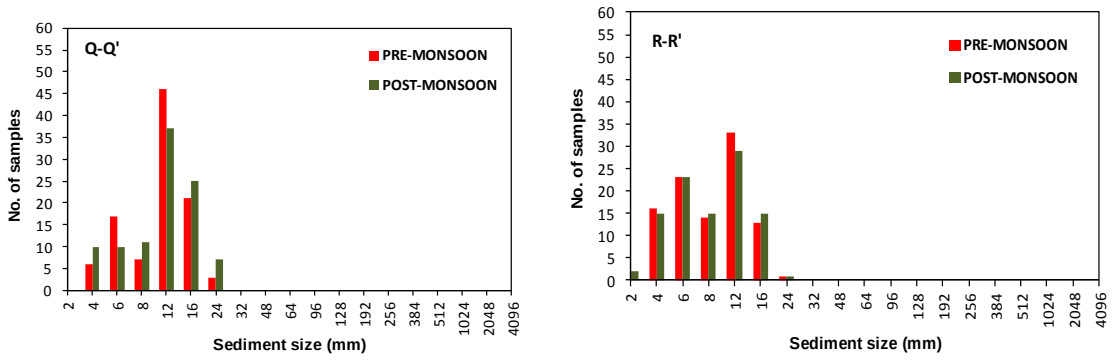

Fig. 4.1.12- Profile-wise distribution of coarse sediments (>2mm) along the study reach of Chel River (Pre- monsoon and Post-monsoon of 2017).

In the study reach of the Chel River, coarse sediments size varies with distance downstream of Putharjhora (near the mountain front) till Kranti (near confluence of Chel and Neora River). A closer observance of Fig.4.1.12 show that vertical bars are gradually shifting from eastern end of x- axis towards the west which reveals the fact that the sediment sizes are gradually decreasing as we move downstream. Dominant sediment sizes range from boulders (512- >4096 mm) in the upper segment (Reach-A), cobbles (96-128mm) and gravels (12-96mm) in the middle segment (Reach-B) and sand and silt (2-12mm) in the lower segment (Reach-C) of the study reach (Fig. 4.1.12). Within the reach-A (from Putharjhora to Odlabari), the sediments are much unsorted in nature and the largest boulders encountered are having intermediate axis of 2.05m. This reach is also hugely dotted with plenty of medium and small size boulders (Plate- 4.1.15 and 4.1.16). The presence of such large sized boulders is the proxy of river's energy to erode and transport sediments to this much distance from the upper catchments and also the intensity of extreme floods resulting in huge debris flow. From Odlabari to Nipuchapur Tea Garden (Reach-B), up to a distance of 26kms, cobbles and gravels having intermediate axis size ranging from 12-128mm are sampled. Only along the cross profiles L-L' and M-M' sediments of size 8mm were sampled in insignificant frequency along each profile. In the lower most reach-C (from Nipuchapur Tea Graden to Kranti), upto a distance of 34 kms, the sediment size decreases significantly due to decreased carrying capacity of river and thus there is generally absence of pebbles and cobbles. The sampled sediments range from 2mm to 48mm in size which falls under the category of small

gravels, sand and silt. Entering this segment, river starts depositing even the finer suspended particles and thus areas of clay deposition have also been observed during the field surveys.

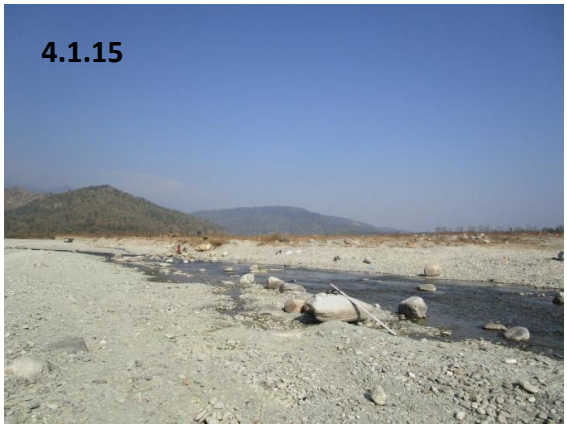

Plate 4.1.15-4.1.16 Numereous large size boulders strewn across at the cross profile A-A' near Putharjhora Tea Garden.

4.1.10.1 Mean sediment size distribution

The mean coarse sediment size analysis shows that it ranges from 7.6mm to 96.8 mm during the pre-monsoon and 7.5mm to 98.44 mm during the post-monsoon season. The sediment size decreases sharply between the distance 4kms and 6kms downstream in the upper segment and between 24 kms and 26kms downstream in the lower segment of the study area (Fig. 4.1.13). The annual mean coarse sediment size of the entire study reach is 42.8mm. The variation of mean coarse sediments in different sites of 2 kms interval during pre-monsoon and post-monsoon from the annual mean shows that the variation is high up to a distance of 20kms downstream (near Mech Busti) and further downstream the variation becomes much lesser. The highest mean coarse sediment size variation from the annual mean sediment size was recorded in cross profile B-B' (4kms downstream) of 8.7mm whereas the least variation of 0.05mm was recorded in cross profile Q-Q' (32kms) downstream. Such variation in mean coarse sediment sizes with distance shows channels annual adjustments with the variation in discharge.

Table 4.1.6- Mean sediment size variability during pre and post monsoon, 2017.

Distance (km)	Pre-monsoon mean sediment size (mm)	Post-monsoon mean sediment size (mm)	Annual mean sediment size (mm)
0	96.8	98.44	97.62
2	89.81	92.13	90.97
4	66.49	83.86	75.18
6	63.55	64.4	63.98
8	54.22	56.12	55.17
10	43.16	46.91	45.04
12	48	49.67	48.84
14	43.2	45.8	44.5
16	46.2	47.35	46.78
18	36.28	41.53	38.91
20	37.22	42.8	40.01
22	33.4	34.13	33.77
24	36.6	38.63	37.62
26	14.6	14.9	14.75
28	11.3	11.99	11.65
30	7.6	7.5	7.55
32	9.8	10.11	9.96
34	8.04	7.91	7.98

Source- Field survey, 2017

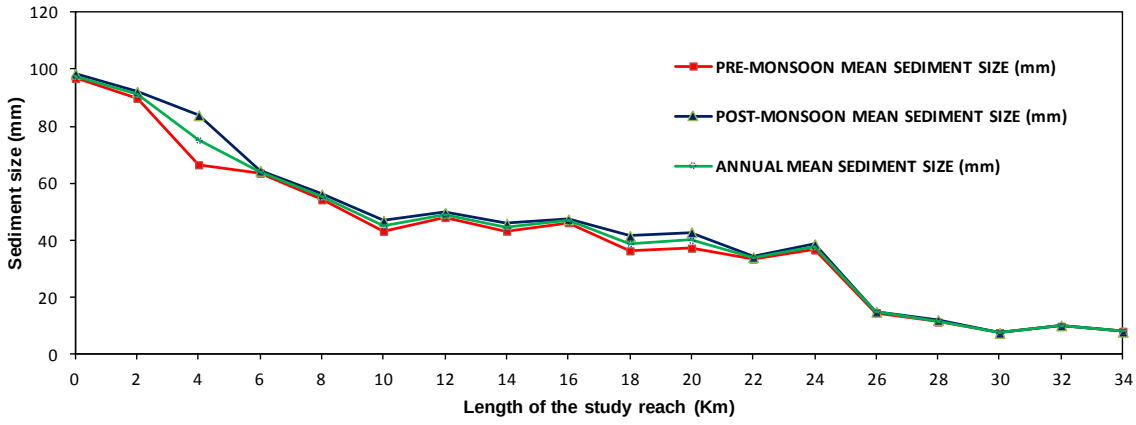

Fig.4.1.13- Mean sediment size distribution along the cross profiles at 2kms interval along the study reach in the year 2017.

4.1.11 Estimation of Discharge and Sediment output

Long term hydrological data is not available for chel River basin. The CWC Chel gauge site at Odlabari records only gauge height, but CWC did not provide the data.

Therefore, much popular and widely used SWAT model has been applied in the present study to understand the role of discharge and sediment load on the channel dynamics of the Chel River. The study found a very higher level of correlation between the water outflow and sediment outflow.

4.1.11.1 Methodology

SWAT 2012 hydrological model was run successfully with Arc GIS 10.1. This model subdivides the DEM into sub-basins and hydrological characteristics of each basin is estimated based on topography, landuse, soil and other factors of the watershed (Olivera et al.,2006). Actually, the basin is sub divided into Hydrological Response Units (HRUs) based on the Landuse, soil types and slope conditions. SWAT model ultimately gives the daily, monthly or annual estimated runoff for long time period.

For the present study DEM, Land use, slope, soil and meteorological data were feed into the SWAT 2012 model. The DEM was projected in WGS 1984 UTM zone 45N and then was used for delineation of watershed and sub-basins. Further flow accumulation, flow direction, stream network was prepared and several flow outlets were selected. Then projected LULC, soil, slope data were given into the model. Meteorological data collected from Global weather data for SWAT (http://global weather.tamu.edu/home/view) relating to daily precipitation, minimum and maximum temperature, relative humidity, solar radiation and wind speed were also fed into the model. The hydrological processes of the sub-basins were estimated by the following water balance equation:

$$SW_t = SW + \Sigma^{t}_{i=1} (R_{it} - Q_I - ET_i - P_i - QR_i) \quad \ldots\ldots\ldots\ldots\ldots\ldots\ldots\ldots\ldots\ldots\ldots\ldots\ldots\ldots\ldots\ldots\ldots\ldots \quad (8)$$

Where, SW defines the soil water content minus the wilting- point water content and R, Q, ET, P, QR are defined as daily precipitation (mm), runoff, evapotranspiration, percolation and ground water flow respectively.

4.1.11.2 Surface runoff estimation

Surface runoff is the water volume which flows over the earth surface according to the slope based on the Hortonian principles. Actually SWAT 2012 model simulates surface

runoff based on the landuse, soil,antecedent soil moisture condition and meteorological data as inputs (Arnold et al.,1998) by using Soil Conservation Service (SCS) curve number method (USDA, Soil conservation Service,1972). The equation of the runoff estimation is the following:

$$Q_{surf}=(R_{day}-I_a)^2/(R_{day}-I_a+S)\ldots\ldots(9)$$

Where Q_{surf} is the accumulated runoff of rainfall excess (mm of H_2O) in m^3/s, R_{day} defines rainfall depth on the day (mm of H_2O),I_a is initial abstractions which comprises surface storage interception and infiltration prior to runogg and S denotes retension factor (mm of H_2O).

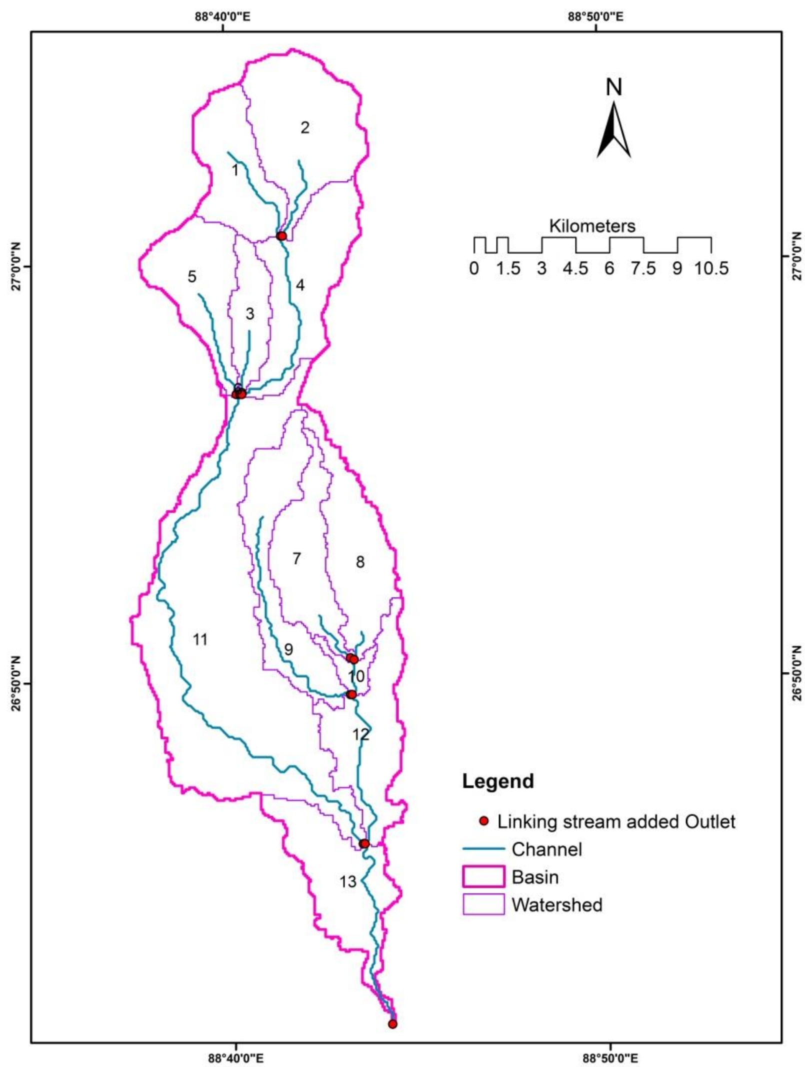

Figure.4.1.14 Generation of Sub-Basins and outlet poins in SWAT 2012.

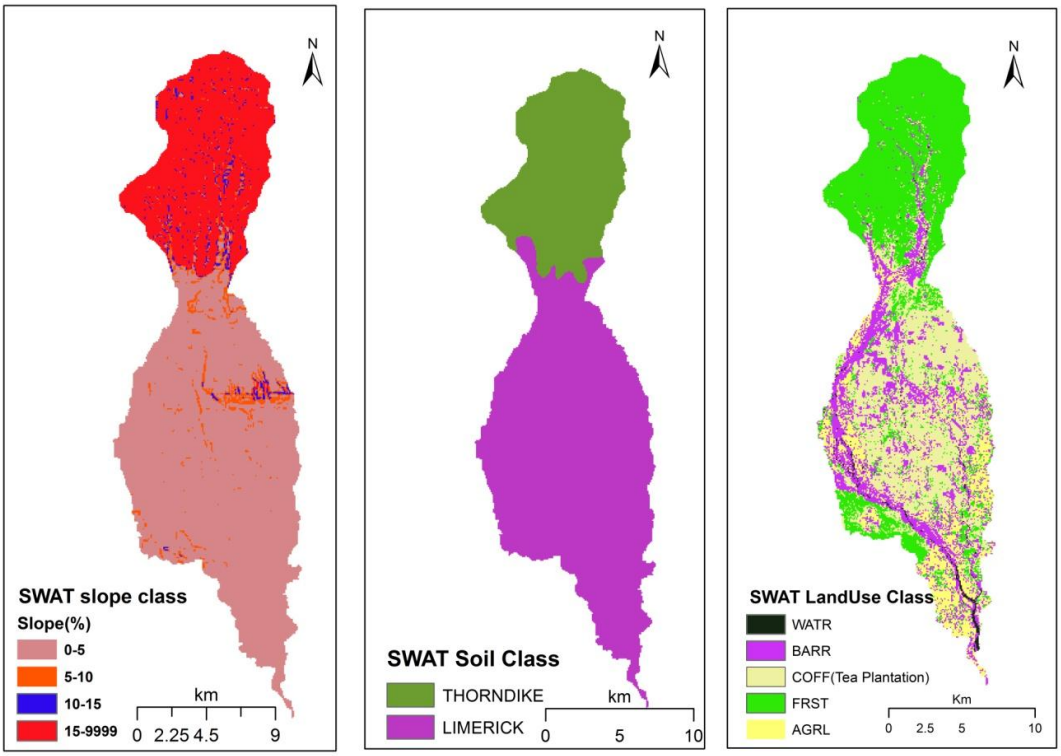

Figure 4.1.15 SWAT 2012 reclassified slope map, Soil map and Landuse map.

Table 4.1.7 Sub-Basin wise mean water and sediment outflow

SUB-BASIN	SEDIMENT (In tons)			WATER (In cumec)	
	Mean sediment in	Mean sediment out	Mean in channel sedimentation	Mean Flow in	Mean Flow out
1	1075278.42	1075278.42	0	34.69	34.69
2	1855337.58	1855337.58	0	53.18	53.17
3	746862.61	746862.61	0	17.99	17.99
4	5880635.11	2120408.33	4001407.68	134.84	134.83
5	3206609.88	3603233.31	0	35.09	35.09
6	8398.99	8064.46	0	0.06	0.06
7	2431171.6	2429797.49	0	33.24	33.23
8	3490900.23	3490900.23	0	38.93	38.94
9	3364123.2	3363940.23	0	35.81	35.81
10	6213519.83	1131154.08	5232331.46	76.61	76.60
11	18971609.43	3667370.68	14309341.71	333.56	333.51
12	6255183.11	2150372.42	4291309.17	146.84	146.83
13	8867001.17	7583175.56	1394103.89	516.22	516.19

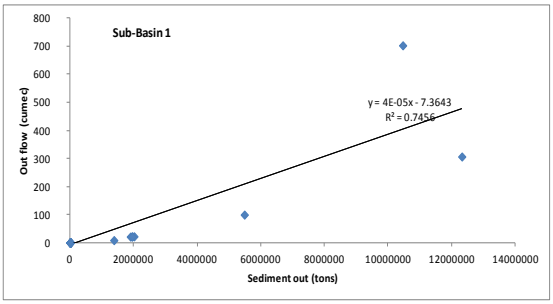
Sub-Basin 1
y = 4E-05x - 7.3643
R² = 0.7456
Out flow (cumec)
Sediment out (tons)

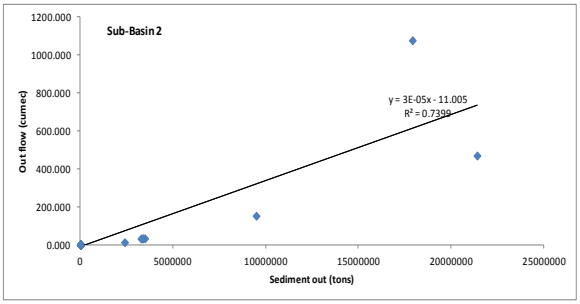
Sub-Basin 2
y = 3E-05x - 11.005
R² = 0.7399
Out flow (cumec)
Sediment out (tons)

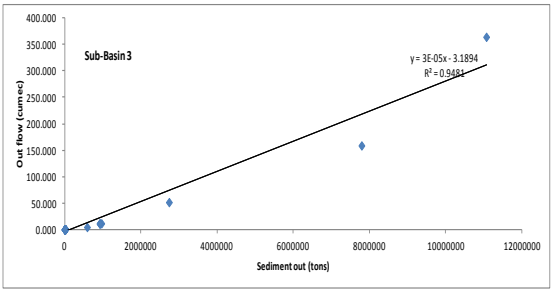
Sub-Basin 3
y = 3E-05x - 3.1894
R² = 0.9481
Out flow (cumec)
Sediment out (tons)

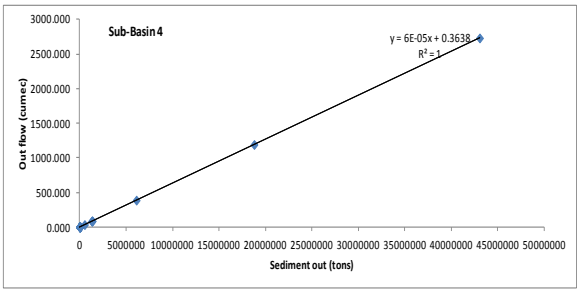
Sub-Basin 4
y = 6E-05x + 0.3638
R² = 1
Out flow (cumec)
Sediment out (tons)

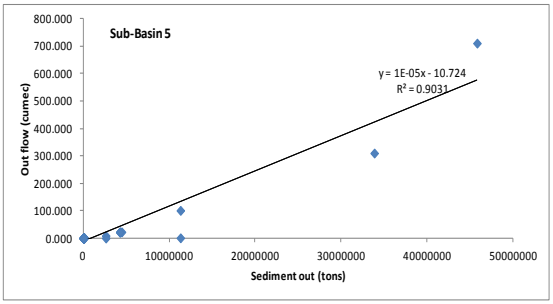
Sub-Basin 5
y = 1E-05x - 10.724
R² = 0.9031
Out flow (cumec)
Sediment out (tons)

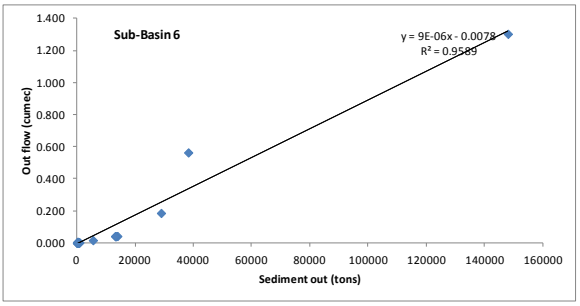
Sub-Basin 6
y = 9E-06x - 0.0078
R² = 0.9589
Out flow (cumec)
Sediment out (tons)

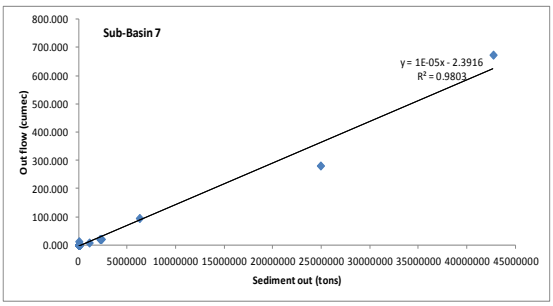
Sub-Basin 7
y = 1E-05x - 2.3916
R² = 0.9803
Out flow (cumec)
Sediment out (tons)

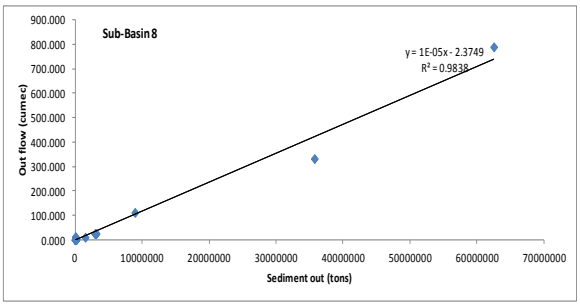
Sub-Basin 8
y = 1E-05x - 2.3749
R² = 0.9838
Out flow (cumec)
Sediment out (tons)

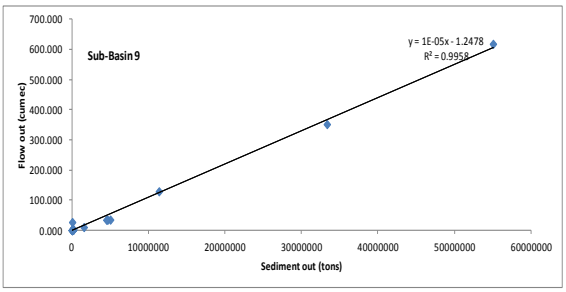
Sub-Basin 9
y = 1E-05x - 1.2478
R² = 0.9958
Flow out (cumec)
Sediment out (tons)

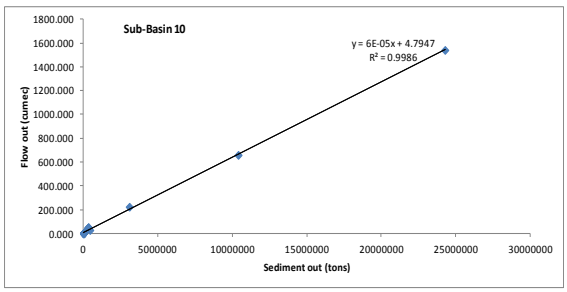
Sub-Basin 10
y = 6E-05x + 4.7947
R² = 0.9986
Flow out (cumec)
Sediment out (tons)

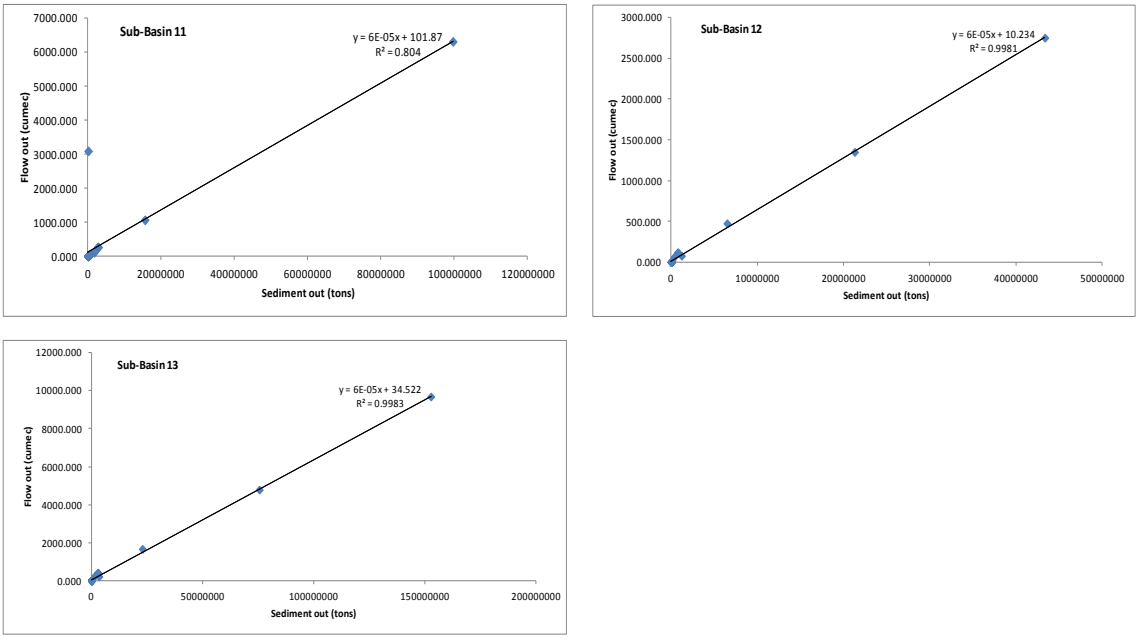

Figure 4.1.16 Correlation between sub-basin wise Sediment out and water outflow

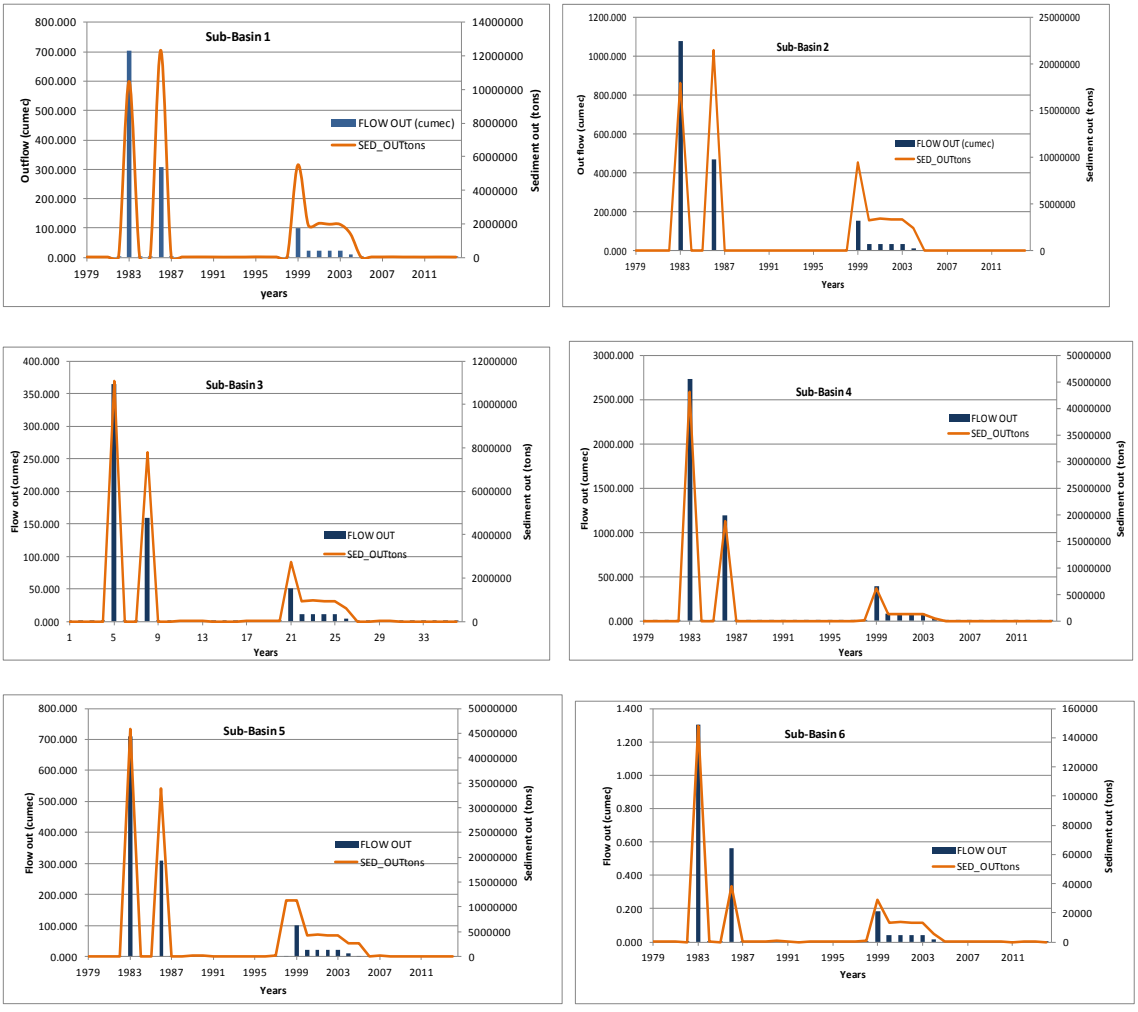

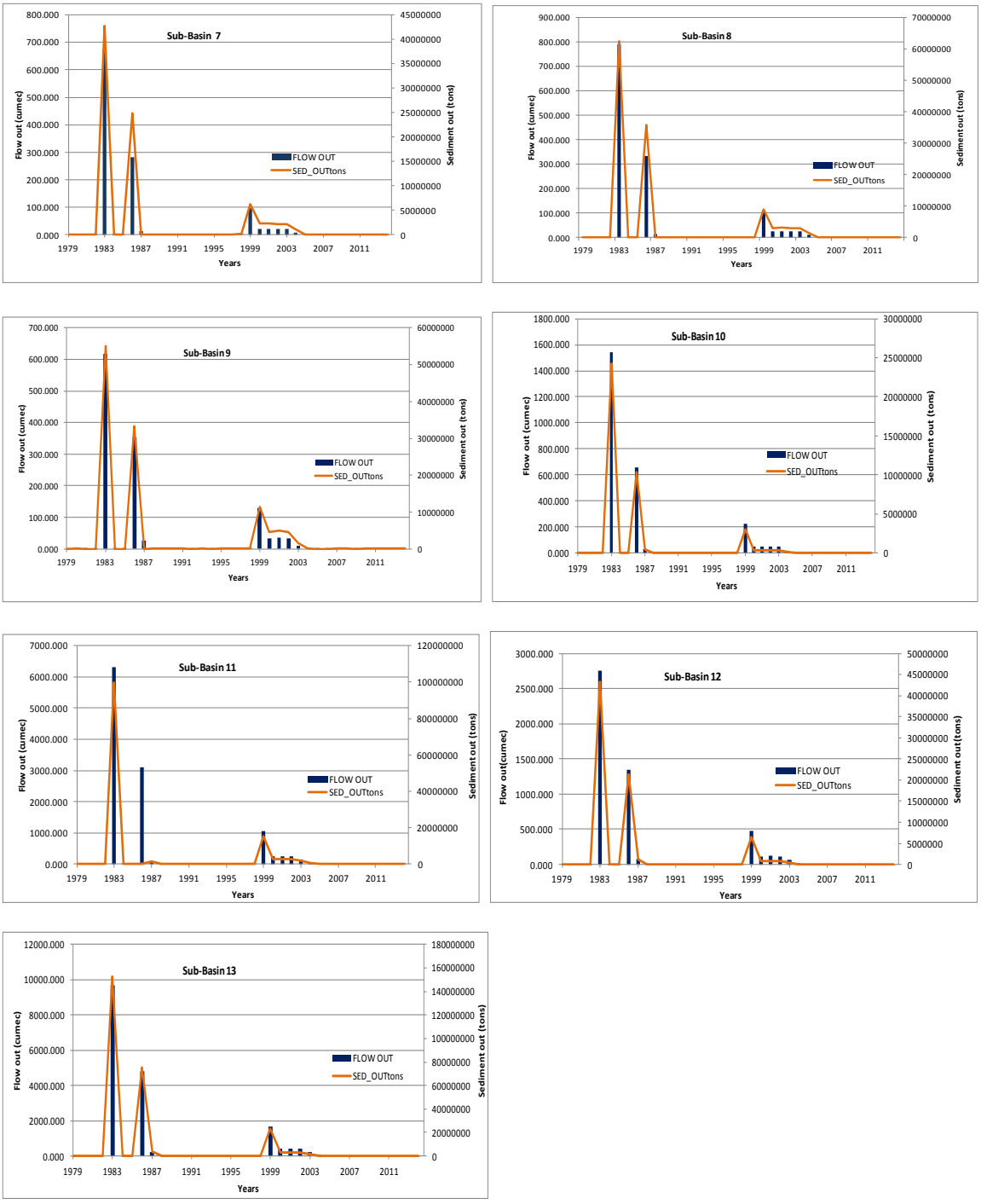

Figure 4.1.17 Sub-Basin wise annual water out and Sediment out.

The Chel basin was divided into 13 sub-basins. The study finds a strong correlation between flow out and sediment out (Fig.4.1.16). The spatial analysis shows that in all the basins the values of water in and water out are almost equivalent whereas in

channel sediment deposition is absent within the upper basins (basin 1,2, and 3) except basin 4 (Table 4.1.7). There is significant mean in-channel sediment in basins 10,11,12,13 and 4. Basin 4 though lies at the apex of the piedmont surface displays good amount out sedimentation deposition as main channel flows through it and thus this reach experience huge amount of sediment deposition consisting of very large boulders. Basins 10,11,12,13 are located in the piedmont or the alluvial reach of the basin which is in conformity with results of bank erosion and accretion in 4.4 section of the thesis. The temporal analysis show generation of water flow out (Discharge) peaks mainly twice during the whole assessment period. A major peak is observed during 1982-1987 and another secondary peak was observed during 1998-2005 (Fig. 4.1.17). Since sediment outflow is strongly correlated with discharge, the sediment outflow curve also displays major peaks during these two time periods. These two peaks resemble high energy catastrophic events which caused maximum discharge and consequent maximum sediment out flow. During rest of the time of entire assessment period, the channel out flow was minimum and thus is the sediment outflow. The peaks seem to be responsible for computation of higher rates of erosion and accretion in the Putharjhora-Kranti reaches of the Chel River (Table 4.4.1 and 4.4.2). In the multi-temporal assessment of erosion and accretion rates, it was found that both erosion and accretion rates were quite higher during late 1980s to early 2000s (details in 4.4 section). Since 1970s the accretion rates are higher than the erosion rate in the reach from Putharjora to Kranti. This is in conformity with the results derived from SWAT analysis wherein lower sub-basins display higher rates of in-channel sedimentation (Table 4.1.7).

Major Findings:

- The entire cross profiles are asymmetric in nature. The profiles are much changeable with several peaks and lows suggesting a number of channels filled with water and are separated by sand bars of different heights. Thus, they display braided pattern of flow for much of the study reach.
- The sinuosity index (SI) value of 1.13 (computed from Landsat 8 OLI&TIRS, 01.12.2017) also suggests that the studied reach of Chel River is slightly braided in nature.

- The mid-channel bars are mostly devoid of vegetation, and are usually composed of coarse bed materials.
- Flow depths are mostly less, usually at the most a few meters during pre and post -monsoon season.
- Much of the length of the study reach, channel banks are composed of coarse material and lacks vegetation; therefore, lack of cohesion of channel banks is observable.
- During the monsoon months when the flow depth or discharge increases, the amount of shear stress exerted on the banks usually is greater due to asymmetric nature of cross profiles, becomes sufficient to entrain bank materials, and thus instead of increase in depth the channel width increases locally.
- This means that when the flow becomes strong and shears enough to transport sediment; it begins the channel to widen itself. Thus, as with majority of the braided rivers world over, Chel River too depicts classic example of greater amount of aggradation than the transport and clearance of sediments downstream.
- Thus, Chel River always maintains flow depths to just greater than threshold depths.
- The study area is characterized by great temporal and spatial variation of depth and velocity, which indicates the unsteady and non-uniform flow of water.
- The values of Reynolds Number at all the cross sections during both pre-monsoon and post-monsoon are more than 10000, indicating the turbulent flow pattern in the study area.
- Pre-monsoon season display sub-critical flow of water as all the cross sections measures Froude number <1. Whereas during post monsoon season cross sections 1,3,14 & 16 experienced Super critical flow with Froude number 1.23,1.17,1.13 and 1.18 respectively. Rest of the cross sections exhibits Fr<1. Thus, altogether it can be said that the Chel River display sub-critical nature of flow.

- Surface water velocity fluctuates along the channel in both pre and post monsoon depending on distribution of depth, shape, channel widening and contraction, slope of river bed, presence of mid-channel bars and pool-riffle sequence,etc. During pre-monsoon the highest surface water velocity is measured at cross profile B-B' (1.11 m/sec) and the lowest velocity was measured at cross profile R-R' (0.46 m/sec). Surface water velocity during post monsoon was recorded highest at cross profile C-C' (2.16 m/sec.) and lowest at cross profile M-M' (0.41m/sec). In general, the velocity decreases downstream but a major spike in surface velocity is observed near cross section N-N' immediately below the confluence of Kumlai River with Chel near Rajadanga, due to increase in amount of discharge, and associated reduction in bed friction.
- Highly fluctuating discharge of Chel River can be well related with the lack of vegetation in- stream and along stream banks which leads to non-cohesive channel bars and boundaries. These non-cohesive or less cohesive sediments both in-stream and on channel boundaries are continuously worked and reworked by the flowing water, leading to multi-thread, shallow, ever changing braiding pattern of flow.
- SWAT 2012 was run for the estimation of flow out and sediment out of the Chel river basin. The study found a strong correlation between the flow out and sediment out from all the sub-basins. Major peaks in flow out and sediment out were observed during 1980s and another 1999-2000.

Conclusion

The analysis done in the present sub-chapter reveals the fact that the study reach of the Chel River is characterized by shallow multiple channels with asymmetric cross sections. There is great spatial and seasonal variability in velocity, discharge and sediment output. The flow is turbulent, non-uniform and overall sub-critical in nature. Altogether the study reach display almost all the characteristics of a braided channel pattern.

4.2 Channel Dynamics

Introduction

Rivers are highly sensitive to environmental conditions (Eaton et al.,2010; Rozo et al.,2014), and especially alluvial channels are inherently dynamic in nature, responding to the variations in water and sediment inputs (Midha and Mathur,2014). Alluvial rivers can respond and readjust at a range of rates to the variations caused by water and sediment inputs, active tectonics and human activities at a range of spatial and temporal scales (Sinha and Ghosh, 2012; Heitmuller, 2014). Natural or anthropogenic input alterations into the river systems results in changes in the planform/channel pattern, sinuosity, and braiding Index (Knighton, 1984). Any changes, whether natural or anthropogenic, can initiate a departure from a state of dynamic equilibrium (Winterbottom, 2000; Petts and Gurnell, 2005). This may in turn, result in channel instability causing changes in channel form and pattern (Yang *et al.,* 1999; Surian and Rinaldi, 2003; Wellmeyer *et al.,* 2005; Kummu *et al.,* 2008; Yao *et al.,* 2011; Gupta *et al.,* 2013; Midha and Mathur, 2014).

Channel dynamics represent an integral component in the evolution of vast alluvial floodplain as well as a disturbance regime vital for floodplain patterns and maintenance of high level of biodiversity (Midha and Mathur, 2014). Channel migration with bank erosion, accretion, and down cutting is a natural phenomenon for an alluvial river. However, with the growth of human population world over the impact is evident. Humans are emerging as rather dominating factor than the natural ones. Developmental activities like reservoir construction, restricting the lateral movement of river through embankments, sand and boulder mining, land use alterations and infrastructure construction along the river banks have altered the natural geomorphological dynamics of river (Gregory and Park,1974; Knighton,1989; Kondolf, 1997; Surian,1999; Surian and Rinaldi, 2003; Batalla *et al.,* 2004; Vanacker *et al.,* 2005; Wellmeyer *et al.,* 2005). Channel instability cause damages to riverine infrastructure and also alteration of aquatic and riparian ecosystems. Thus, it poses challenges for engineers, scientists, and managers on how to best accommodate societal needs with the structure and processes of nature. Understanding the planform dynamics of river channels has important implications for

maintaining biodiversity (Naiman *et al.,* 1993; Hughes, 1997; Ward *et al.,* 1999) and minimizing flood damage too (Holburt, 1984). Investigations of historical channel change provide insight into how stream channels respond to flood events. With this information, land and resource managers are able to make decisions that minimize social costs (*e.g.*, flood damage to property) and maximize the ecological benefits of flooding (*e.g.*, rehabilitating riparian vegetation and deterring the proliferation of exotic species) (Tiegs and Pohl, 2005). Driven by these objectives channel planform dynamics has been studied world over. Ollero (2010) assessed the channel dynamics and consequent floodplains changes in the middle Ebro River, Spain over 80 years and proposed feasible floodplain management solutions. Similarly, Tiegs and Pohl (2005) studied the response of the Colorado River's planform to the fluctuations in hydrology during the period 1976-2000 and thereby assisted land managers in figuring out an appropriate flow regime for proposed rehabilitation of native riparian vegetation. Within our country, Midha and Mathur (2014) have assessed the planform dynamics along a 6o kms reach of Sharda River during 1977 and 2001 in the Terai region of Northern India and established that the altered dynamics is threatening the future of critical wildlife habitats in Kishanpur Wildlife Sanctuary and North Kheri Forest Division in the state of Uttar Pradesh. Thus, an improved understanding of river channel change processes is imperative for improving river engineering and environmental management as well.

The Chel basin is a part of the region popularly known as 'Dooars' which is characterized by channel migration, flooding and avulsion. It falls in the zone of transition between the dissected upper Himalayan hill surface and the lower gently rolling Teesta- Brahmaputra plains, and is popular for notorious incidents of channel avulsion and river capture activities (Chakraborty and Mukhopadhyay, 2014). Because of its straddle like situation with two distinct physiographic units, Chel basin has varied geomorphologic problems. The hilly terrain in the north above the elevation 350m experience rapid overland flow, erosion and landslides whereas its piedmont in the intermediate and alluvial plain in the south is observing large scale sediment deposition, rise in valley floor and consequent shifting of channels (Lama and Maiti, 2019).

In the present sub-chapter, an attempt to reconstruct the channel planform changes of the river Chel has been done over the period between 1955-2017 using Topographical sheets, multi- temporal Landsat images and supplemented by field work. Further geomorphological interpretation of dynamism revealed and documented has been provided. Channel dynamics has been attempted to understand through changes in channel morphology, centreline migration, bankline migration, channel width and length variation, active channel area variation, sinousity index variation, braiding index variation and braid-channel ratio variation.

4.2.1 Study Reach

Chel lies to the left of river Tista after Lish and Gish and joins Neora to become Dharala Nadi at 88° 44' 13"E, 26° 41' 45.6"N which ultimately merges with mighty Tista about 13kms downstream. The study area extends between 26° 41' 30" and 27° 5'15" north latitudes and longitudes 88° 37'00" and 88° 45' 15" east.

The study reach for the present chapter extends from near the confluence point of Manzing and Sukha Khola with Chel River near Putharjhora Tea Garden, near the mountain front below Gorubathan to confluence Point of Chel River with Neora River (Fig. 4.2.1). The straight valley length of the reach is 20.93 kms. But for the ease of description and understanding, the study reach was divided into three smaller reaches from north to south:

1. Reach-A (Putharjhora Tea Garden to Odlabari rail-road bridge)
2. Reach-B (Odlabari rail-road bridge to Nipuchapur Tea Garden)
3. Reach-C (Nipuchapur Tea Garden to Kranti)

The divisions of the reaches noted above were based on hard points located along the river. The first hard point was the Odlabari rail-road bridge and the second hard point was near Nipuchapur Tea Garden where channel migration during the entire assessment period of 62 years was observed to be negligible.

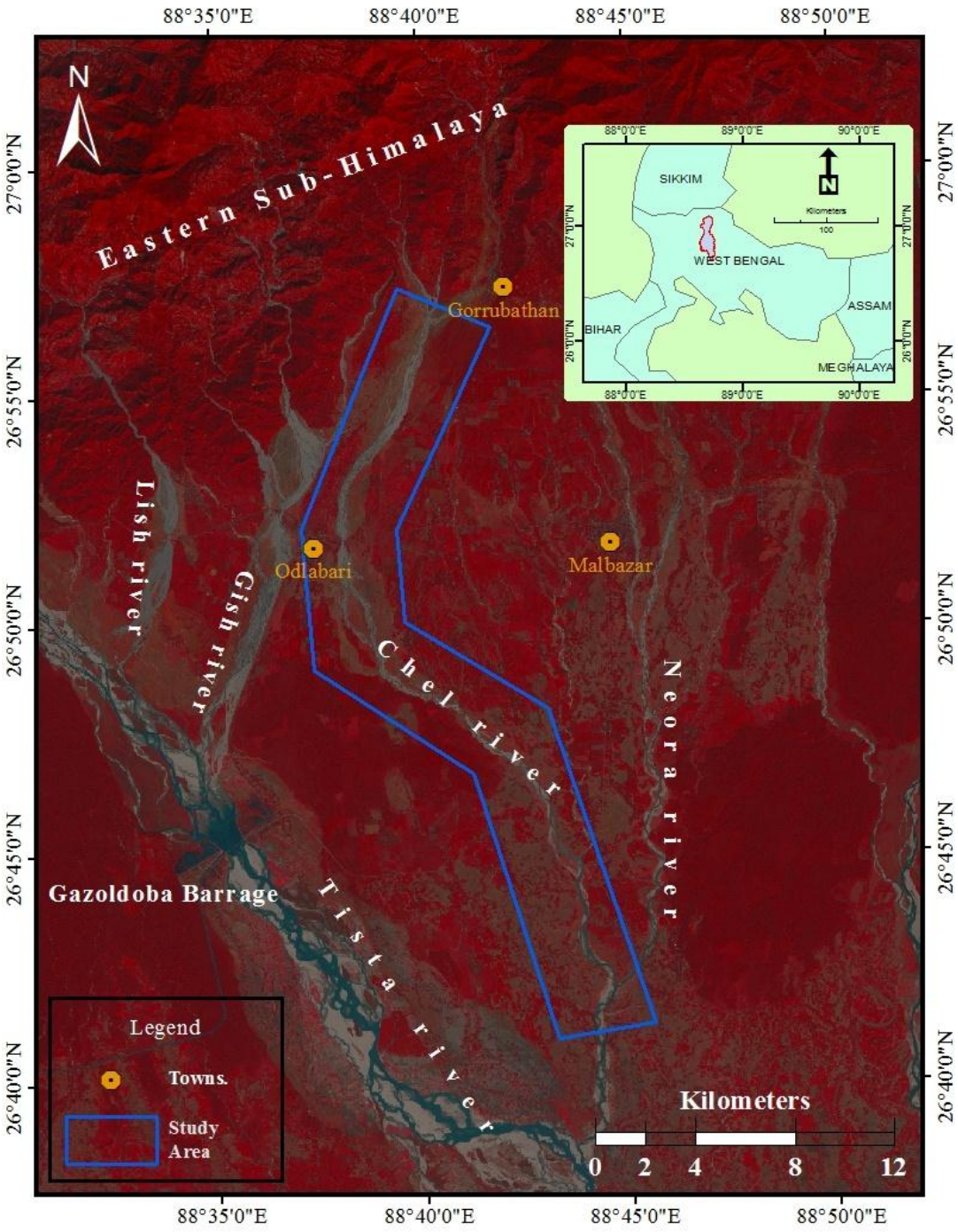

Figure 4.2.1 Pan Sharpened Landsat 8 OLI/ TIRS image (1 December 2017, Path and Row- 139/41) showing the study section of river Chel (Map of part North- East India showing location of Chel river basin in the inset).

Note: The image is a standard false color composite where the red, green and blue band has been assigned Green, Red and Near Infrared colors, respectively.

4.2.2 Data and Methodology

Different methods applied for the fulfillment of objectives are discussed below**.**

4.2.2.1 Data and image processing

This study uses topographical maps and multi temporal Landsat data to quantify and analyze the dynamics of River Chel from 1955 to 2017. A single Landsat scene (Path/ Row: 139/41; 149/41 for 1976 image) covers the entire study area. Similarly, one US AMS Series –U502 topographical map too covers the entire study area. Whereas two sheets of Survey of India topographical maps (78B/9 & 78B/10) topographical maps cover the study area. Therefore, six Landsat scenes (1976, 1987, 1994, 2005, 2010, and 2017) were collected from the USGS site (http://earthexplorer.usgs.gov/). One 1: 250,000 scale U.S. Army corps of Engineers NG 45-8, Series –U502 topographical map (1955) was acquired from the University of Texas site (https://legacy.lib.utexas.edu/maps/india.html) and two 1:50,000 scale topographical maps(Map no.- 78 B/9 and 78B/10) surveyed during 1969-71 were obtained from the Survey of India (SOI).Therefore the study will confine with six epochs(1955-1970,1970-1976, 1976-1987,1987-1994,1994-2005,2005-2010, and 2010-2017). There exists a large data gap from 1955 until 1970, from 1976 to 1987 and from 1994 until 2005. Variation in the length of epochs is due to availability of topographical maps and cloud-free Landsat scenes. All the Landsat scenes were downloaded from the USGS through their data visualization tool GloVis. (Table 4.2.1). All the Landsat images were acquired for months of October to December as during this time of the year generally the region is cloud free being dry season and the discharge is sufficient to fill the main channel normal (non-flood water level of the river) and at the same time relatively constant from year to year (Fig. 4.2.2).

ArcGIS (version 10.1; ESRI,Redlands,CA) software package has been used for preparation of GIS database relating to historical channel position and movement throughout the entire study period of 62 years. All the images were processed through ERDAS imagine (v. 9.0) software and then were georeferenced based on Universal Transverse Mercator (UTM) projection system (Northern hemisphere 45 zone and world geodetic system (WGS) 84) manually using GCPs collected during GPS survey. All the

GCPs representing permanent features like, road intersections, corners of large buildings, bridges etc were well distributed throughout the scenes, and the registration resulted a Root Mean Square Error (RMSE) of <0.5 pixels. A first-order polynomial transformation with nearest neighbor resampling technique was applied to analyze channel planform dynamics of river Chel from 1972 -2017. Finally, each image was clipped using an area of interest (AOI) file derived from a vector dataset.

Table 4.2.1- Map sources used in the study

List of map sources used in this study with some important parameters.

Types of data	Publisher	Index/ map no.	Survey year	Scale	Spatial coverage		
Edition-2 Army Map Service (AMS) Series-U502	USArmy Corps of Engineers	NG 45-8	compiled in 1955 from half-inch series,1: 126.720,SOI,1930-33	1:2,50,000	Jalpaiguri and Kochbehar District		
Topographical maps	Survey of India	78 B/9 and 78 B/10	1969-1971	1:50,000	Darjiling, Jalpaiguri and Dinajpur District		
Satellite images	Satellite/ sensor	**Path/Row**	**Date of acquisition**	**Resolution (Meter)**	**Projection**	**WRS type**	**Bit depth**
	Landsat 1-5 MSS	149/41	30.11.1976	60	UTM/WGS 1984	1	8
	Landsat 4-5 TM	139/41	31.12.1987	30	UTM/WGS 1984	2	8
	Landsat 4-5 TM	139/41	18.12.1994	30	UTM/WGS 1984	2	8
	Landsat 4-5 TM	139/41	13.10.2005	30	UTM/WGS 1984	2	8
	Landsat 4-5 TM	139/41	14.12.2010	30	UTM/WGS 1984	2	8
	Landsat 8 OLI/TIRS	139/41	01.12.2017	30 (15m for PAN)	UTM/WGS 1984	2	16

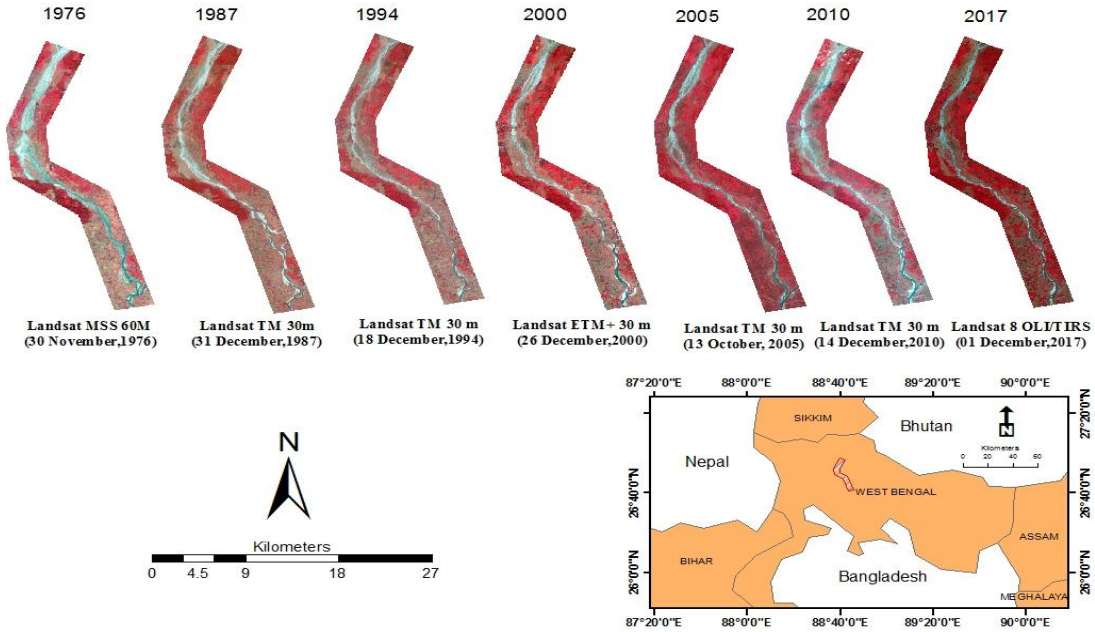

Figure 4.2.2 Temporal Landsat images used in the study showing morphological changes over time.

4.2.2.2 Delineation of channel boundary

For assessing various channel characteristics mentioned above channel boundary delineation is imperative. Now herein channel boundary has been delineated from both topographical maps and Landsat images. The author didn't encounter any confusion for delineating channel boundaries from topographical maps owing to its clear demarcation in the maps but the confusion really stroked for delineating channel boundaries from Landsat images of 1976 and latter. A bunch of previous studies demonstrate the availability of techniques ranging from manual digitization to automatic digitization to extract river boundaries from Landsat images. Herein automatic technique for extraction of river banks was attempted but the idea had to be dropped as the results were unreliable due to similarities in spectral reflectance of several riverine features. Studies done in other parts of the world (Yang *et al.*1999; Gupta et al. 2013) have similarly found manual digitalization superior than the automatic digitization for delineation of river bank from Landsat multispectral data. So manual digitization technique was preferred over automatic one and the channel boundaries were digitized from each Landsat image, using a combination of bands (1-6-7) which has been found by Yang *et al.* (1999), an effective band combination to display river channels at normal water level.

Now there is some difference of opinion in defining the channel- bank limit among the geoscientists. Nicoll and Hickin (2010) digitized the channel outlines of confined meandering rivers at 23 locations in Alberta and British Columbia, Canada to understand planform geometry and channel migration using a strict geomorphologic approach wherein boundary of water limit was taken as edge of the channel because this boundary is clearly visible in multispectral Landsat image. However, this approach cannot be used in my study area having low discharge and braiding nature of flow. Almost in entire study reach, the channel cross sections are broad and shallow. So, a small change in water level can therefore give misleading large changes in the positions of the channel boundaries. To avoid this problem, channel bank limits were defined using a non-morphological variable, namely soil-vegetation limit. This method of defining channel bank limits was adopted by Lawler (1993), Gurnell (1997); Yang *et al.* (1999), Tiegs and Pohl (2005), Dewan *et al.* (2017) etc. Soil- vegetation limit approach presume that river

channel limit is an elongated area wherein stream flow occurred with sufficient frequency, energy and duration to prevent the incidence of vegetation, and therefore 90% of this area is either bare soil or water (Gurnell, 1997; Yang *et al.*, 1999, Tiegs and Pohl, 2005). This method effectively overcomes the problem of inconsistencies in channel planform delineation due to varying water levels (Gurnell, 1997). Due to its simplicity and practicality, this method has been used successfully and widely in different climatic regions of the world (Lawler, 1993, Gurnell, 1997; Yang *et al.*, 1999, Tiegs and Pohl, 2005, Midha and Mathur, 2014, Dewan *et al.*, 2017). Author performed digitization of channel boundary on-screen from each Landsat image at 1:5000. Finally, a georeferenced spatial dataset, representing Channel banklines, for each topographical map and Landsat image was created (Fig. 5.5). Bhunia *et al.* (2016) have used single sensor Landsat-Thematic Mapper (TM) of 1989,1999,2005 and 2010 to show the channel dynamics of a reach of river Ganga in the southern Vaishali district of Bihar. They argue that observing images of common projection minimizes the error due to temporal changes.

4.2.3 Channel Dynamics

Channel dynamics of Chel River were studied through the assessment of channel characteristics which comprise changes in channel morphology, channel centerline migration, bank line migration, length, width, sinuosity, braiding index, and braid-channel ratio.

4.2.3.1 Channel morphology dynamics

In order to understand morphological changes, a map showing reach wise temporal morphological changes from 1976-2017 was prepared (Fig.4.2.4). Further a combined configuration map was also prepared by superimposing temporal vector files showing epochal changes (during 1955-2017) in the channel location (Fig.4.2.5). These two maps were used to assess the changes in morphology by visual inspection. A typology mainly based on the methods proposed by Goswami et al. (1999) for planform changes was established (Midha and Mathur (2014). It helped as a reference to classify the observed geomorphological changes. The different types of morphological changes observed during the entire assessment period were: neck cut-off and consequent

straightening of course; Changes in channel width; development and abandonment of anabranches; and shifting of meander bends.

A meander bend was observable at the very beginning of assessment period (i.e., in 1955) near Kranti in the Reach-C. In the next 15 years, it's observable that the meander's intensity has increased further (Fig. 4.2.3 A) in 1970 and by 1976 we see a complete neck cut-off (Fig. 4.2.3 B). Thus, the river has straightened its course by abandoning the meander loop. Notably, this straightening has decreased the length value by 1.94 km in the Reach-C and by 2.10 km in the overall length of the river during the period 1970-1976 (Table 4.2.6).

The Chel River experienced several episodes on contraction, expansion, osilation and straightening during the assessment period of 62years as shown by the channel configuration maps of the seven periods between 1955 and 2017 (Fig.4.2.4 & 4.2.5).

4.2.3.2 Centerline and Bankline dynamics

To understand the centerline and bankline migration dynamics, transects were drawn at 1km interval perpendicular to the general trend of the 1994 polygon along the 36 kms long study reach of River Chel from near Putharjhora T. E to its confluence with River Neora near Kranti. Thus altogether 35 transects ($T_1 - T_{35}$) were drawn and the entire study reach was divided into three smaller reaches namely Reach –A (T1-T11), Reach-B (T11-T25) and Reach-C (T25-T35) (Fig.4.2.6).

Migration distances of Centrelines, right banks and left banks were computed based on works of Leopold (1973), Gurnell et al. (1994), Yang et al. (1999) and Giardino and Lee (2011). The centerline and banklines of earliest channel (1955) were taken as the origin (Yang et al. 1999) and then centerline and banklines of the later dates were overlaid on the previous ones. The distance between the points of intersection between the centerlines and banklines along transects for subsequent years were measured (Chakraborty and Mukhopadhyay, 2014). Migration distances thus computed were treated as vectors, in a sense it has both numerical values as well as assigned directions. A positive value for rightward movement of channel and negative value for leftward movement of the channel were assigned.

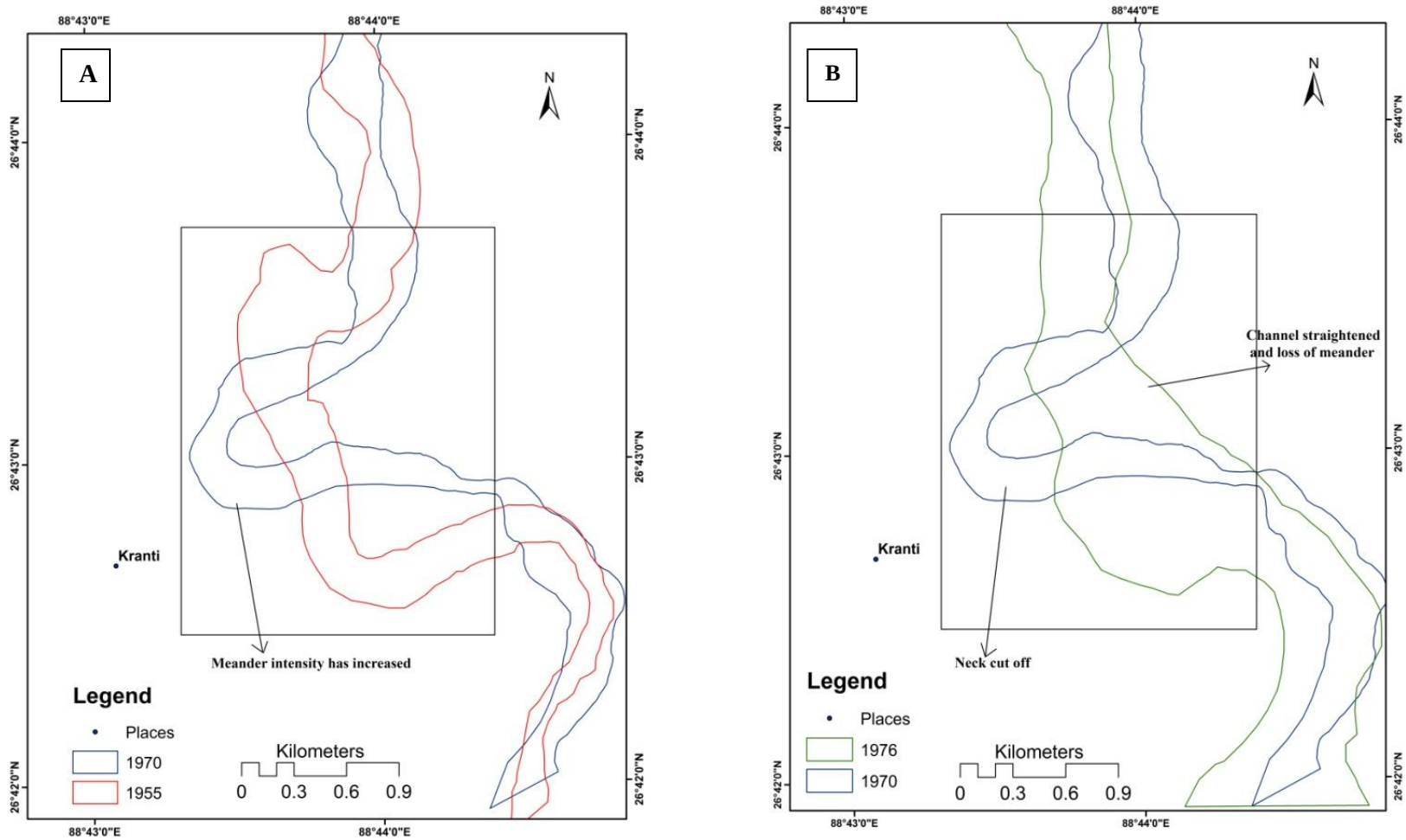

Figure 4.2.3 Channel polygons of 1955, 1970 and 1976 illustrating the episode of channel straightening through neck cut-off in Reach-C of the Chel River.

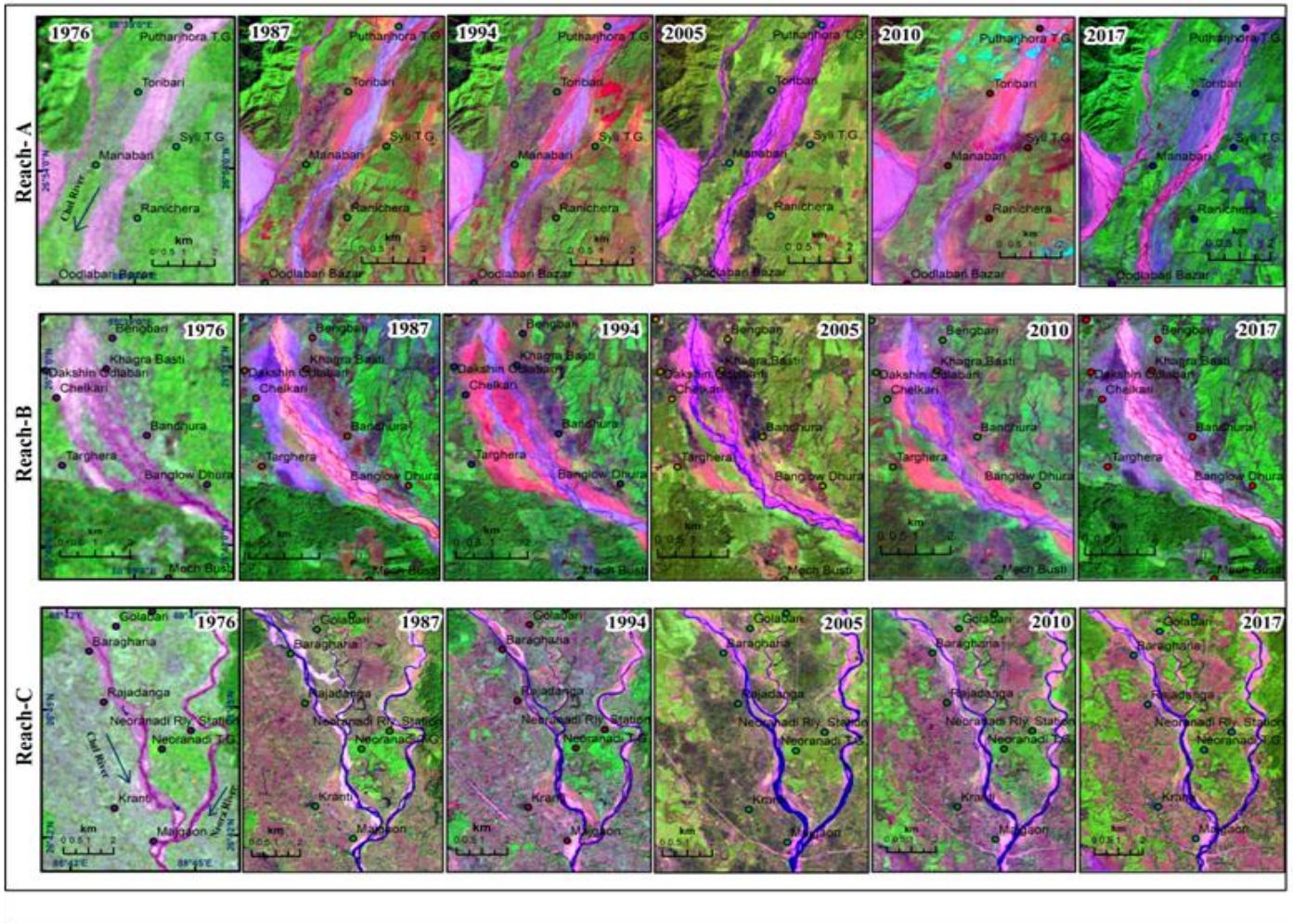

Figure 4.2.4 Reach-wise morphological changes over time.

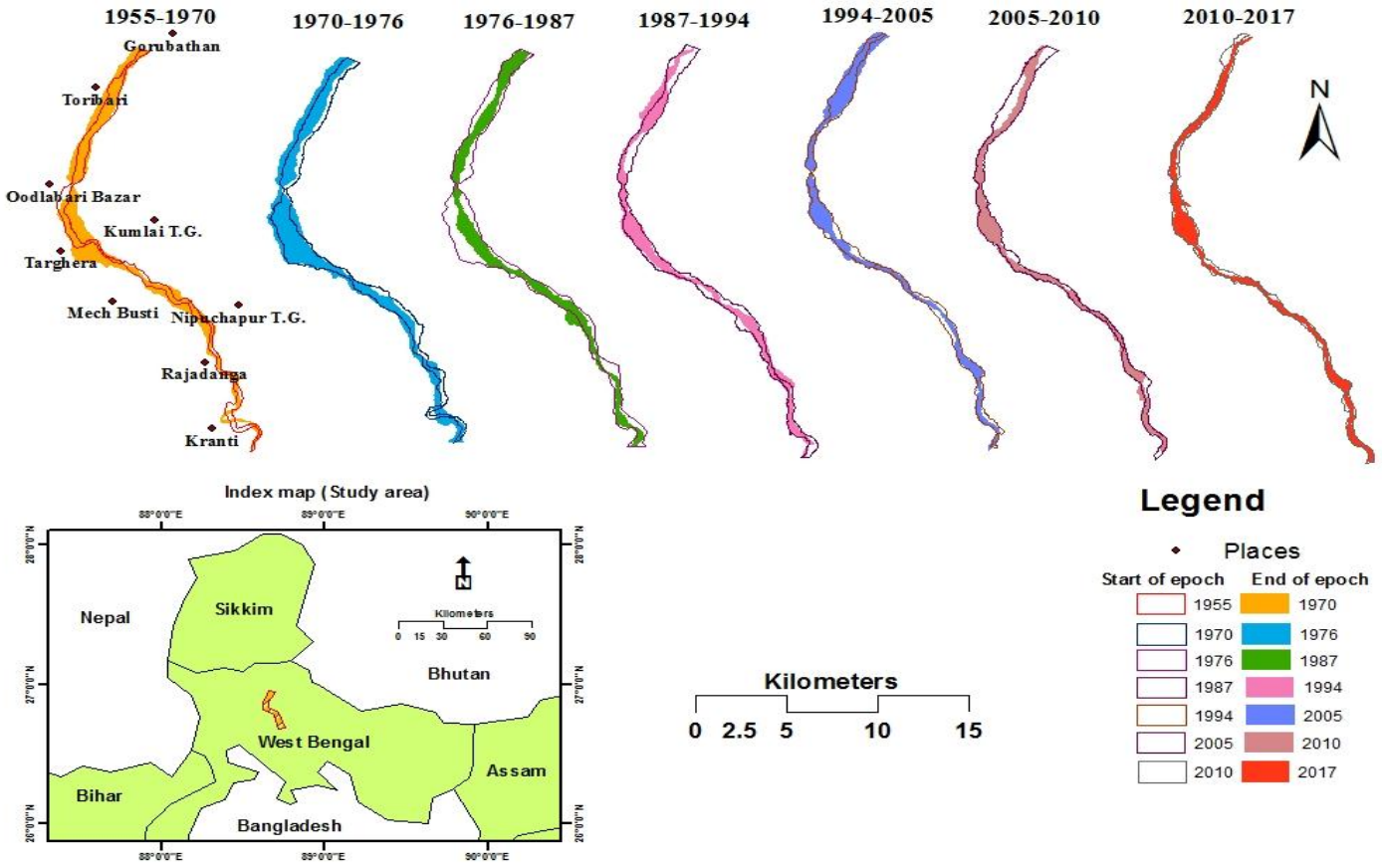

Figure 4.2.5 Channel configuration maps of Chel River, showing epochal change in channel location. Channel at the start of the epoch is shown by hollow polygon, at the end with solid fill.

4.2.3.2.1 Channel centerline dynamics

Channel centerlines were drawn along the centre of the active channels for the straight reaches and along the cut banks for the meandering reaches (Chakraborty and Mukhopadhyay 2014). The 1955's centerline was assumed or taken as the base centerline and all the subsequent channel centerlines were overlaid and their movements along transects have been calculated. Channel centerline migrations were measured using "line tool" under "measure tool" of ArcGIS. Study on channel centerline migration is assessed through temporal transect wise, reach wise and total migration.

Measurements of lateral centerline migration are summarized in Table- 4.2.2. The general trend of channel centerline movement is towards rightward (Fig.4.2.8). The Y- axes of these graphs are kept with same scale so that logical comparison can be made. Out of 35 transects only 9 transects (T12, T13, T14, T15, T21, T27, T29, T33 and T34) shows leftward movement of centerline. T14 exhibit maximum total leftward movement of -1081.57 m with yearly average of -17.44m whereas T27 demonstrates the minimum leftward centerline movement of -22.98 m with annual average of -0.37m. Among the rightward movements, transects T17 records the maximum movement value of 1747.49m with annual average movement of 28.19 m whereas T7 exhibit least movement of 72.2 m only with annual average movement of 1.16m.

Transects T12, T19, T20, T21, T22, T25, T27, T28, T31, T32 and T35 are relatively stable, with very little changeable curves (Figure 4.2.8). Sixteen transects (T1, T2, T3, T6, T7, T8, T9, T10, T11, T23, T24, T26, T29, T30 and T30) are moderately stable. Whereas the reach between Oodlabari TG and Mech Busti is highly unstable with eight transects (T4, T5, T13, T14, T15, T16, T17 and T18) having very high irregular curves (Fig.4.2.8). The chronological superimposition of centerline shapefiles, i.e., overlay operation, reveals several interesting facts (Fig.4.2.9). It uncovers a general picture that the maximum centerline migration has occurred in the middle reach followed by upper reach and the lowermost reach.

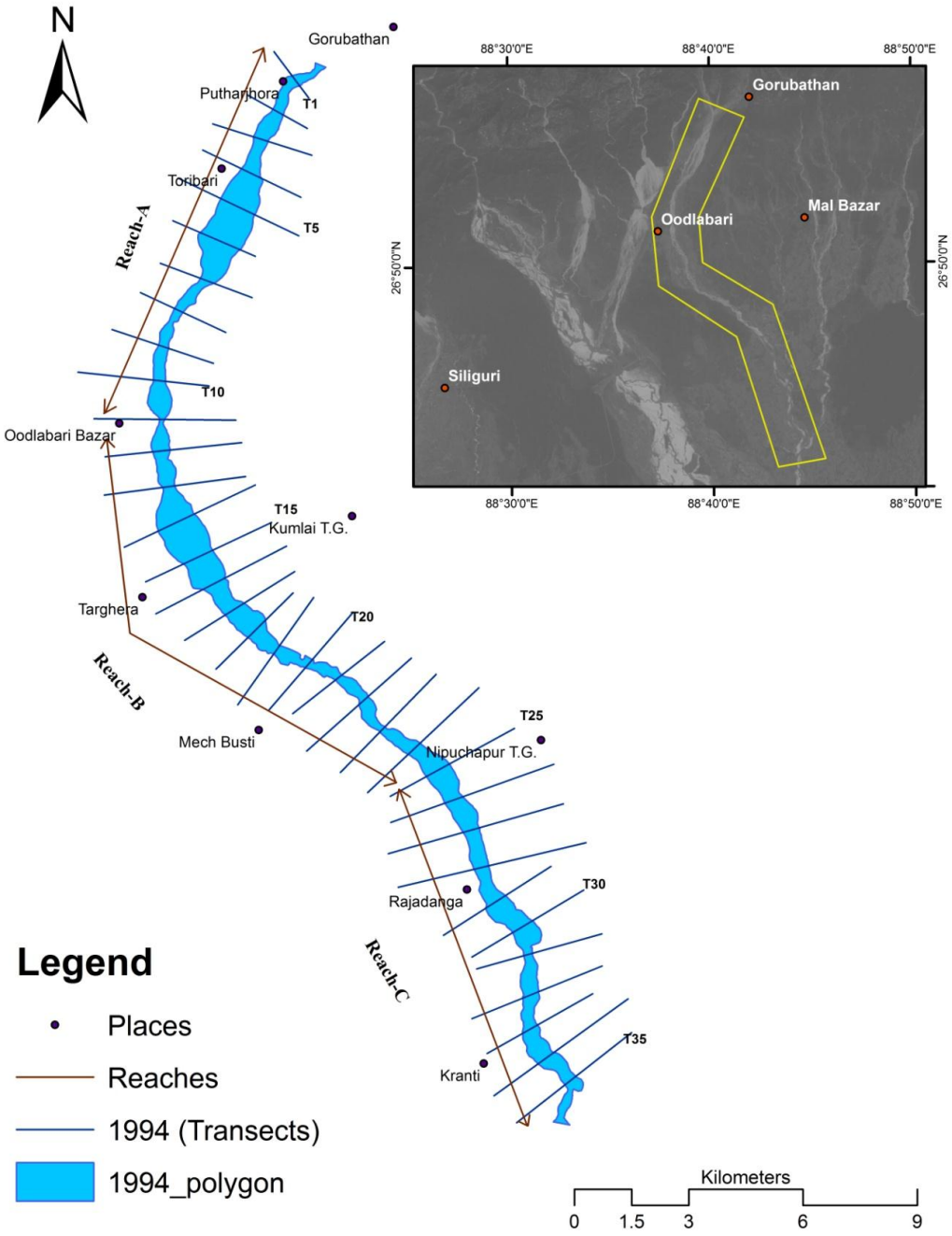

Figure 4.2.6 Location of transects at 1kms interval. Polygon encompass all mid channel bars.

The reason behind the severe centerline dynamics along the middle reach of Chel can be attributed to bottleneck effect of NH-31C Bridge and NEFR Siliguri- Alipurduar Railway Bridge near Odlabari on immediate downstream channel hydraulics of Chel (Fig. 4.6.4). To the immediate downstream of these two bridges the river becomes much shallower and wider. This results in the oscillating movement of centerline on the wider cross profile. There exists a large vegetative bar (1.06 km^2 according to Landsat-8 OLI & TIRS dated- 07.12.2017) 2kms downstream of the bridge. This bar diverges the flow and often results in oscillation of main flow thus centerline to the east or west of the vegetative bar in downstream direction.

The centerline migration in the upper reach is mainly controlled by huge aggradation process. The reach upstream of NH-31C Bridge near Odlabari experience incessant aggradation of huge Himalayan detritus (Plate 4.6.29). This is developing a huge alluvial fan over which River Chel flows in braided pattern wherein the channel bifurcates into multiple channels and flows between the alluvial bars. Since most of these bars are unstable, the channels change their positions and thus the main channel too.

The lower reach is characterized by lowest level of centerline dynamics yet the reach records an average figure of 5.36 m/yr centerline migration during the whole assessment period. The lower reach begins beyond the straight-line distance of 19.22 kms from the mountain front. Thus, there is very little effect of aggradations process to such distance. The on bed and banks sediments are mainly coarse sand and silts. The number of channels in this reach becomes very few, at times attains single channel flow and exhibits sinuous to meandering channel pattern.

The study of temporal trends in the total centerline migration distance conforms to the above-mentioned findings. The centerline migration distance has remained well below the 1kms mark for most of the historical period except during 1955-1970 and 1970-1976 periods in the middle reach of the Chel River. This spike in the centerline migration distance can be attributed to the massive flood of 1968 which lashed havoc in the Darjeeling Himalaya (Plate 4.2.1). It's very possible that the huge discharge having high velocity and armored with huge quantity of sediments widened the channel width by 2-3 times. Thus, the main channel and its centerline oscillated much over the newly gained

cross bed surface in the subsequent years. The bottleneck impact of two bridges near Odlabari on the immediate downstream morphology of river and the flow divergence role played by large vegetative mid channel bars seems to be the reasons behind the exhibition of centerline migration distance of over 2kms in the middle reach of the Chel River.

Plate 4.2.1 Field Photograph taken on 10.09.2017 displaying first railway pier from left bank over Chel River at Odlabari showing clearly CWC marked Highest Flood Level recorded during 1968.

Table 4.2.2 Statistics of centerline migration dynamics over time.

Centerline movement											
Sl. No.		1	2	3	4	5	6	7	8	Total migration (m)	Average migration(m y^{-1})
Time		1955	1970	1976	1987	1994	2005	2010	2017		
Years (accumulative)		1	16	22	33	40	51	56	62		
TRANSECTS	T1	0	278.1	646.92	-283.3	-84.69	112.9	245.05	-444.4	470.58	7.59
	T2	0	382	312.15	66.1	-146.86	180	-645.23	-12.6	135.56	2.19
	T3	0	517.39	15.66	-85.1	25.6	190.97	-461.4	-44.37	158.75	2.56
	T4	0	605.29	-97.42	-167.48	-122.01	679.02	-979.7	218	135.7	2.19
	T5	0	528.15	-2.16	-13.37	-232.35	731.77	-916.72	103.6	198.92	3.21
	T6	0	343.12	-258.91	35.24	13.34	601.22	-524.6	108.79	318.2	5.13
	T7	0	-163.06	103.94	163.71	9.03	377.99	-539.9	120.49	72.2	1.16
	T8	0	-236.26	153.54	581.19	-1.66	178.95	-177.73	1.75	499.78	8.06
	T9	0	-153.25	164.81	680.6	18.34	-53.87	240.4	-90.24	806.79	13.01
	T10	0	-58.76	195.53	576.94	-115.75	280.42	-90.3	-146.19	641.89	10.35
	T11	0	-105.99	676.51	-243.14	-8.69	277.62	-16.34	4.55	584.52	9.43
	T12	0	-170.51	117.42	115.58	-44.68	24.71	-300.19	167.5	-90.17	-1.45
	T13	0	74.21	-1056.5	283.73	6.71	206.37	-246.82	14.04	-718.26	-11.58
	T14	0	57.15	-1232.92	837.92	-619.16	876.66	-712.9	-288.32	-1081.57	-17.44
	T15	0	-14.65	-1049.97	613.22	-435.05	657.39	-914.9	79.05	-1064.91	-17.18
	T16	0	1463.36	-1456.69	135.29	210.69	226.21	-233.25	115.6	461.21	7.44
	T17	0	2841.63	-2448.93	547.17	395.84	246.3	-165.66	331.14	1747.49	28.19
	T18	0	715.56	-895.61	350.21	502.03	491.02	-528.54	278.5	913.17	14.73
	T19	0	341.97	-73.11	173.2	189.02	43.7	-214.32	257.9	718.36	11.59
	T20	0	32.18	272.34	57.74	113.5	108.64	-144.64	82	521.76	8.42
	T21	0	-125.63	139.5	25.17	-162.59	74.92	48.03	-135.64	-136.24	-2.20
	T22	0	340.98	90.78	153.14	-29.44	-15.48	97.2	72.52	709.7	11.45
	T23	0	631.7	-756.823	674.75	354.36	-493.71	325.96	-151.16	585.077	9.44
	T24	0	642.47	-431.16	540.14	59.95	-46.35	-127.08	137.14	775.11	12.50
	T25	0	-43.82	264.9	155.79	120.8	-177.89	-170.43	-17.15	132.2	2.13
	T26	0	508.13	103.53	415.39	-5.89	-363.78	35.56	-81	611.94	9.87
	T27	0	-75.82	203.62	74.62	-22.17	-142.04	-56.4	-4.79	-22.98	-0.37
	T28	0	232.35	84.28	-37.81	-232.8	254.9	-216.74	-16.47	67.71	1.09
	T29	0	-108.71	-280.5	658.47	-473.48	448.6	-342.9	42.1	-56.42	-0.91
	T30	0	-147.87	292.36	298.58	-386.79	586.42	-478.22	-15.5	148.98	2.40
	T31	0	-181.43	190.17	17.78	172.07	15.27	164.45	-120.74	257.57	4.15
	T32	0	-122.95	590.57	66.72	-282.31	-0.29	-39.51	56.75	268.98	4.34
	T33	0	573.12	-935.25	-32.66	267.82	41.8	-249.24	-12.59	-347	-5.60
	T34	0	-783.56	-419.85	-59.39	384.8	-169.8	234.51	-184.63	-997.92	-16.10
	T35	0	-6.94	137.52	386.94	152.6	-73.3	31.73	-82.7	545.85	8.80

Note: + (positive) denotes Rightward migration ; - (negative) denotes Leftward direction.

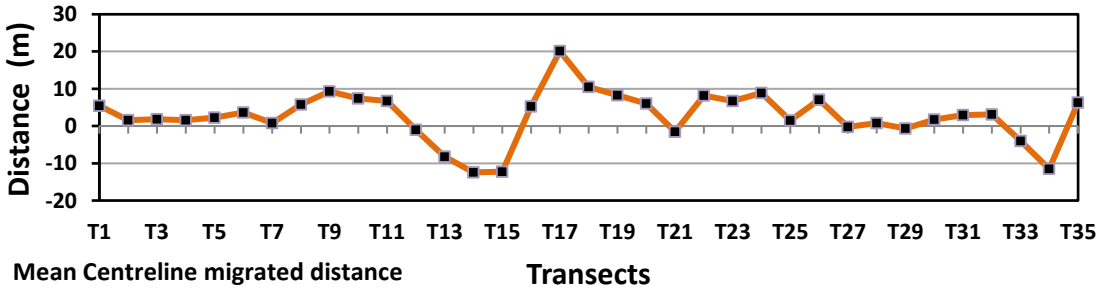

Figure 4.2.7 Transect wise mean centerline migrated distance of Chel River (1955-2017).

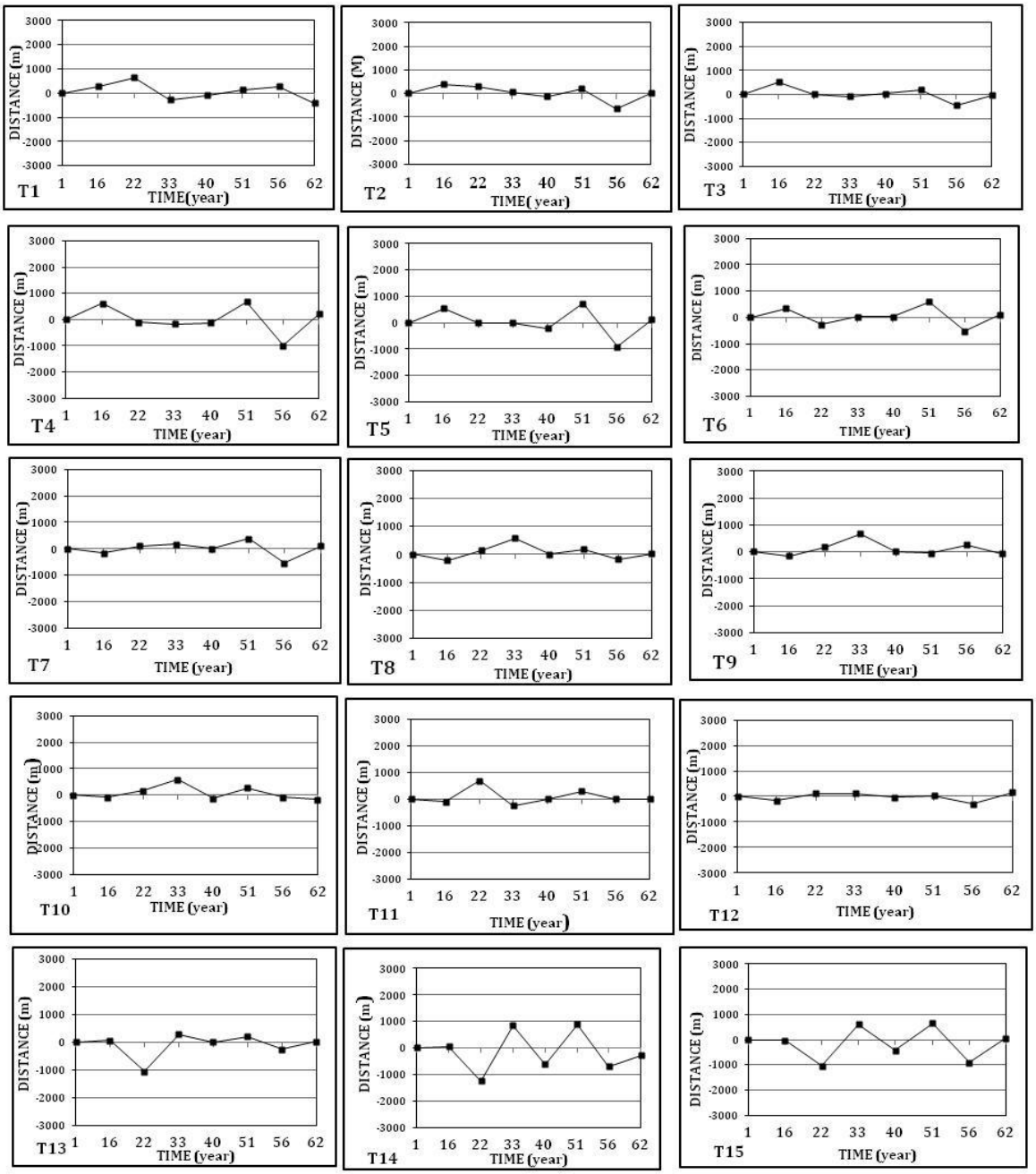
T1
T2
T3
T4
T5
T6
T7
T8
T9
T10
T11
T12
T13
T14
T15
DISTANCE (m)
TIME (year)
3000
2000
1000
0
-1000
-2000
-3000
1 16 22 33 40 51 56 62

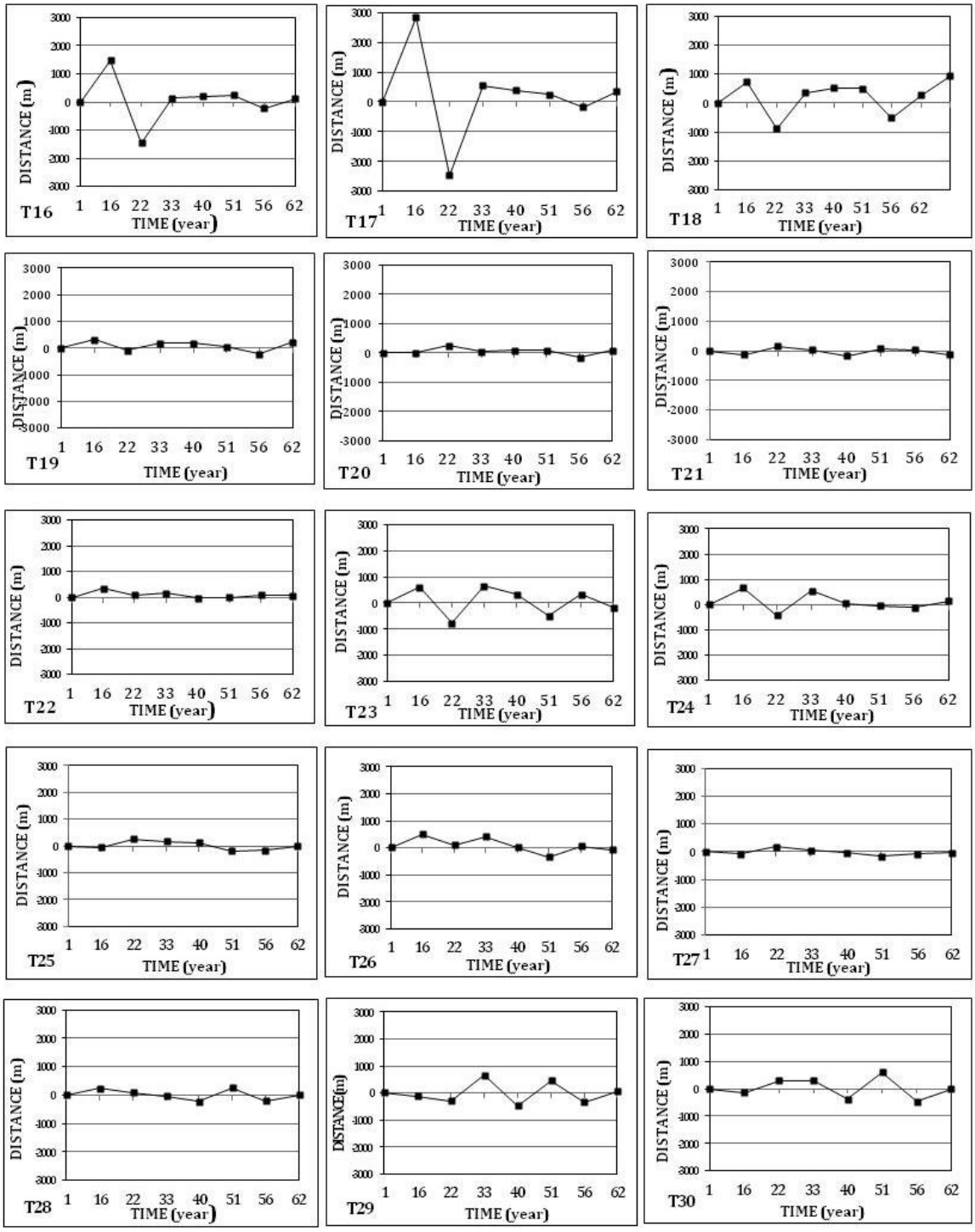
T16
T17
T18
T19
T20
T21
T22
T23
T24
T25
T26
T27
T28
T29
T30
DISTANCE (m)
TIME (year)
3000
2000
1000
0
-1000
-2000
-3000
1 16 22 33 40 51 56 62

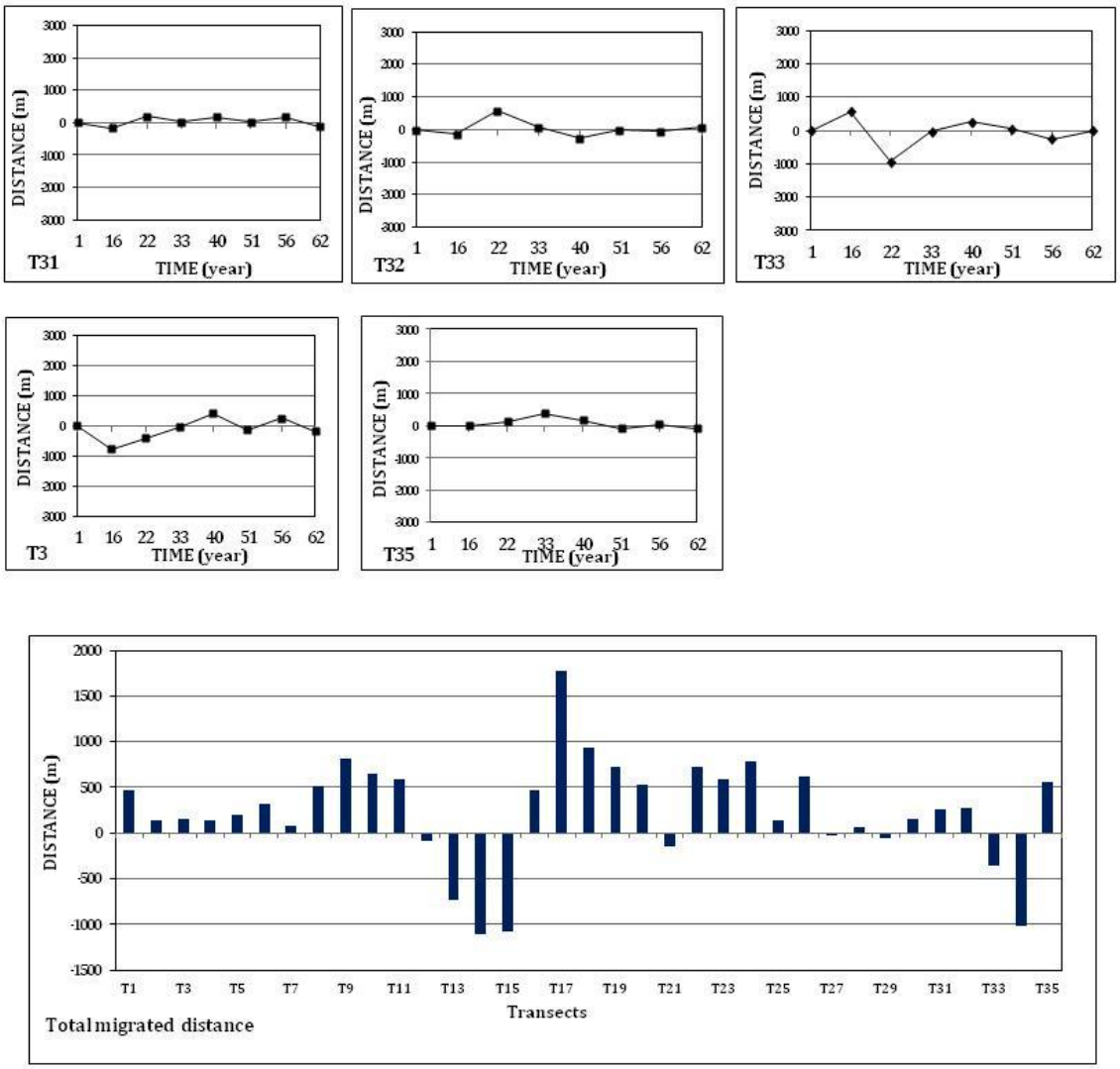

Figure 4.2.8 Channel centerline migration over time.

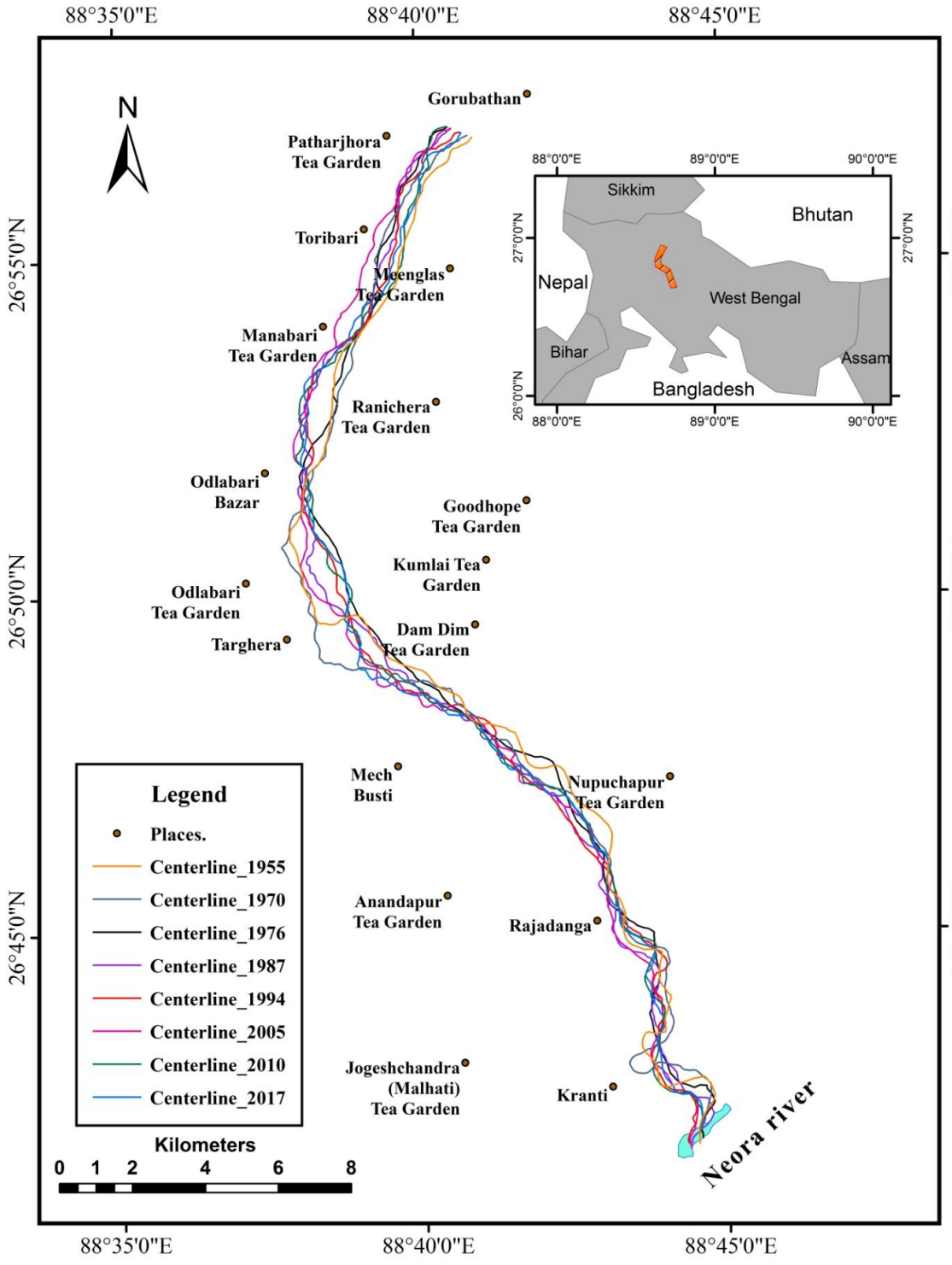

Figure 4.2.9 Temporal trends in total centerline migration distance for the Chel River (1955-2017).

4.2.3.2.1.1 Channel centerline prediction of Chel River in 2025 and 2035 using linear regression method

Time series forecasting is an important technique of forecasting in which past observations of the same variable are collected and analyzed to develop a model describing the underlying relationship. The model is then used to extrapolate the time series into the future. This modeling approach is particularly useful when little knowledge is available on the underlying data generating process or when there is no satisfactory explanatory model that relates the prediction variable to other explanatory variables. Much effort has been devoted over the past several decades to the development and improvement of time series forecasting models (Zhang,2001). Despite availability of many techniques, the identification of erosion susceptible locations and predication of riverbank erosion is difficult due to dynamic and stochastic nature of the river channels (Winterbottom and Gilver,2000). Many numerical models such as support vector machine (SVM), autoregressive integrated moving average (ARIMA), and artificial neural network (ANN) have been used in the fluvial geomorphology to model and predict the riverbank erosion probability or location of the channel bank lines (Sreenu and Teja 2015; Akhter et al. 2019; Pareta and Goswami,2021). Few other studies propose a hybrid approach to time series forecasting. Zhang, 2001 have proposed a similar hybrid approach wherein he combines a linear model ARIMA with non-linear model ANN to take advantage of unique strengths of both models. His empirical results with real datasets clearly suggest that the hybrid model is able to outperform each component model used in isolation. However, most of these above cited models are not only computationally complex and data intensive rather considering the detailed datasets required to calibrate, run and validate, these models are generally non-existent in developing countries (Bordoloi et al.2020). Few geomorphologists have therefore attempted an integration of relatively less data demanding Graf's model (Graf,1984) in the GIS environment to predict the bank lines and erosion probability (Winterbottom and Gilver 2000; Bordoloi et al.2020).

Few others have chosen even simpler model of simple linear regression method to predict the channel bank line or erosion hazard reaches (Richard et al.2005; Heo et al. 2009; Das et al.2012; Deb and Ferreira 2015).

Considering the non-uniform or gaps inherent in Landsat time-series and paucity of time available for detailed analysis in this study, a linear regression method is used here to determine the channel centerline position of the Chel River in 2025 and 2035 using the historical values from digitized shape files. The detail methodology of digitization of bank line shape files from historical satellite images are discussed in section 4.2.2.2 of this thesis. However, it is to be noted that prediction/forecasting of channel centerline position is difficult for a plethora of variables like rainfall, discharge, landuse, anthropogenic activity etc. govern it. Active neotectonics, high rainfall, high volume of sediment flux and increasing human intervention which characterize the eastern Himalayan piedmont surface makes the study area highly unstable which creates impediments for any long-term forecasting of channel dynamics of the Chel river. Therefore, a short-term prediction of channel centerline for River Chel has been attempted here with the assumption that all the controlling factors will stay constant during the period.

Details on measurements of lateral centerline migration and future distance prediction is summarized in Table 4.2.3. None of the 35 transects shows a linear progression of migration distance in relation to elapse of time. It has been observed that the centerlines are migrating non-linearly throughout the assessment period and simple linear regression modelling suggests that this trend of non-linear shifting will continue even in the future as well (Table 4.2.3). The analysis has identified two reaches having highest predictive centerline migration distance with highest R^2 values. The first reach is from transect 8 to transect 11 wherein the highest predicted centerline migration distance of 1360 m (west) from the base year position of 1955 is likely to occur along the T9 transect by the year 2035. This reach falls immediately upstream of Odlabari rail and road bridge hosting Manabari Tea estate, few patches of agricultural lands and most importantly upper section of Odlabari town (Fig. 4.2.11). The second reach is from transect 17 to transect 22 consisting of western bank of lower reach that hosts extensive forest land under Apalchand Reserve Forest. Herein transect 18 is likely to attain highest predictive migration distance of 1206.3 m by 2035 from its base year position of 1955. This suggests greater threat to flora and fauna of the reserve forest. Transect 21 is likely to maintain its eastward migration trend even in the future. Based on the predictive

centerline position of 2035, a buffer polygon of width 578m i.e., the average width of the river in whole assessment period of 62 years is created and the same was overlaid on recent google earth images (dated: 17.08.2018) to predict the extent of hazard in these two zones (Fig. 4.2.12 and Fig. 4.2.13). It is evident that these two reaches are much likely to observe the greatest brunt of soil erosion and consequent implications. If unchecked, the westward migration of River Chel in Zone-1 is much likely to erode away the narrow interfluvial strip of land (1km approx. in width at its narrowest part) between Chel and River Ghish. The erosion process may be very gradual or it may be in the form of an avulsion. Similarly, a significant area of Apalchand Reserve Forest is much likely to get eroded in the Zone-2. Even a forest village named Mech Busti will lose much of its cultivation lands spread across its eastern fringe. Thus, the predictive channel dynamics is likely to damage cultural elements (i.e. human habitation, agricultural lands and roads and infrastructures) in the Zone-1 and physical elements (i.e. natural vegetation) in the Zone-2. Therefore, investment of much focus and attention for proper bank strengthening and management works along these two reaches becomes suggestive and imperative too.

The third reach of very small distance is identified at transects 33 and 34. This reach is typical and special in the sense that the channel will maintain its eastward movement along these transects in the future too as suggested by the model. These transects are just 1-2 km upstream of the current confluence point of Chel and Neora. The predictive eastward movement of centerline implies greater erosion of land at Majgaon (literally meaning "Village in the middle"), which is an interfluve between Chel and Neora Rivers. If the River Neora is having a tendency of westward movement and continues in the near future too then there is high probability of huge erosion of interfluvial land at Majgaon and consequently the confluence point will shift northward obliterating the southern landmass of the present Majgaon village.

The westward movement of River Chel implies further increase in length of eastern tributaries which may be accompanied by the shifting of confluence points too. It also implies more loss of arable land along the west bank and increase in areas by almost equal quantity under gravel point bars along the eastern banks. There may be increase in areas under mid-channel bars and development of few permanent riverine bars too.

The riparian population who loose arable land and properties along the west bank will pursue agrarian activities on the ever-increasing point bars or deposited landmass along the eastern bank. But the agriculture will be only seasonal i.e., paddy and vegetables, for being low lying the newly deposited land will be inundated during flood water level. Thus, people will pursue other viable options in the surrounding like boulder and sand mining, fishing, forest clearing etc. which will further heighten anthropogenic imprints in the basin. Certain percentage of population may migrate temporarily or permanently in hope of attaining a stable source of income. This can disrupt the existing and already distorted socio-economic fabric of the communities living within and vicinity of the basin.

Time period		1955-1970	1955-1976	1955-1987	1955-1994	1955-2005	1955-2010	1955-2017	1955-2025	1955-2035	R	R^2
Years (accumulative)		15	21	32	39	50	55	62	70	80		
		Observed Centerline migration trend (m)							Predictive centerline migration trend (m)			
Transects/Cross-sections	T1	278.1	925.02	641.72	557.03	669.93	914.98	470.58	709.61	733.22	0.25	0.06
	T2	382	694.15	760.25	613.39	793.39	148.16	135.56	283.04	211.49	-0.59	0.34
	T3	517.39	533.05	447.95	473.55	664.52	203.12	158.75	239.26	177.99	-0.73	0.53
	T4	605.29	507.87	340.39	218.38	897.4	-82.3	135.7	129.29	49.77	-0.57	0.32
	T5	528.15	525.99	512.62	280.27	1012.04	95.32	198.92	301.59	253.34	-0.39	0.15
	T6	343.12	84.21	119.45	132.79	734.01	209.41	318.2	408.39	450.87	0.46	0.21
	T7	-163.06	-59.06	104.65	113.68	491.67	-48.23	72.26	236.85	293.29	0.60	0.36
	T8	-236.26	-82.72	498.47	496.81	675.76	498.03	499.78	838.61	1001.59	0.90	0.82
	T9	-153.25	11.56	692.16	710.5	656.63	897.03	806.79	1153.48	1359.64	0.94	0.88
	T10	-58.76	136.77	713.71	597.96	878.38	788.08	641.89	1035.00	1199.21	0.90	0.81
	T11	-105.99	570.52	327.38	318.69	596.31	579.97	584.52	723.88	825.53	0.81	0.66
	T12	-170.51	-53.09	62.49	17.81	42.52	-257.67	-90.17	-81.63	-87.31	-0.12	0.01
	T13	74.21	-982.29	-698.56	-691.85	-485.48	-732.3	-718.26	-807.59	-873.27	-0.47	0.22
	T14	57.15	-1175.77	-337.85	-957.01	-80.35	-793.25	-1081.57	-884.79	-969.27	-0.41	0.17
	T15	-14.65	-1064.62	-451.4	-886.45	-229.06	-1143.96	-1064.91	-1058.70	-1177.03	-0.60	0.36
	T16	1463.36	6.67	141.96	352.65	578.86	345.61	461.21	242.26	165.66	-0.39	0.16
	T17	2841.63	392.7	939.87	1335.71	1582.01	1416.35	1747.49	1414.27	1397.80	-0.06	0.00
	T18	715.56	-180.05	170.16	672.19	1163.21	634.67	913.17	1054.01	1206.29	0.73	0.53
	T19	341.97	268.86	442.06	631.08	674.78	460.46	718.36	749.34	828.41	0.89	0.80
	T20	32.18	304.52	362.26	475.76	584.4	439.76	521.76	659.61	747.42	0.92	0.84
	T21	-125.63	13.87	39.04	-123.55	-48.63	-0.6	-136.24	-73.36	-79.45	-0.21	0.04
	T22	340.98	431.76	584.9	555.46	539.98	637.18	709.7	740.24	804.21	0.95	0.86
	T23	631.7	-125.123	549.627	903.987	410.277	736.237	585.077	734.78	801.99	0.49	0.24
	T24	642.47	211.31	751.45	811.4	765.05	637.97	775.11	493.79	905.55	0.43	0.18
	T25	-43.82	221.08	376.87	497.67	319.78	149.35	132.2	288.49	305.45	0.24	0.06
	T26	508.13	611.66	1027.05	1021.16	657.38	692.94	611.94	753.95	760.77	0.08	0.01
	T27	-75.82	127.8	202.42	180.25	38.21	-18.19	-22.98	22.43	9.72	-0.29	0.08
	T28	232.35	316.63	278.82	46.02	300.92	84.18	67.71	69.70	30.86	-0.71	0.51
	T29	-108.71	-389.21	269.26	-204.22	244.38	-98.52	-56.42	77.26	118.19	0.42	0.18
	T30	-147.87	144.49	443.07	56.28	642.7	164.48	148.98	386.57	444.61	0.53	0.28
	T31	-181.43	8.74	26.52	198.59	213.86	378.31	257.57	431.85	530.04	0.96	0.92
	T32	-122.95	467.62	534.34	252.03	251.74	212.23	268.98	314.17	329.69	0.19	0.03
	T33	573.12	-362.13	-394.79	-126.97	-85.17	-334.41	-347	-463.13	-563.34	-0.66	0.43
	T34	-783.56	-1203.41	-1262.8	-878	-1047.8	-813.29	-997.92	-951.30	-936.13	0.20	0.04
	T35	-6.94	130.58	517.52	670.12	596.82	628.55	545.85	821.81	945.43	0.90	0.81

Table 4.2.3: The assessment of channel centerline shifting and prediction of channel centerline using linear regression method.

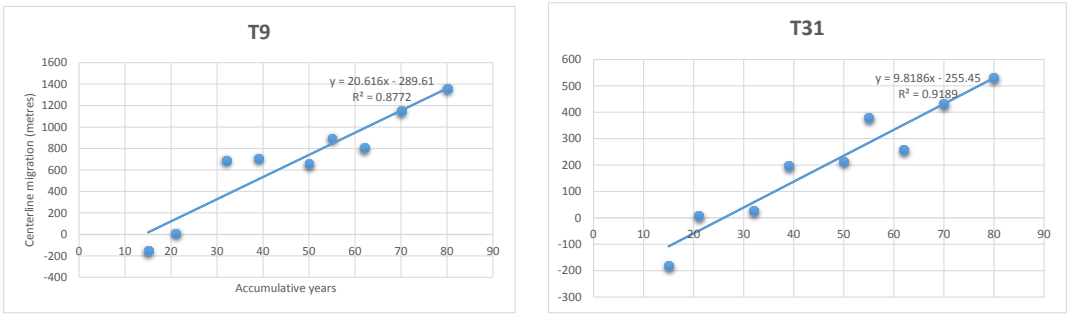

Fig.4.2.10 Prediction for centerline in 2025 and 2035 using linear regression method

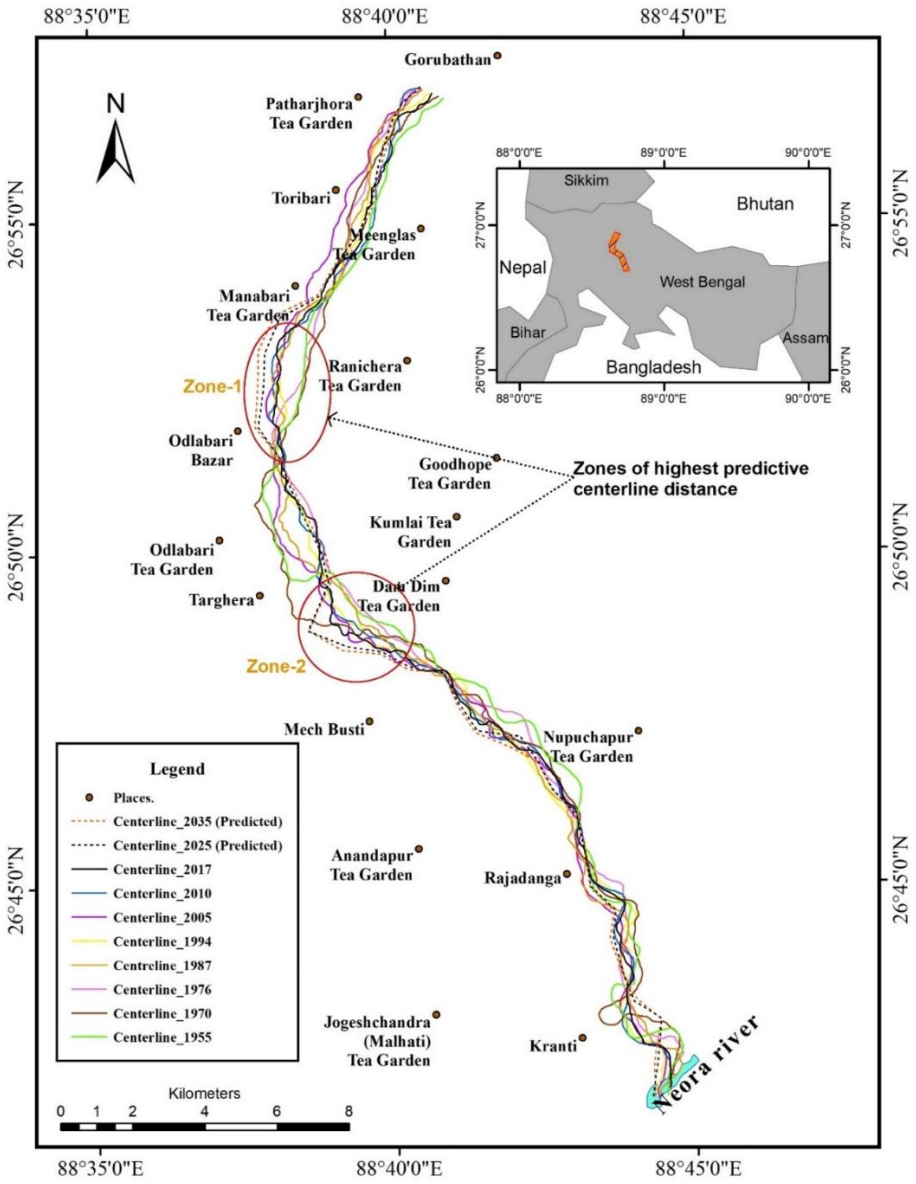

Fig.4.2.11- Predicted centerline migration of River Chel

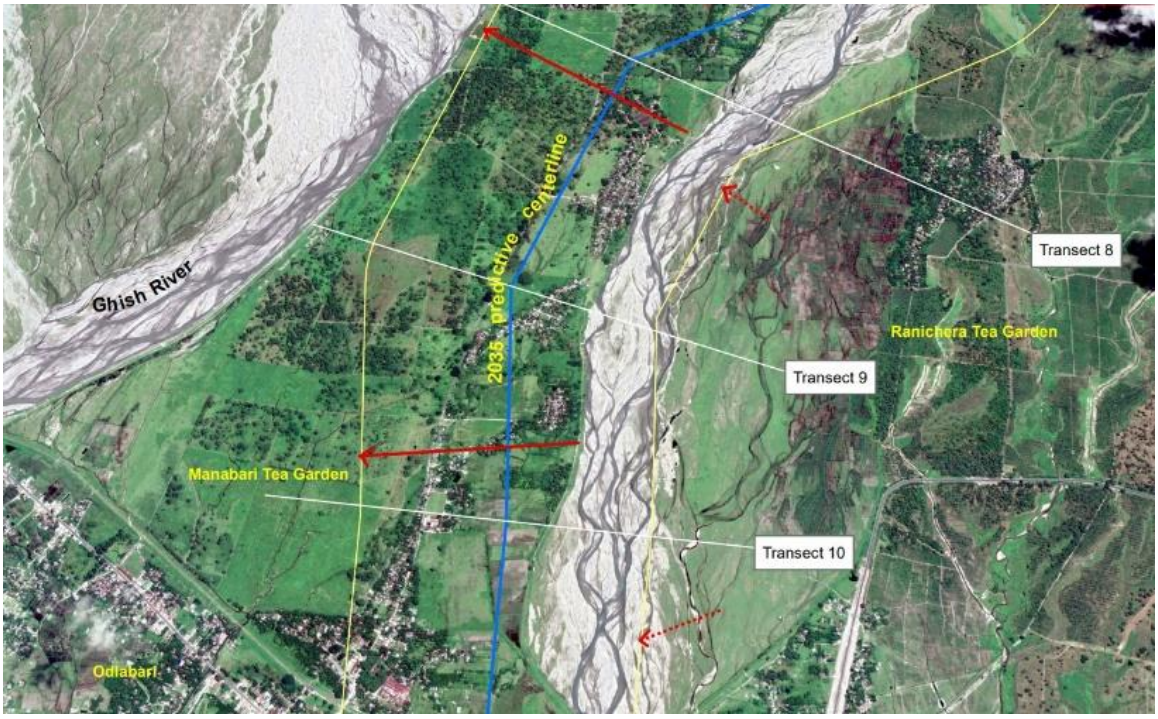

Fig.4.2.12- Hazard assessment at zone-1(Google Earth image- 17.08.2018)

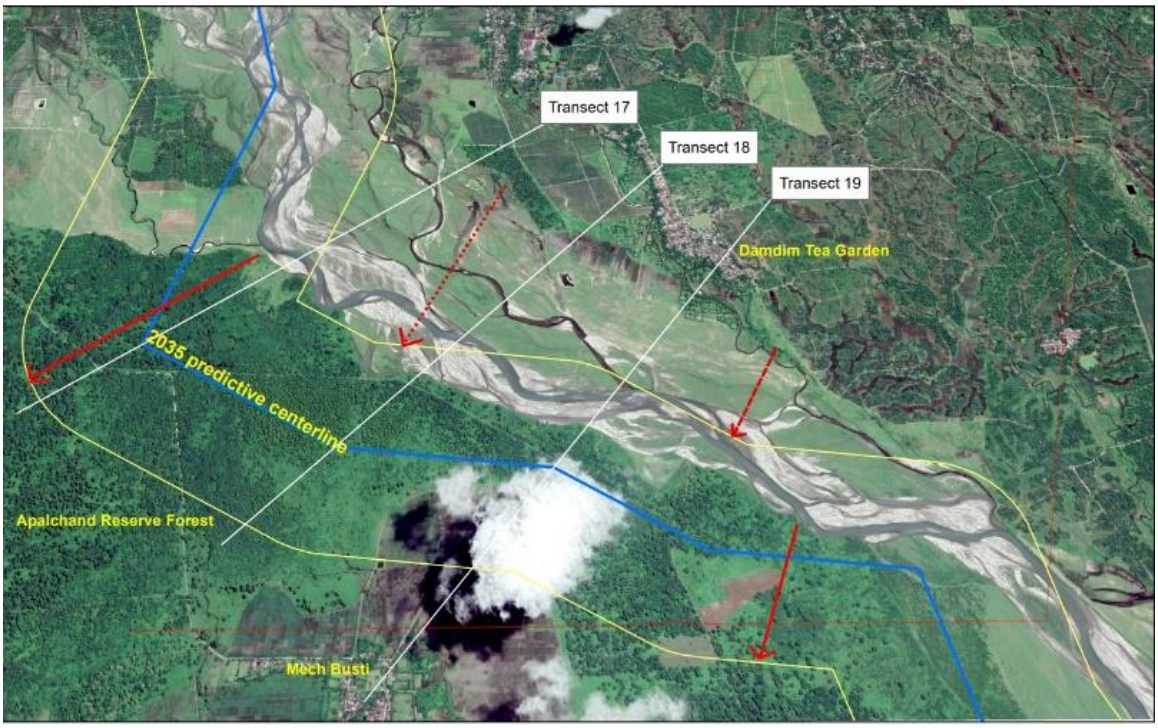

Fig.4.2.13- Hazard assessment at zone-2 (Google Earth image- 17.08.2018)

4.2.3.2.2 Channel bankline dynamics

Channel bank limits were defined using a non-morphological variable, namely soil-vegetation limit. This method of defining channel bank limits was adopted by Lawler (1993), Gurnell (1997); Yang et al. (1999), Tiegs and Pohl (2005), Dewan et al. (2017) etc.

4.2.3.2.2.1 Right bank line dynamics

The statistics on temporal right bank migration are summarized in Table-4.2.4. Only 10 transects shows an overall leftward direction movement while rest of the 25 transects show rightward direction migration. The stretch from T12 to T15 displays the maximum leftward migration. During the whole assessment period; T13 exhibits the maximum total leftward movement of right bank by a distance of -632.9 m. The least total leftward movement of -51.01m was observed for right bank.

The stretches near T11, T19, T20, T21 are relatively stable, as depicted by less fluctuating curves (Fig. 4.2.14). T19 is unique and interesting by the fact that it has recorded only rightward movement of right bankline (positive values) during the whole assessment period of 62 years. This implies to the fact that the stretch near T19 has experienced only erosion and progressively moved into Apalchand Reserved Forest near Mech Busti at a modest rate of $12.89m^{-1}$. All other transects are unstable but T4,T5,T16,T17,T23 can particularly be categorized as highly unstable stretches. Highly fluctuating curves of these transects suggest the same. T17 has recorded highest movement of right bankline by a distance of 2455.2m during the 16^{th} year of assessment period in 1970.

In terms of total migration, T23 has recorded maximum lateral right bank movement distance of 1527.35m. The minimum movement of only 36.57m was recorded in the stretch near T27. The above-mentioned figures are among the overall 35 transects and among rightward moving transects too. Among the leftward moving transects T13 scores the highest lateral movement distance of -632.9m and least distance of -51.01m in stretch near T5(Table 4.2.4).

Now in terms of the mean rate of migration, T23 scores the highest rate of right bank line migration of 24.63m $^{-1}$ whereas T5 has the lowest of 0.82m^{-1}.

Table 4.2.4 Statistics of right bank migration over the period 1955 to 2017

Right Bankline movement											
Sl. No.		1	2	3	4	5	6	7	8	Total migration (m)	Average (m y^{-1})
Time		1955	1970	1976	1987	1994	2005	2010	2017		
Years (accumulative)		1	16	22	33	40	51	56	62		
TRANSECTS	T1	0	454.77	479.04	-114.53	-142.5	148.2	104.9	-365.28	564.6	9.11
	T2	0	409.37	323.41	51.21	-60.95	26.37	-21.62	-564.59	163.2	2.63
	T3	0	5.09	308.96	-318	130.1	90.77	-390.07	-10.4	-183.55	-2.96
	T4	0	220.27	246.2	-492.56	404.03	122.98	-549.73	-62.2	-111.01	-1.79
	T5	0	324.9	293.93	-394.12	384.9	6.99	-658.13	-9.48	-51.01	-0.82
	T6	0	381.09	346.19	-335.57	201.08	78.38	-603.83	16.45	83.79	1.35
	T7	0	87.31	344.57	-251.9	-62.4	293.63	-226.32	-18.15	166.74	2.69
	T8	0	69.9	300.4	-44.61	18.71	35.6	-33.12	10.4	357.28	5.76
	T9	0	215.83	362.77	-12.95	-12.78	55.39	-4.57	-23.6	580.09	9.36
	T10	0	362.68	223.44	1.23	-14.71	8.12	12.38	-38.7	554.44	8.94
	T11	0	154.95	140.9	3.81	-29.75	25.01	5.1	-25.4	274.62	4.43
	T12	0	-567.03	417.87	-242.31	35.2	24.47	8.94	-28.33	-351.19	-5.66
	T13	0	0.1	282.39	-1050.34	96.6	56.6	60.3	-78.55	-632.9	-10.21
	T14	0	-12.06	233.85	-549.36	72.53	28.55	-11.06	-31.23	-268.78	-4.34
	T15	0	65.18	242.45	-754.61	124.51	-3.25	-16.56	82.24	-260.04	-4.19
	T16	0	1564.53	105.42	-1052.64	-115.1	17.9	42.83	-143.65	419.29	6.76
	T17	0	2455.2	-326.05	-1484.22	-208.7	173.32	82.4	76.42	768.37	12.39
	T18	0	702.55	-31.79	47.91	-160.95	347.25	106.43	-159.21	852.19	13.75
	T19	0	386.77	159.78	21.46	74.3	34.76	57.11	65.21	799.39	12.89
	T20	0	74.25	142.34	-10.96	82.6	111.6	23.7	-49.42	374.11	6.03
	T21	0	35.6	211.49	-88.5	-310.11	54.32	-15.8	-4.32	-117.32	-1.89
	T22	0	549.3	30.18	24.8	-154.96	30.68	80.43	53.06	613.49	9.90
	T23	0	454.66	1006.07	-298.93	349.1	68.72	-16.55	-35.72	1527.35	24.63
	T24	0	612.51	47.35	58.38	10.2	16.78	-7.29	3.71	741.64	11.96
	T25	0	71.54	79.85	688.41	-417.3	-166.26	32.28	-123.86	164.66	2.66
	T26	0	533.29	304.31	72.64	28.34	-244.67	-83.38	56.08	666.61	10.75
	T27	0	142.76	211.08	13.34	-39.28	-249.75	71.06	-112.64	36.57	0.59
	T28	0	338.61	93.71	-48.61	-105.16	-68.59	24.85	-7.82	226.99	3.66
	T29	0	-42.28	52.54	159.7	-14.35	-9.3	-4.08	-31.5	110.73	1.79
	T30	0	133.03	273.97	-1.62	24.75	16.81	-11.79	0.27	435.42	7.02
	T31	0	-47.9	360.5	-186.63	8.99	63.56	287.53	-189.69	296.36	4.78
	T32	0	13.19	476.7	-183.99	-2.15	-41.3	-34.84	-58	169.61	2.74
	T33	0	474.87	-608	-79.3	8.48	71.11	-50.84	31.97	-151.71	-2.45
	T34	0	-955.64	850.65	-139.15	17.66	42.13	7.43	-0.68	-177.6	-2.86
	T35	0	221.52	257.5	70.1	218.24	-8.51	25.28	-88.16	695.97	11.23

Note: + (positive) denotes Rightward migration ; - (negative) denotes Leftward migration.

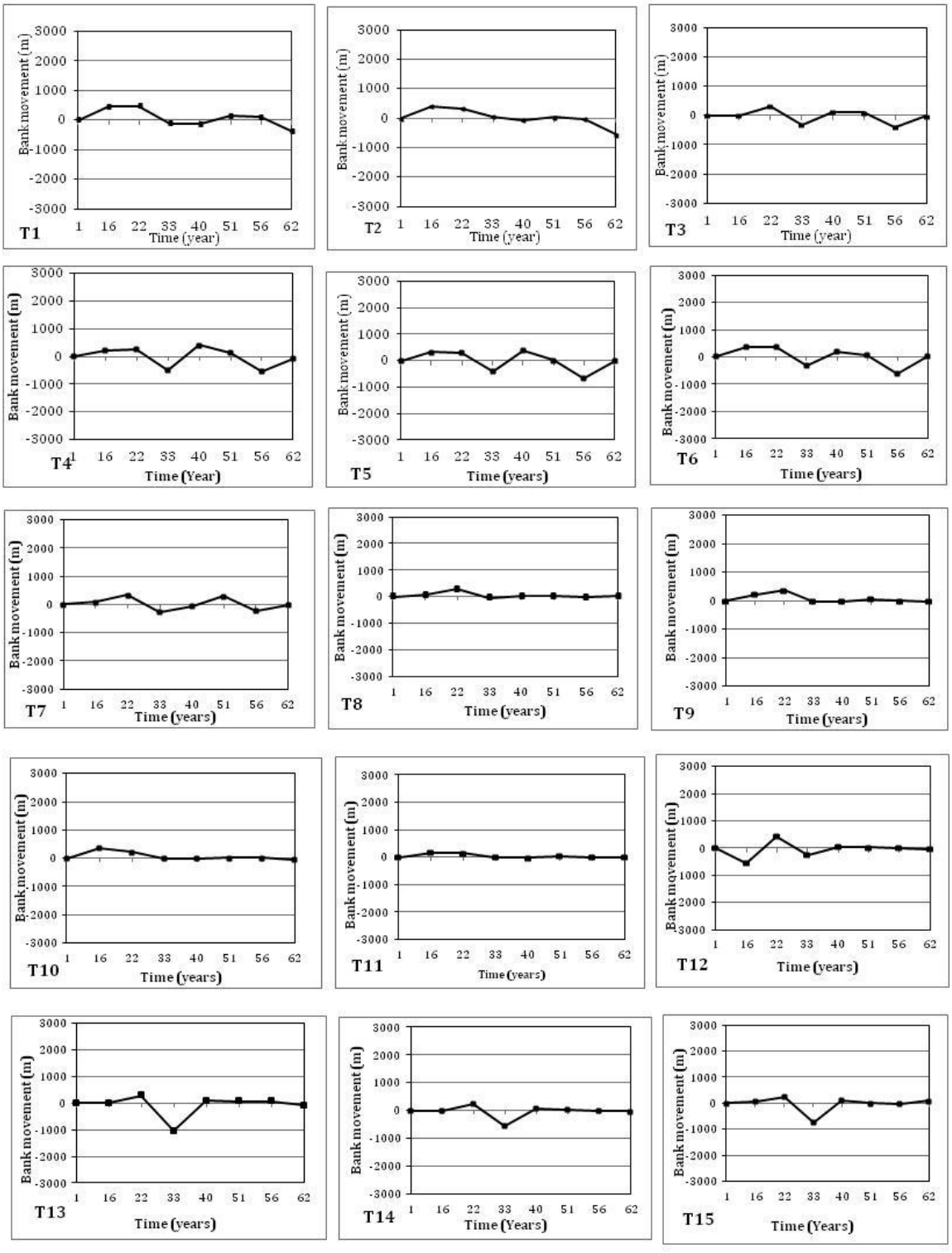
Bank movement (m)
3000
2000
1000
0
-1000
-2000
-3000
1 16 22 33 40 51 56 62
Time (year)
T1
T2
T3
Time (Year)
T4
Time (years)
T5
T6
T7
T8
T9
T10
T11
T12
T13
T14
Time (Years)
T15

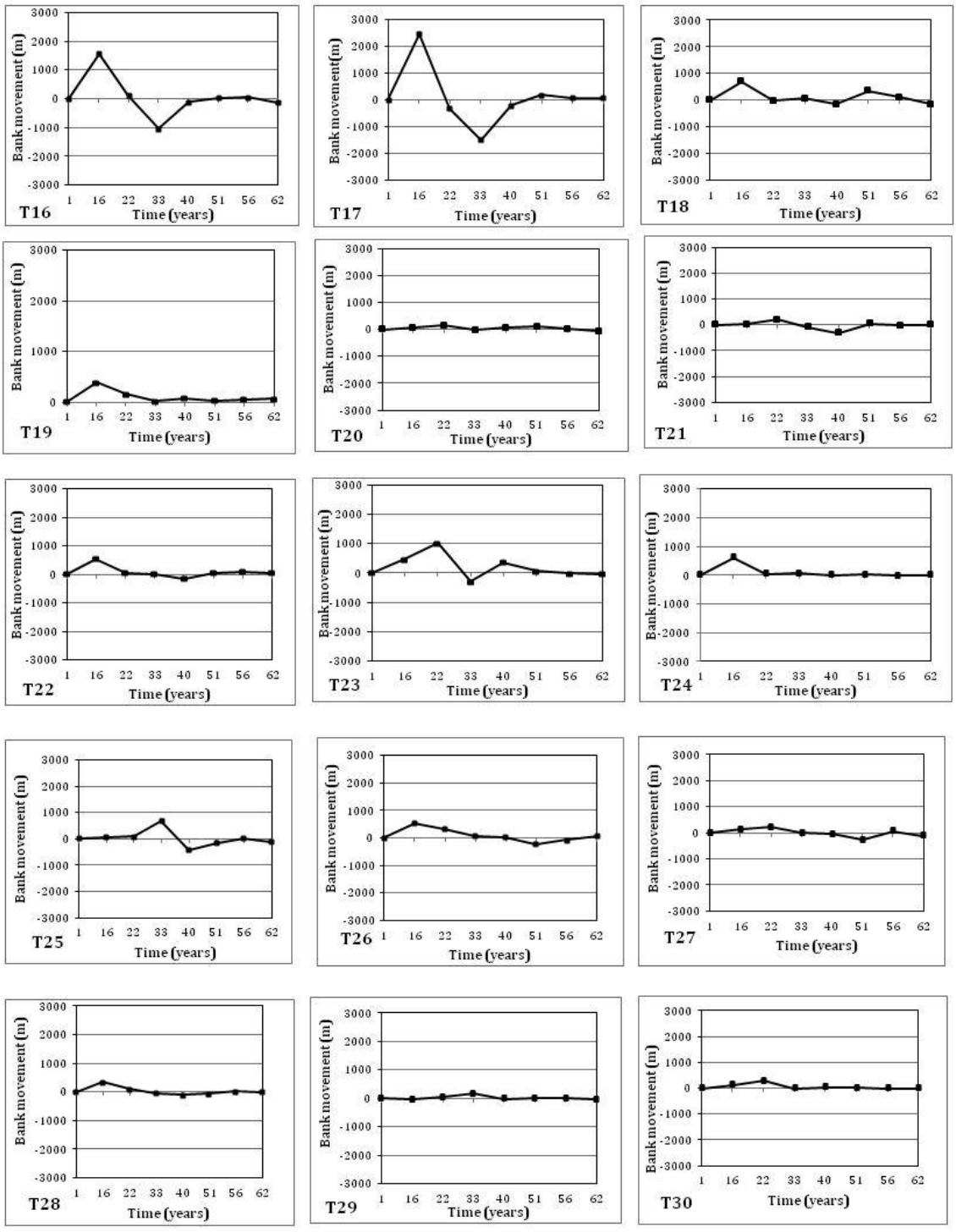
Bank movement (m)
Time (years)
T16
T17
T18
T19
T20
T21
T22
T23
T24
T25
T26
T27
T28
T29
T30

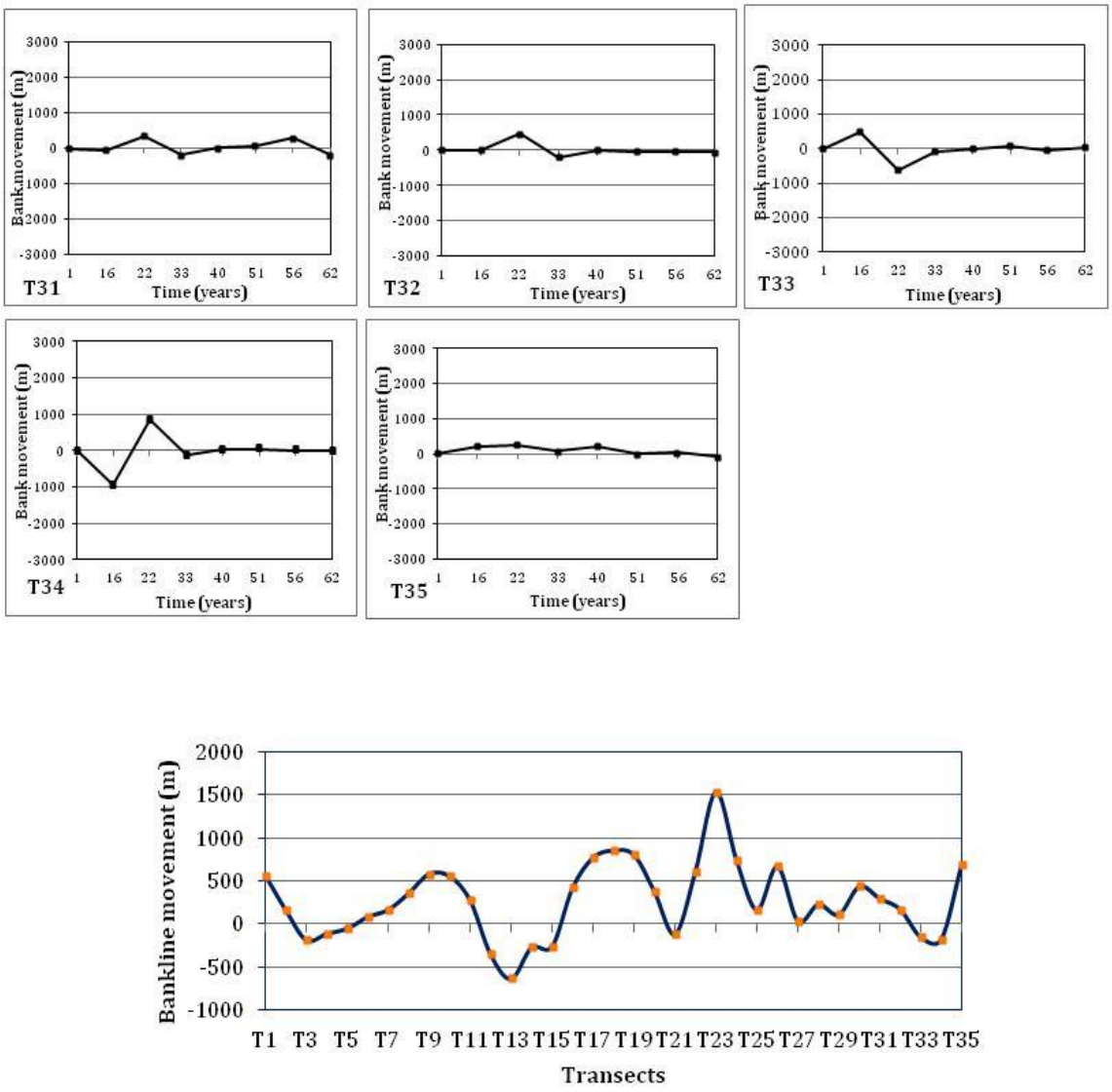

Figure 4.2.14 - Right bank migration during the period 1955-2017.

4.2.3.2.2.2 Left bank line dynamics

The statistics on temporal left bank migration are summarized in Table-4.2.5. Out of 35 transects only 07 transects show an overall leftward direction movement while rest of the 28 transects depict rightward migration (Fig.4.2.15). Keeping conformity with the right bankline, the left bankline too the continuously stretching from T12 to T15 displays the maximum leftward migration. This implies the fact that banks along the left bankline was eroding whereas the right bankline was moving towards the river bed during the

assessment period somewhere maintaining the width of the river. During the whole assessment period; T14 exhibits the maximum total leftward movement of left bank by a distance of -1005.3 m. The least total leftward movement of -79.48 m was observed for T29. The stretches near T4, T5, T6, T7, T21, T32, and T35 are relatively stable, as depicted by less fluctuating curves (Fig.4.2.15). All other transects are unstable. T1, T2, T13, T14, T33 are particularly highly unstable stretches as suggested by more fluctuating curves of these transects. T33 has recorded highest movement of left bankline by a distance of 943.17m during the 22nd year of assessment period in 1976.

In terms of total migration, T18 has recorded maximum lateral left bank movement distance of 1266.29 m. The minimum movement of only 34.65m was recorded in the stretch near T21. The above-mentioned figures are among the overall 35 transects and among rightward moving transects too. Among the leftward moving transects T14 scores the highest lateral movement distance of -1005.3m and least distance of -79.48m in stretch near T29.Now in terms of the mean rate of migration, T18 scores the highest rate of left bank line migration by 20.42m $^{-1}$ whereas T21 has the lowest of 0.56m $^{-1}$ (Table 4.2.5).

Table 4.2.5 Statistics of left bank migration over the period 1955 to 2017

		Left Bank movement									
Sl. No.		1	2	3	4	5	6	7	8	Total migration (m)	Average ($m\ y^{-1}$)
Time		1955	1970	1976	1987	1994	2005	2010	2017		
Years (accumulative)		1	16	22	33	40	51	56	62		
TRANSECTS	T1	0	-266.5	206.67	-147.92	780.76	-598.4	592.3	-51.56	515.35	8.31
	T2	0	-487.85	405.5	-311.75	626.35	-299.26	178.12	35.32	146.43	2.36
	T3	0	-97.23	222.9	38.41	354.23	-347.48	-24.05	29.7	176.48	2.85
	T4	0	-104.59	236.31	184.24	11.92	-118.6	-77.15	47.12	179.25	2.89
	T5	0	90.38	241.54	39.23	-34.7	-6.28	-51.6	3.59	282.16	4.55
	T6	0	-66.62	237.84	42.18	55.77	-12.63	-92.95	10.4	173.99	2.81
	T7	0	-78.27	227.56	29.75	128.38	-56.37	-95.51	2.1	157.64	2.54
	T8	0	-179.55	431.02	208.25	413.83	-25.15	-13.21	-33.51	801.68	12.93
	T9	0	-222.96	370.44	206.64	556.36	-110.5	-4.76	162.5	957.72	15.45
	T10	0	-202.63	165.34	422.69	398.13	-97.8	21.81	38.74	746.28	12.04
	T11	0	-190.24	641.1	253.17	32.09	-53.63	-24.65	139.39	797.23	12.86
	T12	0	-532.87	25.6	274.59	32.03	-36.23	-66.4	6.06	-297.22	-4.79
	T13	0	-861.69	-409.74	444.3	114.06	-152.26	-69.92	201.82	-733.43	-11.83
	T14	0	-812.47	-311.7	266.97	-68.23	-38.2	-58.29	16.62	-1005.3	-16.21
	T15	0	-894.24	-144.25	75.93	-19.52	82.5	-57.94	28.91	-928.61	-14.98
	T16	0	-159.15	93	-2.47	128.71	258.85	-29.21	107.61	397.34	6.41
	T17	0	-304.53	-175.22	309	-315.31	519.17	125.44	423.88	582.43	9.39
	T18	0	-192.94	207.12	360.95	-204.33	543.94	375.66	175.89	1266.29	20.42
	T19	0	231.82	-18.35	301.44	46.28	78.7	-72.57	268.63	835.95	13.48
	T20	0	152.78	124	-39.51	178.73	-109.99	-19.09	0.6	287.52	4.64
	T21	0	20.78	6.63	39.25	-71.57	60.52	-25.7	4.74	34.65	0.56
	T22	0	-36.42	269.81	100.2	59.18	-28.03	4.56	331.61	700.91	11.31
	T23	0	-752.52	722.77	440.05	872.57	457.81	-286.93	-270.91	1182.84	19.08
	T24	0	51.6	246.61	-23.87	308.63	204.97	-67.07	-30.09	690.78	11.14
	T25	0	-203.65	232.14	87	21.89	204.93	-3.66	3.39	342.04	5.52
	T26	0	-213.61	486.84	145.52	93.11	18.73	-23.74	20.83	527.68	8.51
	T27	0	-81.43	245.24	38.42	-131.04	-8.98	-9.3	-1.94	50.97	0.82
	T28	0	152.75	201.62	-117.36	-100.71	-6.14	14.41	-5.17	139.4	2.25
	T29	0	-48.16	-255.48	473.41	-319.98	83.1	-15.34	2.97	-79.48	-1.28
	T30	0	-58.87	190.65	397.62	-399.79	4.48	101.08	-35.85	199.32	3.21
	T31	0	-17.7	182.98	14.86	30.55	-23.23	145.56	-45.29	287.73	4.64
	T32	0	155.66	211.28	-18	21.91	-25.13	-25.64	61.51	381.59	6.15
	T33	0	568.57	-943.17	101.83	-8.17	11.76	14.55	3.45	-251.18	-4.05
	T34	0	-742.28	-26.52	403	-34.01	184.1	-14.86	8.04	-222.53	-3.59
	T35	0	-3.08	109.94	268.43	174.21	56.05	14.88	-48.8	571.63	9.22

Note: + (positive) denotes Rightward migration ; - (negative) denotes Leftward direction.

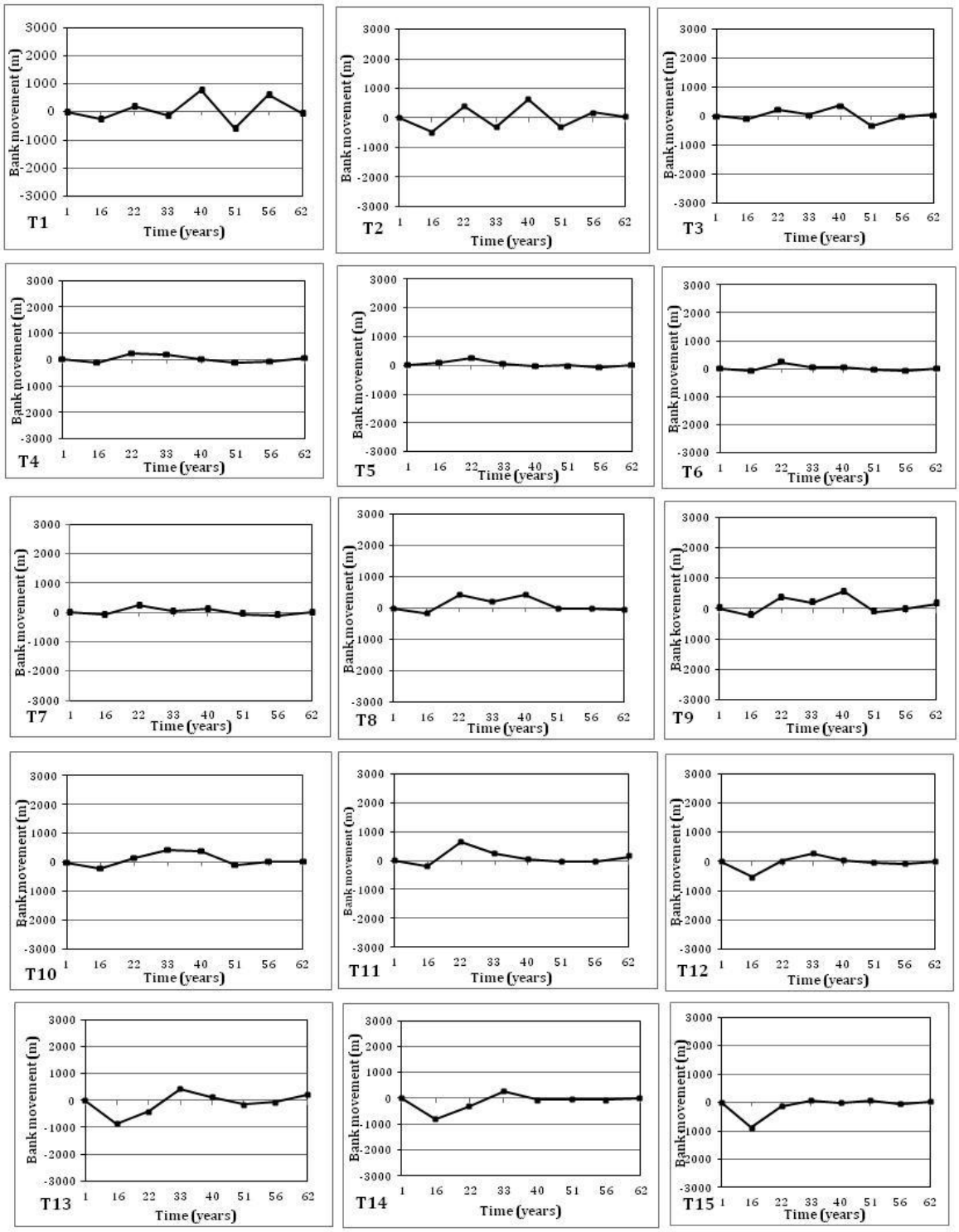
Bank movement (m)
3000
2000
1000
0
-1000
-2000
-3000
1 16 22 33 40 51 56 62
Time (years)
T1
T2
T3
T4
T5
T6
T7
T8
T9
T10
T11
T12
T13
T14
T15

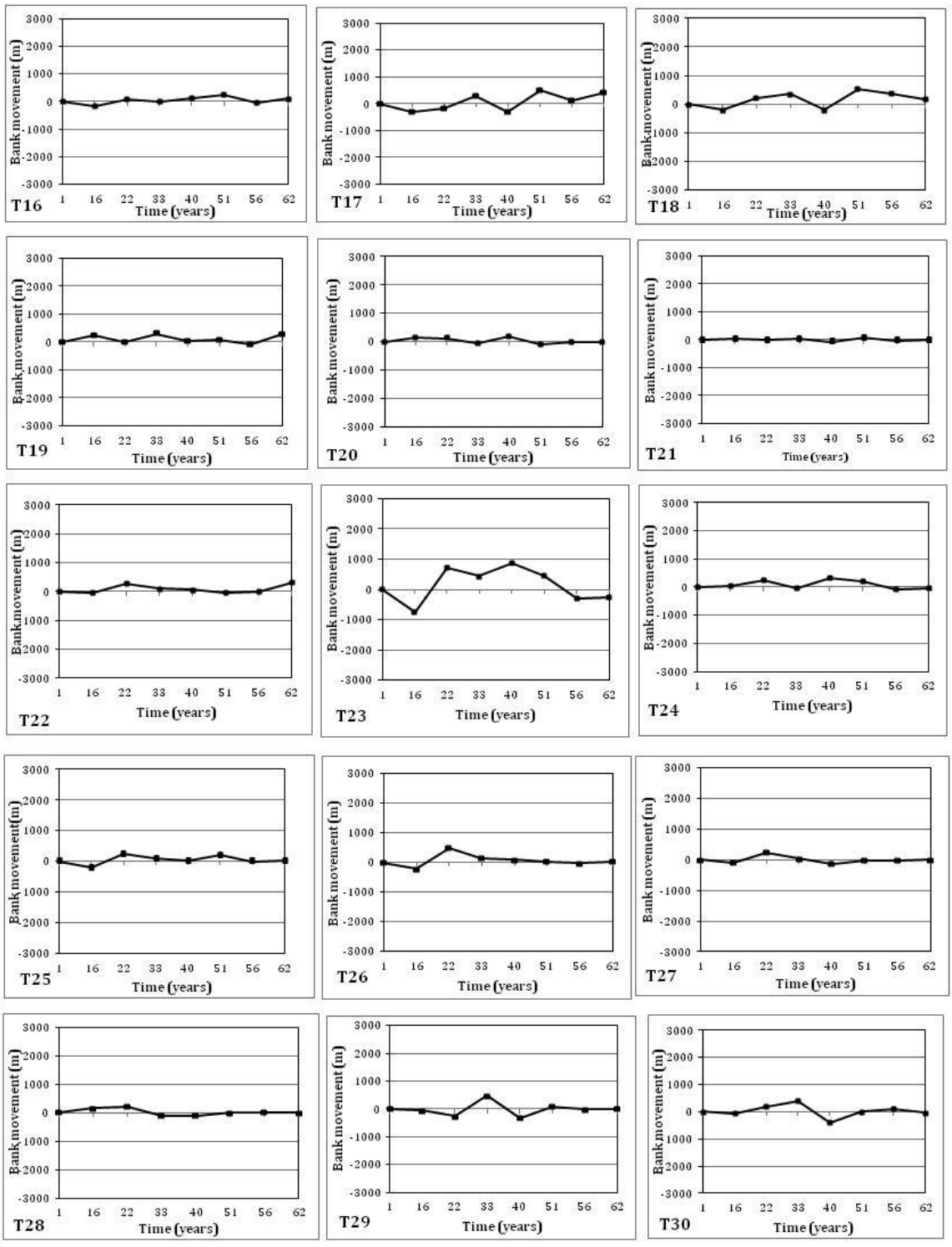
Bank movement (m)
Time (years)
T16
T17
T18
T19
T20
T21
T22
T23
T24
T25
T26
T27
T28
T29
T30

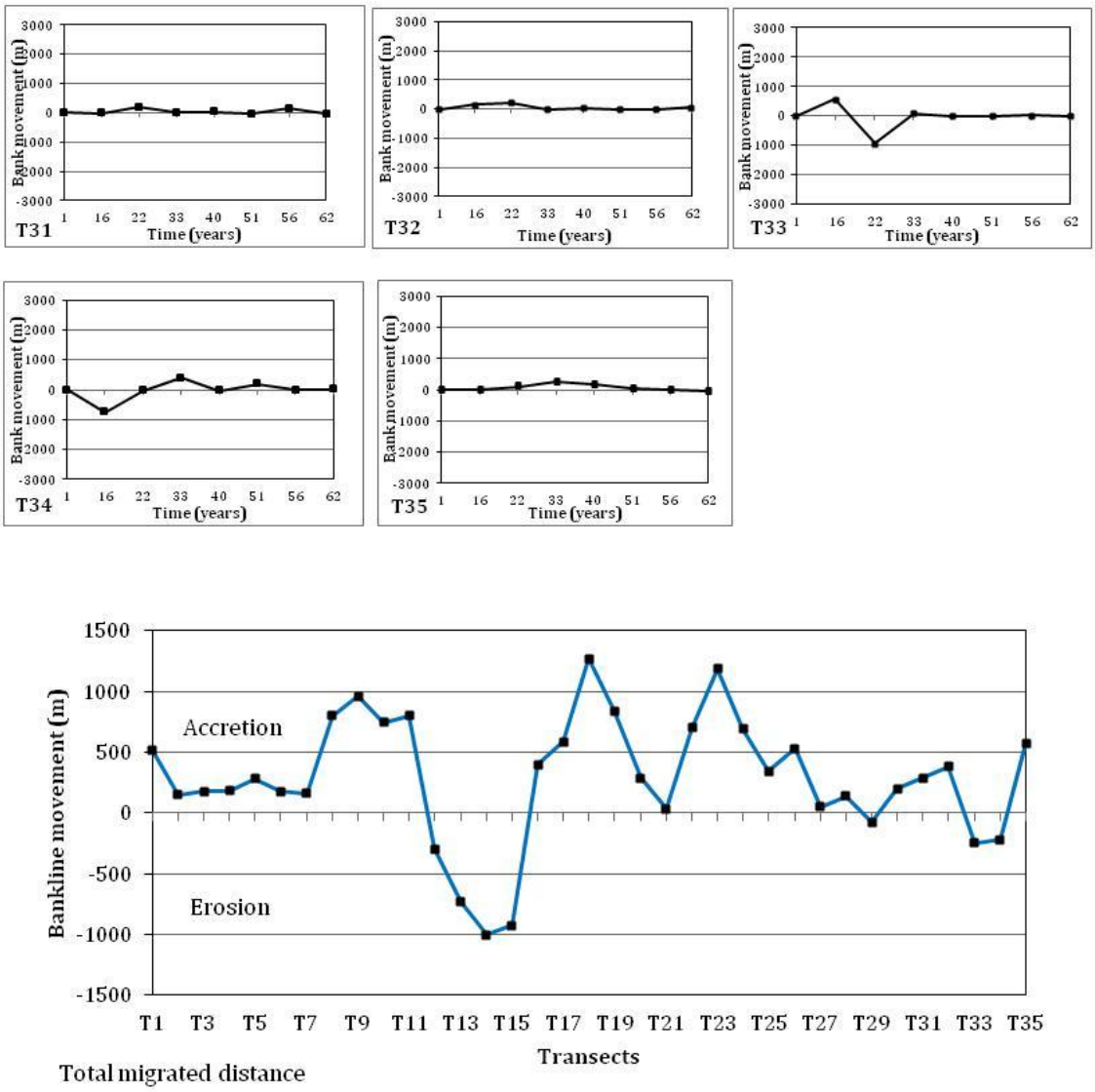

Figure 4.2.15 Left bank migration during the period 1955 to 2017.

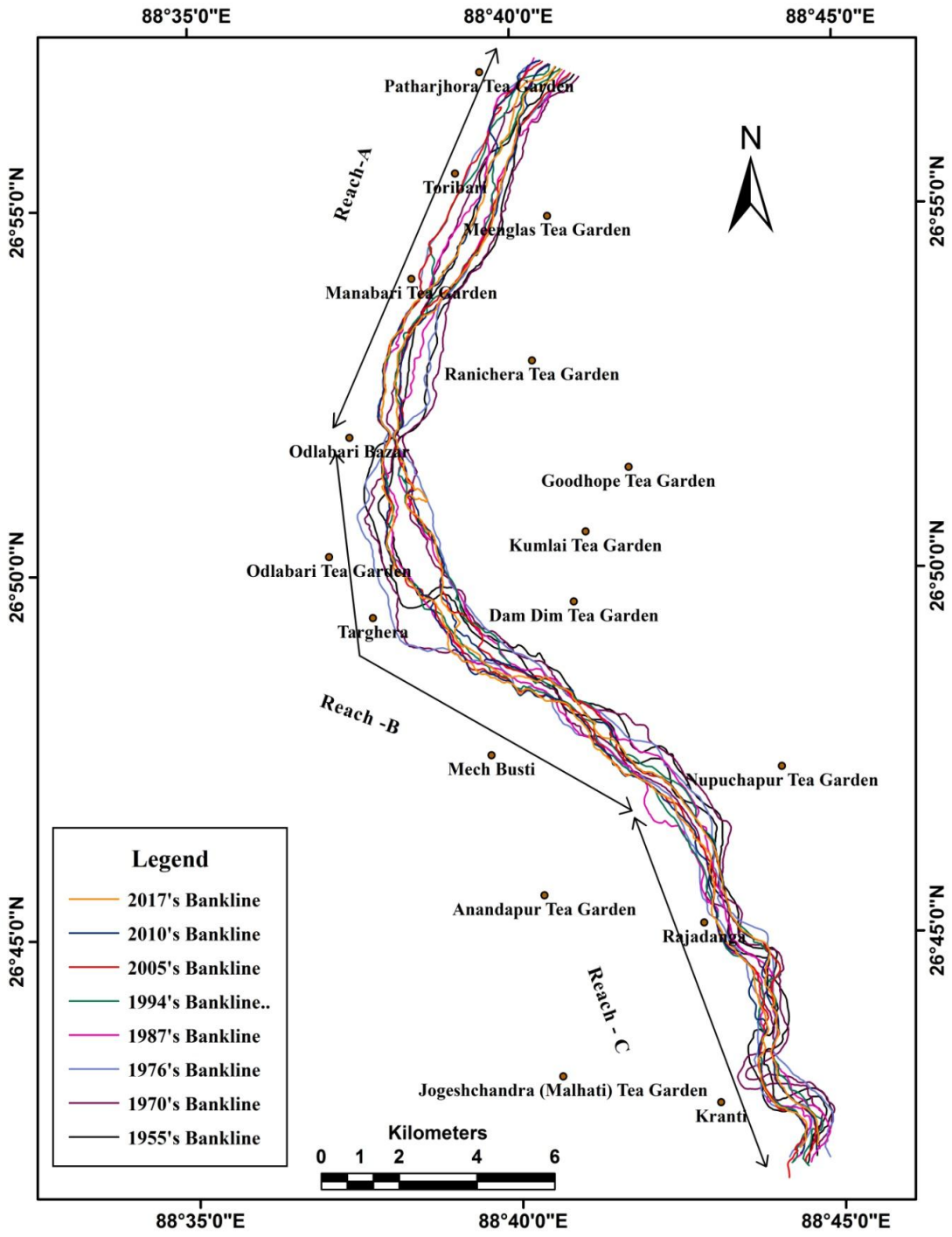

Figure 4.2.16 Bankline migration during the period 1955-2017.

4.2.3.3 Dynamics in Channel Length and active channel area

Channel length was measured along the line equidistant and parallel to the left and right banks of the channel polygon (Midha and Mathur, 2014). Following method as adopted by Tiegs and Pohl (2005), and active channel area was computed for each temporal polygon wherein areas of vegetative mid-channel bars (>1.5 km^2) were excluded.

4.2.3.3.1 Channel length

Channel length dynamics has been studied for whole 62 years (1955 to 2017) from toposheets and Landsat images. After computation it was found that the total channel length has consistently decreased from 37.49 kms during 1955 to 33.59 kms in 2017(Table 4.2.6). There has been channel length variability observed at reach scale in different time phases. The channel length measured ranges from lowest of 10.4 kms in 1970 at Reach A to highest of 13.73 kms in 1955 at Reach A again. Highest gain in channel length of 3.13 % was computed for Reach-A in 1994 whereas highest loss in channel length (14.99%) was recorded in 1976 for Reach-C. The highest loss in channel length in 1976 in Reach-C can be explained through neck-cut off process observed in Reach-C which straightened the channel and thus reduced the channel length considerably (Fig. 4.2.3 B). Unlike active channel area, the Chel River never experienced large variation in its length and has shortened by 4kms loosing 10.4% of its original length in 1955 during the entire assessment period (Fig. 4.2.17).

Table 4.2.6 Reach wise temporal channel length changes from 1955 to 2017 (values in the parenthesis indicate percentage change from previous year).

Reach	Length(km)							
	1955	1970	1976	1987	1994	2005	2010	2017
A	10.59	10.4 (-1.8)	10.49 (+0.87)	10.54 (+0.48)	10.87 (+3.13)	10.61 (-2.39)	10.75 (+1.32)	10.9 (+1.4)
B	13.73	12.53 (-8.74)	12.28 (-2)	11.99 (-2.36)	12.08 (+0.75)	12.2 (+1)	12.16 (-0.33)	12.25 (+0.74)
C	13.17	12.94 (-1.75)	11 (-14.99)	11.07 (+0.64)	10.87 (-1.8)	11.15 (+2.58)	10.62 (-4.75)	10.44 (-1.69)
Total	37.49	35.87 (-4.32)	33.77 (-5.85)	33.6 (-0.5)	45.9 (-36.6)	33.96 (-26.01)	33.53 (-1.27)	33.59 (-0.18)

4.2.3.3 .2 Area

There seems clear influence of channel dynamics on active channel area too. Much variability in the active channel area has been recorded in different time periods (Table 4.2.7). The active channel area ranged from a minimum of 3.25km^2 in 1955 (Reach-C) to the maximum value of 12.68km^2 in the year 1976 (Reach-B). The most notable and maximum gain of channel area of 147.33% was recorded for 1970 in Reach-B. The gain seems to be due to channel widening as a consequence of huge flood of 1968. The other notable gains were 68% in 1970 (Reach-a) followed by gain of 40.03% in 2005 (Reach-A). The significant losses recorded were: maximum of 45.27% during 1976-1987 (Reach-B) followed by 35.91% during 2005-2010 (Reach-A), then 30.1% and 25.57% during 1976-1987 in (Reach-A) and (Reach-C) respectively. It's noteworthy that for the first time the period 1976-1987experienced significant loss of active channel area along all the three reaches which was otherwise continuously gaining area since the beginning of assessment period in 1955. This significant loss of active area can be seen as a self-recovery mechanism of channel from the extreme event of devastating flood of 1968 which had eroded and widened the channel almost by double and a gain of (+87%) of channel area was recorded during the period 1955-1970 (Table-4.2.7). This gaining of channel area continued further during 1970-1976 as it was still easier for river to erode its weaker and less vegetative banks as a result of devastating flood. But the rate of gaining of channel area was much lower (+19.42%) during 1970-1976. It seems during the twelve years between 1976-1987 much of channel banks got stabilized and strengthened due to regeneration of vegetation and thus accretion dominated over erosion along all the reaches. Since then, the changes in channel area have remained much stable within percentage change limit of 20. The overall percentage change in the active channel area of Chel River during the whole assessment period of 62 years (1955-2017) is negligible value of (-1.1%) but the loss is significant since 1976 (Fig. 4.2.17).

Table 4.2.7 Reach wise channel area variation of the Chel River from 1955 to 2017 (values in the parentheses indicate percentage change from previous year.

Reach	Area (sq. km)								
	1955	1970	1976	1987	1994	2005	2010	2017	Overall (% change)
A	5.06	8.5 (+68)	9.4 (+10.6)	6.57 (-30.1)	5.17 (-21.3)	7.24 (+40.03)	4.64 (-35.91)	3.53 (-23.92)	(-30.2)
B	4.31	10.66 (+147.33)	12.68 (+18.94)	6.94 (-45.27)	6.11 (-11.96)	6.01 (-1.64)	6.03 (-0.33)	5.44 (-9.78)	(+26.2)
C	3.25	4.47 (+37.54)	6.14 (+37.36)	4.57 (-25.57)	4.85 (+6.13)	3.74 (-22.9)	3.85 (-2.94)	3.51 (-8.83)	(+8)
Total	12.62	23.63 (+87.24)	28.22 (+19.42)	18.08 (-35.93)	16.13 (-10.79)	16.99 (+5.33)	14.52 (-14.54)	12.48 (-14.05)	(-1.1)

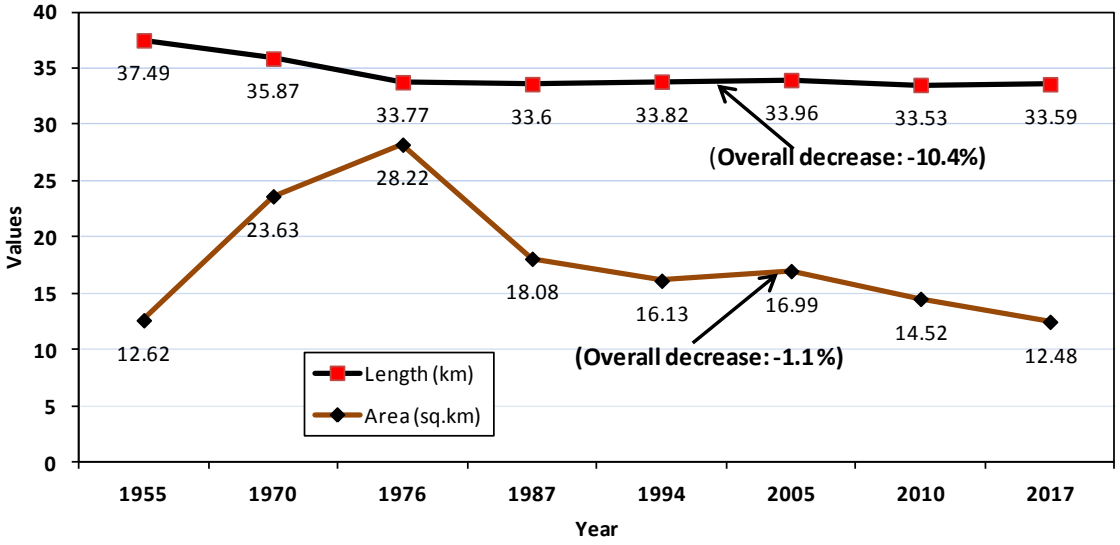

Figure 4.2.17 - Variation in channel length and area from 1955 to 2017 in the Chel River.

4.2.3.4 Variation in channel width

Channel width variation has been studied along the study reach along transects drawn at an interval of 1kms (Fig.4.2.6) from SOI topographical map of 1955 and 1970 and temporal Landsat images of 1976, 1987,1994,2005,2010 and 2017. The active channel width was measured along each transects from one bank line to another and thus includes all the mid channel bars. The details of the measurements are summarized in (Table-4.2.8). The mean channel width values consistently decreased since 1976 and have reached to 418.16m during 2017. The extent of channel width dynamics recorded is +94.6%, +30.6%, -35.1%, -14.8%, +15.4%, - 15% and -19.6 %, for periods 1955-1970, 1970-1976, 1976-1987, 1987-1994, 1994-2005, 2005-2010 and 2010-2017 respectively.

The devastating flood of 1968 can be attributed for more than double increase in mean channel width from 369.02 m in 1955 to 716.75m in 1970. The year wise plotting of channel width along different transects clearly demonstrates that total channel width was always under 1500m with only exception observed with channel width curve of 1976 spiking up to a width value of 2610.3m along transect 17 near Targhera in upper middle reach (Fig.4.2.18). The figure also reveals highly fluctuating temporal channel width curves in the middle reach (T_{10}-T_{25}) followed by moderately fluctuating curves in the upper reach and less fluctuating curves (always marked below 1km mark) in the lower reach. The mean channel width curve shows a constant decline of width values since its highest mark of 911.43m in 1976 to the present day (2017) mean width of 418.16m, almost equivalent to the initial mean channel width of 369.02m of 1955 (Fig.4.2.19).

Further the channel width dynamics were studied for the period 1976-2017 in detail by selecting transects at Manabari (Reach-A), Chelkari (Reach-B) and Baragharia (Reach-C) as representative of each reach. The computed values are summarized in (Table-4.2.9). It is evident from the computation that channel width has decreased significantly in all the segments. In Manabari, the channel width has decreased from 643.64m in 1976 to 435.6m in 2017. Chelkari and Baragharia have experienced a reduction of 832.23 m and 456.81m respectively during the same time period. The extent of channel width reduction is -32.32%,-46.54% and -63.38%, respectively, for these three stations of Segments A-C for the entire assessment period. The satellite images also show significant channel width reduction near these locations (Fig.4.2.20 a-c). These findings are in consistent with dynamics of centerline and bank lines recorded above which reinforces the fact that middle reach is highly unstable followed by moderately unstable upper reach and comparatively stable lower reach.

Table 4.2.8 Transect wise temporal variation in channel width.

Transects	1955 Width (m)	1970 Width (m)	1976 Width (m)	1987 Width (m)	1994 Width (m)	2005 Width (m)	2010 Width (m)	2017 Width (m)
T1	139.71	686.78	1204.7	1232.1	320.2	1042.2	557.3	232.3
T2	124.58	633.33	1012.6	1350.4	661.5	1002.1	802.1	206.7
T3	350.6	745.48	906.2	522.1	314.7	745.7	375.3	337.3
T4	753.93	940.76	1020.5	347.7	740.3	981.5	502.4	407.2
T5	794.54	1047.9	1100.3	670.4	1145.2	1102.7	506.8	483.7
T6	669.79	979.16	1091.7	713.2	865.7	1005.3	438.9	441.9
T7	426.61	581.94	710.3	415.8	220.5	574.2	445.5	427.4
T8	565.84	781.7	907.2	647.4	242.1	312.1	293.4	331.2
T9	492.42	984.85	107.9	842.1	276.4	445.7	446.4	269.7
T10	496.85	1120.8	1150.8	733.9	323.5	432.8	427.3	345.5
T11	207.27	226.52	632	378.4	310.7	405.4	423.6	267.7
T12	601.04	564.62	960.5	442.4	451.4	516.8	589.2	541.2
T13	311.86	1070.62	1820.1	331.3	311.2	523.5	652.1	506.6
T14	366.43	1183.28	1760.8	942.8	1084.8	1146.2	1194.7	1131.5
T15	439.1	1296.36	1807.7	961.3	1112.4	1002.1	1062.6	1126.4
T16	157.99	1920.29	1900.4	853.1	612.2	376.8	445.4	197.4
T17	121.48	1270.89	2610.3	1042.3	992.8	641.6	613.8	265.5
T18	185.46	888.71	1105.1	751.8	813.3	582.5	732.4	406.2
T19	243.65	393.97	570.4	291.6	316.7	275.5	402.8	125.2
T20	424.99	340.75	362.1	392.3	298.9	512.3	567.8	516.4
T21	368.5	370.37	585.2	452.5	226.3	211.9	223.4	218.7
T22	343.19	905.42	660.8	591.8	372.2	434.3	512.4	237.9
T23	316.63	989.56	887.1	861.2	462.5	982.7	1081.2	1462.3
T24	285.46	833.69	640.7	723.4	431.4	211.2	275.8	302.2
T25	401.69	676.58	522.2	1121.1	695.2	329.5	352.3	239.3
T26	205.88	653.56	712.5	631.7	574.1	315.7	253.6	285.8
T27	193.26	455.52	380.3	356.8	452.7	216.4	292.2	186.7
T28	239.77	402.72	330.3	402.2	401.4	331.1	345.7	345.6
T29	301.22	303.12	610.7	301.1	613.2	512.3	523.9	492.3
T30	327.35	536.56	673.1	278.7	703.2	704.3	602.3	637.3
T31	315.93	286.73	477.3	264.2	246.4	336.8	474.2	325.7
T32	732.36	334.92	582.6	412.1	403.3	372.4	361.7	256.8
T33	354.21	229.8	557.2	371.1	384.8	452.8	383.4	406.8
T34	526.56	127.55	1021.1	465.7	511.6	374.7	405.6	396.9
T35	129.67	321.27	517.2	321.6	372.2	301.3	312.2	274.2
Mean Channel Width (m)	369.02	716.75	911.43	611.93	521.86	563.27	510.85	418.16
Mean Channel Width (km) % age change in parenthesis	0.37	0.72 (+94.6%)	0.94 (+30.6%)	0.61(-35.1%)	0.52(-14.8%)	0.6 (15.4%)	0.51(-15%)	0.41(-19.6%)

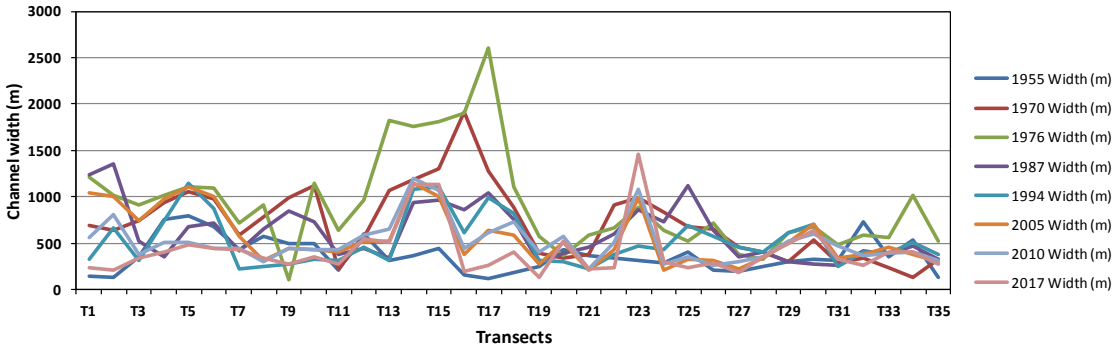

Figure 4.2.18 - Transect-wise channel width variation in the Chel River from 1955 to 2017.

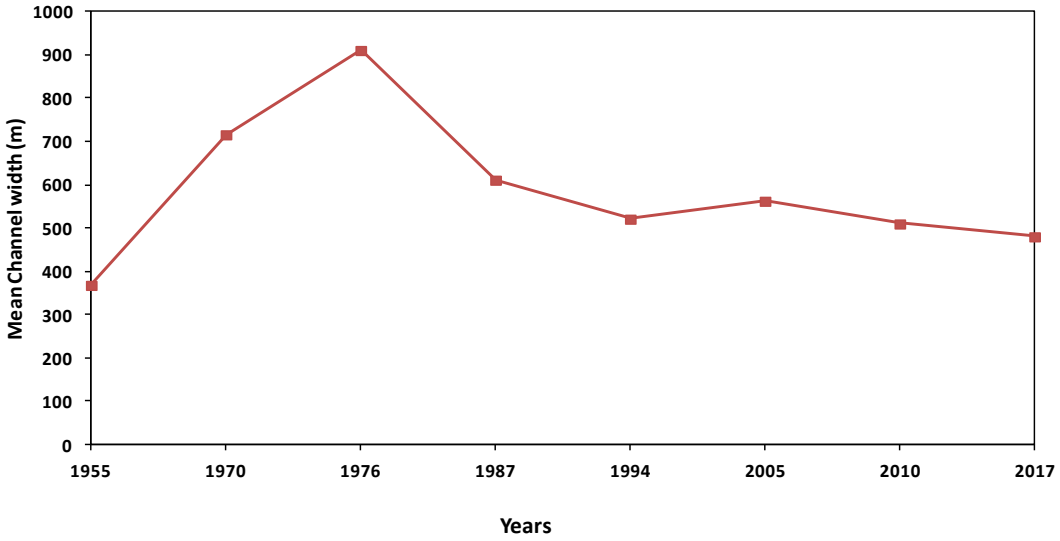

Figure 4.2.19 -Mean channel width variation from 1955-2017 in the Chel River.

Table 4.2.9 Channel width variation at Manabari, Chelkari and Baragharia as representative of Reach A-C respectively from 1955-2017.

Reach	Year	Width (m)
Manabari (Reach-A)	1976	643.64
	1987	449.62
	1994	228.91
	2005	551.5
	2010	489.03
	2017	435.6
Chelkari (Reach-B)	1976	1788.5
	1987	764.15
	1994	968.8
	2005	1048.49
	2010	1055.59
	2017	956.07
Baragharia (Reach-C)	1976	720.75
	1987	521.23
	1994	507.85
	2005	274.73
	2010	220.9
	2017	263.94

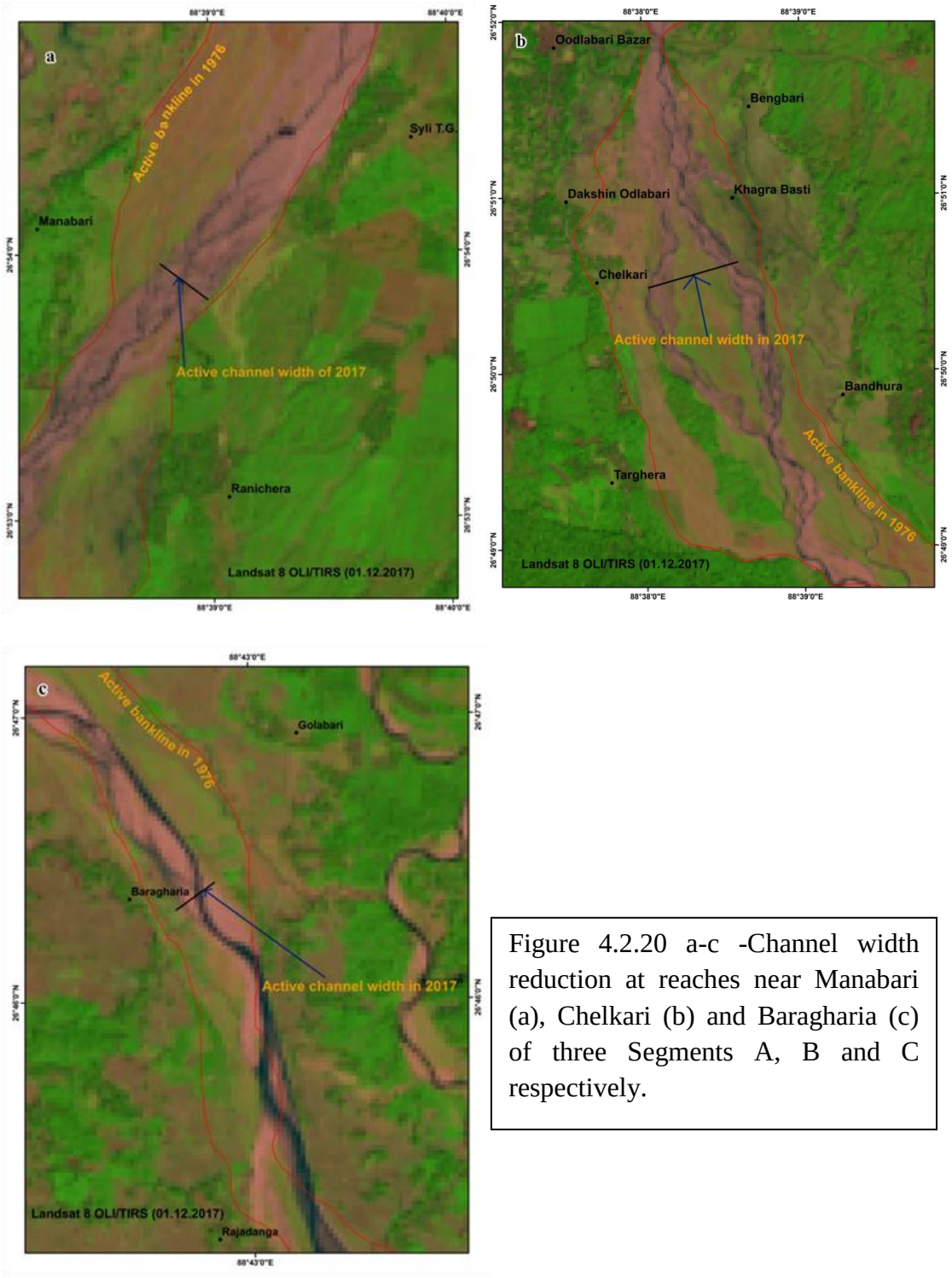

Figure 4.2.20 a-c -Channel width reduction at reaches near Manabari (a), Chelkari (b) and Baragharia (c) of three Segments A, B and C respectively.

4.2.3.5 Sinuosity, Braiding Intensity, and Braid-Channel Ratio

Detailed study on planform dynamics has been attempted through application of several Channel planform indices namely Sinousity Index, Braiding Index, and Braid-

Channel Ratio. Sinuosity, Braiding Index and Braid-Channel Ratio have been calculated only for the period 1976-2017 from Landsat Images. Computation of these parameters from topographical maps was avoided as they display poor details on channel morphology. Changes in channel Braiding Index was computed adopting method given by Brice (1964). Whereas measurement of changes in channel Sinousity Index and Braid-channel Ratio was achieved through Friend and Sinha's method (1993). Each index has been discussed and calculated below;

Sinousity Index has been calculated following Friend and Sinha's method (1993). Accordingly, the sinuosity index, P, is defined as

$$P= Lcmax/LR, \quad (1)$$

Where LR is the overall length of the channel-belt reach measured along a straight line, and Lcmax is the mid-channel length of the same reach, or the mid-channel length of the widest channel, where there is more than one channel. Sinousity Index in fact is a measure of bending of a river. Lower value of it implies the channel is near to straight course and higher values shows more sinuous course.

There are mainly three indices for estimation of Braiding index, viz. Braiding Index (BI) by Brice, Braiding Parameter (Bo) by Rust and Braid-Channel Length ratio (B) by Friend and Sinha. I have employed braiding index (BI) by Brice, 1964 as:

$$BI= 2(\Sigma L_i)/L_r \quad (2)$$

Where Li is the length of all the islands and/or bars in the reach, and L_r is the length of the reach measured midway between the banks of the channel belt (Brice, 1964).

Braid-channel ratio (B) has been measured following Friend and Sinha, 1993 using the relation:

$$B=Lctot/Lcmax, \quad (3)$$

Where Lctot is the sum of the mid-channel lengths of all the segments of primary channel in a reach, and Lcmax is the mid-channel length of the widest channel through the reach.

A higher value of braid-channel ratio means higher braiding of the river which means multiple numbers of channels. In fact, greater braid index implies an unstable river condition. The lowest value of Braid-Channel ratio is 1 that implies a single channel flow with no mid-channel bars.

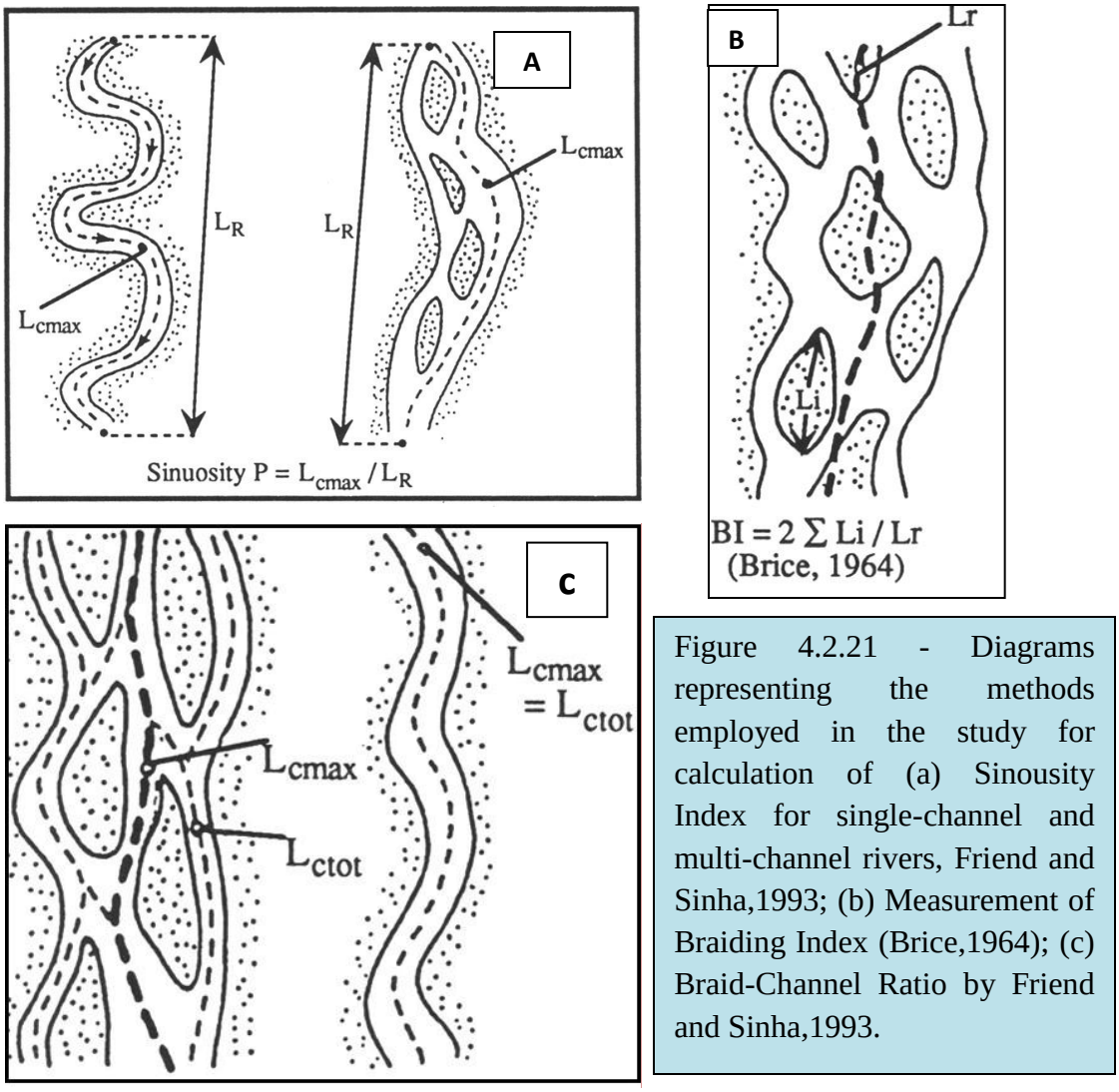

Figure 4.2.21 - Diagrams representing the methods employed in the study for calculation of (a) Sinousity Index for single-channel and multi-channel rivers, Friend and Sinha,1993; (b) Measurement of Braiding Index (Brice,1964); (c) Braid-Channel Ratio by Friend and Sinha,1993.

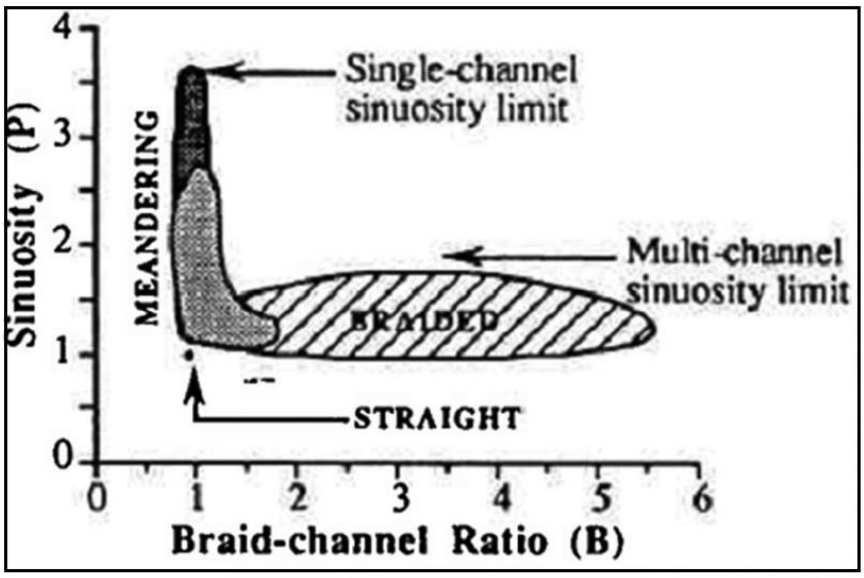

Figure 4.2.22 -Determination of channel pattern based on Sinousity (P) and Braid-channel Ratio (B), Friend and Sinha,1993.

Table 4.2.10 Reach-wise temporal dynamics in planform.

Reach	year	Lctot (km)	Lcmax(km)	Li(km)	Lr(km)	Sinousity Index (P)= Lcmax/LR	Braiding Index, Brice 1964 (B)=2(?Li)/Lr	Braid-channel ratio, B= Lctot/ Lcmax
	1976	16.18	11.23	8.26	10.45	1.07	1.58	1.44
	1987	14.19	11.6	7.08	10.46	1.11	1.35	1.22
A	1994	12	11.83	8.83	10.8	1.1	1.64	1.01
	2005	22.1	11.66	14.13	10.6	1.1	2.67	1.89
	2010	14.23	11.73	4.04	10.7	1.1	0.76	1.21
	2017	13.76	11.8	5.25	10.84	1.1	0.97	1.17
	1976	26.1	11.5	9.69	12.24	0.94	1.58	2.27
	1987	24.23	11.49	8.73	11.98	0.96	1.46	2.11
B	1994	16.01	11.61	8.82	12.04	0.96	1.46	1.38
	2005	22.32	12.32	10.96	12.2	1.01	1.8	1.81
	2010	21.29	11.21	12.67	12.7	0.9	2.01	1.9
	2017	17.5	11.53	7.4	12.23	0.94	1.21	1.52
	1976	19.71	14.84	6.69	10.9	1.36	1.23	1.33
	1987	15.34	15.34	1.65	11.29	1.36	0.29	1
C	1994	13.98	13.98	7.6	10.81	1.29	1.4	0.98
	2005	14.82	14.82	5.75	11.26	1.32	1.02	0.96
	2010	15.51	15.51	4.68	10.52	1.47	0.89	1
	2017	15.46	15.46	6.77	10.46	1.48	1.29	1

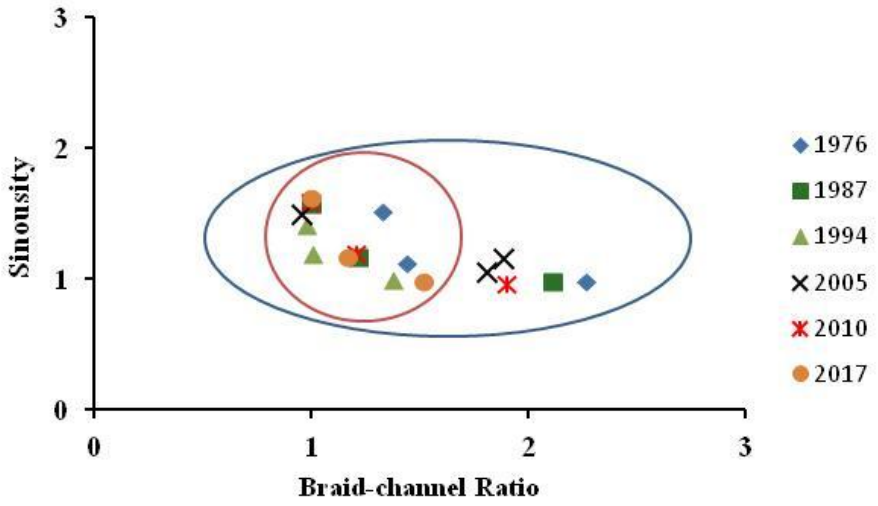

Figure 4.2.23 Temporal variability of Sinousity(B) and Braid-channel Ratio (P) of River Chel.

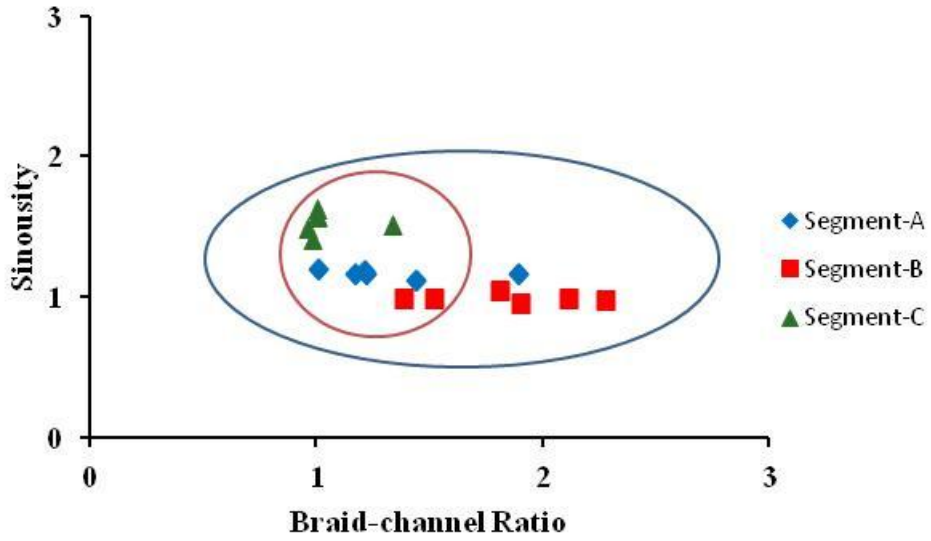

Figure 4.2.24 - Reach- wise temporal variability of Sinousity (B) and Braid-channel Ratio (P) of River Chel.

Computation of planform indices reveals the fact that there are visible trends of decreasing sinuosity and BI of river Chel. Decreasing trend of channel width has already been established in the earlier paragraphs. This decreasing trend in channel width, sinuosity and braiding index seems to be due to construction of embankment and

channelization. There are good number of documented evidences of decreasing width, sinuosity and BI in other parts of the world which validates the fact that channel narrowing begins rapidly after channel confinement.

The sinuosity index and Braid-Channel Ratio values has been computed for each segment or reach of the river for a period of 41 years (from 1976 to 2017) and it reveals the fact that sinuosity values are generally low and constant but Braid-Channel Ratio values are comparatively much variable and horizontally much scattered (Table 4.2.10 and Fig.4.2.23). Friend and Sinha (1993) have used the similar indices for the study of measuring channel morphological variability of Gandak, Burhi Gandak and Bagmati River of India. A river will be of straight pattern when B=1 and P=1 (Figure 4.2.22) because a reach with a single channel with no braids will have a value of 1 for B and will be equal to Sinousity value (P). The horizontally elongated shape of plotted points in a scatter diagram with Braid-Channel ratio values along the abscissa and Sinuosity values along the Ordinate, suggests braided channel pattern, whereas vertically elongated shape points towards the meandering channel pattern (Fig. 4.2.22).

In the present study, the plotting of Segment or Reach wise braid-channel ratio against the sinuosity index (Fig.4.2.23) exhibits that sinuosity values are less variable as compared to braid-channel ratio values. The lowest sinuosity value of 0.9 has been observed during 2010 in Segment-B whereas the highest sinuosity value of 1.48 has been observed during 2017 in Segment-C. Similarly, the lowest braid-channel ratio value of 0.96 is observed during 2005 in the Segment-C whereas the highest braid-channel ratio value of 2.27 is observed during 1976 in Segement-B (Table 4.2.10). Overall, the horizontally scattered points suggest of moderately braided channel pattern of the river (Fig. 4.2.23). The values of braid-channel ratio have consistently decreased since its highest mark of 2.27 in 1976 to lowest value of 0.96 in 2005 and then by 2017, the values in each segment became near 1 which is suggestive of the fact that Chel river is gradually transforming itself from a braided channel to a straight one. The recent years clustering of points which otherwise were scattered horizontally and elongated further confirms the transition of channel form from braided to straight. The Reach wise plotting of points suggests that Segment- B is the most braided reach followed by Segment-A and

Segment-C. Segment-C has always been a near straight reach throughout the assessment period of 41 years (Fig. 4.2.24).The consideration of Sinousity and Braiding Index for the entire study reach of Chel River reveals the fact that channel configuration dynamics led to an overall decrease of braiding index by 20.6% and a negligible increase of sinuosity index by 4.5% in 41 years i.e., from 1976 to 2017 (Table 4.2.11 & Fig.4.2.25).

Table 4.2.11 Temporal variation in Sinousity and Braiding Index values of entire study reach from 1976-2017 (values in the parentheses indicate percentage change from previous year).

Year	Sinuosity Index	Braiding Index
1976	1.12	1.46
1987	1.14(+1.8%)	1.03 (-29.5%)
1994	1.12 (-1.8%)	1.5 (+45.63)
2005	1.14 (+1.8%)	1.83 (+22%)
2010	1.16 (+1.8%)	1.22 (-33.33%)
2017	1.17 (+0.9%)	1.16 (-4.92%)
Overall % change	(+4.5%)	(-20.6%)

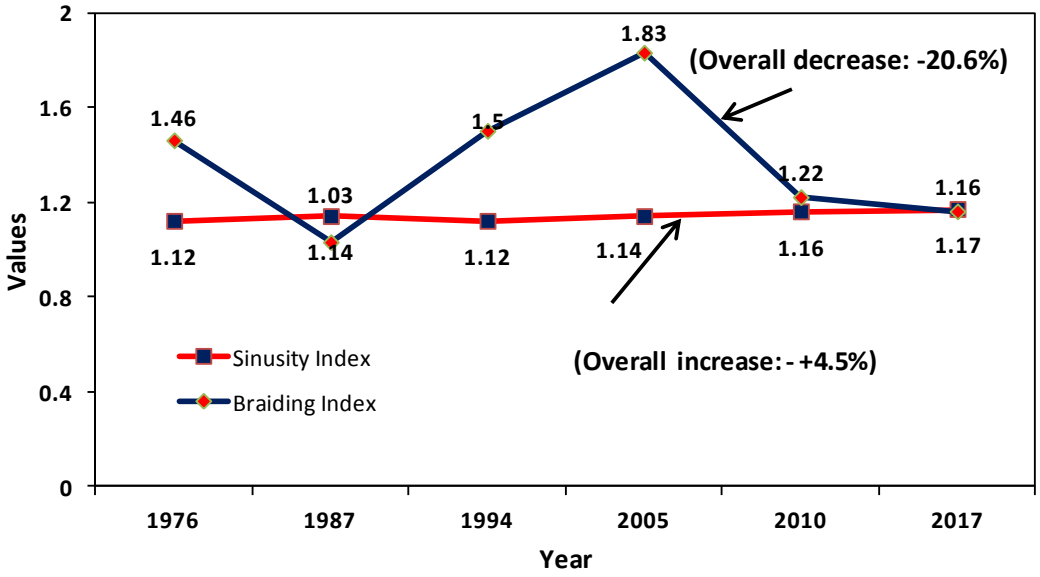

Figure 4.2.25 Variation in Sinousity Index and Braiding Index values from 1976 to 2017 in the Chel River.

Major Findings

- The general trend of channel centerline migration is rightward. Out of 35 transects only along 9 trancests leftward movement of the centerline was observed.
- In conformity with the channel centerline, both right and left banklines depicts rightward migration.
- The total channel length has consistently decreased 37.5 km during 1955 to 33.6 km in 2017.
- Much variability in the active channel area has been recorded during the entire assessment period.
- The mean channel width has consistently decreased since 1976 and has reached to 418.16m in 2017.
- Computation of planform indices shows decreasing trends of Sinuosity and braiding index.
- The decreasing trend in channel width, BI and sinuosity seems to be due to heavy extension of embankments.

Conclusion

The present sub-chapter considerably establishes the fact that Chel River has undergone various phases of planform changes during the assessment period of 62 years from1955-2017. The significant changes observed were increased instability in terms of channel widening, increasing number of neck cut-offs, occurrences of avulsions, decreasing sinuosity, braiding intensity and channels' overall westward movement of the river.

4.3 Confluence Dynamics

Introduction

Channel confluences form an important component of the river systems as they influence morphology and hydrology of the reaches both upstream and downstream of the confluence (Roy and Sinha, 2007). From hydraulic perspectives, river confluences are active sites for occurrence of turbulence with convergent and divergent movements, resulting in upwelling and down welling of flows and formation of lateral vortex (Morisawa, 1968). Stevaux et al., 2009 describes channel confluences as sites of drainage systems with complex hydraulic interactions provided by the integration of two different flows which constitutes an environment of "competition and interaction" with gradual dynamism in flow velocity, river discharge and structure, physical and chemical properties of water and channel morphology. Thus, it's not hard to imagine the implications of shifting of such complex sites. The implications can be far reaching and multi-faceted i.e., hydrological, morphological, engineering related, basin management, religious belief etc. The dynamics of confluence points affects the availability of water and pattern of sediment dispersal in different reaches and around the confluence points (Roy and Sinha, 2007). From engineering point of view, such movements triggers scouring or aggradation and thus poses threats to riverine infrastructures. In India, confluence points bear aesthetic and mythological significance too, as confluence points of many great rivers are revered as holy place and many religious institutions are located at such confluences. Roy and Sinha, 2007 argues that study of river confluence dynamics also holds significance geologically as confluences generate peculiar sedimentary facies and the understanding of confluence dynamics can provide significant insight to alluvial architecture around the confluences. River confluences along the Ganga River also hold archeological significance as a number of human settlements have been reported around the Ganga- Yamuna confluence (Williams and Clarke, 1984, 1995).

Inspite of so much significance,there is limited number of studies on confluence dynamics in Ganga plains (Tangri, 1986; Roy and Sinha, 2005, 2007). In the vicinity, channel confluence studies are almost non-existent. Recent works on lower Jaldhaka river

system exhibit channel confluence dynamics in the Dooars region of Sub-Himalayan West Bengal (Chakraborty and Datta,2013 and Chakraborty and Mukhopadhyay,2014).

In the present section movements of two confluence points namely, Chel-Kumlai confluence and Chel-Neora confluence in the lower Chel-Neora river system has been analyzed using multi- temporal Landsat Images and topographical sheets. The various fluvial processes responsible for confluence dynamics and the morphological implications of such confluence dynamics have been examined for. The temporal scale of the study spans 62 years (1955-2017) and establishes the fact that the confluence points of the rivers have shifted both upstream and downstream during the assessment period.

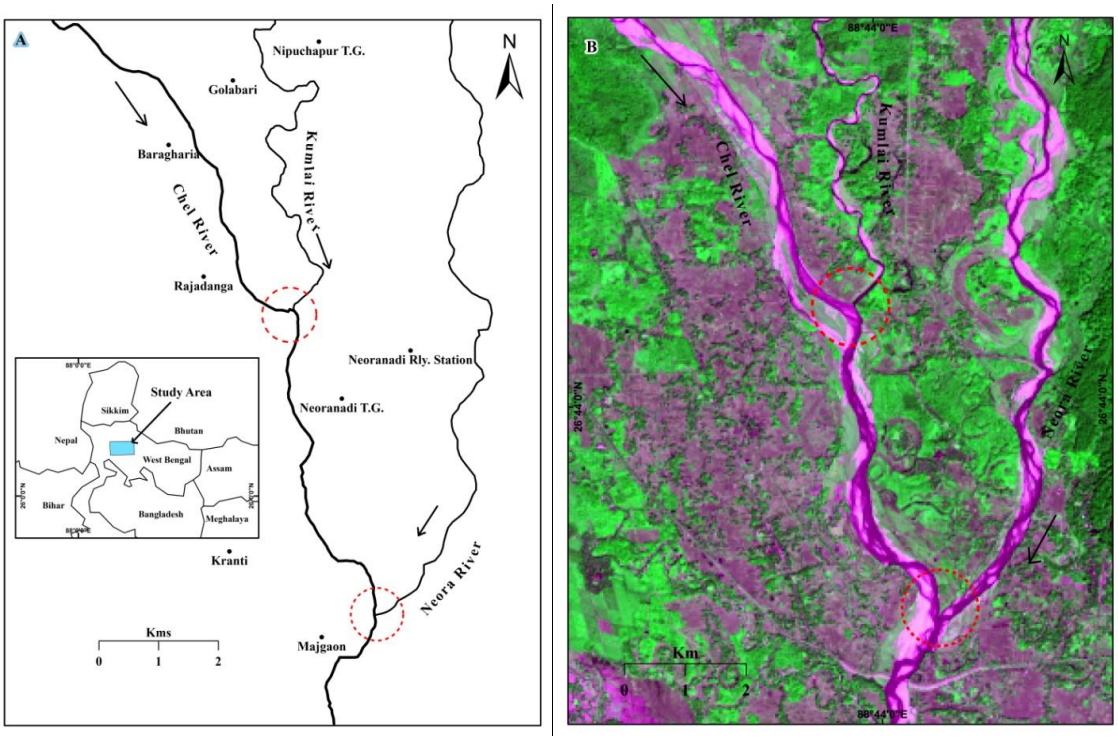

Figure 4.3.1 (A) Base map showing the study area in the Sub-Himalayan West Bengal. (B) Landsat 8 OLI / TIRS image of 1st December, 2017. Red dotted circles represent two confluence points, the Chel-Kumlai confluence and Chel-Neora confluence, under investigation.

4.3.1. Study area

The lower Chel river system under study is located between 26°41'N and 26°47'30"N latitudes and between 88°41'E and 88°46'30"E longitudes (Fig. 4.3.1). It

forms a part of an elongated area that spreads in west-east direction and is a zone of transition between Eastern Sub -Himalayan Mountains and North Bengal Gangetic plains. This part of the foothill region to the east of Teesta River is popularly known as the "Dooars" spreads over Darjeeling, Jalpaiguri and Alipurduar districts of West Bengal. The region is dissected heavily by parallel and sub-parallel rivers of Himalayan origin in almost north-south direction. Few rivers originating in the piedmont and foothill serve as tributaries of major river of Himalayan origin.

The foothill situation makes the region ideal for aggradations. The rivers originating from different elevations of Himalaya, flowing southwards suddenly loose considerable gradient, velocity and thus transporting capacity before reaching the plains. Therefore, large amount of Himalayan detritus composed of large-medium and small sized boulders, cobbles, pebbles, sand, silt particles etc. gets deposited at or near the break of slope, transforming the region into a region of coalescing alluvial fans. These alluvial fans are being dissected into a bunch of interfluves by numerous southward flowing rivers which disperse and grades the sediments distance wise to a great extent and thus we find presence of fine silt and clay beyond a distance of 25kms (approx.) from the mountain front. The piedmont surface is inclined in the root part between 25‰ and 10‰, before gradually declining to 5‰ and less, and at a distance of 30 km from the mountains to below 2‰ in areas not affected by uplift (Starkel et al.2008). The continuous aggradations fill- In the channels resulting in rise of river beds and thereby cause river migration mostly through avulsions during floods.

The region thus exhibits a geomorphic mosaic of high elevated terraces, channels, channel bars, flood plains, The signatures of spatio-temporal adjustments of rivers to the variation in controlling factors of tectonic, hydrologic, geomorphic and anthropogenic origin are strewn all over the region in the form of paleochannels, meander cutoffs, avulsion marks, misfit streams, ox-bow formations, crevasse splays etc.

Kumlai origantes from Sakam Reserved Forest at an elevation of 300m(approx.) in the piedmont surface below Gorubathan and meets Chel to its left bank near Rajadanga at an elevation of 105m above msl. On the other hand, Neora River originates in the Lesser Himalayan region at an elevation 2200m and flowing southwards it joins the Chel also

from the left near Majgaon downstream of Kranti at an elevation of 94 m above mean sea level.

4.3.2. Data used and methodology

This study uses topographical maps and multi-temporal Landsat images to map the temporal variation of confluence points and channel positions during 62 years from 1955 to 2017. Therefore, six Landsat scenes (1976, 1987, 1994, 2005, 2010, and 2017) with Path/ Row: 139/41; 149/41 for 1976 image were collected from the USGS site (http://earthexplorer.usgs.gov/). One 1: 250,000 scale U.S. Army corps of Engineers NG 45-8, Series –U502 topographical map (1955) was acquired from the University of Texas site (https://legacy.lib.utexas.edu/maps/india.html). All the Landsat scenes were downloaded from the USGS through their data visualization tool GloVis.

ArcGIS (version 10.1; ESRI,Redlands,CA) software package have been used for preparation of GIS database relating to temporal channel configuration maps. All the images were processed through ERDAS imagine (v. 9.0) software and then were georeferenced based on Universal Transverse Mercator (UTM) projection system (Northern hemisphere 45 zone and world geodetic system (WGS) 84) manually using GCPs collected during GPS survey.

Junction angles between channel courses at the confluence points were measured as the angle between the tangents on the curved thalweg from the confluence point of the two channels (Roy and Sinha, 2007). The morphological implications of confluence dynamics were analyzed through three parameters namely, sinuosity, braiding, and channel width. The sinuosity and braiding intensity were computed following Friend and Sinha (1993). Native knowledge about the area was also applied.

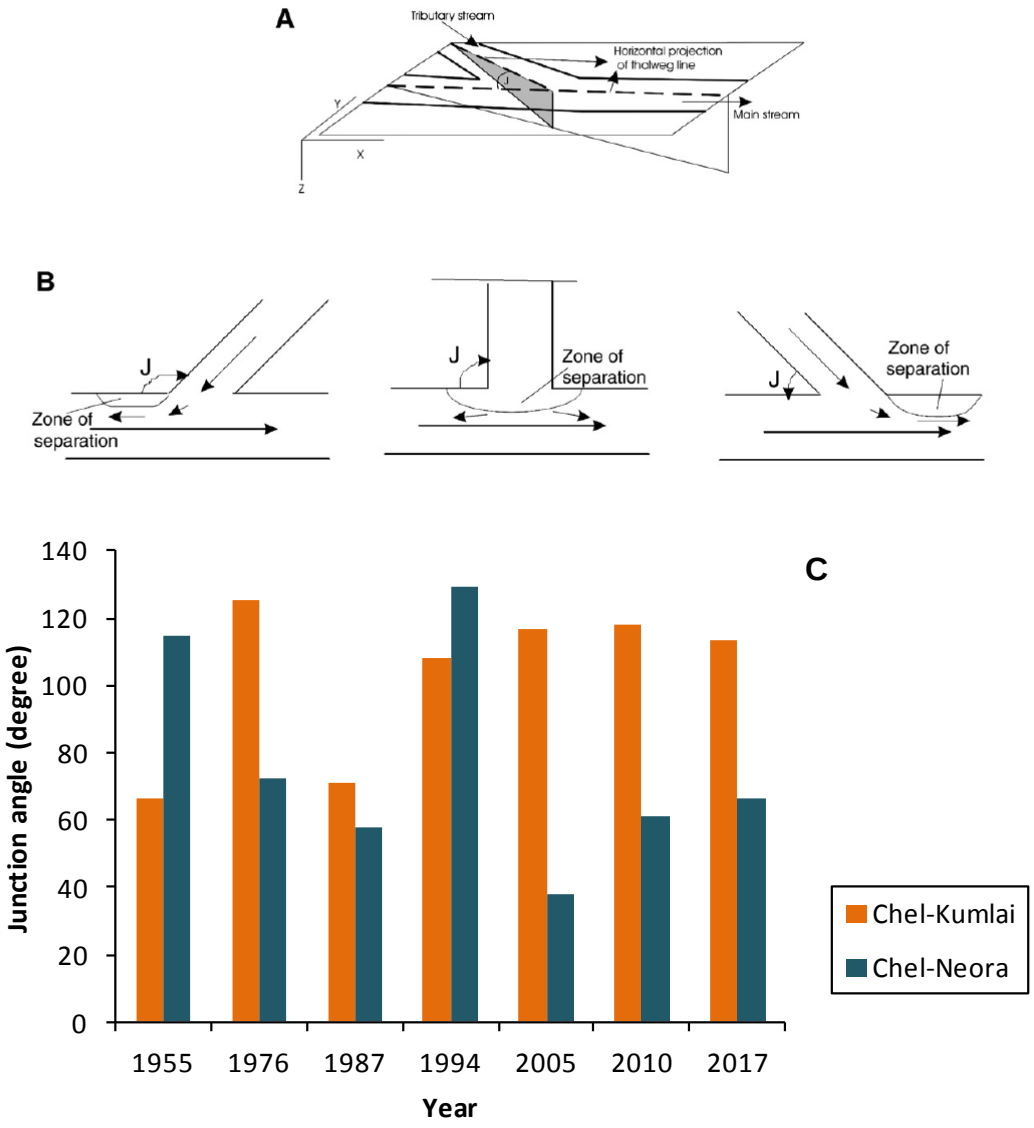

Figure 4.3.2. (A) Measurement of junction angle (adapted from Roy and Sinha,2007). (B) Relation between junction angle and zone of separation; low junction angle favours mouth bar formation immediately downstream of the confluence point (adapted from Roy and Sinha,2007) (C) Plot showing variation in junction angle for the Chel-Kumlai and Chel-Neora confluences for the period 1955-2017 (computed by the author).

Table 4.3.1 Computed values of junction angle variation for Chel-Kumlai and Chel-Neora confluence points during 1955-2017.

Year	Junction angle (Degree)	
	Chel-Kumlai	Chel-Neora
1955	66.5	115
1976	125	72.5
1987	71	57.5
1994	108	129
2005	117	38
2010	118	61
2017	113.5	66.5

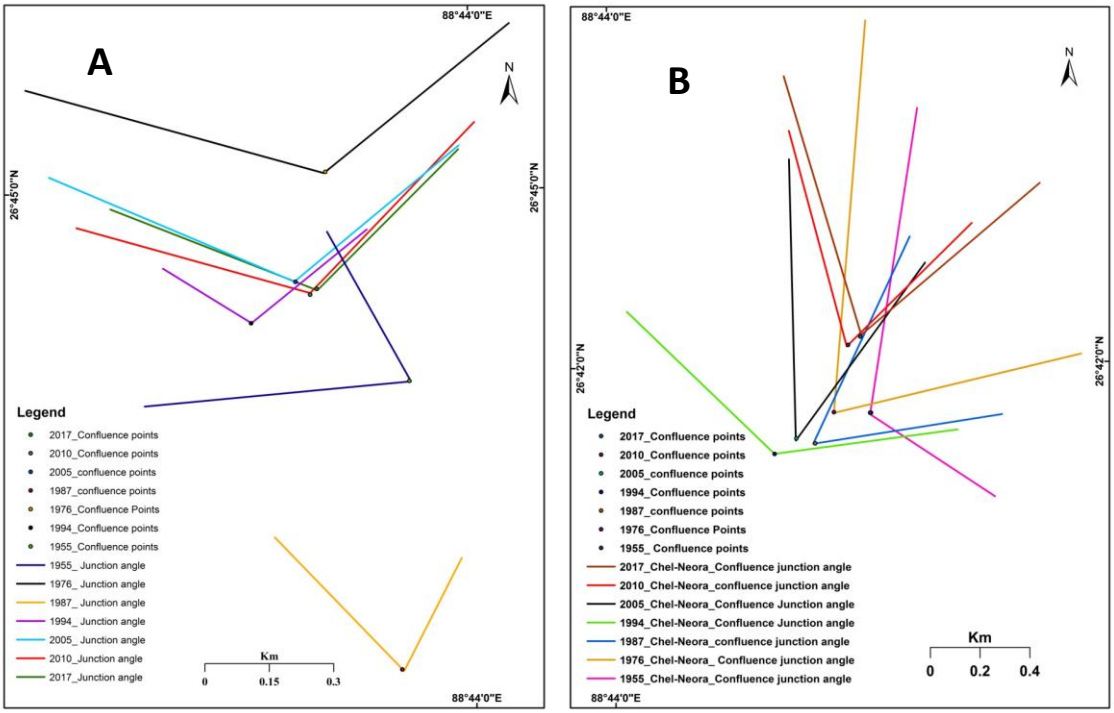

Figure 4.3.3 Channel confluence junction angle dynamics of (A) Chel-Kumlai and (B) Chel-Neora rivers during 1955-2017.

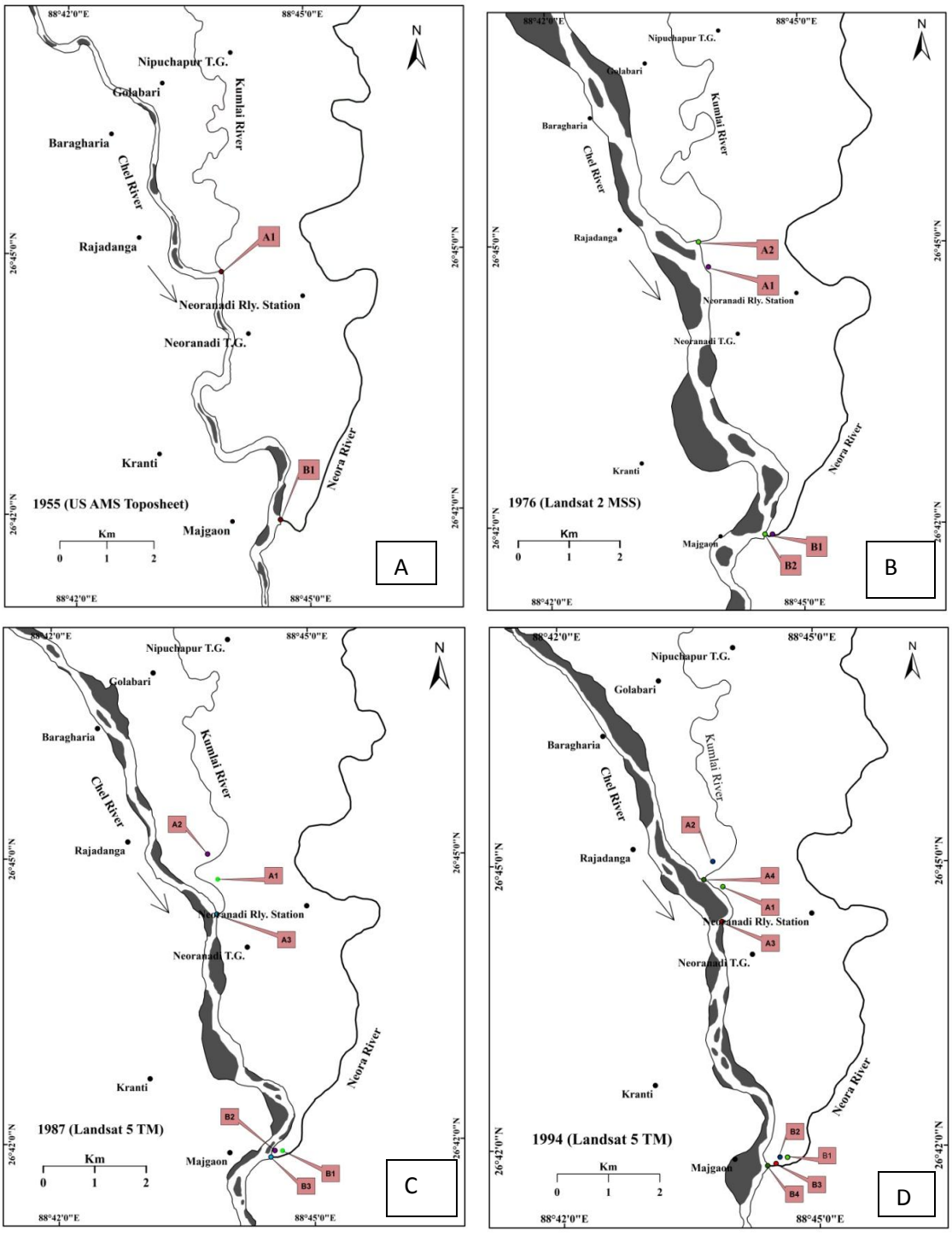
88°42'0"E
88°45'0"E
N
Nipuchapur T.G.
Golabari
Baragharia
Chel River
Kumlai River
Rajadanga
Neoranadi Rly. Station
Neoranadi T.G.
Kranti
Neora River
Majgaon
26°45'0"N
26°42'0"N
A1
B1
1955 (US AMS Toposheet)
Km
0 1 2
A
A2
B2
1976 (Landsat 2 MSS)
B
A3
B3
1987 (Landsat 5 TM)
C
A4
B4
1994 (Landsat 5 TM)
D

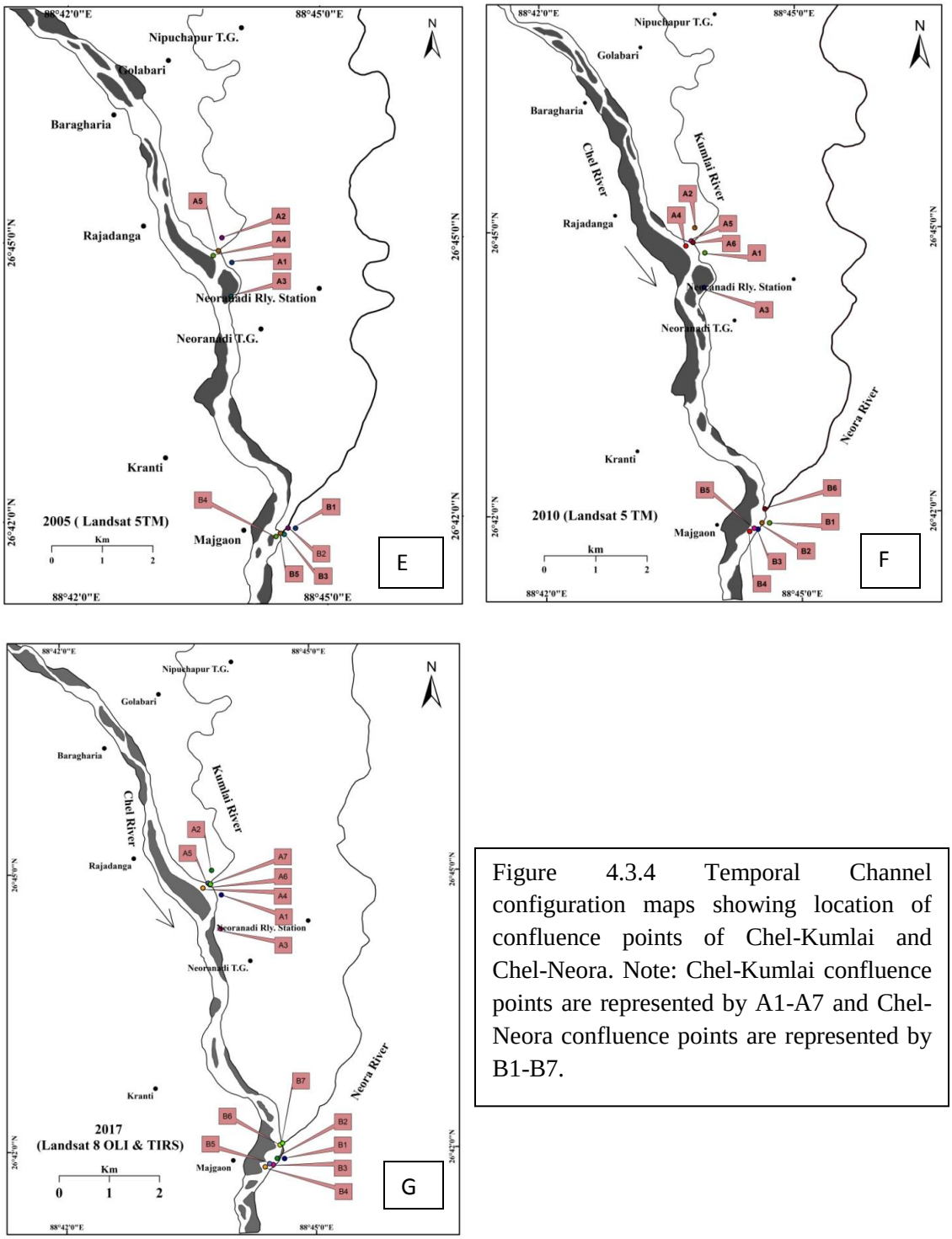

Figure 4.3.4 Temporal Channel configuration maps showing location of confluence points of Chel-Kumlai and Chel-Neora. Note: Chel-Kumlai confluence points are represented by A1-A7 and Chel-Neora confluence points are represented by B1-B7.

4.3.3. Description of Confluence dynamics

The Chel and Kumlai rivers formed a confluence (A1) in 1955 (Fig.4.3.4A) near Rajadanga. While at the same time Chel- Neora confluence point (B1) was near Majgaon. Systematic reconstruction of channel configuration shows that the width of river Chel near the confluence has increased manifold from 189.3 m to 679 m during the period 1955-1976 which brought the left bank of Chel river nearer to river Kumlai. Consequently, the earlier lower course of river kumlai has been engulfed into river chel thereby the Chel-Kumlai confluence point has shifted by 531m upstream to A2 (Fig. 4.3.4B). The junction angle between the Chel-Kumlai has increased almost by double and sinuosity of Kumlai has decreased. During the same period, the river Chel has shifted westward along with increase in channel width downstream of Kranti. This has resulted in westward shift of confluence point between Chel and Neora by 154m to B2 (Fig.4.3.4B). During the period 1976-1987, the confluence area between the Chel and Kumlai experienced huge aggradation most probably due to increased bank erosion in the upstream reaches. There has been a marked reduction in the width of Chel river from 679m in 1976 to mere 202.2 m in 1987 near the confluence and river chel has shifted towards the right bank. This aggradation has pushed the Chel and Kumlai rivers southward resulting in downstream movement of the confluence point from A2 to A3 by 1192 m (Fig. 4.3.4C). The Chel-Neora confluence too experience downstream movement by 150.46m during the period 1976-1987 due to accretion only. Within the next seven years a major flow separation develops around 900m upstream of Rajadanga in North-East direction, thus main channel (flow) avulsed through the earlier interfluve and captures the lower Kumlai river by 1994 thereby moving the confluence upstream by 885 m (A4) (Fig. 4.3.4D). It is notable that Kumlai River was almost completely stable during the period. It was due to flow separation of Chel River that a mid-channel bar of size 392 km^2 has come into existence. Further there has been a significant increase in the channel width of river Chel from 177.5 m in 1987 to 548.2m in 1994 just upstream of confluence point. Chel river is cutting short the Kumlai river and flow through its course but at the same time the secondary channels of the Chel river still flow through its earlier course. During the same period the Chel avulsed occupying pre-existing flow course seen during 1976 thereby shifting westward and restricting its flow towards the right bank

downstream of Kranti and almost reach upto village Majgaon. Whereas Neora river is stable during this time period. This local avulsion of Chel seems responsible for the downward shift of confluence point from B3 to B4 by 168.13 m (A4). By the year 2005 the Chel-Kumlai confluence point experience further upstream movement from A4 to A5 by 158m. This upstream movement of confluence point can be attributed to the increase in the size of mid-channel bar developed during 1987-1994 and further leftward movement of main flow of Chel. In the downstream, the Chel-Neora confluence point also exhibits an upstream movement from B4 to B5 by 110m (Fig.4.3.4E). The straightening and westward movement of Neora River decreasing the junction angle is responsible for the same. The flow separation that was observed since 1994 at a distance of around 900m upstream of Rajadanga and was present during 2005 window has been transformed into a single flow and significantly the flow in restricted to the left bank of the Chel river in 2010 window. The confluence point has shifted downstream from A5 to A6 by 55.27m (Fig.4.3.4F). The Chel-Neora confluence point moves 431.82 m upstream from B5 to B6 during 2005-2010 due to eastward movement of river Chel being forced by the increment in the size of point bar east of Majgaon. The period during 2010-2017 exhibits upstream movement of Chel-Kumlai confluence by 22 m due to little eastward movement of river Chel. During the same period Chel-Neora confluence moved upstream from B6 to B7 by 66m (Fig.4.3.4G).

4.3.4. Fluvial mechanisms of Confluence Dynamics

Table 4.3.2, Fig. 4.3.5 and Fig. 4.3.6 summarize the confluence dynamics of the lower Chel-Neora river system and probable fluvial mechanisms behind such dynamism. Note worthily, there are few points that emerge from the study. Firstly, there has been a net upstream shifting of both the confluence points (~ 310.62m for Chel-Kumlai confluence and~ 318.81m for Chel-Neora confluence), but there is no definite trend of movement. The confluence points' movements were variable in different direction and movement rate was also variable. Secondly, various fluvial processes are involved in such confluence movements viz. avulsion, river capture, agradation, variable junction angle. Lastly, there are significant morphological alterations in the lower Chel system during the assessment period which seems to correspond with the confluence dynamics.

4.3.4.1 Avulsions

Avulsion is defined as the sudden and abrupt change in a river course. Floods during the rainy season are often related with the triggering of avulsions (Jones and Schumm, 1999; Jain and Sinha, 2003, 2004; Leir et al., 2005; Mitra et al., 2005). Hydrological variability (mainly flood magnitude), lateral erosion and local aggradations also serve as the triggering factors for avulsion of a channel into nearby channel (Roy and Sinha, 2007). In the study area, the Chel-Neora confluence point moved downstream from B3 to B4 by168.13m during 1987-1994 (Table 4.3.2). Chel avulsed occupying preexisting flow course seen during 1976 thereby shifting westward and restricting its flow towards the right bank downstream of Kranti and almost reach upto village Majgaon. Neora River is stable during this time period (Fig.4.3.6C). Large variability in flood magnitude is characteristics of Sub-Himalayan North Bengal Rivers and thus favors channel instability and cause channel avulsion. So hydrological readjustment can be attributed as the main factor behind the movement. The Chel basin exhibits a classic example of a basin straddle in the zone of transition between the dissected upper hill surface and the lower gently rolling plains (Lama and Maiti, 2019), which favors large scale aggradation, rise in valley floor and consequent channel migration mostly through avulsion during floods. Low stream power, gentle gradient, high sediment yield and proximal positions of rivers are likely to cause avulsions and hence the movement of confluence points.

Table 4.3.2 Summary of spatio-temporal channel confluence dynamics, probable reasons and morphological implications.

Period	Direction of confluence movement	Total shift	Causative process	Morphological changes	Remarks
Chel-Kumlai confluence					
1955-1976	Upstream in Northern direction	A1-A2 (~531m)	Width increment of river Chel and capuring of lower course of Kumlai	P decreased from 1.37 to 1.2 and B increased from 1 to 1.66 for Chel. P increased from 1.59 to 1.77 and B remained unchanged at 1 for Kumlai; J increases.	Net movemet of Chel-Kumlai cofluence (A1-A7) is 310.62m in N-W direction.
1976-1987	Downstream in Southerly direction	A2-A3(~ 1192 m)	Aggradation, width reduction and westward movement of Chel	P decreases from 1.2to 1.19 and B decreases from 1.66 to 1.36 for Chel. P decreases from 1.77 to 1.44 and B remained unchanged at 1 for Kumlai; J decreases.	
1987-1994	Upstream in N-W direction	A3-A4(~904.34 m)	Flow separation ,diversion of main flow of Chel towards the left bank and river capture	P decreases from 1.19to 1.18 and B increases from 1.36 to 1.53 for Chel. P increases from 1.44 to 1.53 and B remained unchanged at 1 for Kumlai; J increases.	
1994-2005	Upstream in N-E direction	A4-A5(~158 m)	Little increment in channel width of river Chel	P decreases from 1.18to 1.11 and B increases from 1.53 to 1.57 for Chel. P remains stable at 1.53 and B remained unchanged at 1 for Kumlai; J increases.	There is no definite trend of the confluence dynamics.
2005-2010	Downstream in S-E direction	A5-A6 (~55.27 m)	Little Westward movement of river Chel	P increases from 1.11to 1.18 and B decreases from 1.57 to 1.53 for Chel. P increases from 1.53 to 1.58 and B remained unchanged at 1 for Kumlai; J remains unchanged.	
2010-2017	Upstream in N- E direction	A6- A7(~22 m)	Little eastward movement of river Chel	Both P and B remains unchanged at 1.18 and 1.53 respectively for Chel. Both P and B remains unchanged at 1.58 and 1 respectively for Kumlai; J decreases.	
Chel-Neora confluence					
1955-1976	Westward direction	B1-B2 (~154m)	Westward shift of river Chel	P decreased from 1.5 to 1.31 and B remains unchanged at 1 for Neora; J decreases.	Net movemet of Chel-Kumlai cofluence (B1-B7) is 318.81m in northly direction.
1976-1987	Downstream in S-W direction	B2-B3(~150.46 m)	Aggradation	P increased from 1.31 to 1.43 and B too increases from1 to 1.21 for Neora; J further decreases.	
1987-1994	Downstream in S-W direction	B3-B4(~168.13m)	Local avulsion	P decreased from 1.43 to 1.41 and B too increases from1.21 to 1.4 for Neora; J increases.	
1994-2005	Upstream in N-E direction	B4-B5 (~110m)	Westward movement and straighning of course of Neora before confuence	P decreased from 1.41 to 1.32 and B too decreases from 1.4 to 1.29 for Neora; J decreases.	There is no definite trend of the confluence dynamics.
2005-2010	Upstream in N-E direction	B5-B6(~431.82m)	Little eastward movement of river Chel before confluence and river capture	P decreased from 1.32 to 1.23 and B too decreases from 1.29 to 1.27 for Neora; J increases.	
2010-2017	Upstream in N-E direction	B6-B7(~66m)	Eastward movement of river Chel	P decreased from 1.23 to 1.19 and B too decreases from 1.27 to 1.25 for Neora; J increases.	

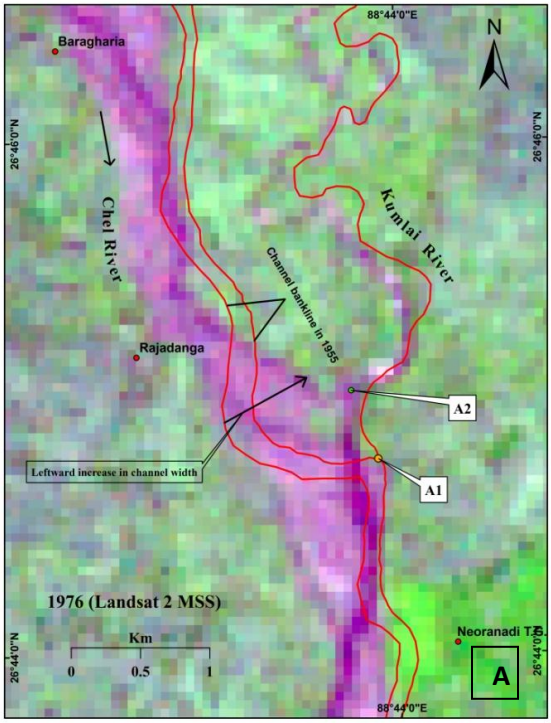
88°44'0"E
N
Baragharia
26°46'0"N
Chel River
Kumlai River
Channel bankline in 1955
Rajadanga
A2
Leftward increase in channel width
A1
1976 (Landsat 2 MSS)
Km
0
0.5
1
Neoranadi T.G.
26°44'0"N
A
88°44'0"E

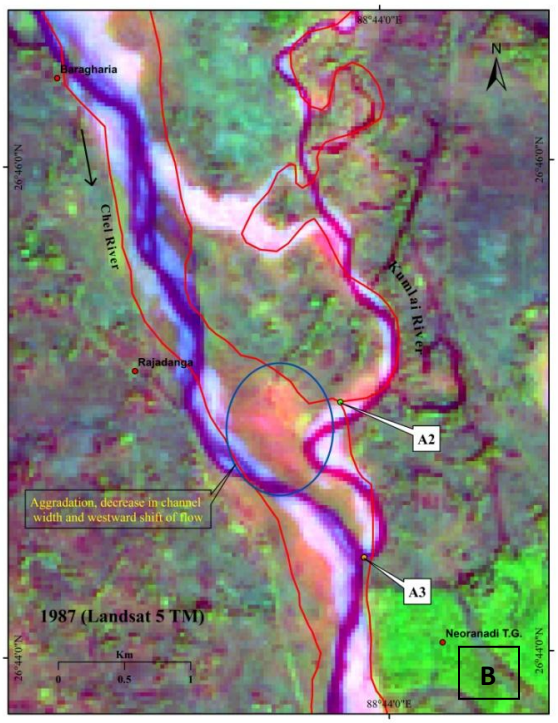
88°44'0"E
N
Baragharia
26°46'0"N
Chel River
Kumlai River
Rajadanga
A2
Aggradation, decrease in channel width and westward shift of flow
A3
1987 (Landsat 5 TM)
Km
0
0.5
1
Neoranadi T.G.
26°44'0"N
B
88°44'0"E

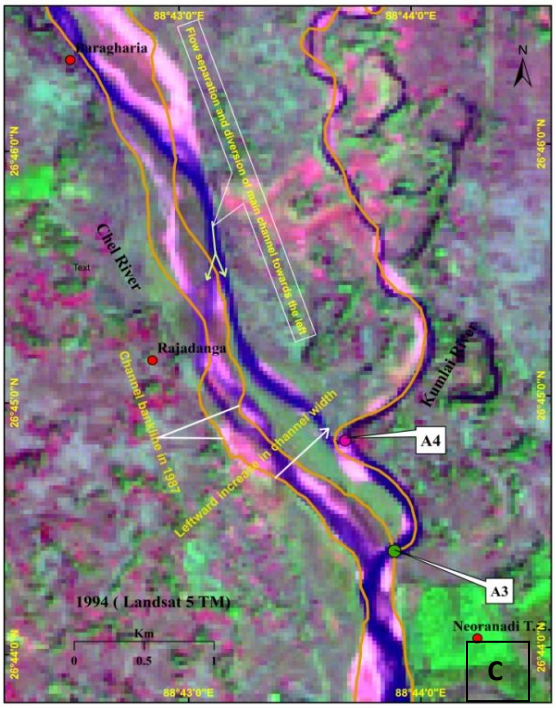
88°43'0"E
88°44'0"E
N
Baragharia
26°46'0"N
Flow separation and diversion of main channel towards the left
Chel River
Rajadanga
Channel bankline in 1997
Leftward increase in channel width
Kumlai River
A4
A3
1994 (Landsat 5 TM)
Km
0
0.5
1
Neoranadi T.G.
26°44'0"N
C
88°43'0"E
88°44'0"E

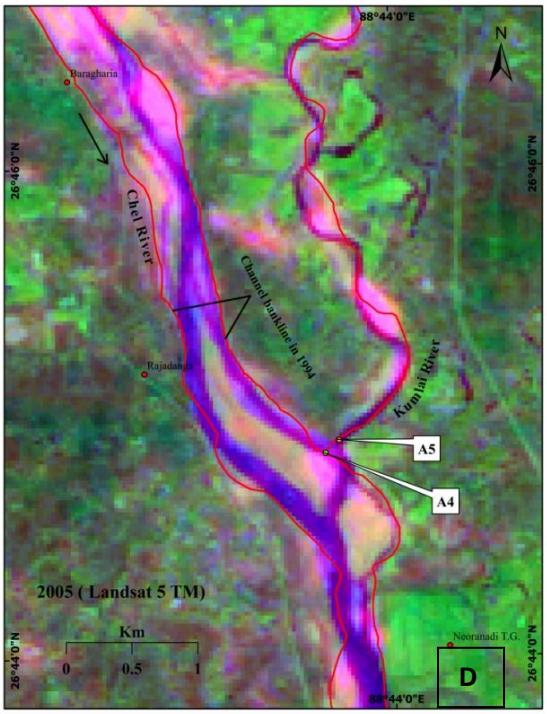
88°44'0"E
N
Baragharia
26°46'0"N
Chel River
Channel bankline in 1994
Rajadanga
Kumlai River
A5
A4
2005 (Landsat 5 TM)
Km
0
0.5
1
Neoranadi T.G.
26°44'0"N
D
88°44'0"E

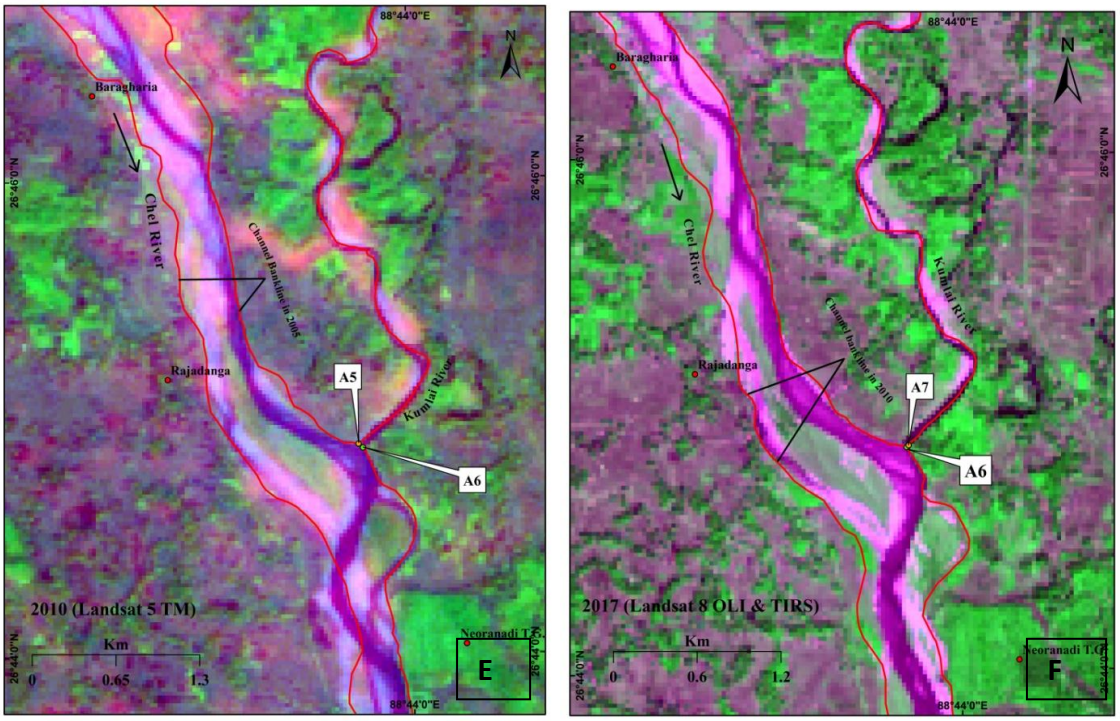

Figure 4.3.5 Enlarged representations of channel confluence point dynamics between the Chel-Kumlai Rivers during the period 1955-2017 and probable reasons.

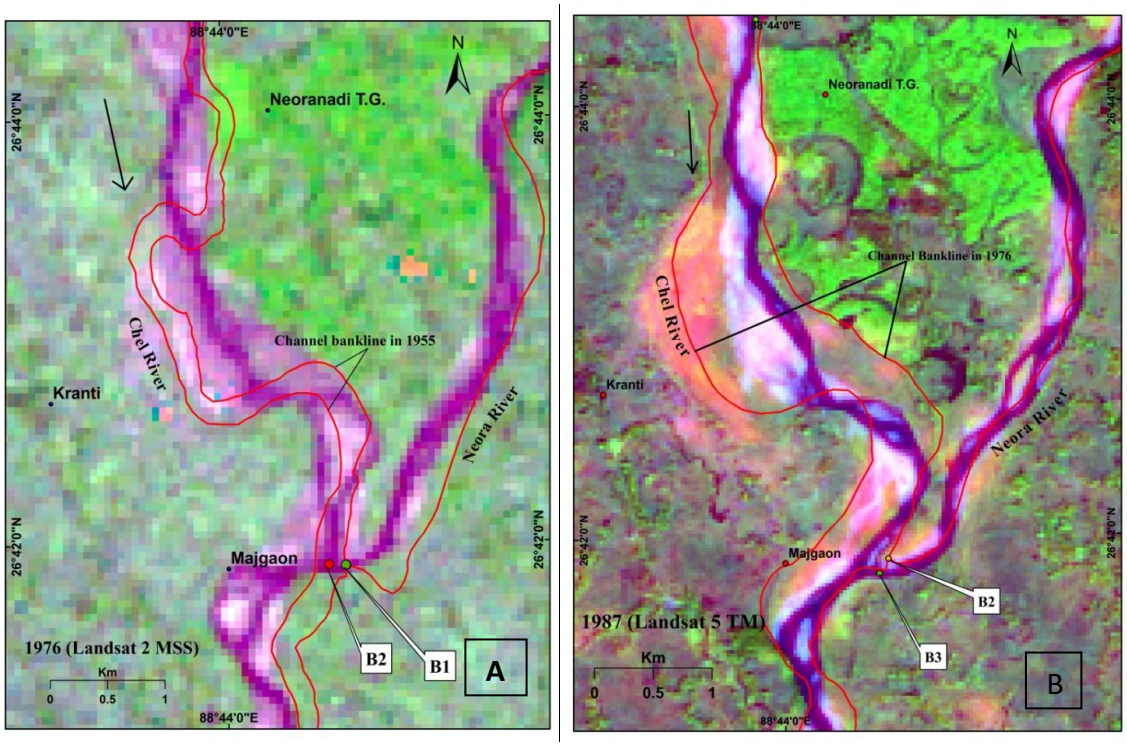

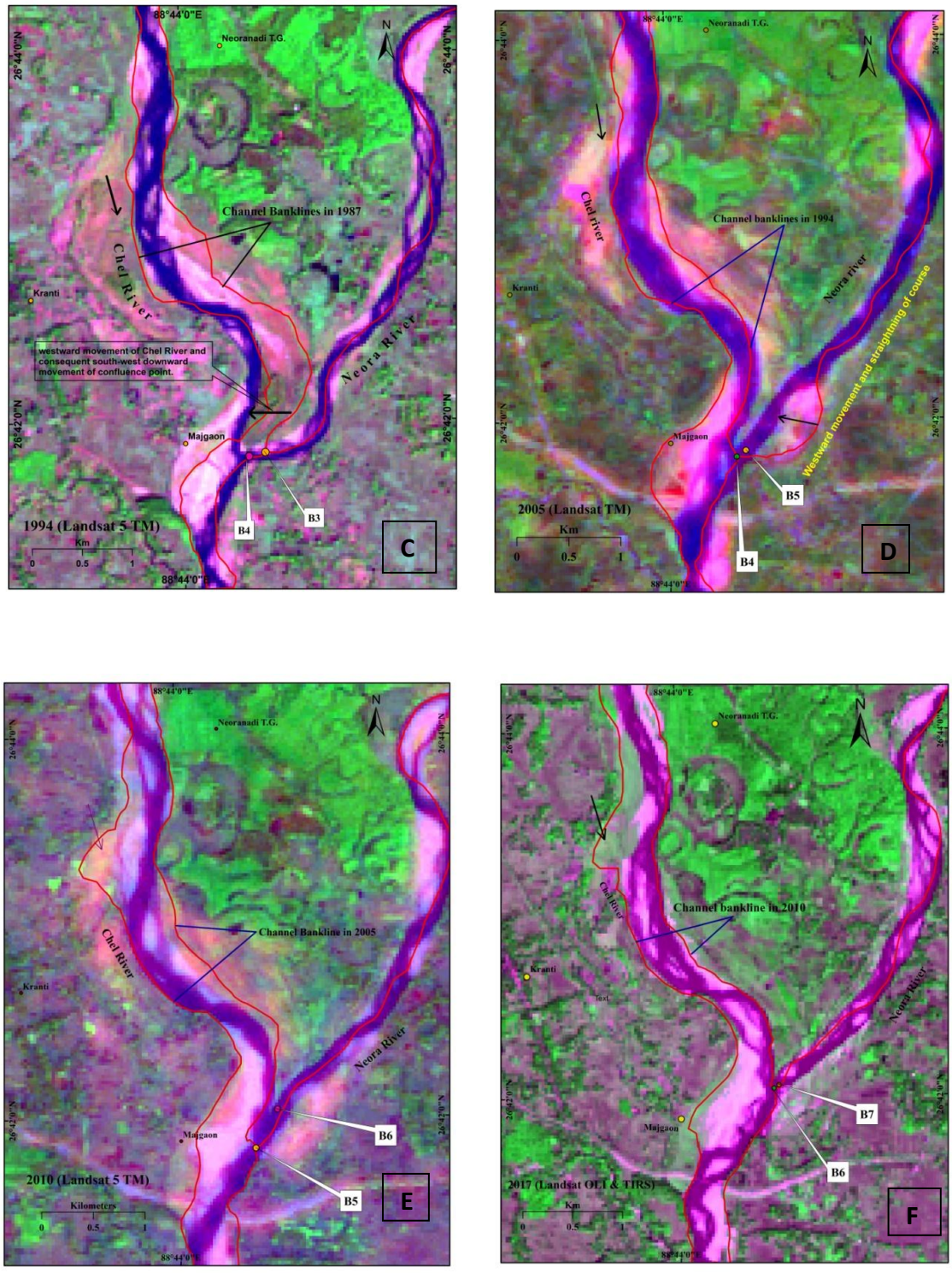

Figure 4.3.6 Enlarged representations of channel confluence point dynamics between the Chel-Neora Rivers during the period 1955-2017 and probable reasons.

Further the southern tip of the basin also falls within a distance of 50km from the mountain front, so role of tectonics in triggering such avulsions cannot be ruled out. Results on avulsion mechanism in the study area are comparable and related to the studies on eastern Ganga plains (Jain and Sinha, 2003, 2004; Sinha et al.,2005) and lower Jaldhaka-Diana River system, Jalpaiguri (Duars), West Bengal (Chakraborty and Datta, 2013).

4.3.4.2 Aggradations

The Chel-Kumlai confluence and Chel- Neora have shifted downstream between 1976-1987 from A2-A3 and B2-B3 respectively (Table 4.3.2). These downward movements can be asserted to the mechanism of aggradation in the confluence area. The transition of degradational to aggradational regime around 1980s is well evident in the Landsat images of 1987 in the form of large bars in the confluence area (Fig.4.3.5B). An increased sediment budget due to bank erosion in the upstream reaches would encourage aggradation in the confluence area downstream due to reduced velocity and gradient (Roy and Sinha, 2007). The development and increment in the size of bars have pushed the primary channels of Chel, Kumlai and Neora farther from each other in the confluence area and thus the confluence points have moved downstream (Fig.4.3.5B and Fig.4.3.6B).

Alterations in the degradational and aggradational regimes in a selected reach over time in a large river system such as Ganga is much likely to respond to the fluctuations in monsoonal strength (Gibling et al., 2005). Such fluctuations would therefore move the confluence point upstream and downstream in a major way on a longer time scale (Roy and Sinha, 2007). Few studies have documented the systematic upstream migration of major confluence points in the Ganga plain due to increased accretion of rivers in response to increased erosion in the Himalayan catchments and base level changes due to sea-level fluctuations during late Pleistocene- Holocene (Tangri,1986; Singh,1987). Few workers have attributed the role of tectonic tilting in channel shifts in the Ganga plain, probably during early Holocene (Mitra et al., 2005). The principal cause of aggradations around the confluence area in the study area is hydrological changes induced by the fluctuations in amount of monsoonal rains and large scale erosion in the catchment area

due to clearing of natural forests for making way for tea and beetle nut plantations seems most likely among all possible causes.

4.3.4.3 River Capture

River capture is essentially caused by local base level difference between two channels which in turn controls the erosional potential. The captured river has a higher base level and lower erosion potential whereas the predatory stream has a lower base level and higher erosion potential (Roy and Sinha,2007). The predatory river captures the lower reaches of another river and results in the upstream movement of the confluence point. River capturing is an important fluvial mechanism by which river enlarges its drainage network and thereby significantly alters the landscape evolution. It also impacts the distribution of discharge and sediment within and among the drainage basin in a very significant way. Mather (2000) has documented the transfer of~ 15% of water and sediment budget due to river capture in Sorbas basin of SE Spain during Plio-Pliestocene period. While most of the river capture has been reported from the tectonically active mountain river basins (Brookfiled, 1998; Mather, 2000; Mather et al., 2000), a few reported examples from Ganga plains can be cited here. The capturing of lower reaches of Bhakla River by Rapti River during avulsion which left upper reach of Bhakla River left as misfit channel (Richards et al., 1993). The capturing of lower part of Garra River by Ganga River during 1990 and 2000 and consequent upstream movement of confluence point by~ 7.5km has been well described (Roy and Sinha, 2007). Documented events of river capture in the alluvial plains of Dooars region of Sub-Himalayan west Bengal is almost non-existent. The only instance is the capturing of lower reach of Diana River by Jaldhaka river during 1970-1990 thereby shifting the confluence point upstream by 11 kms (Chakraborty and Datta,2013; Chakraborty and Mukhopadhyay,2014). For the present study of Chel basin, the instance of river capture of very local nature is observed twice for Chel and Kumlai River. During the period 1955- 1976, the channel width of Chel increases manifold eastwards coupled with eastward shifting of main flow. This led to the complete planation of earlier interfluves area and thereby Chel captured the lower reach of Kumlai River which led to upstream movement of confluence point by~ 531m from A1 to A2 (Fig.4.3.5A & Table-4.3.2). Period 1976-1987 witnessed major accretion

near the confluence point which pushed the two rivers farther and consequently the confluence points moved downstream. But during 1987-1994, a flow separation develops above Rajadanga and the eastern flow avulse through the accretion area developed during 1976-1987 and captures the lower Kumlai, thereby shifting the confluence point upstream by~904.34m from A3 to A4 (Fig.6.5C & Table 6.2).

4.3.4.4 Stream junction angle

The junction angle between the main stream (M) and tributary stream (T) depends on their relative gradient (S_M/S_T) (Horton, 1970; Howard, 1971). A wide junction angle indicates a higher slope of the tributary stream relative to the main stream and a low angle indicates nearly equal slopes (Roy and Sinha, 2007). Therefore, the confluences with wider junction angles are more dynamic and are likely to erode, migrate, avulse and create flooding. In contrary to this the confluences with lower junction angles would be more stable. Any change in the junction angle would therefore is much likely to manifest itself through channel stability and or channel dynamism (Roy and Sinha, 2007). Measurements of junction angles for both Chel-Kumlai and Chel-Neora show that the angles have been significantly variable during the assessment period. Computed junction angle values for Chel-Kumlai were much variable compared to the Chel-Neora junction angle (Table 4.3.1). This is manifested in terms of the fact that the amount of confluence points shifts for Chel-Kumlai has been recorded much larger than the Chel-Neora confluence.

At the Chel-Kumlai confluence, the junction angle shows a very sharp increase during 1955-1976, followed by a steep decrease during 1976-1987 and again followed by a period of sharp increase during 1987-1994. After 1994 the junction angles remained almost stable between 100 to 120 degrees. This indicates that the slope ratio (S_M/S_T) must have increased manifold during 1955-1976 and 1987-1994 which facilitated to erode its banks and capturing of the lower reaches of the Kumlai River thereby moving the confluence points upstream (Fig.4.3.5A & 4.3.5C). The decrease in slope ratio (S_M/S_T) during 1976-1987 as evident from the low junction angle indicates that the relative slope of Kumlai (tributary) has decreased with respect to that of the Chel (main stream) and

this encouraged deposition of sediments in the confluence area resulting in bar formation thereby downward shifting of confluence points.

For the Chel-Neora confluence, a moderate level increase in junction angle is witnessed during 2005-2010 (Table 4.3.1). It seems, this mild increase in junction angle have increased the slope ratio (S_M/S_T) during the period which allowed the Chel to widen its width by eastward erosion thereby capturing the lower reach and shortening the Neora River. Consequently, the confluence point has migrated upstream by~ 431.82m during this period (Table-4.3.2 & Fig.4.3.6E).

Figure 4.3.7 Google Earth Image (12.05.2017) showing confluence of Chel and Kumlai Rivers near Rajadanga.

Plate 4.3.1 Confluence of Chel-Neora,near Majgaon during January,2014.

4.3.4.4 .1 Channel confluence junction angle prediction of Chel River using linear regression method and its impact

Taking into consideration all the similar limitations and assumptions as discussed in predictive centerline migration distance section (4.2.3.2.1.1), an attempt is made here to predict the short-term channel confluence or junction angles dynamics using a linear regression method. Details of both observed and predictive channel junction angle dynamics is summarized in Table-4.3.3. It is observed that the junction angle of Chel-Kumlai increased almost consistently since 1987 and this trend is likely to continue even in the future. The confluence angle will attain a value of almost 132 degrees by the year 2035. Overall, the junction angle of Chel-Kumlai have registered a net increase of 47 degrees within 62 years of assessment till 2017 and this value is likely to increase to 65.4 degrees if we increase the assessment period till 2035. While in the case of Chel-Neora confluence, the junction angles have been comparatively fluctuating. The junction angle values are likely to decrease further in the future and will approximately attain a value of about 43 degrees by the year 2035. Within the 62 years of assessment period, this

confluence point has registered a net decrease of 48.5 degrees and the value is further likely to attain a value of 72 degrees if we increase the assessment period to 2035.

From the predictive values it seems the Chel-Kumlai will experience increased instability which will lead to more erosion and less accretion near the confluence zone. The erosion may be a gradual one wherein the interfluvial land like permanent or semi-permanent bars near the confluence will be slowly eroded away or it may be sudden event like an avulsion during high flow period and thus the confluence point will shift upstream. This implies shortening of length of both the rivers or most likely of Kumlai. Whereas the confluence zone of the Chel-Neora will experience increase in sedimentation or accretion as suggested by decreasing predictive junction angle values. The increase in sedimentation brings stability near the confluence zone. There will be new bar formation or the increment in sizes of the existing ones. These bars will gradually push the main flow of both channels farther from each other and thus eventually the confluence points will move downstream. This implies gain in the length of both or any of the two channels. This also implies that humans will lose arable land near the confluence of Chel-Kumlai whereas development of new bars will serve as patches for seasonal cropping near Chel-Neora confluence zone. Overall, the River Chel is likely to get more dynamic near Chel-Kumlai and less dynamic near Chel-Neora confluence zone reaches in the near future.

Years/Time period		Observed Junction angle trend (degree)							Predicted Junction angle trend(degree)		R	R^2
		1955	1976	1987	1994	2005	2010	2017	2025	2035		
Channel Confluence/Junction	Chel-Kumlai	66.5	125	71	108	117	118	113.5	125.1	131.9	0.72	0.53
	Chel-Neora	115	72.5	57.5	129	38	61	66.5	51	43.1	-0.63	0.4

Table 4.3.3 The assessment of channel junction angle variation and prediction using linear regression method

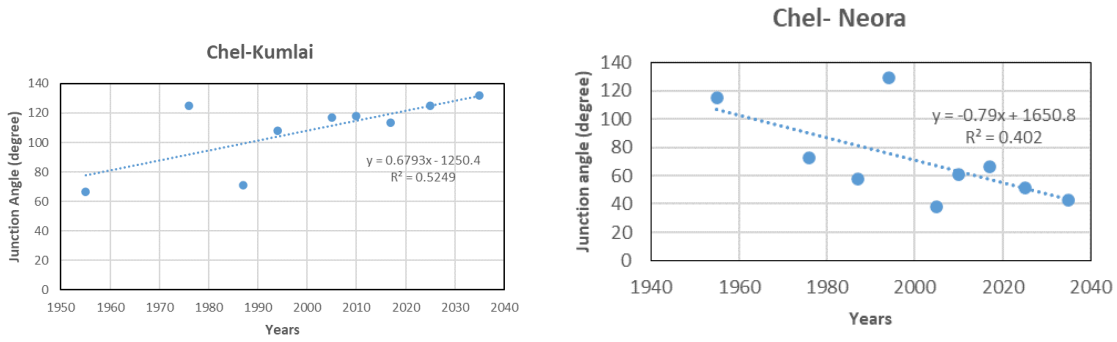

Fig.4.3.8 Prediction for channel junction angle variation of the Chel river in 2025 and 2035 using linear regression method.

Major findings

- The present study exhibits well that the two major confluence points of lower Chel system namely, Chel-Kumlai and Chel- Neora were dynamic and moved both upstream and downstream during the assessment period spanning 62 years. Some of the movements were massive but some years confluences also recorded almost no movements. Confluence points have registered net upstream movement by 310.62m and~318.81m for Chel-Kumlai and Chel-Neora respectively.
- Inspite of being in close vicinity, the two confluence points recorded variable amount of movement. Chel-Kumlai confluence point was more dynamic than the Chel-Neora confluence during the six inter-phases of assessment period. There seems no particular trend in the confluence dynamics for both confluence points.
- There are several processes responsible of these confluence movements viz. avulsion, cut-offs, river capture and aggradation. We observed that river capture has moved the confluence point upstream whereas aggradation resulted in downstream shifting of confluence point. The avulsion mechanism is responsible for both upstream and downstream movement.
- Hydrological variability in terms of flood magnitude seems to be the important factor triggering avulsions. The fluctuation in the monsoonal strength can likely be seen as reason for hydrological variability which alters degradation and

aggradation regimes in the study area as described by Gibling et al.,2005 for Ganga River system.

- North Bengal Rivers are significantly influenced by structural and tectonic controls too. So, the role of tectonics in confluence dynamics of study area cannot be ruled out.
- Junction angle also play an important role in confluence dynamics. Measurements of confluence junction angles shows that sharp decrease in junction angle encouraged aggradation near the confluence resulting in bar development thereby moving the confluence downstream. Whereas the sharp increase in junction angle increased instability and moved the confluence point upstream mostly through river capture and avulsion.
- There are significant morphological changes in terms of sinuosity, braiding intensity and channel width in the rivers during the assessment period which seems to correspond to the confluence movements.

Conclusion

Channel confluence dynamics is the manifestation of dynamism of main channel along with its tributaries induced by multiple factors. Thus, an attempt was made to reconstruct the historical channel confluence dynamics in the lower Chel-Neora river system to understand the trend of confluence dynamics and probable factors driving such movements. The study found that there was large variability in the amount of confluence dynamics in the region during the entire study period. The confluence point movements have been erratic without displaying any specific trend. Aggradations, avulsions and river capture processes were found to be the major factors behind the confluence dynamics. Further study coupled with tectonics and long-term hydrological data can give deeper insight into the mechanism and causative factors of confluence dynamics of the region.

4.4 Erosion and Accretion

Introduction

Changes in channel forms and patterns are rivers' response to Channel dynamism induced by the natural or anthropogenic factors in channel. Bank erosion and accretion is one of the many geomorphologic manifestations of such change. Channel dynamism of river Chel is causing large scale erosion along its course and is damaging Tea Gardens, forests and agricultural lands (Plate 4.4.1-4.4.5). Therefore, a study on the computation of areas of erosion and accretion along a reach (Putharjhora- Kranti) of river Chel has been attempted in this section over the period of 62 years (1955-2017) using georefrenced topographical sheets, multi- temporal Landsat images, and supplemented by fieldwork.

Plate (4.4.1-4.4.5) Huge erosion along the right bank of river Chel shrinking the Apalchand Reserve forest (4.4.1); Tree trunks lying on the river bed after being washed

from Apalchand Reserve Forest by river erosion (4.4.2); erosion of agricultural land along left bank near confluence with Neora River (4.4.3); Extensive left bank erosion near, 4kms downstream of Chel,Sukha and Manzing khola confluence. Note: Unvegetative remaining footpath shown in red circle seems to be eroded away recently during last monsoonal high flow. (Photograph taken on 05.02.2017) (4.4.4); and Bank erosion along the right bank in the downstream direction at South Odlabari Tea Garden (4.4.5)

4.4.1 Study reach

The study reach for the present study extends from near the confluence point of Manzing and Sukha Khola with Chel River near Putharjhora Tea Garden, near the mountain front below Gorubathan to confluence Point of Chel River with Neora River (Fig. 4.2.1) in the downstream. The straight valley length of the reach is 20.93 kms.

4.4.2 Data and methodology

Details of data used and their sources are given in the table 4.2.1. The study deploys an overlay analysis methodology of seven temporal datasets using a combination of georefrenced topographic maps and Landsat images spanning over 62 years (from 1955 to 2017). Field works were conducted to verify the results computed in GIS and for collection of field photographs.

4.4.2.1 Delineation of channel boundary

Channel banklines were delineated using non-geomorphological approach which presumes that river channel limit is an elongated area wherein stream flow occurred with sufficient frequency, energy and duration to prevent the incidence of vegetation, and therefore 90% of this area is either bare soil or water (Gurnell, 1997; Yang *et al.*, 1999, Tiegs and Pohl, 2005). Proper on-screen digitization of banklines produced a georeferenced dataset and a channel configuration map were created (Fig. 4.2.5).

4.4.2.2 Determination of erosion and accretion areas

River bank changes were analysed by superimposing the digitized banklines for each of the seven data sets using the ArcGIS software and its extensions. The seven periods are 1955 to 1970 (15 years), 1970 to1976 (6 years), 1976 to 1987 (11 years),

1987 to 1994 (7 years), 1994 to 2005 (11 years), 2005 to 2010 (5 years), and 2010 to 2017 (7 years). The overlaying of banklines for each time period revealed the areas of erosion and accretion.

Then the areas of erosion and deposition were digitized and thus revealed after superimposition for each time period to create polygons that represented the difference between the two bank lines. If the developed polygon was positioned to right of the right bank of base year, it represented an erosion polygon: if the polygon was positioned to the left of the right bank of base year, it represented the accretion polygon. For the left bank, the same process was repeated but unlike right bank, here polygons to the right and left of the base year represented accretion and erosion polygons (Fig.4.4.1). Adding the areas of these polygons gave the total eroded and accreted areas of the time period.

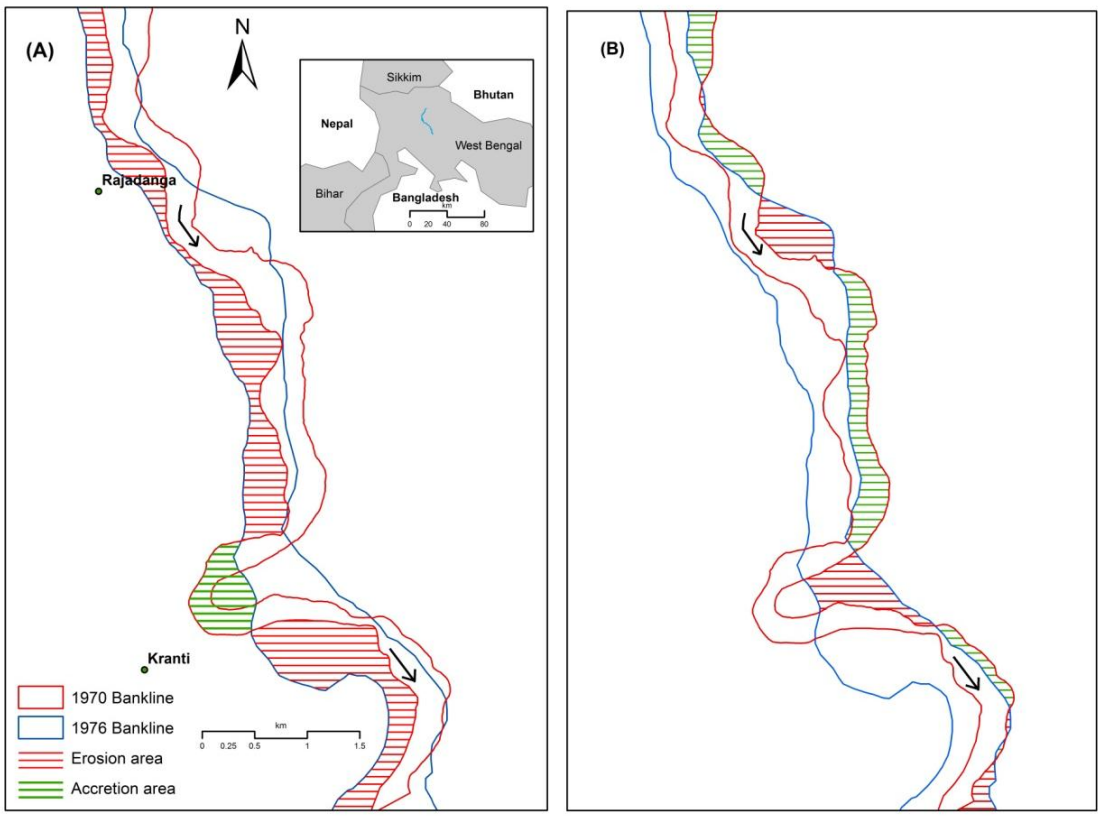

Fig. 4.4.1 Enlarged area demonstrates an example for the identification of erosion and accretion areas between transects 27 and 35. (A) Erosion and accretion areas along the right bank of river Chel during 1970-1976. (B) Erosion and accretion areas along the left bank of river Chel during 1970-1976.

4.4.3 Areas of erosion

The total area of bank erosion from 1955-2017 equaled 34.8 km^2, of which 12.36 km^2 were on the left bank and 22.4 km^2 were on the right bank (Table-4.4.1) Further 342 erosion plots were identified (all plots >1m^2 has been considered, plots <1m^2 were neglected). On the left bank there are 166 erosion plots smaller than 1 km^2 which totaled 8.52 km^2 (69.16 % of the total area). In contrast, there are only 2 erosion plots larger than 1km^2 but their cumulative area equaled 3.8 km^2 (30.84 % of the total area).

Along the right bank there are 168 erosional plots are less than 1 km^2 of size which equaled 8.07 km^2 (35.8 % of the total area). In contrast, there are only six erosional plots larger than 1km^2 but their cumulative area was 14.17 km^2 (64.2 % of the total area).

Table 4.4.1: Area of riverbank erosion along the study reach of River Chel from 1955-2017.

	Area of erosion (sq.km.)		
Time span	**Left Bank**	**Right Bank**	**Total**
1955-1970	5.77	7.88	13.65
1970-1976	1.77	7.84	9.61
1976-1987	0.31	1.14	1.45
1987-1994	1.344	2.082	3.426
1994-2005	1.81	1.741	3.551
2005-2010	0.76	1.172	1.932
2010-2017	0.6	0.546	1.146
Total (1955-2017)	12.364	22.401	34.765

4.4.4 Areas of accretion

The total area of bank accretion from 1955-2017 equaled 35.16 km^2, of which 18.99 km^2 were along the left bank and 16.17 km^2 were on the right bank (Table-4.4.2) Further, 363 accretion plots were identified. On the left bank there are 166 accretion plots smaller than 1 km^2 which totaled 14.26 km^2 (76.13 % of the total area). In contrast, there are only 3 accretion plots larger than 1km^2 but their area equaled 4.47km^2 (23.86 % of the total area).

Along the right bank there are 191 accretion plots are larger than 1 km^2 of size which equaled 8.68 km^2 (52.93 % of the total area). In contrast, there are only 3 accretion plots larger than 1km^2 but their area totaled 7.72 km^2 (47.07 % of the total area).

4.4.5 Annual rates of bank erosion and accretion

The total area eroded along the study reach amounts to 13.65 km^2 from 1955 to 1970; 9.61 km^2 from 1970 to 1976; 1.45 km^2 from 1976 to 1987; 3.43 km^2 1987 to 1994; 3.55 km^2 from 1994 to 2005; 1.93 km^2 from 2005 to 2010 and 1.15 km^2 from 2010 to 2017. These total figures give way to annual bank erosion rates of 0.92 km^2/y, 1.6 km^2/y, 0.13 km^2/y, 0.49 km^2/y, 0.33 km^2/y, 0.38 km^2/y, 0.17 km^2/y respectively (Table-4.4. 2 & 4.3.3). The total area accreted along the study reach equaled 2.32 km^2 from 1955 to 1970; 5.17 km^2 from 1970 to 1976; 11.85 km^2 from 1976 to 1987; 5.4 km^2 1987 to 1994; 2.7 km^2 from 1994 to 2005; 4.4 km^2 from 2005 to 2010 and 3.32 km^2 from 2010 to 2017. These figures translate into annual accretion rates of 0.15 km^2/y, 0.88 km^2/y, 1.08 km^2/y, 0.77 km^2/y, 0.25 km^2/y, 0.88 km^2/y, and 0.47 km^2/y, respectively (Table-4.4.3).

Table 4.4.2 Area of riverbank deposition along the study reach of River Chel from 1955-2017.

	Area of accretion (sq.km.)		
Time span	**Left Bank**	**Right Bank**	**Total**
1955-1970	0.794	1.527	2.321
1970-1976	4.72	0.45	5.17
1976-1987	5.23	6.62	11.85
1987-1994	3.67	1.734	5.404
1994-2005	1.6	1.1	2.7
2005-2010	1.632	2.763	4.395
2010-2017	1.34	1.98	3.32
Total (1955-2017)	18.986	16.174	35.16

Table 4.4.3 Mean annual rates of bank erosion and accretion along the study reaches from 1955 to 2017.

Time span	Erosion rate (sq.km/y)	Accretion rate (sq.km/y)
1955-1970	0.92	0.15
1970-1976	1.61	0.88
1976-1987	0.13	1.08
1987-1994	0.5	0.77
1994-2005	0.33	0.25
2005-2010	0.38	0.88
2010-2017	0.17	0.47

4.4.6 Spatial and temporal distribution of erosion and accretion along the study reach

Areas of erosion and accretion along the right and left banks of Chel River are shown in (Fig.4.4.2). The table-4.4.1 depicts that during the entire assessment period of 62 years the areas under erosion was highest (13.65 km^2) during 1955-1970 followed by the period 1970-1976 wherein erosion exceeded far more than accretion along the right bank. Rest of the assessment periods record that the accretion values are greater than the erosion values, except during 1994-2005 wherein the erosional area is 1.81 km^2 against the accretion area of 1.6 km^2. The maximum amount of erosional area (7.8 km^2) was recorded during 1955-1970 along the right bank, while maximum accretion area (6.62 km^2) was recorded during 1976-1987 again along the right bank. Over the entire 62 years of assessment period, 12.36 km^2 area was eroded along the left bank against the 18.9 km^2 of accretion along the left bank. This means that during the last 62 years 6.49 km^2 of land has been gained along the left bank of river Chel. In contrary to left bank, the right bank of river Chel is more prone to erosion. The right bank recorded 22.8 km^2 equivalent of erosion against 16.17 km^2 of accretion. Except during 1976-1987 and last two epochs (2005-2010, 2010-2017), erosion exceeded deposition along right bank. The highest amount of erosion recorded during 1955-1970 can be attributed to the major flood of 1968. The huge amount of flood water widened the otherwise narrow channel to accommodate the excess amount of water laden with huge quantity of sediments. There is

not much difference in the amount of erosion along right and left banks during 1955-1970 as the flood water flowed through channel covering its entire width. The period 1970-1976 saw receding of flood water and water mainly flowed along the right bank guided by the tiltation of the basin towards the right as suggested by the basin asymmetry factor (Af) of 40.31 in sub-chapter - 4.5 and relief profiles showing surface gradient direction from east towards the west (Fig.2.2). Therefore, the period 1970-1976 recorded very high amount of right bank erosion and high amount of area under accretion along the left bank. Then after the accretion process has dominated and therefore, we find reduction in the width of the channel. The channel has progressively narrowed and the erosion is mostly concentrated along the right bank due to tiltation of whole basin towards the south-west of the flow of the main channel (Table-4.4.1 and 4.4.2).

4.4.7 Accuracy of results

Cloud free Landsat images of minimum water level differences were selected and author as single operator digitized multi-temporal channel boundary to achieve highest level of accuracy yet there can't be scope for denial of the fact that while working with multi-temporal dataset on Remote sensing and GIS, positional inaccuracies may crop up due to procurement of maps and images from different time period and at different scale. In this study, one of the possible error sources is the different map scale of Topographical maps (1955 AMS with 1:2, 50,000 and 1970 SOI with 1:50,000 map scale) and the different spatial resolutions of the Landsat MSS (60m) and ETM & OLI/TIRS (30m) images.

Further, systematic and random errors of the sensors themselves could have affected the delineation of channel boundary (Dewan *et al.,* 2017). Mixed color composition of pixels in multispectral Landsat images along the transition zones posed as a challenge and can be considered as another source of error that precluded us from deciding the exact line of channel boundary along some short reaches. This misjudgment of channel boundary can have a significant implication in area calculation whether erosional or accretional.

Other sources of error inherent in our methods include those associated with polygon delineation and variability in the time that elapsed between the cessation of flood events

and the collection date of the image data. Despite everything, the work embodies measurement accuracy of satisfactory level and documents information on erosion-accretion scenario of the River Chel along its alluvial reach.

Major findings

1. In the studied reach of Chel River, the area of bank retreat from 1955-2017 totaled 34.77 km^2, of which 22.4 km^2 were recorded along the right bank whereas 12.36 km^2 were along the left bank. Thus right bank is more erosion prone than the left bank.

2. The areas eroded were 13.65 km^2 during 1955 to 1970, 9.61 km^2 during 1970 to 1976, 1.45 km^2 from 1976-1987, 3.43 km^2 from 1987-1994, 3.55 km^2 from 1994-2005, 1.93 km^2 from 2005-2010, and 1.15 km^2 from 2010-2017.

3. The areas accredited were 2.32 km^2 from 1955 to 1970, 5.17 km^2 from 1970 to 1976, 11.85 km^2 from 1976-1987, 5.4 km^2 from 1987-1994, 2.7 Km^2 from 1994-2005, 4.4 km^2 from 2005-2010 and 3.33 km^2 from 2010-2017.
4. There is no noticeable trend in the mean annual rates of erosion and deposition in the study reach. The values are all fluctuating during the study period.
5. Spatially, the right bank Oodlabari Bazaar-Nipuchapur Tea Garden section has suffered the most extensive bank erosion, whereas Rajadanga- Kranti section of the study reach sustained minimal bank erosion.

Conclusion

An attempt to compute the areas of channel erosion and accretion was made in the present sub-chapter to understand the temporal and spatial distribution of bank erosion and accretion from 1955 to 2017. Non-geomorphological approach was followed for delineation of channel boundaries from multi-temporal Landsat images. The study shows a phase of major channel widening thus dominancy of channel bank erosion from 1955 to 1976. This phase can be related well with the catastrophic flood of 1968 which damaged Darjeeling Himalaya in a very large scale. Then a major phase of accretion was

observed during 1976-1987. Gradually now the channel has attained the earlier width of 1955. Characteristically erosion is dominant along right bank whereas accretion is along the left bank. This implies westward movement of the main channel induced by the tectonic tilt of the basin towards the south-west direction. The study thus documents the fact that the reach under study has experienced large spatio-temporal variation in the areas under erosion and accretion and this variation seems to be largely guided by the flood and tectonic tiltation of the basin.

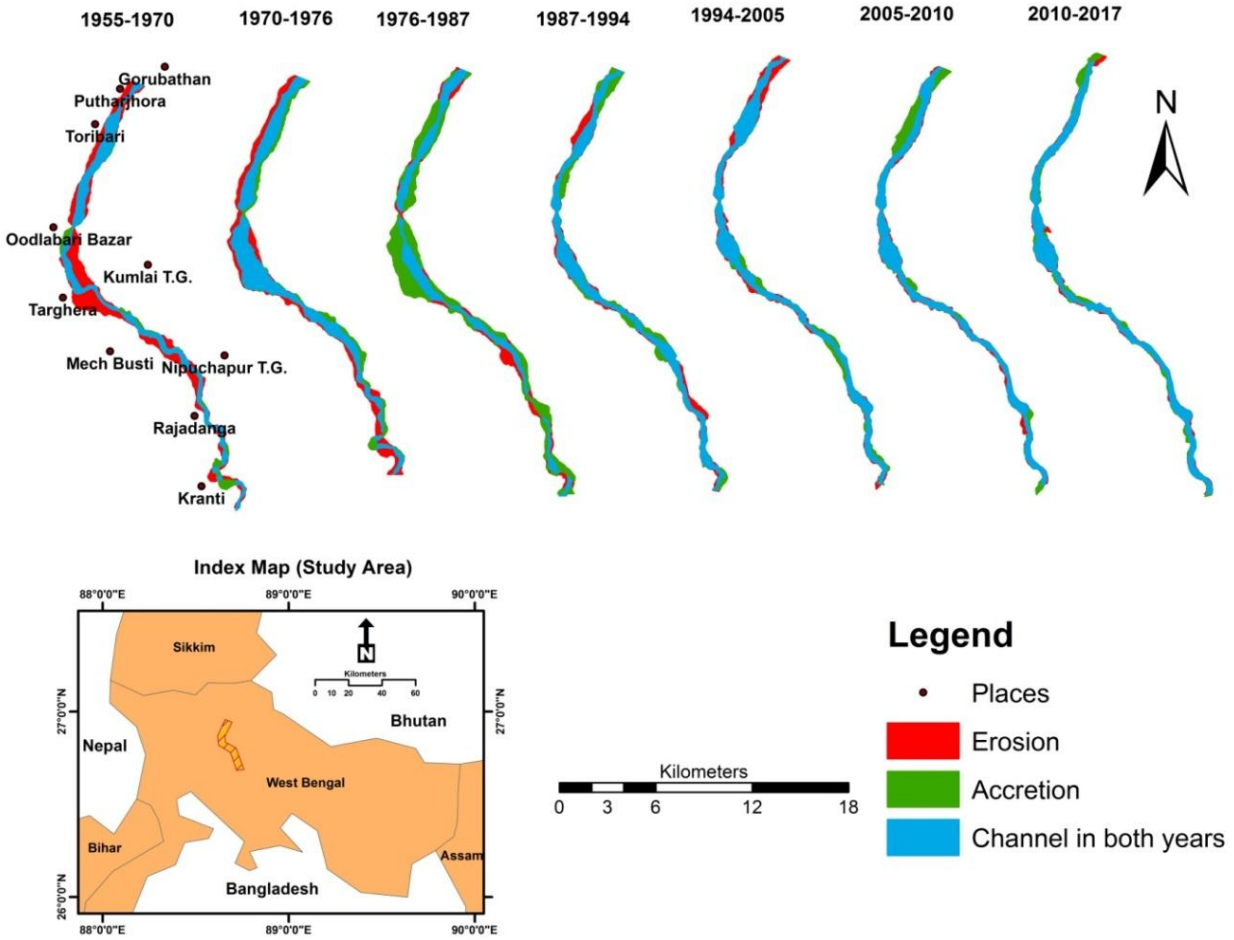

Fig. 4.4.2 Spatial patterns of erosion and accretion areas along the Chel River.

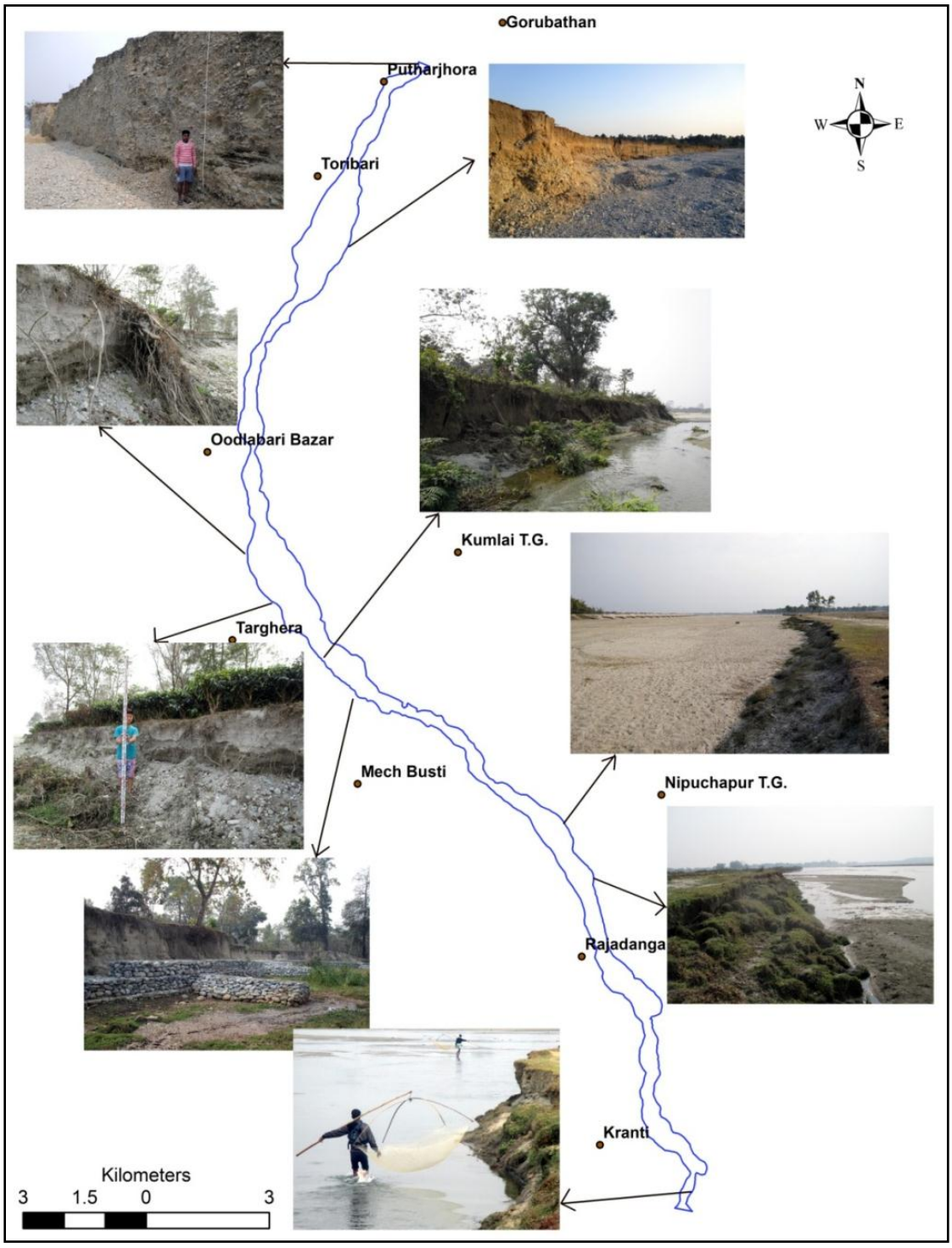

Fig.4.4.3 Field photographs showing bank erosion along the entire study reach of Chel River.

4.5 Role of Tectonics

Introduction

The present existing landforms are the result of complex interplay between the endogenic and exogenic forces working upon earth's surface. Himalayan topography is a direct consequence of the convergence of Indian plate with the Eurasian Plate. This convergence of two continental plates has developed three major thrusts namely Main Central thrust (MCT), Main Boundary Thrust (MBT) and Main Frontal Thrust (MFT) which traverse the east-west elongated Himalayan ranges and divides it into three tectonic belts. Apart from these major thrusts, there are numerous smaller and regional level faults and thrusts all across the Himalaya. The variable rate of convergence further creates a complicated environment for landform evolution. Under this background, the study of active tectonics and its implication on geomorphology and drainage characteristics and response mechanism of landform and channels become very interesting and imperative as well. The understanding of geomorphologic processes and features are essential to get an insight into the tectonics that shapes them and the response of landform to the tectonics. Keller (1986) opines that for the study of active tectonics, geomorphic indices are very useful as they are capable of detecting particular areas of a region that is experiencing and adjusting to the varying rates of active tectonics. The study of active tectonics, and in particular those areas with relatively high activity, in the Holocene and late Pleistocene, is important to evaluate the Earthquake hazard (Keller and Pinter 2002). Mukul et al. (2017) demonstrate that the evolution of the landscape can be studied quantitatively using digital elevation data.

The geomorphic indices have been used the world over as an effective tool for the identification and spatial variation of relative active tectonics. Wells et al. (1988), used geomorphic index (K) of around 100 mountain fronts along with the long profile of numerous rivers, radiometric dating and conducted several field studies to assess the regional variations in active tectonics along a segmented convergent plate boundary, along Pacific coast of Costa Rica. Ramiez-Herrera (1998) applied a combination of geomorphic indices and morphometric evidence approach in faulted

mountain fronts of Acambay Graban to assess the evidence of spatial variation of relative active tectonics in Mexico. Silva et al. (2003) used Mountain-front sinuosity index (Smf) and Valley floor/width ratio (Vf) and their regression to assess the tectonic activity of the Mediterranean coast of South-East Spain. Similarly, El. Hamdouni R. et.al. (2007) used the resulted values of few geomorphic indices such as drainage basin asymmetry (Af), Stream length gradient index (SL), hypsometric integral (Hi), ratio of valley floor to valley height (Vf), index of drainage basin shape (Bs), and index of mountain front sinuosity (Smf) to combine and yielded Index of relative active tectonics (Iat), which was divided into four classes from very low to very high tectonic activity. They tested this newly devised concept and method in the southwest border of the Sierra Nevada in southern Spain and divided the landscape into four classes of relative tectonics. Troiani and Seta (2008) used the integration of stream length gradient index (SL) and amplitude of relief (Ar) for detecting the impact of neotectonics on the development of a small Tarugo river basin (92 Sq.kms) in the Northern Marchean Apennines (Central Italy). Dehbozorgi et al. (2010) have applied the method of Index of relative active tectonics (Iat) devised by El. Hamdouni R. et.al. (2007) to assess tectonic activity in the Sarvestan area, Central Zagros, Iran and divided the study area into four parts. In India, too geomorphic indices have been used widely as an important tool to study active tectonics as is evident from studies of. Rana et.al (2016) in Alaknanda Valley, Garhwal Himalaya, Kothyari and Rastogi (2013) in upper Narmada valley, Dhanya (2014) in Achankovil river basin, Kerela, Mukul et. al (2017) in Relli river basin, Darjeeling Himalaya, Mandal and Sarkar (2016) in Chel river basin, North Bengal, West Bengal to name a few. A similar kind of study to assess the implications of neotectonism in the Chel basin has been attempted here with SRTM DEM based geomorphic indices which are considered to be very useful in active tectonic studies (Keller 1986; Keller and Pinter 2002; Ramiez-Herrera 1998; Bull and McFadden 1977; Azor et al. 2002). The reason for selection of the Chel river for the present study was prompted by the fact that the Chel river drains through the major Himalayan faults and flows towards the North Bengal plain which is part of tectonically active Himalayan region and its foreland, thus gives an opportunity to test response of drainage lines and watershed to the

neotectonics. Further, the entire course of the Chel is accessible to verify the results generated by remote sensing and GIS.

Rivers originating in the Eastern Himalaya and draining towards north Bengal plains are characterized by highly incised mountainous course with elongated, asymmetric drainage basins and low sinuous mountain fronts. All these drainage and basin characteristics indirectly point towards the response of rivers and whole watersheds to the prevailing neotectonic activities. The present work tries to analyze and elucidate the response of drainage, topography, and watershed as a whole of Chel river basin to the neotectonics of the region, through some selected geomorphic indices computed from SRTM DEM.

4.5.1 Regional geological Setting

Regional geological setting of Chel River basin is discussed in Chapter-2 in detail.

4.5.2 Data and method

In the present study, two SRTM DEM 1 Arcsec (n26_e088_1arc_V3 and n27_e088_1arc_V3) with 30m resolution were used for extraction of geomorphic indices to access the implications of tectonic activities in the Chel river basin. The DEMs were downloaded from U.S. Geological Survey website using the Earth explorer interface: http://earthexplorer.usgs.gov/. as GeoTiff raster files, mosaicked them into one and then our watershed was clipped out from. Other relevant and related information were collected from SOI toposheets (Sheet no. 73B/9 and73B/10 having R.F -1:50,000). The geological map was prepared by consulting geological map published by Geological Survey of India (1990). ArcGIS 10.1 along with many DEM processing extensions were used for the analysis. The accuracy of C30N SRTM data in comparison to C90 is found to be more and owing to its better vertical accuracy, has been suggested for all future geographic studies (Mukul et al. 2017). Since the accuracy and usability of resultant geomorphic indices for the Chel river basin depend highly on the accuracy of the DEM used, its accuracy measurement becomes imperative. Thus, the accuracy of SRTM DEM was cross checked and tested

before the generation of geomorphic indices of Chel basin. In order to evaluate the accuracy, elevation values of 23 spot heights were collected from SOI toposheet (1:50,000) and corresponding values were extracted to perform a linear regression analysis (Fig.8.1). The analysis resulted in a best-fit plot with a correlation coefficient of 0.99 (Fig.8.2) and root mean square error of ±81 m. This validates the use of SRTM DEM 1Arc sec (30m resolution) in the extraction of geomorphic indices for the present study.

The following geomorphic indices typically used to identify neotectonics in river basins: relief ratio, drainage basin asymmetry, basin elongation ratio, hypsometric integral, stream length gradient index, mountain front sinuosity index and valley floor width-to-height ratio (Bull and McFadden 1977; Strahler 1952; Schumm 1956; Pike and Wilson 1971; Hack 1973; Gardner et al. 1987) have been applied to Chel river basin. Geomorphic indices which need elevation for their computation are Relief ratio, Stream length gradient index, valley floor width-to-height ratio, hypsometric integral etc. whereas drainage basin asymmetry, transverse topographic symmetric factor, Basin shape index (Bs) are few geomorphic indices that require length or area for its computation (Mukul et al. 2017).

Table 4.5.1 Geological and *Lithostratigraphic* units of Chel basin ,compiled from Geological and Mineral map of West Bengal, GOI,1999 and Mitra et al. 2010 and references therein.

Abbreviation	Units & age	Group	Lithology
Q2b	Baikunthapur Formation (Holocene)	--------	Sand,silt & clay
Q1c	Middle to Upper Chalsa Formation (Pleistocene)	----------	Boulders,Gravels,pebbles,sands and silts
Ptb	Buxa Formation (Proterozoic)	Daling	Predominantly dolostone, cherts and variegated slates.
Ptr	Reyang Formation (Proterozoic)	Daling	Ortho-, and protoquartzite variegated slates ancrphyllites
Ypt2l	Lingtse Granite Gneiss (Proterozoic-II)	Darjeeling Gneiss	Sheared, streaky, porphyritic biotite gneiss.
Ptd2	Chungthang Formation (Proterozoic)	Daling	Calc-gneiss, calc-granite, augen gneiss, marble, sillimanite gneiss, graphite schists; etc.

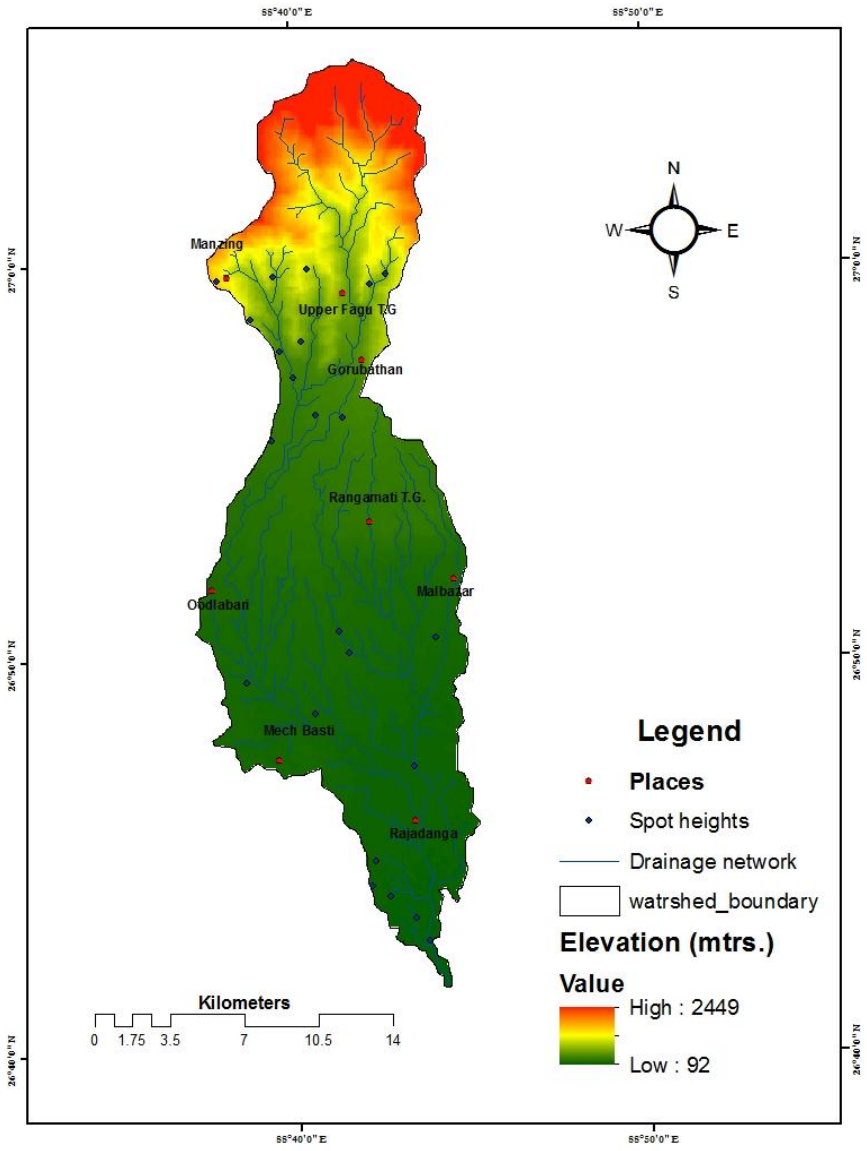

Figure 4.5.1 Location of spot heights, used for accuracy measurement of SRTM DEM.

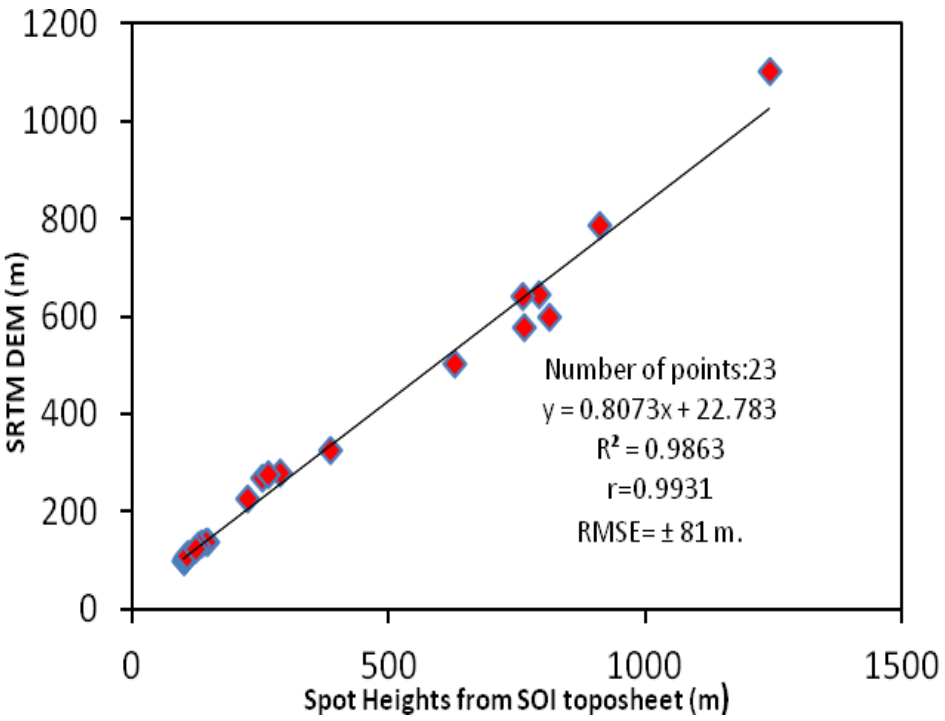

Figure 4.5.2 Correlation plots of spot heights derived from SOI toposheets and corresponding points on SRTM DEM.

4.5.3 Geomorphic indices of the Chel basin from the SRTM DEM

A bunch of previous research suggests the potentiality of geomorphic indices in the identification of geomorphologic characteristics in the tectonically dominated landscape (Keller and Pinter2002; Silva et al. 2003; Bull and McFadden 1977; Burbank and Anderson 2001; Kale 2014).

Geomorphic indices also act as reconnaissance tools to assess the association between tectonics and basin morphology and recognize recent geological deformation as well (Kale 2014).Commonly used geomorphic indices such as Relief ratio (Rh), Drainage basin asymmetry (Af),Basin Shape Index (Bs), Hypsometric curve and Hypsometric Integral, Stream length gradientindex (SL), Valley floor width-to-height ratio (Vf), Index of Mountain front sinuosity (Smf), Transverse topographic symmetry factor (T), Longitudinal Profile has been used in the present study and the methodology used has been discussed in detail below.

4.5.3.1 Relief ratio (Rh)

The relief ratio (Rh) is computed from the elevation of the river source (ZS), river mouth (ZM), and the maximum watershed length (L). Schumm 1956 describes relief ratio as the grade of the river and is derived as follows:

$$\text{Relief Ratio (Rh)} = \frac{ZS - ZM}{L} \quad (1)$$

The ZS and ZM values for Chel River are 2400 m and 92 m respectively. The maximum watershed length (L) is 42.6 km. From the above values, the relief ratio (Rh) computed was 54.12.

4.5.3.2 Drainage basin asymmetry (Af)

The drainage basin asymmetry is used to show asymmetry of drainage networks and basin as a result of tectonic tilting at both local and regional scale (Keller and Pinter 2002; Garrote et al. 2008; Hare and Gardner 1985; Cox 1994; Özkaymak and Sözbilir 2012; Giaconia et al. 2012).

The asymmetry factor (AF) can be represented as the percent of the area of the basin that is found on the right bank side of the mainstream (while looking downstream) to the whole area of the basin (Vijith et al. 2015) and is defined as:

$$AF = \frac{AR}{AT} X100 \quad (2)$$

Where Ar is the area of the basin to the right of the trunk stream and At is the total area of the drainage basin. AF is applied over a relatively large area or at the scale of a drainage basin (Hare and Gardner1985). AF value close to 50% shows little or no tilting perpendicular to the direction of main stream but an Af factor above or below 50 may result from basin tilting, as a consequence of either active tectonics or lithologic structural controlled differential erosion (El. Hamdouni R. et.al. 2007).

With Ar=129.4 km^2 and At=321 km^2 the drainage basin asymmetry factor for the Chel basin is 40.31which implies basin is tilted towards the right (looking downstream) (Fig. 4.5.3 a-b).

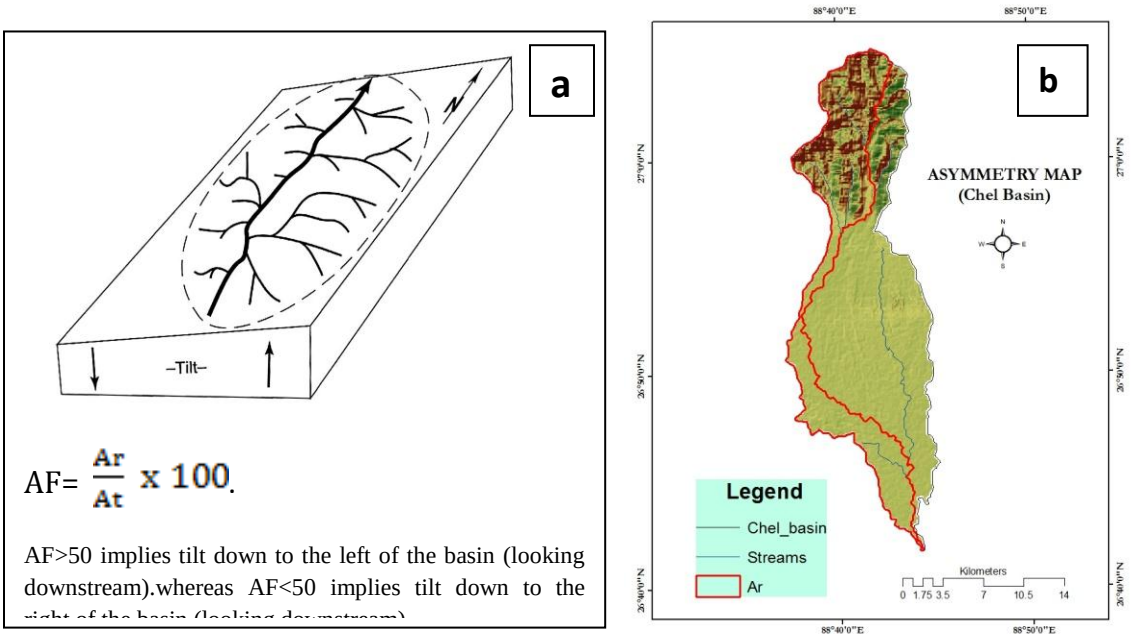

Figure 4.5.3 a. Block diagram shows the effect of an asymmetry factor with a left side tilt on tributaries lengths (From Keller and Pinter 2002, figure 4.3, p. 125). b. Tectonic tilting of Chel Basin, 40.31% area of basin is to the right side of trunk stream.

4.5.3.3 Basin Shape Index (Bs)

Basin elongation ratio (Re) is area related morphometric variable that quantitatively describes the planimetric shape of a basin, and thus, indirectly provides information about the degree of maturity of the basin landscape (Kale and Shejwalkar 2008). Bull and McFadden (1977) point out that basin draining tectonically active areas are generally more elongated and become more circular with the ending of uplift. The reason behind such transformation is because the Stream Energy is mostly directed towards the down cutting in the drainage basins near the tectonically active mountain fronts whereas the slow rate of uplift permits widening of basins near the mountain fronts. Molin et al. (2004) opine that elongated basin shapes are also associated with high local relief and steep valley slopes.

Ramiez-Herrera (1998) [5], expressed elongation Ratio by an equation:

$$Bs = Bl / Bw \quad (3)$$

where Bl is the length of the drainage basin calculated from its mouth to the most distant drainage divide and Bw is the width of the basin measured at its widest point (Fig.4.5.4). Drainage basin shape of river Chel was measured following Ramiez-Herrera (1998) and with Bw value of 12.38 km and Bl value of 43.48 km, the Bs value thus obtained is 3.46.

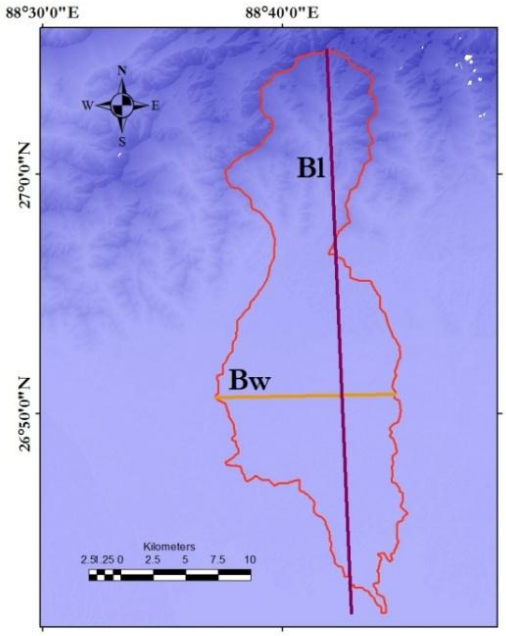

Figure 4.5.4 Basin shape index (Bs) calculation of Chel basin following Ramiez-Herrera, 1998.

4.5.3.4 Hypsometric curve and Hypsometric Integral

Hypsometry is the computation of relation between area and corresponding elevation slab of a basin (Strahler 1952; Langbein 1947). Thus hypsometric curve facilitates comparison of areas of varying sizes and elevations and consists of a normalized cumulative area along the x-axis and normalized elevation along the y-axis. The consequent shape of the curve obtained, gives an indication of the geomorphic processes operating in a watershed (Strahler 1952). A convex curve indicates a young basin categorized by irregular relief demonstrating active tectonics, whereas a concave curve is related to an old basin where alluvial or fluvial processes dominate. A concave-convex curve (S-shape) is an indication of a mature basin where

tectonics and erosion work in near equilibrium (Strahler 1952). A basin's relief can be quantified easily by the hypsometric integral (HI). The HI can be calculated from the area under the curve, and it expresses, in percentage, the volume of the original basin that remains unaltered. Hypsometric curves are obtained by plotting the proportion of the total height (h/H) against the proportion of the total area (a/A) of the basin, where H is the total relative height, A is the total area of the basin and "a" is the area of the basin above a given line of elevation h (Keller and Pinter 2002). Following Pike and Wilson (1971), HI can be calculated as follows:

$$HI = \frac{h_{mean} - h_{min}}{h_{max} - h_{min}} \quad (4)$$

Where h_{mean}, h_{min}, and h_{max} are the mean elevation, minimum elevation, and maximum elevation of the watershed respectively. The HI values range between 0 and 1 with values close to 0 indicating the basin to be at an old-age stage and values close to 1 indicating a youthful stage (Strahler 1964). The basin at the youthful stage is characterized by rugged relief and deep incision, whereas old-age basins have subdued relief (Keller and Pinter 2002; Strahler 1964).

Mature basins are in the intermediate stage where the geomorphic progression occurs at near stability. The HI is expressed as a percentage and is an indicator of the remaining volume of the original basin (Ritter et al. 2002). The hypsometric integral is also an indication of the 'cycle of erosion' (Strahler 1952; Garg S.K. (1983). The Hypsometric Integral (H.I.) of Chel basin is 0.15 indicating the basin in senile stage and only 15% of the original landform is yet to be removed by the erosion agents (Fig.4.5.5). The higher H.I. values indicate much area under the hypsometric curve that is still to be eroded and thus indicate a young landform and vice-versa.

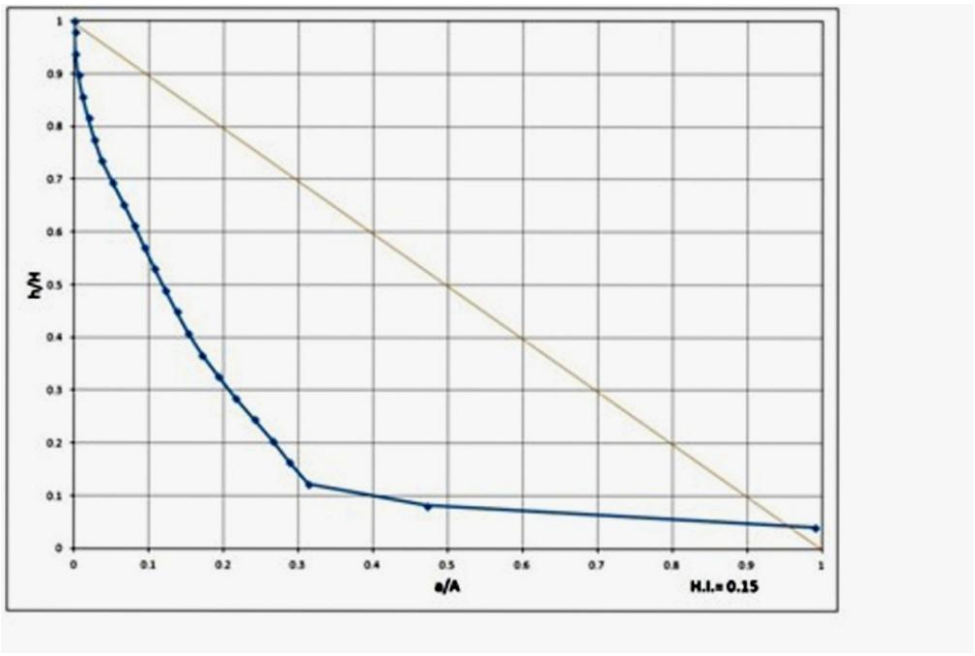

Figure 4.5.5 Hypsometric Curve of Chel Basin

4.5.3.5 Stream length-gradient index (SL)

Stream Length-Gradient Index (SL Index) is considered as one of the quantitative geomorphic parameters incorporated in the morphotectonic analysis (Hack 1973). Tectonic upliftment of a basin and consequent higher vertical erosion and stream profiles changes can be attributed to the SL gradient Index (Vijith 2015).

Lithology, erosional process and tectonic forces greatly affect the morphology of a drainage basin (Keller and Pinter 2002; Dehborzogi et al. 2010; Hack 1973; Giaconia et al. 2012). For areas with abrupt changes in stream profiles, stream pattern and slope, the SL index has proved to be an excellent method to evaluate the ongoing processes of uplift (Štěpančíková et al. 2008; Toudeshki and Arian 2011). Nevertheless, the effectiveness of the parameter in detecting local active structures has not been confirmed for small catchments and/or in regions where tectonic activity is subtle (Chen et al. 2003) and references therein; (Troiani and Della Seta 2008). In small river basins, the contribution of the lithological effect to anomalous values of the SL Index seems indistinguishable from the tectonic one (Troiani and Della Seta 2008). However, in spite of all the difficulties, SL index has been widely used as a

proxy to identify areas of anomalous uplift within a landscape (Kale and Shejwalkar 2008). In tectonically active regions, and at the basin scale of investigation, the SL index can be a useful tool to detect tectonic displacement (Keller and Pinter 2002; Chen et al. 2003; Zovoili 2004).

The stream length gradient index (SL) also shows the association between tectonics, stream power, and rock resistance (Hack 1973; Keller and Pinter 2002) and is computed using the following equation:

Stream Length Gradient Index,

$$SL = \frac{\Delta H}{\Delta L} \times L \qquad (5)$$

Where ΔH is the difference in elevation, and ΔL the length of the stream reach where the index is to be computed. Thus (ΔH/ΔL) is the gradient of the stream reach. The L is the channel length from the drainage divide to the center of the reach (Fig. 4.5.6). Stream power is a function of water, slope, and discharge.

Thus, any alter in slope induced by tectonic deformation or differential rock resistance from lithological variation leads to change in stream power and gets reflected in abnormal SL values.

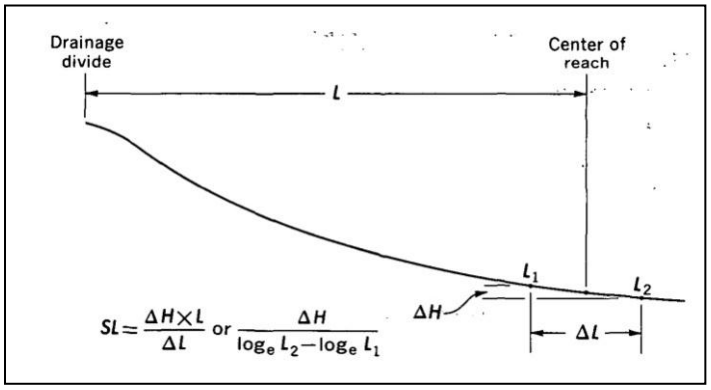

Figure 4.5.6 Schematic diagram for calculation of Stream length Gradient after After Hack J.T., 1973.

The values of SL were computed along the river Chel through demarcation of the watershed, generation of contour at equal intervals, measurement of the values of H

and L using ArcGIS 10.1on a mosaic of SRTM DEM. SL gradient index for Chel River was calculated for its whole length at every 2km unit lengths and corresponding elevation values were extracted from the DEM. The SL gradient values thus computed for every 2km unit length for 28 segments ranges widely from 23 to 950. SL index can be used to recognize recent tectonic activity by identifying irregularly high index values of a particular rock type, as the value of the SL index increases as rivers flow over active uplifted areas (Keller and Pinter 2002; Troiani and Della Seta 2008). The sudden increase in SL gradient index values can be attributed to zones of higher tectonic activity or zones of lithological transition (Fig. 4.5.7). The SL values thus generated along the river Chel ranges widely from 23 to 950.

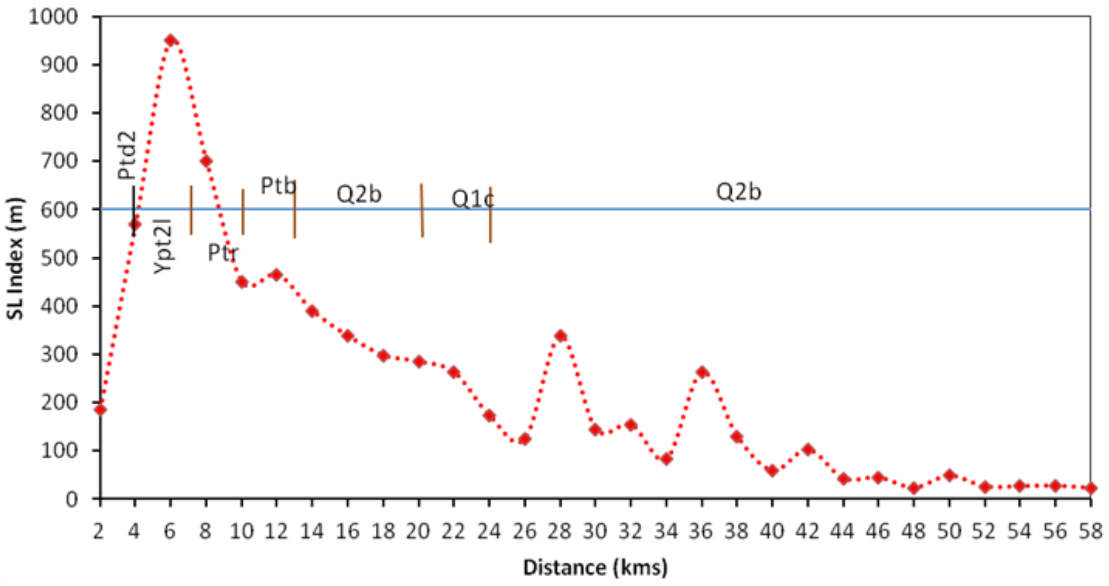

Figure 4.5.7 SL gradient Index of Chel River with lithological boundaries. Note the sudden increase in SLvalues in uniform lithology. (Consult table-1 for details of litho units)

4.5.3.6 Valley floor width-to-height ratio (Vf)

The U- and V-shaped valleys can be identified by the valley floor width-to-height ratio, Vf; (Wells et al. 1988) geomorphic index, which is defined as:

$$Vf = \frac{2Vfw}{Eld + Erd - 2Esc} \quad (6)$$

Where Erd and Eld are elevations of the right and left valley divides respectively, Esc the valley floor elevation, and Vfw the valley floor width (Fig.8.8a). Values closer to 0 implies V-shaped and those close to1 or above 1 implies U shaped valleys. The V-shaped valleys indicate the presence of areas affected by tectonic uplift. The U-shaped valleys indicate the attainment of erosion at the base level (Keller 1986; Keller and Pinter 2002). The Vf for the Chel river basin was computed for every 2kms of the channel length where SL was computed from its mouth up to the mountain front. The Vf values range from 0.1 to 3.67 within this stretch of 14km. The upper catchment of Chel Basin is characterized by V shaped valleys and unpaired terraces induced by tectonic uplift (Fig. 4.5.8b & 4.5.9; Plate 4.5.1).

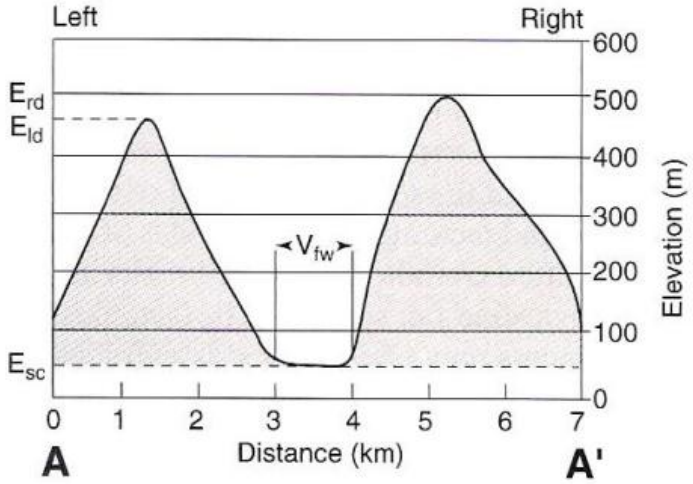

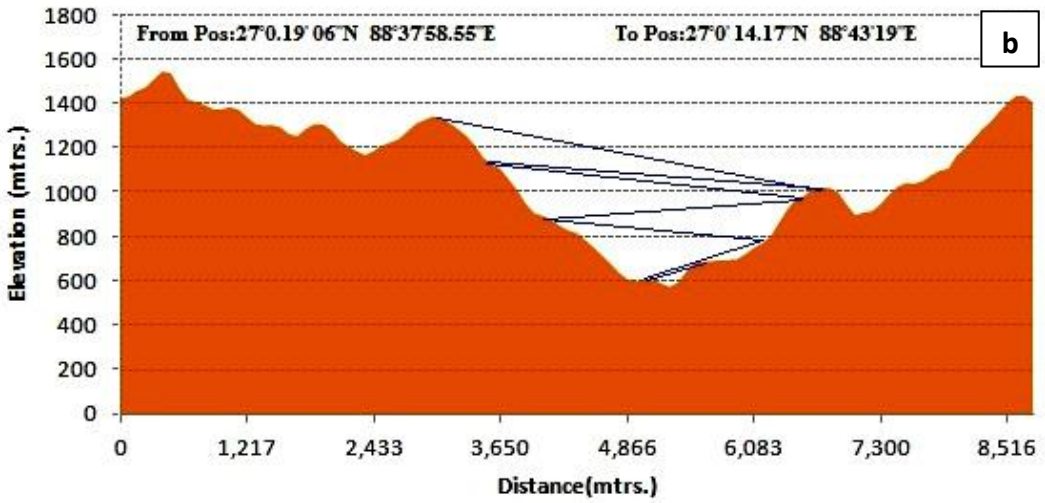

Figure 4.5.8 a- An idealized diagram illustrating how Vf is calculated. Right and left is determined by looking downstream. (Modified from Keller and Pinter 2002, figure 4.16, p. 139); b- Transverse valley profile of the Chel River sculpted by unpaired terraces connected by blue lines.

Plate 4.5.1 Field photograph showing highly incised valley floor of Chel with multiple terrace development on the right side of flow in the upper course around 4kms upstream of Gorubathan(view towards north).

Figure 4.5.9 Google Earth image showing highly incised valley floor with multiple terrace development on the left side of flow in the upper course near Ambiok T.E.(view towards north east) .

4.5.3.7 Index of Mountain front sinuosity (Smf)

Bull and McFadden (1977) and Bull (1978) defines Index of mountain front sinuosity, Smf as

$$Smf = \frac{Lmf}{Ls} \quad (7)$$

Where Lmf is the length of the mountain front along the foot of the mountain where a change in slope from the mountain to piedmont occurs; and Ls is the straight line length of the mountain front (Fig. 4.5.10A &B).

Smf shows a relationship between erosive processes that tend to erode a mountain front, making it more sinuous through rivers and active vertical tectonics that tend to produce straight mountain fronts, which are often coincidental with active faults or folds (Keller 1986; Bull and McFadden 1977). That is, mountain fronts with active

tectonics and active uplift are straight giving the lower value of Smf whereas the regions which have lower or no active tectonics and consequent low rate of upliftment, the erosional processes along the mountain front will dominate and thus will produce more sinuous mountain front resulting in higher Smf.

Smf can be easily calculated from topographical maps or aerial photographs. But the accuracy of value depends upon the scale (Bull and McFadden 1977). Large-scale maps such as Topographical maps and aerial photography which generally have higher resolution gives a higher level of accuracy compared to small-scale maps (>1:250,000) which gives approximate values of Smf due to the lower resolution. Lower the value of Smf higher is the level of active tectonics and vice –versa. Smf approaches 1.0 for the most tectonically active mountain front whereas as the rate of upliftment decreases, the erosional processes carve a much broad and sinuous mountain front leading to higher Smf value. Smf values lower than 1.4 signifies tectonically active (Keller 1986; Rockwell et al. 1985) whereas inactive mountain fronts where initial mountain front may be more than 1 km away from the present erosional front are usually associated with higher Smf values (>3) (Bull and McFadden 1977).

Silva et al. (2003) have calculated the index of mountain front sinuosity using a topographical map at scale 1:50,000 in the two most prominent crustal-scale structures of the Mediterranean sector of Spain: The Eastern Betic Shear Zone (EBSZ) and the Valencia Trough. The authors have divided mountain fronts into three classes on the basis of Smf values:

Class-I (Active Tectonics) - Linear Mountain Fronts (Smf<1.5)

Class-II (Moderate Tectonics) - Irregular Mountain Fronts (Smf ranges from 1.8-2.3)

Class-III (Inactive) – Highly Sinuous Mountain Fronts (Smf ≥2.8).

Here the mountain front sinuosity Index of Chel basin has been attempted from SOI toposheet no 73 B/9 at 1:50,000 scale (Figure 4.5.11) and with Lmf = 8.9 km and Ls= 4.4.km, the Smf value so calculated is 2.02. So based on (Keller 1986; Silva et al.

2003; Rockwell et al. 1985), mountain front sinuosity of Chel basin falls under Class-II of moderate tectonics characterized by irregular mountain front (Plate 4.5.2 & Fig.4.5.11).

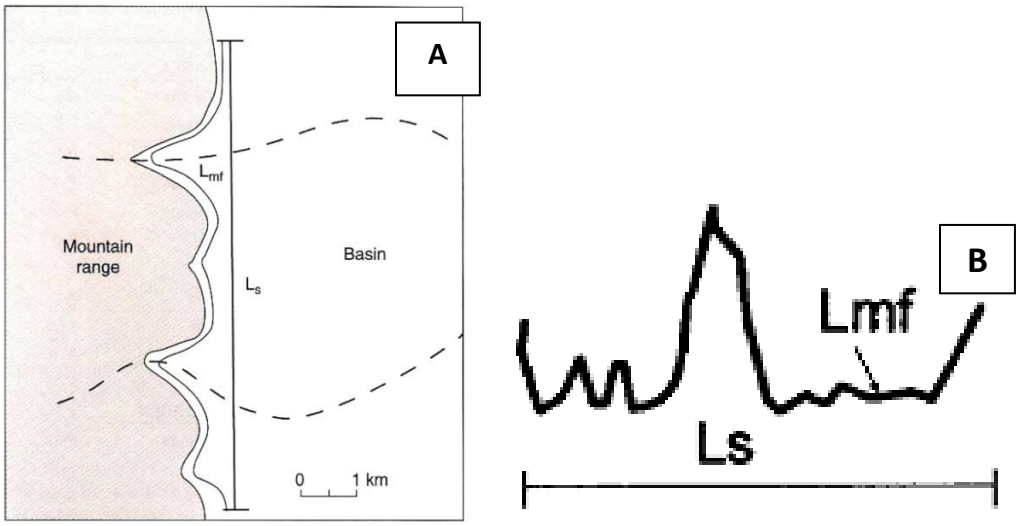

Figure 4.5.10- A. Calculating Mountain front sinuosity (Smf) index (Modified from Keller and Pinter 2002, figure 4.14, p.137); B. Showing total length of mountain front (Lmf) and straight-line length (Ls) of the mountain front (after Bull and McFadden, 1977).

Plate 4.5.2 Mountain front of Chel Basin (View from south-east).

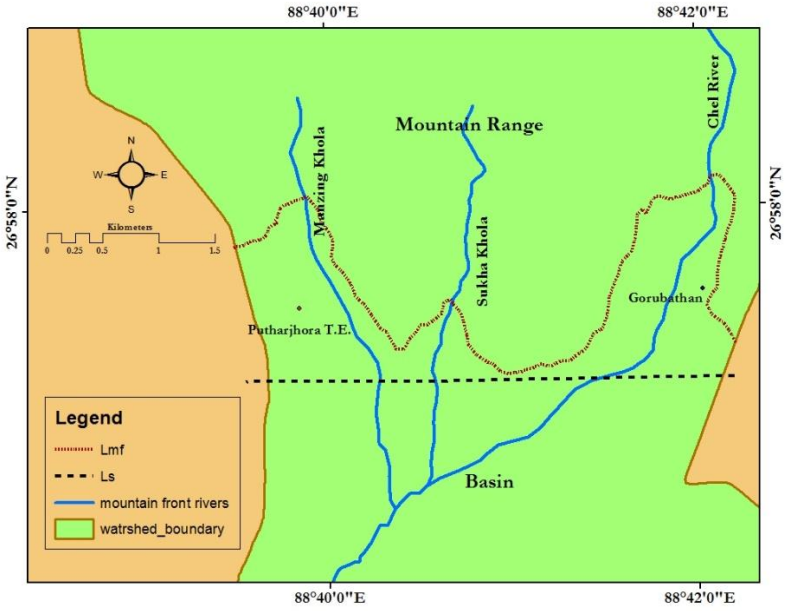

Figure 4.5.11 Mapping of mountain front, Lmf and Ls of Chel basin (Source- SOI toposheet 1970).

4.5.3.8 Transverse topographic symmetry factor (T)

The transverse topographic symmetry factor is another important quantitative geomorphic parameter for the evaluation of tilt of a basin. The T factor can be calculated using the equation:

$$T = Da/Dd \quad (8)$$

Where Da is the distance from the midline of the drainage basin to the midline of the active meander belt. Dd is the distance from the basin midline to basin divide. Generally, the value of T ranges from 0 to 1 and the values close to 0 indicate an absolute symmetric basin, while values close to 1 indicate highly asymmetric basin.

This method was first devised and applied by Cox in the year 1994 to the southwestern Mississippi Embayment infer west-southwestward as preferred stream migration. The observed T values for Chel basin is ranging from 0.15 to 0.91 which implies ground tilting of the basin.

4.5.3.9 Longitudinal Profile

Longitudinal profile of a stream can provide clues to underlying materials as well as an insight into the geologic processes and geomorphic evolution of the area (Giaconia et al. 2012; Jain et al. 2006; Hack 1957; Ambili and Narayana 2014) . The longitudinal profile of a stream channel can be drawn graphically by a plot of altitude in (ordinate) as a function of horizontal distance in (abscissa). Longitudinal river profiles can be interpreted as arising from the balance between erosion and uplift rates. This profile provides an interpretation of the surface history of the river channel as they depict the origin of the river channel and it can be interpreted based on the shape of the curves (Ferraris and Pazzaglia 2012). Concave profiles represent a long-term equilibrium between uplift and erosion rates, while concave - convex profiles with erosion steps in the middle reach indicate a long-term predominance of erosional processes. Convex profiles are characteristic of the areas where the uplift is dominant (Giaconia et al. 2012).

A longitudinal profile of river Chel was prepared by extracting and placing elevation values against the length. The profile thus obtained was subjected to smoothening technique available in MS Excel to avoid any unnecessary large misleading fluctuations. The prepared longitudinal profile indicates the presence of a few knick points at the steeper mountainous course of the river (Fig. 4.5.12).

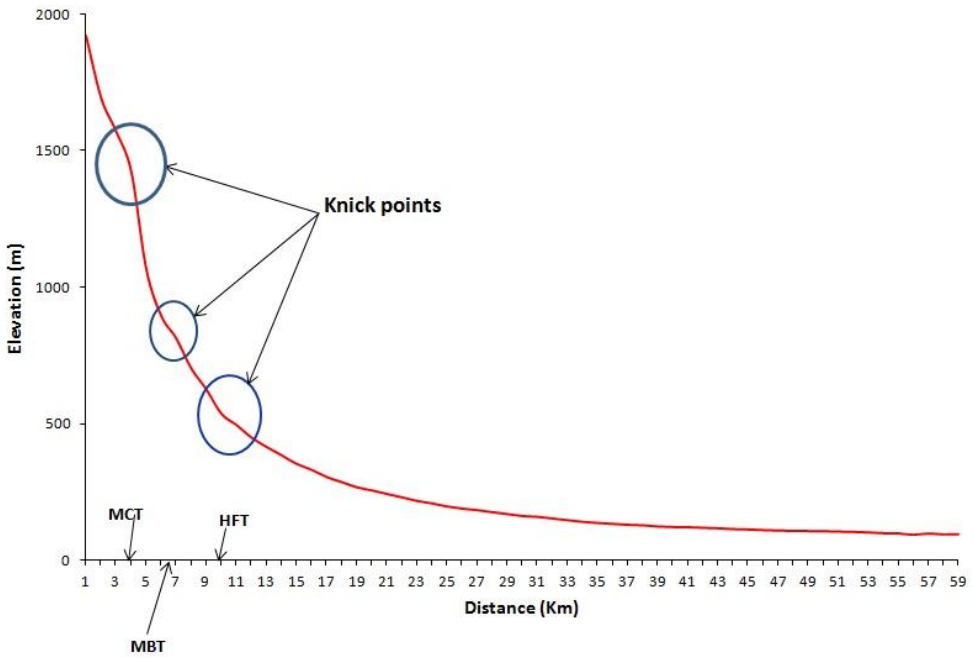

Figure 4.5.12 Longitudinal profile of the Chel river with Knick points.

4.5.4 Combination of geomorphic indices with geology

The combination of assessed indices with the geology of the basin gives an elaborate picture of the influence of neotectonics and its implications on the basin morphology and consequent river characteristics (Fig. 4.5.13). This includes SL, T, and AF which shows the variation of SL values along the river, direction of channel shifting from the basin midline and direction of tilt. This allows for assessment of role of varying lithology over the development of SL index values and since the maximum variation of SL values are observed above mountain front in the multi litho zone of transitional boundary between Ptd2, YPt2l and Ptr whereas largest variation is observed in a single unit of rock (Q2b), it can be inferred that there is an influence of both lithology and tectonics over the drainage characteristics of Chel river basin. Thus, this strongly advocates the argument that active tectonics is influencing and shaping the basin characteristics of Chel river basin.

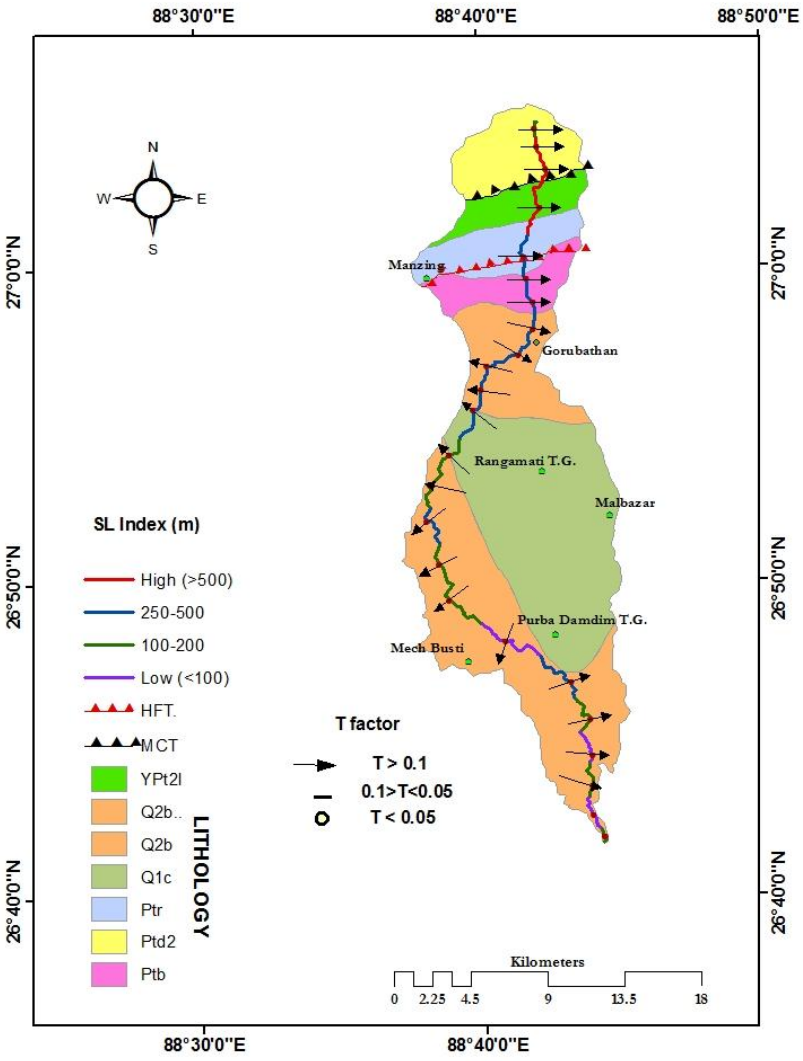

Figure 4.5.13 Map showing cumulative effect of lithology, transverse topographic symmetric factor (T), SL gradient index and major structural features present in the Chel river basin. YPt2l-Lingtse Granite Gneiss (Proterozoic-II), Q2b= Baikunthapur Foration (Holocene), Q1c= Middle to upper Chalsa formation (Pleistocene), Ptr = Reyang formation (Proterozoic), Ptd2= Chungthang Formation (Proterozoic), Ptb= Buxa Formation (Proterozoic).

Major Findings

- The Relief ratio (Rh) calculated for the Chel basin indicates that the river's gradient is steep (~0.054).

- Drainage basin asymmetry factor indicates possible tectonic tilting of the basin and deviation of AF from the central value of 50 indicates basin asymmetry due to tectonic tilting. Af calculated for Chel basin is ~40.31 (<50) which implies the basin is tilted towards the right (looking downstream). Longer length of eastern tributaries compared to the western tributaries further testifies this asymmetry (Fig. 2.5).

- The Basin shape index calculated for Chel basin following Ramirez- Herrera (1998) is 3.46, which indicates that it is an elongated basin and according to (Bull and McFadden 1977), basins draining tectonically active areas are more elongated and become more circular with the ending of uplift.

- The Hypsometric curve shows a relationship between the degree of erosion, dominant hillslope processes and landscape evolution. The hypsometric curve of river Chel shows a steep initial fall with an increasing distance from the equilibrium line then followed by long gentle gradient and finally becoming almost parallel to the abscissa. Such curves indicate high stream erosion which denuded the basin to a large extent and gave the basin characteristics of an old stage of erosion cycle. Hypsometric Integral (H.I.) value of 0.15 indicates very little (only 15%) of the total basin area is present to be removed by the erosion agents. The very steep nature of the hypsometric curve can be attributed to the tectonic activity rather than the normal fluvial processes.

- The valley floor width-to-height ratio (Vf) is considered to a robust proxy of active tectonics. The Vf values for the Chel basin were computed from its source up to the mountain front i.e. only for the mountainous part at the 2km interval for a total length of 14 km. The Vf values thus computed are all <0.7 till 10 km indicating a vertical erosion in response to uplift resulting in tectonically induced V-shaped river valleys. The Vf values at 12km and 14 km are 3.67 and 3.5 respectively suggesting broader river floors then onwards (downslope) due to the comparatively greater lateral erosion of valley sides over weak tectonics.

- Cross-examination of assessed geomorphic indices with geology signifies the presence of tectonic activity in the basin which is responsible for the evolution of basin to its present-day morphology and is reflected in river characteristics and basin as a whole.

Conclusion

An analysis of selected geomorphic indices derived from freely available SRTM DEM was made to assess the impact of neotectonics in the drainage and landform development of the Chel river basin. The accuracy measurement performed to assess the usability of the DEM, validated the use of SRTM DEM 1Arc sec (30m resolution) in the extraction of geomorphic indices for the present study. Relief Ratio (Rh) of 54.12 indicates high gradient, Basin shape index of 3.46, implies an elongated and active basin, Vf values <7 to 10kms from the source indicates then presence of tectonically induced V-shaped valleys in the catchment areas. hypsometric integral value (HI) of 0.15 implies that the basin is active but mature, drainage basin asymmetry factor (Af) of ~40.31 (<50) implies the basin is tilted towards the right (looking downstream), however transverse topographic symmetric factor (T) indicates two directions of tilt, that is, the catchment area above the mountain front of the basin is tilted towards the east whereas the rest of the basin is tilted towards the west (looking downstream). This opposing direction of tilt can be attributed to the prevailing active tectonics along the major Himalayan thrusts. This differential tectonics is reflected in the sudden increase of SL Index values in the reach where the river traverses these active major thrusts. The concave hypsometric curve with steep initial fall with increasing distance from the equilibrium line followed by long gentle slope and finally almost horizontal tail with very low elevation indicates an active but old drainage basin.

This is further supplemented by a concave longitudinal profile with the presence of many knick points in proximity to major thrusts. Altogether it may be concluded that analysis of geomorphic indices suggests Chel river basin has undergone a differential level of neotectonic activity and the trend of severity generally decreases from north to south. The chapter very well explains the tectonic reason behind the west ward

movement of the main channel and consequent evolution of channel morphology. There are no right bank tributaries of River Chel except Manzing khola and sukha khola in the upper catchment as main channel flows along the western edge of the basin for most of its length from Putharjora to kranti. Therefore, nearly all the tributaries have developed on the left of the main channel and are longer than the west bank tributaries. Further the presence of neo tectonically active faults implies potential localization of stress and gradual development of seismic zones, which may lead to large earthquake hazards in the Darjeeling and Sikkim Himalaya. A large number of settlements and infrastructures (like Dams over Tista) are likely to bear the brunt of large seismic events and consequent landslide hazards. Therefore, strict adherence to national and international norms relating to earthquake resilient buildings and land use practices becomes imperative as basic mitigation measures in the region.

4.6 Role of Anthropogenic activities

Introduction

The densely settled piedmont zones of young mountains constitute an example of areas where human activity is superimposed on changes induced by natural forces (Tiwari 2000; Liebault and Piegay 2002; Starkel et al. 2008). On a regional scale, the tectonically active Darjeeling-Sikkim Himalayas, with lithology, which is prone to the mass movement, receive the highest annual rainfall along the whole Himalayan front (Starkel 1972; Dhar and Nandargi 2000; Soja and Starkel, 2007). Their margins and piedmont, as a transitional zone down to the lowland plains, is under the strong influence of the adjacent mountains. The nature and extent of the Himalayas impact on their piedmont is largely a product of adjustments in the fluxes of water and sediment (Starkel and Basu 2000; Grujic et al. 2006; Ghosh and Carranza 2010). Both are frequently accelerated by various forms of human activity such as agriculture, logging, mineral extraction, and road building at the mountain margin (Froehlich and Starkel 1993; Tiwari 2000).

The present-day economy of the Darjeeling-Sikkim Himalayan margin and piedmont depends mainly on tea estates established in the late 19th century (Ray 2002; Prokop and Sarkar 2012). Cultivation of other crops (e.g., rice, millet, areca nut) is largely for local consumption (Bhandari and Kale 2009). A significant part of the region constitutes reserved forest, and tea gardens. Forestry based on commercially valuable trees and tourism is an important contributor to the economy, as well as being an employer of large numbers of people (Government of West Bengal 2008- 2009; Madhusudan 2011).

Like other Himalayan margin and piedmont environments, the study area has been experiencing heightened human pressures resulting in environmental degradation from a variety of causal factors, such as deforestation, sediment mining, bridge construction, extensions of embankments, and growth of tourism etc The human activities observed in the basin are boulder, pebble and sand mining (especially mechanized in-stream mining), embankment construction, road and rail bridge, landuse change, road widening,

concretization of flood plains etc. The present section seeks to assess, understand and gather the evidences of the role of these human activities on Chel River's dynamism.

4.6.1 Sediment Mining

Alluvial channels have historically been an attractive source of sand and gravel for a variety of construction activities. The floodplains and terraces are mostly the sites of sediment storage in stream systems and can contain large quantities of boulders, gravels and sands that can be mined economically (Langer 2003). There are several advantages for the aggregate operators in using river sediment (Kondolf 1994), such as: (a) the material is already granulated, rounded, well-sorted, and generally clean (lacking cement and weak materials, and relatively free of interstitial fine sediment); (b) the source of material is generally close to destination or to the markets for the product, reducing transportation costs; (c) active channel sediments can be easily extracted (deep quarrying is not necessary), require little processing, and are periodically replaced from upstream during high flow events.

The study reach is characterized by highly fluctuating discharge, copious amount of aggradations due to break of slope situation and erodible banks. This altogether has resulted in development braided channel pattern with ever changing bars. The upper catchment experience surface runoff and landslides during high intensity concentrated rainfall months and adds more sediment to the channel downstream. These sediments are available for easy extraction directly from the river bed and surrounding terraces right from Putharjhora (near mountain front and tip of break in slope) upto confluence of Chel with River Neora. It's not certain when sediment mining began in the Chel basin but through surveys among locals it was understood that a major peak in the demand for sediments from chel basin came during the construction of Teesta Barage at Gazoldoba during 1980s.The barrage construction was completed in 1987 but the barrage operation of the water diversion was started at the end of 1997 (Ghosh, 2012). Initially only boulders and large sized gravels were extracted but with the growth of demand, extraction of other grades of sediments began. In recent years the development of higher connectivity in the form of better and new roads further has increased the demand.

Further the basin is well linked with major growing towns of north Bengal which has made Chel River a great source of sediments. This has attracted influx of laborers from neighboring areas and far off places from different regions of North Bengal, Bihar and even Bangladesh (Gan 2008). The dwindling Tea industry of the region is also forcing local population to get engaged in the sediment mining process. The same reason is driving locals for coal mining in the nearby Lish and Gish basins. Presently the sediments from the Chel River are a major source for growing construction industries in the region, neighboring states and countries as well. The extraction of sediments is mostly done manually with simple tools throughout the entire stretch of study reach but mechanized extraction to a significant extent was observed upto 10 kilometers upstream and downstream of the Odlabari road and rail bridges (Plates 4.6.5-4.6.8). There are two operational local sediment processing units- one at Toribari, 5 km upstream of Odlabari and another at Odlabari, 1km downstream of Odlabari Road Bridge (Fig.4.6.1 A & 4.6.1 B). The extracted sediments from the river are brought to these processing units and the materials are processed mechanically with the help of sieves of various sizes. The sieved materials are kept separately according to its sizes for ready transportation to places of demand. The common methods of sediment extraction practiced are Dry-pit mining, Wet-pit mining, bar skimping or scrapping and pits on the river terrace or adjacent flood plain.

The types and amount of sediment extraction is seasonal in nature. During dry season all grades of sediments ranging from large boulders to fine sand is extracted directly from the river bed, bars and surrounding terrace of the entire stretch of the study reach. Generally large size boulders are collected from upper section of the Reach-A (Putharjhora-Odlabari), medium size boulders, gravels and little proportion of sand is collected from the rest portion of Reach-A and upper portion of Reach-B (Odlabari-Nipuchapur T.G) whereas sand mining dominates along the rest of Reach-B and entire Reach-C (Nipuchapur T.G.- Kranti) (Plate 4.6.1-4.6.4). With the onset of monsoon season the extraction activities gradually ceases to near bank and higher terrace locations as high flow and water depth hinders the in-stream extraction. This season records the lowest extraction amount in the entire year especially for lower grade sediments and sand. As soon as monsoonal winds weakens and flow velocity and depth lower in the channel by the month of late September and early October, laborers lift the larger sized

boulders first that are brought down to greater distance by the higher monsoonal flow. The cycle continues same way year after year. Various impacts of sediment mining on channel dynamics are discussed below.

Plate 4.6.1 Field photographs showing Boulder lifting at Toribari, Upper Reach; Plate 4.6.2 Mid channel Gravel bar skimping at Odlabari, Middle Reach; Plate 4.6.3 and Plate 4.6.4 Sand mining at Rajadanga, Lower Reach.

Plate 4.6.5, 4.6.6 & 4.6.7 Manual way of sediment extraction wherein crushing and segregation is done on the river bed only; 4.6.8 Mechanized sediment extractions collect large volume but crushing and segregation happens with sieves at processing units.

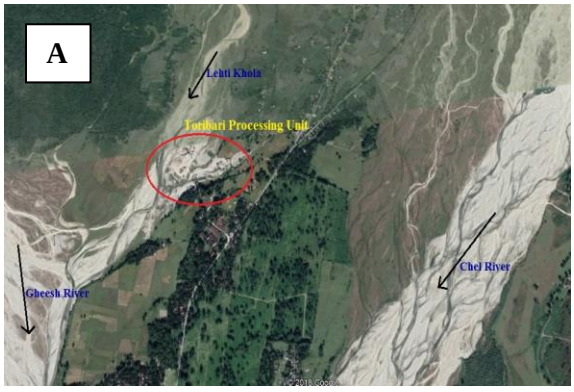

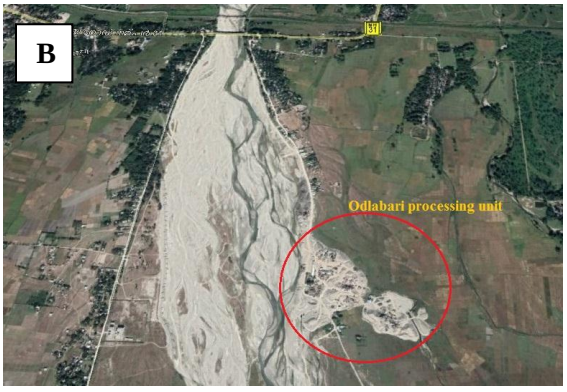

Figure 4.6.1 Google Earth Images showing sediment processing units. (A) at Toribari and (B) at Odlabari.

Plate 4.6.9 Field photograph showing sediment processing unit at Toribari. Plate 4.6.10 Field photograph showing sediment processing unit at Odlabari.

4.6.1.1 Thalweg shifting and instability of channel bars

Thalweg shifting happens when sediment is extracted very close to the river thalweg. The extraction leaves pits of different sizes separated from thalweg by a narrow strip of land. As the water level rises during high flows, the thalweg may capture the pits. Thus, the former off-channel pit transforms into an in-channel pit (Rinaldi et al. 2005).

It has been observed from cross profiles measured at 400m upstream and 400m downstream of the odlabari road and rail bridge respectively that thalweg points have oscillated to the right and left with time (Fig.4.6.2 A & 4.6.2 B). In the upstream cross profile, the thalweg point migrated near to right bank in 2015 from its near left bank position in 2014 and it occupied near center position in the year 2017. In the downstream cross profile, the thalweg has consistently moved towards the center from its near left bank location in 2014. The river exhibits braided channel pattern for much length of the studied reach except the lower reach (Reach-C). In this multi-channel braided system there are multiple lower elevation points with very little variation and are separated by low height bars as exhibited by both cross profiles. In such situation little disturbance of channel bars separating this multiple flow induced by sediment mining is leading to significant shifting of thalweg points. Thus, due to braided channel pattern and greater extent and intensity of sediment mining, thalweg shifting is much dynamic in the Reach-A and Reach-B.

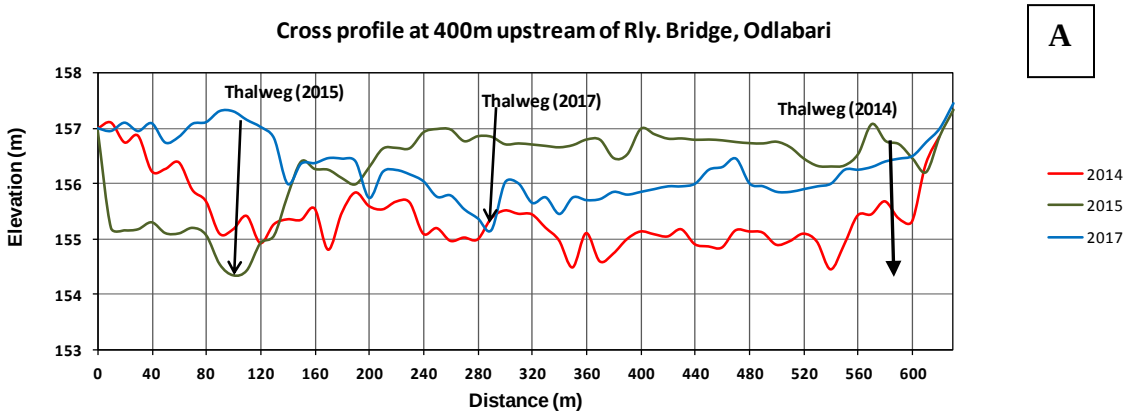

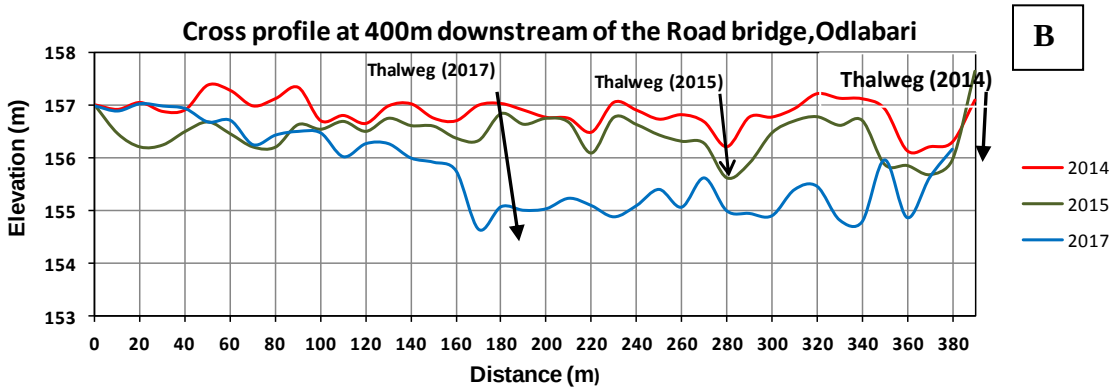

Figure 4.6.2 Cross profiles showing Bed elevation change and movement of thalweg during 2014 and 2017at 400m upstream of Rail Bridge (A) and 400m downstream of the Road Bridge, Odlabari (B).

4.6.1.2 Bed elevation change

In terms of bed elevation, the upstream cross profile exhibits alternate phases of lowering and rise in bed elevation. In the year 2015, its bed elevation has risen by 1.5m on an average throughout the cross-profile length except near the right bank where the bed elevation has gone below the 2014's bed elevation and the new thalweg point has developed at an elevation of 154.54m. The 2017 bed elevation falls almost between the bed elevations recorded in 2014 and 2015. Its observable that the near right bank section experienced deposition of about 2m and rest of the cross-profile length experienced erosion by 1m on average. The fact that this cross profile falls upstream of the twin Odlabari bridges and is nearer to the mountain front explains the bed level rise of 2015 (Fig. 4.6.2 A). Whereas it seems that huge amount of both manual and mechanized sediment extraction activity operating in the region is the most probable cause for the lowering of bed elevation (Fig.4.6.2 B). The downstream cross profile on the other hand exhibits consistent lowering, much on the centre to left bank section of the cross profile. The consistent lowering of bed elevation in the downstream cross profile can be attributed to the coupled impact of bed scouring caused by the increased flow velocity induced by the twin bridges and huge mechanized sediment extraction being very close to the Odlabari processing unit (Fig.4.6.3).

Figure 4.6.3 Huge mechanized mining pits near to Odlabari Processing unit.

4.6.1.3 Shifting of pool-riffle sequence

Pools are defined as topographic lows and riffles are the topographic highs along a longitudinal profile of a stream. Huge extraction activities especially mechanized one is creating artificial pools along the studied reach of Chel River (Plate 4.6.17 & 4.6.18). These artificial pools increase the gradient of the upstream channel from the extraction hole, which leads to headward erosion that will tend to move several kilometers upstream and changes the natural sequence of pool and riffles and then change in channel morphology happens (Ghosh et al.2016).

4.6.1.4 Deformation of channel beds

It's been observed that mining of sediments is deforming the river bed. The mining pits are creating artificial pools and lows which can be considered as topographic negatives whereas the extracted materials are sorted and stored on river bed only which creates temporary topographic positives of mounds ranging anywhere from 1m to 8m height. Some of the spoil dumps at the Odlabari processing unit measures 30m high approximately (plate 4.6.15). These mounds of sediments are stored temporarily from few days to few months. Sometimes it is left till even next season. Some of the

excavation pits on the other hand can also last longer if the river cannot fill it in the next high flow season or if pit remains cut-off and thus abandoned from the main channel flow. These artificial highs and lows are creating defaced channel beds and is affecting river morphology (Plate 4.6.11-4.6.18).

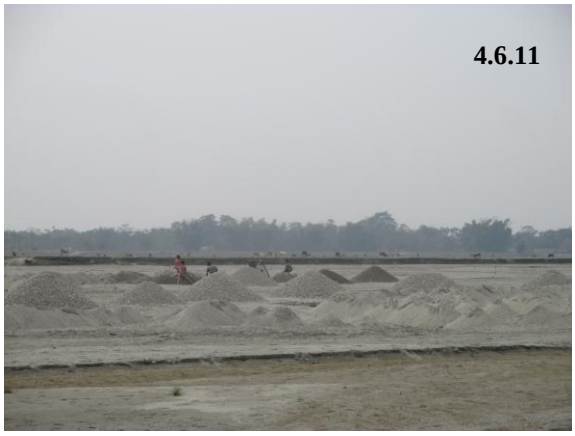
4.6.11


4.6.12

4.6.13


4.6.14


4.6.15


4.6.16

Plate 4.6.11 & 4.6.12 Channel bed deformation due to manual sediment mining; Plate 4.6.13& 4.6.14 mechanised wet pit mining creating huge longitudinal depressions (negative topography); Plate 4.6.15 Dumping of huge amount of sediments at Odlabari processing unit creating positive topography of sediment mounds; Plate 4.6.16 huge elongated mining pit after mechanized lifting of sediments; Plate 4.6.17 and 4.6.18 huge pools created along mechanized wet pit mining sites.

4.6.1.5 Channel planform changes

The values of braid-channel ratio have consistently decreased since its highest mark of 2.27 in 1976 to lowest value of 0.96 in 2005 and then by 2017, the values in each segment became near 1 which is suggestive of the fact that Chel river is gradually transforming itself from a braided channel to a straight one (Table 4.2.10 and Fig. 4.2.23). The recent years clustering of points which otherwise were scattered horizontally elongated further confirms the transition of channel form from braided to straight (Figure 4.2.23). Continuous wet pit mining creates deep elongated riverbed and lack of sediments can be hold partly responsible of this gradual transition (Plate 4.6.14). This limits scope for multi-channel flow.

4.6.1.6 Others Impacts

Due to sediment mining human pressure is increasing on the channel beds. During day time, thousands of people tread the river bed on foot, bicycles and motor bikes. Further sediment transporting vehicles i.e., pickups trucks, full size trucks, tractors, tipper or dumper trucks continuously move on the river bed. All these movements generally happen across riffles as they are the natural topographic highs. Thus, river beds get very

compacted across the riffles and along the haul ways of the river due to continue movement of vehicles. Naturally river needs larger stream power to erode away these human compacted sections of river beds and thus remains largely undisturbed during entire low flow duration whereas river concentrates its energy on loose section of the bed. The vehicular movements also degrade the growth of vegetation on the river beds, banks and on the adjacent floodplains which leads to increased erosion. Further the surface vibration produced from the continuous vehicular movements loosens weak and high bank materials and thus assists in accelerated rate of bank erosion. It was found during field surveys that embankments or natural levees were deliberately broken or lowered for easy and short access of men and vehicles to the river bed (Plate 4.6.19). During the high flow time these points are much likely to be breeched and cause movement of flow towards the low-lying surrounding floodplains. Thus, it also accentuates channel dynamicity. At many a times the sediments are collected from the base of the banks to get the advantage of easy and quick transportation of sediments which leads to diversion of flow towards the banks and cause bank erosion. Further the lifting of specific size sediments and leaving behind the others is disrupting the natural distribution and dispersal of sediments both across and along the channel. This is creating unnatural imbalance in the distribution of critical shear stress ($\boldsymbol{\tau_c}$) both across and along the river channel. Further though the West Bengal Minor Minerals Rules, 2002; Schedule V prohibits extraction of minerals within a distance of 200 m from any hydraulic structure, reservoir, bridge, canal, road and other public works or buildings, it was noticed during the field surveys that sediment extraction in the Chel basin is operating flaunting all rules and regulation according to the ease of miners. Sediment extraction barely 100 meters upstream of the rail bridge and even under the road bridge of Odlabari was noticed, most probably to get the comfort of shade provided of bridges on scorching day of March (Plate 4.6.20 & 4.6.21).

Plate 4.6.19 One of the many human breached embankment points for easy access of man and vehicles into the river.

Plate 4.6.20 Sediment mining operating barely 100m upstream of the Odlabari rail bridge; 4.6.21 Sediment mining operating under the Odlabari road bridge.(Photographs taken- 21.03.2013)

4.6.2 Bridge construction

Human induced modifications through engineering infrastructures like roads, bridges, dams and urban landscape when takes place across and along a river channel, experience severe geomorphologic impacts upon that channel in terms of its transport

capacity, sediment supply, river bed modification, and downstream hazards (Thomas 1956). Several scholars have studied the impact of these infrastructures on river channel and have established about alteration in natural state of the channels (Ismail 2009, Forman and Alexander 1998, Gregory 2006). Bridges, railways and highways which are built to facilitate surface connectivity affects channel morphology negatively much like the dams. Road-stream crossings especially affects both upstream and downstream of channel. It also affects the riverine ecology and habitat (Suvendu 2013, Khalifa et al. 2009, Bouska et al. 2011, Kothyari and Ranga Raju,1992).In the case of Chel River under study, one rail and one road bridge crosses the chel basin from the middle and thus divides the Chel River into two halves of almost equal lengths (Fig.2.13).The road bridge is over NH31 connecting Siliguri and Alipurduar which joins newly built Asian Highway at Telipara, Binnaguri and the rail bridge is over broad gauge line of NEFR (North East Frontier Railway) division connecting Siliguri with Alipurduar. During the construction of bridges, engineers kept the width of bridges minimum for structural efficiency or cost cutting (Biswas and Banerjee, 2018). Chel basin fall within the annual total precipitation range of 250- 500 cm much of which is concentrated in the high sun season from May to June. During 2015 an annual total precipitation of 432.02 cm was recorded at Rangamutee Tea Garden (Fig. 2.4). The concentrated amount of rainfall during monsoon brings down huge sediments and water into the channel but the twin bridges of Odlabari, barely 150m in across length pose as a great impediment for natural passage of water and sediments downstream. Very less spacing between upstream rail bridge and downstream road bridge further aggravates the situation. Presently the channel has been constricted to a greater extent and a bottle neck situation has developed (Fig.4.6.4). The morphological and hydrological alterations that the channel is facing upstream and downstream of these twin bridges are discussed below.

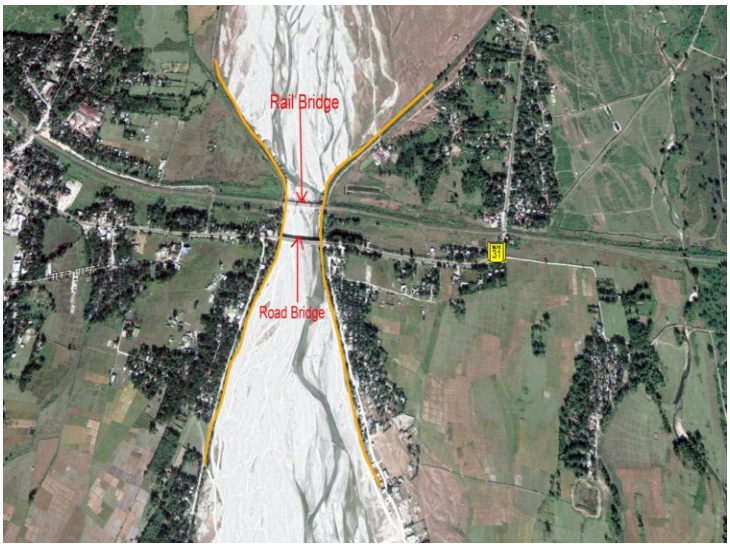

Figure 4.6.4 Bottleneck condition of the River Chel (marked with yellow lines) due to Rail and Road Bridge at Odlabari (Source- Google Earth Image dated. 11.07.2017).

4.6.2.1 Surface Elevation Change

The study established the fact that due to bottle neck condition, the surface terrain in both upstream and downstream of rail and road bridges has undergone change and is observable during even a short period of 2000 to 2011. The upstream section is experiencing increment in elevation in response to sedimentation as is evident from comparison of Aster GDEM, 2011 (30m resolution) with SRTM DEM of 2000 (30m resolution). The areas within elevation zones of 192m-239m and 239m-312m is growing in size and is increasing down slope which implies sediment increment in the upstream of twin bridges (Fig.4.6.5a & 4.6.5b). The bridges hinder the free passage of water and hence the flow velocity gets reduced considerably in the upstream leading to deposition of sediments which the river couldn't carry at that velocity. Whereas opposite scenario is prevailing in the downstream section of the bridges. This stretch is characterized by bed scouring and bank erosion. Unlike upstream of twin bridges, the downstream stretch is experiencing intrusion of low elevation surface zones towards the higher elevation zones in fragmentary but linear pattern which suggests of bed scouring along these linear zones (Fig. 4.6.6a & 4.4.6b). It is quite evident from the comparison of DEMs of 2000 and 2011 that the temporary impounding situation occurs during high monsoonal flow at the upstream of the bridges causing increase in the potential energy of the river which has to

pass through constricted section of the bridges resulting in the increase of downstream flow velocity, i.e., the conversion of potential energy to kinetic energy. This increased velocity translates itself through bed scouring and bank erosion. These findings are well consistent with the bank erosion results in previous chapters wherein the Reach-B (downstream of bridges) accounted for maximum channel migration and consequent bank erosion.

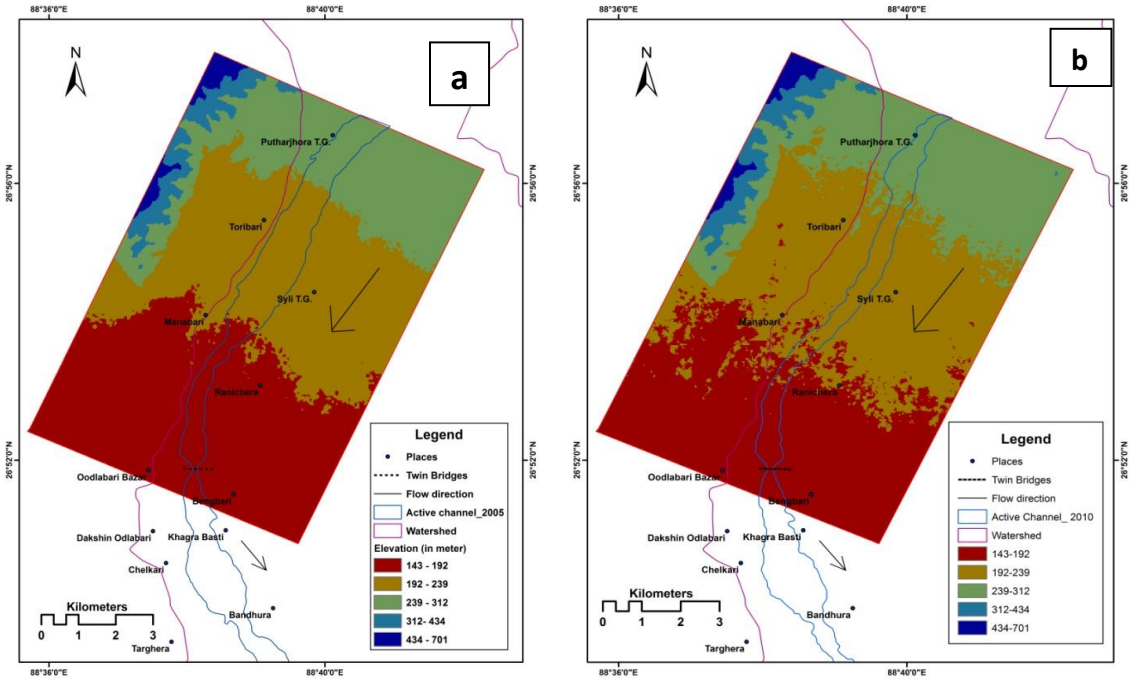

Figure 4.6.5 Surface elevation change from Putharjhora till Odlabari bridges in the upstream section in 2000 (a) and in 2011 (b).

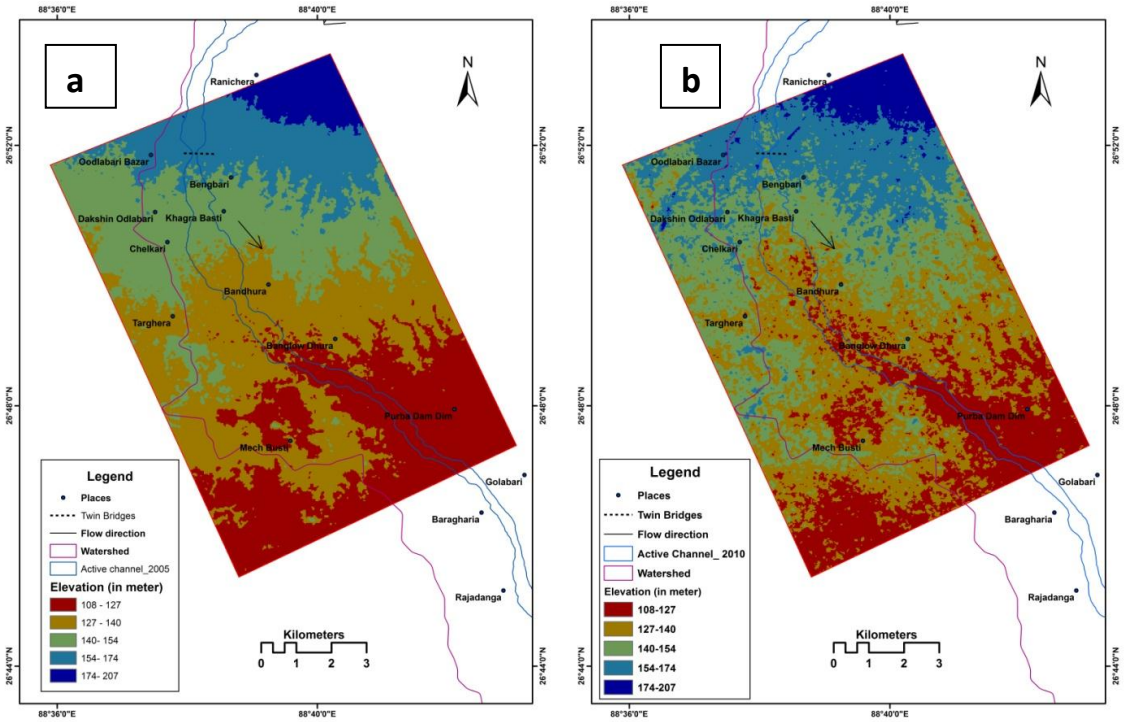

Figure 4.6.6 Surface elevation change from the Odlabari bridges till Purba Damdim in 2000 and in 2011 (d).

4.6.2.2. Channel migration and planform change

The twin bridges have an impact in increasing the dynamicity of the Chel River. Biswas and Banerjee, 2018 have studied the impact of twin bridges on channel planform of Chel River in detail spanning 100 years from 1913-2014. Soon after the construction of rail bridge the river started depositing sediments and well-formed bars appears by the year 1942 (Fig.4.6.7c). From 1913 to1942 there was only rail bridge across its course but with the addition of road bridge soon after 1984, the hydro-morphological impact has amplified manifold. In the subsequent years there have been phases of bar enlargement and modifications. It was observed that the channel width gradually increased and braided channel pattern evolved with increase in number of streams in both upstream and downstream reach of the river.

Based on the six cross sections drawn along the river, they argue that maximum shifting of channel has happened across the cross sections downstream of the twin bridges. Shifting of almost 2.5 kms (approx) has happened since 1913 between downstream of

bridges to Damdim. Further they add that the channel is shifting westward in the upstream and eastward in the downstream of the twin bridges after high flows of 1922-1923,1948,1950,1968,1999 and 2000 (Biswas and Banerjee,2013).

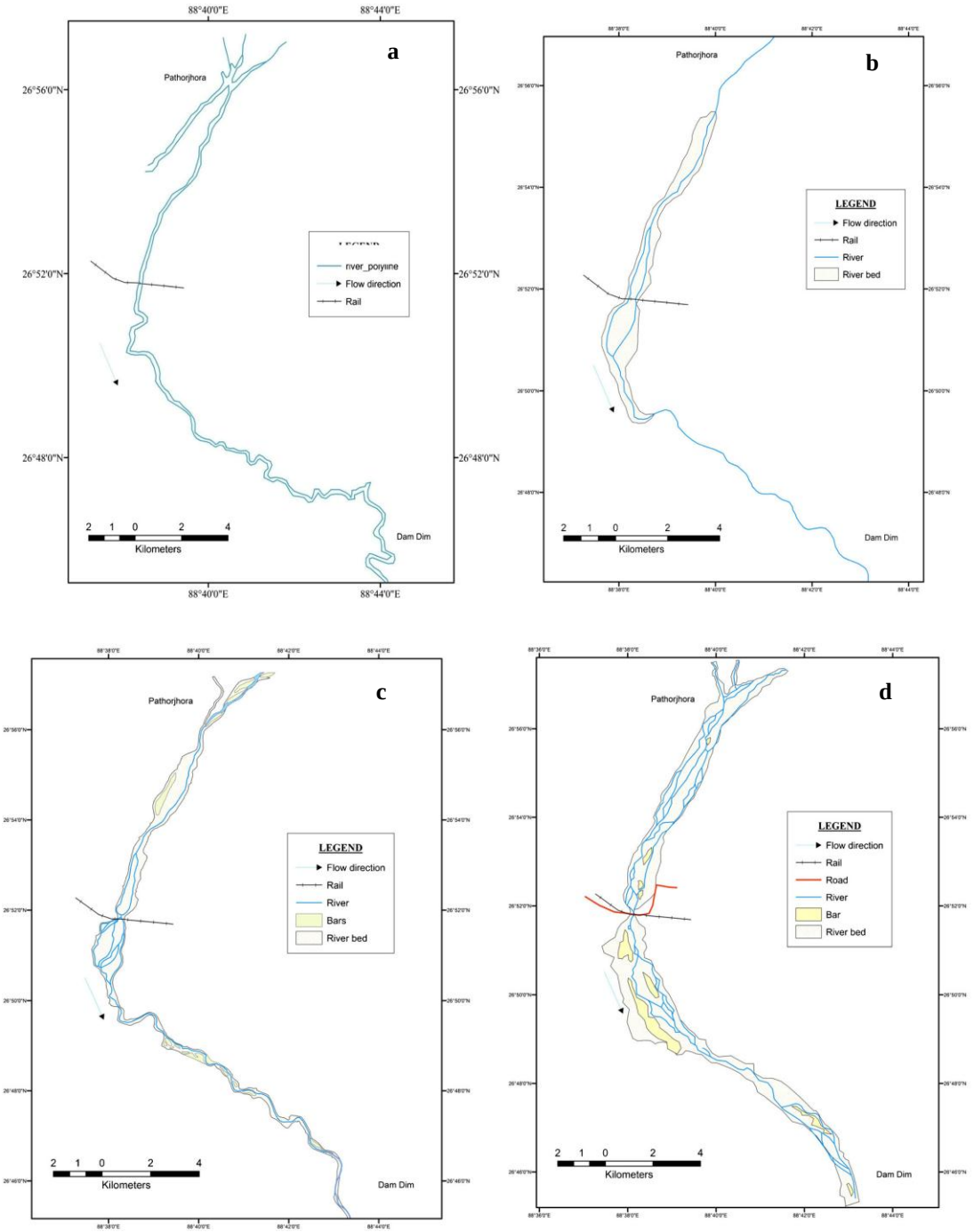

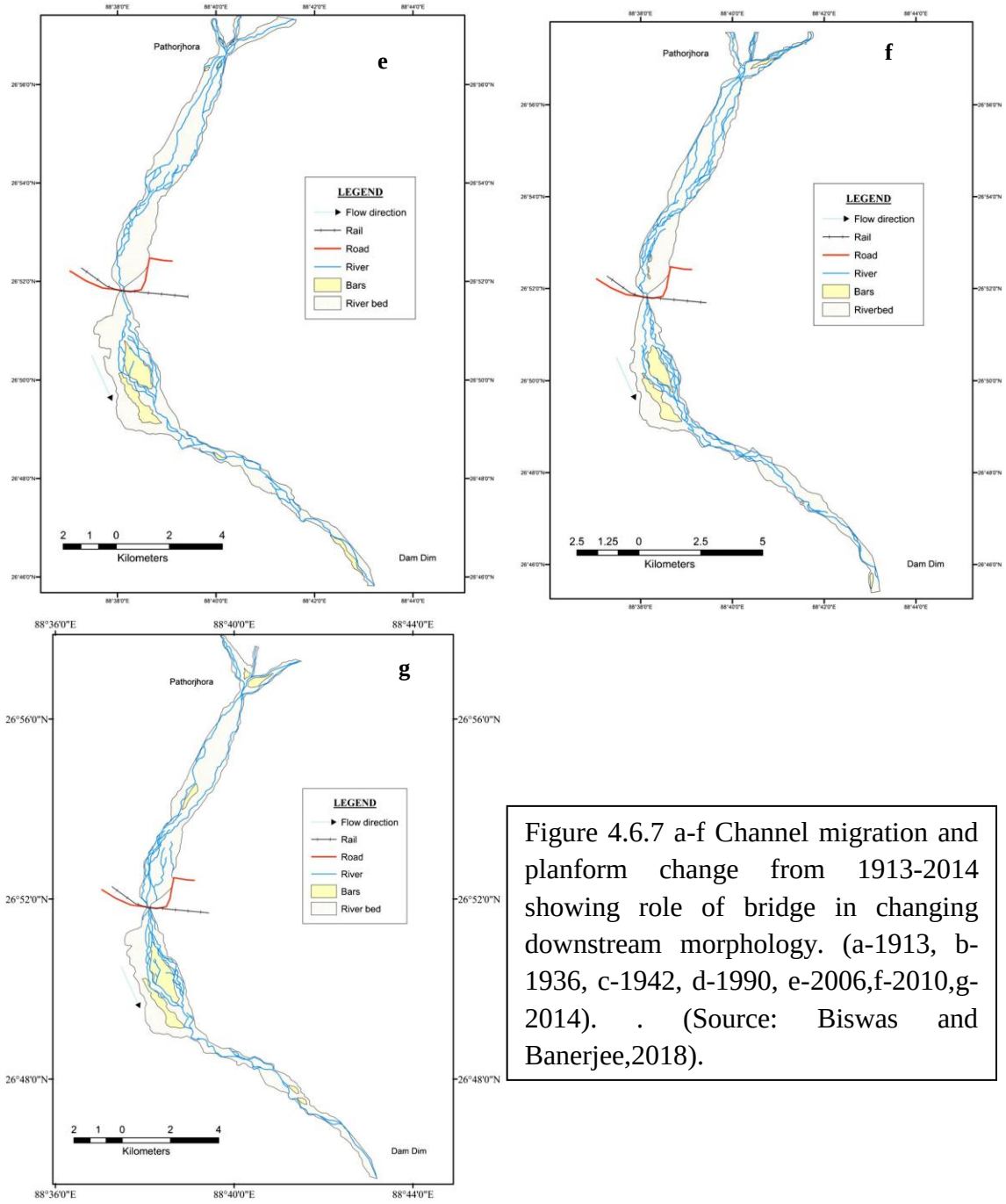

Figure 4.6.7 a-f Channel migration and planform change from 1913-2014 showing role of bridge in changing downstream morphology. (a-1913, b-1936, c-1942, d-1990, e-2006,f-2010,g-2014). . (Source: Biswas and Banerjee,2018).

4.6.2.3 Effects on hydraulic and geometric parameters

The bridges have also impacted the hydraulic and geometric parameters of the river. It has been found that the flow velocity is highest in between the bridges. The same is higher in the downstream of the bridges compared to the upstream section. The higher recorded flow velocity in the downstream section compared to the upstream section of

the bridges plays vital role in bed scouring and bank erosion in the Reach-B (Odlabari-Nipuchapur). Concentration of highest flow velocity between the bridges is causing scouring and incision of bridge piers threatening their stability (Plate 4.6.22 & 4.6.23). This very process seems responsible for damage of old railway bridge and therefore a new bridge has been constructed upstream and is operational presently (Plate 4.6.24). Further the flood prone channel width and width-depth ratio is least in between the bridges whereas it is higher in the upstream section compared to the downstream section of the bridges which is suggestive of back water effect and consequent extended flood plain in the upstream section due to obstruction caused by the bridges (Biswas and Banerjee 2018).

Plate 4.6.22 & 4.6.23 Bed incision at the foot of railway piers.

Plate 4.6.24 Remnants of old damaged railway piers in between functional Rail and Road Bridge at Odlabari. The number of piers in the new railway bridge has been reduced to only two instead of five in the older one.

Figure 4.6.8 Channel widening due to cumulative effects of bottleneck condition and vegetative mid-channel bars in the middle reach of River Chel (Source- Google Earth Image dt. 11.07.2017).

4.6.3 Extension of embankments

The embankments (locally known as *Bandh*) are constricting the active floodplain and thus compelling Chel River to dissipate its energy within the narrow channel bed. During 1970 the total length of embankment was only 14 kms which grew to 41.25 kms in 2017 alongwith 2.53 kms of Dykes. Dykes have been constructed along severe erosion reaches to strengthen embankments. Thus, there has been three times extension in the length of the embankments and now covers almost 58.1% of the total active channel length of 71kms combining both banks (2017) (Fig.4.6.9). Right bankline is almost embanked completely with very little embankment free stretch between Dakshin Odlabari and Targhera. Erection of embankment along almost entire stretch of right bank can be explained by the fact that the area beyond the right bank is largely settlement area and cultivable land and the channel is progressively migrating towards the right as seen in section 4.2.3.2.1. Contrary to this, areas along left bank is physiographically higher than the right bank area as suggested by basin asymmetry factor of 40.31 which implies that the basin is tilted towards the right in the downstream flow direction section 4.5.3.2. Thus, main channel flow reaches near left bank only at or along sites of concave channel bends and thus erosion is confined only along these small and fragmented cut banks (Transverse section A-B in figure 4.6.9). But since main channel flow is mainly concentrated along the left bank, large stable point bars have developed on the inner banks of the channel bend. This development and growth of point bars along the inner banks of left coupled with tiltation towards the right is pushing the main channel more towards the right and thus creating more pressure to the right embankments especially along stretches where channel bends are near to right banks (Transverse section B-C in fig.4.6.9). Thus, it's been noticed that this has resulted in damage of right embankments along these bends (Plate 4.6.25-4.6.28). Few cases of erosion along the banks without embankment has been noticed which falls on the opposite of banks with embankments (Plate 4.6.30 & 4.6.31). The area beyond left bank hosts forests, tea gardens and agricultural land with no large settlements or towns which altogether explains why much length of the left bank is still free from embankments. Almost entire left bank upstream of Odlabari bridges has no embankment and similarly the stretch from Bengabari to Purba Damdim in the downstream still doesn't have any embankment (Fig. 4.6.9). Since

the river is flowing confined between higher terraces along the left bank and heavily embanked right bank, unless and until there is very heavy high flow it cannot access and deposit the sediments in the lower flood plains. Due to this the channel bed is rising constantly and thus the difference between channel bed and embankment heights is decreasing progressively (Plate 4.6.29). This implies ever decreasing threshold level of bank full discharge with higher probability of flood and channel avulsion at lower discharge in the future.

Plate 4.6.25 & 4.6.26 Damaged right embankment at transverse section C-D, (Photograph taken -21.03.2013). Plate 4.6.27 & 4.6.28 Repairing and strengthening of embankment by addition of dykes (Photograph- 10.08.2014).

Plate 4.6.29 Copious sediment aggradations forming huge gravel bars in the immediate upstream of railway bridge, Odlabari. Note the least difference in elevation between the river bed and the embankments.

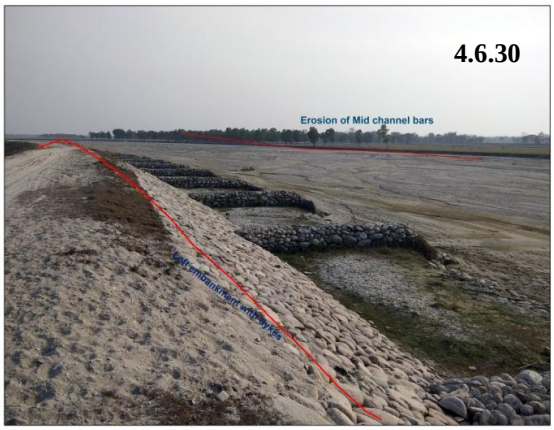

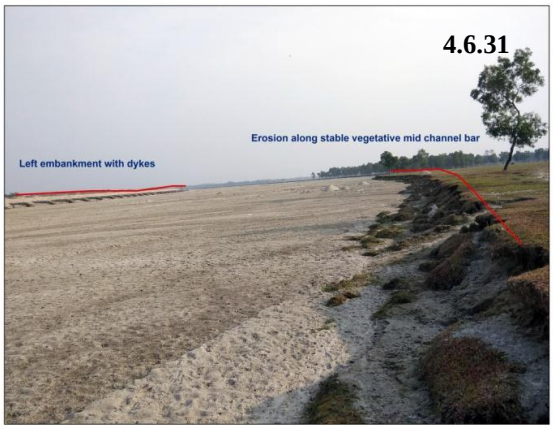

Plate 4.6.30 & 4.6.31 Left embankment with dykes and erosion on the opposite along the mid channel bars near Rajadanga.

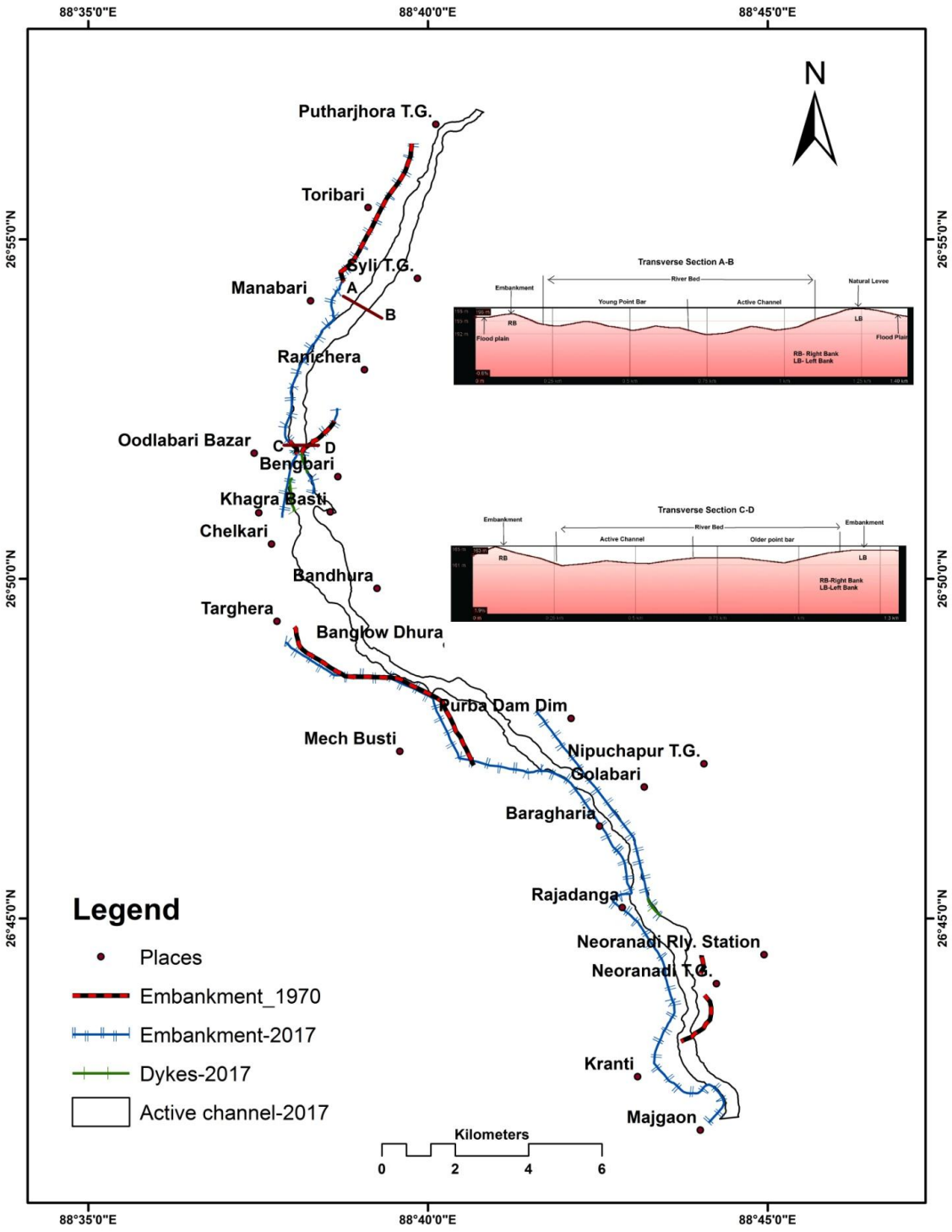

Figure 4.6.9 Extension of Embankments between 1970 and 2017. Source- SOI Topographical Map(1970) and Landsat 8 OLI/TIRS (2017).

4.6.4 Change in Land use

Biswas and Banerjee (2018) have compared the landuse of Chel Basin and surrounding region from 2005 and 2015 classified Landsat images. They found that there have been significant changes in the areas within settlement and tea gardens. The areas within settlement and roads have increased from 5 to 11% and agricultural land from 11 to 30%. Most notably the area with tea gardens has reduced from 25.9% to 10.75 %. Forest coverage also has reduced from 37% to 32%. Scrubland has recorded zero in 2015 compared to 10% in 2005 (Fig.4.6.10). Altogether it can be said that there has been decrease in land under natural elements and increase in land under anthropogenic activities except tea gardens. The altered land uses have negative impact on the channel and it can be seen in the increment of areas within sand and boulder river bed from 5% in 2000 to 9% during 2015. Much of the areas on both side of the river below the twin bridges of Odlabari have been converted into settlement and agricultural land and even the channel bars are cultivated intensively seasonally. During monsoon it's used for paddy cultivation whereas during dry winter season, vegetable is cultivated largely.

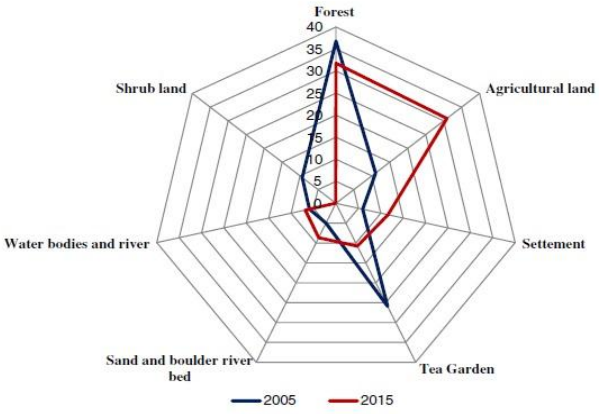

Figure 4.6.10 Graphical representation of LULC change (%) during 2005-2015. (Adopted from Biswas and Banerjee,2018).

4.6.5 Intensive cultivation of channel bars

During field survey it was notified that much of the channel bars (both point bars and mid channel bars are cultivated. Formation of channel bars begins from near Gorubathan as upstream of the channel flow through deep constricted valley. Large beetle nut plantations cover much of the mid channel and point bars from Gorubthan to Putharjhora (Plate 4.6.33). Whereas cultivation of paddy during summer monsoon and vegetable during winter was observed during winter from Toribari till confluence with Neora at Kranti (Plate 9.32).

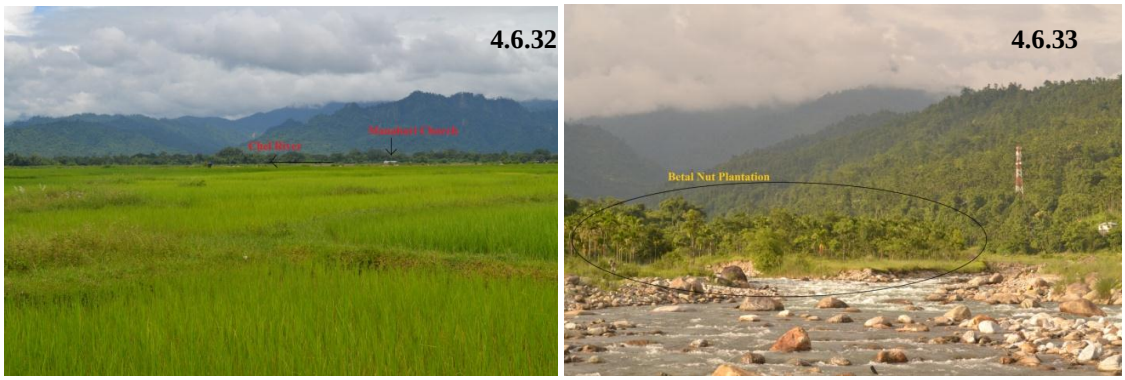

Plate 4.6.32 Extensive Paddy field in the foreground being cultivated on the huge left bank point bar at the upstream of Odlabari Rail Bridge; Plate 4.6.33 Betel Nut plantation on mid channel bar at Gorubathan.

4.6.6 Road Widening

During 2015-2016, the Damdim-Lava Road was widened and repaired thoroughly (Fig.2.13). Fieldworks that coincided during that time revealed the fact that road widening activity affects channel morphology and dynamics mainly in two ways. Firstly, the boulders and loose sediments generated during the slope cutting for road widening were getting dumped into the channel which generally constricts the channel and compels it to divert flow. Sometimes the dumped sediments completely dam the channel and thus creates temporary channel impoundment upstream until discharge and flow velocity increases enough to breach the newly dammed material (Plate 4.6.36 & 4.6.37). Road widening requires slope cutting above the road which destabilize the slope and at times trigger landslides which adds more sediments into the river (Plate 4.6.34 & 4.6.35). Secondly, it increases the demand for sediments of specific grades for laying and pitching on the road. Further huge amount of boulders and sand is needed for repair, extension and construction of new retention walls, culverts, drains and bridges. The sediments from Chel River were entirely used during the entire widening and repairing phase due to its proximity and thus cost efficiency as well. Thus, it was learnt that road widening especially in the upper catchment areas of higher elevation puts on pressure on the channel through both addition and removal of sediments which individually and combinedly increases channel instability and thus dynamicity.

Plate 4.6.34 Road widening at near Ambiok T.G; Plate 4.6.35 Road widening near Chittong Bridge; Plate 4.6.36 & Plate 4.6.37 Dumping of loose sediments generated during road widening into the channel near Chitong Bridge. A dumper/tipper truck marked with red circle can be seen returning after dumping the sediments marked with blue circle, in Plate 4.6.37.

4.6.7 Growth in Tourism

Due to near saturation and degradation in some aspects, of tourism in Darjeeling and Sikkim, the focus and attention is turning into vast, still largely unexplored region of Dooars with immense tourism potentiality. The "Dooars" region also serves as a gateway of tourism to Nepal, Bhutan, Assam and Meghalaya. Thus, the whole region comprising the districts of Darjeeling, Kalimpong, Jalpaiguri and Coochbehar is gaining huge popularity among tourists looking for taste of mountains and riverine landscape, forests and wildlife, lush green tea gardens, adventure, culture etc. The Chel basin in particular falls in the advantageous location as physiographically its upper cathment falls within the lower Himalaya and the middle- and lower-part falls within gently rolling north Bengal plains hosting lush green forets and tea gardens. Three popular tourist towns of its basin

Odlabari, Gorubathan and Malbazar are all within a distance of 70 kms and 60kms from Bagdogra Airport and New Jalpaiguri Railway Station (NJP) respectively. The basin is in high proximity to many tourist spots of the region such as Neora Valley, Jaldhaka Hydel power projects, Murti, Lataguri, Chapramari Forest, Suntale Khola, Jhalong, Bindu. The Department of Tourism, Govt. of West Bengal promotes tourism of the region with the tagline "Majestic Mountains and Mesmerizing Dooars". Thus, huge tourist infrastructures and amenities are growing in the entire basin (Plate 4.6.38-4.6.41). Lot more homestays are opening in the rural areas especially above Gorubathan. Jhandi Eco Hut project in Gorubathan is one such recent and already an established venture. During the months of December and January, people from near and far off places throng to Gorubathan area for picnicking. Mukti Bridge over Chel River at Gorubathan has grown into the most popular Picnic destination of the region. Thus, this massive boom in tourism within and in the region of Chel River basin is and will affect the dynamicity of Chel River.

Plate 4.6.38 Vacant right lower terrace of Chel River just upstream of Mukti Bridge, Odlabari (Photograph- 08.08.2012); Plate 4.6.39 Amenities for tourists and picnickers developed on the same site (13.01.2016); Plate 4.6.40 Close up photograph showing

various amenities developed for tourists and picnickers on the same site (13.01.2016); Plate 4.6.41 Billboard erected by Department of Tourism, Govt. of West Bengal along roadside at Odlabari T.G. near Targhera showing master plan to convert Gazaldoba region into a mega Tourism Hub(Photograph taken-15.01.2016).

4.6.8 Coal mining

During field works it was noticed that Chel River basin bears very small and fragmentary pockets of coal seams with very little volume of very low-quality coal at the confluence zone of Chel, Manzing and Sukha Khola. Due to little volume and poor grade, commercial mechanized mining has not developed as it is not cost effective but because of diminishing tea industry, some locals especially from Putharjhora T.G and Gorubathan areas excavate these coals illegally. The coal is collected in rice sacks manually and transported in cycles mostly during night. They sell it at the rate of Rs. 200-300 mostly to the restaurant and dhaba (local name for *roadside informal budget restaurants*) owners of Odlabari and Malbazar. This coal mining activity though very small in extent and volume can destabilize the upslope and down slope of the mining hole, pits or seams. Thus, it may cause landslide of smaller to larger extent which adds more sediment to the channel and increase its dynamicity.

Major Findings

- Sediment mining destabilizes the channel bars separating multi channels and thus results in migration of thalweg line during little high flow. It is also responsible for lowering and rising of the channel beds.
- Mechanised sediment extraction along wet pits is creating elongated depressions which force water to flow concentrated through these depressions. These pits act as large pools storing much of the water during the low flow time and thus deprives surrounding and downstream reaches by not letting enough flow to reach these areas.
- Mechanised wet pit mining also disrupts the natural pool riffle sequence and deforms the channel beds. Sediment mining creates both negative and positive topography in the form of mining pits and sediment storing mounds respectively.

- Human alteration in the form of twin bridges at Odlabari is disrupting the natural state of hyrological and geometrical properties of the upstream and downstream section of the bridge. The twin bridges have constricted the channel to such an extent that there is large scale variation in the elevation surface, velocity, transport capacity and erosion and deposition in the upstream and downstream of the bridges.
- The embankments have grown in length. It has constricted the flood plain and has disconnected the main channel from its flood plain to a large extent. It reduces elevation gap between embankments or natural levees and river channel bed due to constant aggradations, the threshold level of bankfull discharge and increasing the likeliness of embankment breaching even in low flow.
- The areas covering settlement and roads have increased from 5 to 11% and agricultural land from 11 to 30%. Most notably the area with tea gardens has reduced from 25.9% to 10.75 %. Forest coverage also has reduced from 37% to 32%. Scrubland has recorded zero in 2015 compared to 10% in 2005. Altogether it can be said that there has been decrease in land under natural cover and increase in land under anthropogenic activities except tea gardens. The altered land uses have negative impact on the channel and it can be seen in the increment of areas within sand and boulder river bed from 5% in 2000 to 9% during 2015.

Conclusion

River Chel is not yet a regulated river in terms of damming or any other major engineering infrastructure but with the growth of human population in the region, the impact of human activities on the river has become observable. The study finds that though the net impact is not large yet but the rate is very high and, in the future, the human impact in channel dynamism is estimated to grow manifold and thus demands greater monitoring of anthropogenic activities at basin level.